

AUTOMOTIVE SUSPENSION SYSTEM MODELLING AND CONTROLLING



Thesis submitted in fulfilment of the requirement for the degree
of Doctor of Philosophy

By

ALI IBRAHIM HASSAN AL-ZUGHAIBI

Mechanics, Material and Advanced Manufacturing

Cardiff School of Engineering

Cardiff University

United Kingdom

2019

Publications:

Ali Al-Zughaibi and Huw Davies. 2015. Controller Design for Active Suspension System of $\frac{1}{4}$ Car with Unknown Mass and Time-Delay. International Journal of Mechanical, Aerospace, Industrial, Mechatronic and Manufacturing Engineering Vol: 9, No: 8.

Ali Al-Zughaibi, Yiqin Xue, and Roger Grosvenor. 2018. A New Insight into Modelling Passive Suspension Real Test Rig System, Quarter Race Car, with Considering Nonlinear Friction Forces. Proceeding of the IMechE, Part D: Journal of Automobile Engineering.

DOI: 10.1177/0954407018764942.

Ali Al-Zughaibi. 2018. Experimental and Analytical Investigations of Friction at Lubricant Bearings in Passive Suspension Systems. An International Journal of Nonlinear Dynamics and Chaos in Engineering Systems, Springer, 94(2), P.1227-1242. (Open Access)

DOI: 10.1007/s11071-018-4420-x.

Ali Al-Zughaibi, Yiqin Xue, Roger Grosvenor, and Aniekan Okon. 2018. Design and Investigation of PA Controller for Driving Nonlinear Electro Hydraulic Actuator with New Active Suspension System Model. Proceeding of the IMechE, Part D: Journal of Automobile Engineering.

DOI: 10.1177/0954407018822254.

DECLARATION

This work has not been submitted in substance for any other degree or award at this or any other university or place of learning, nor is being submitted concurrently in candidature for any degree or other award.

Signed (Ali Al-Zughaibi) Date

STATEMENT 1

This thesis is being submitted in partial fulfilment of the requirements for the degree of PhD

Signed (Ali Al-Zughaibi) Date

STATEMENT 2

This thesis is the result of my own independent work/investigation, except where otherwise, and the thesis has not been edited by third party beyond what is permitted by Cardiff University's policy on the Use of Third-Party Editors by Research Degree Students. Other sources are acknowledged by explicit references. The views expressed are my own.

Signed (Ali Al-Zughaibi) Date

STATEMENT 3

I hereby give consent for my thesis, if accepted, to be available for photocopying and for inter-library loan, and for the title and summary to be made available to outside organisations.

Signed (Ali Al-Zughaibi) Date

ABSTRACT

In both academic and industrial fields, suspension system modelling and associated control design influence vehicle response. Ideal hydraulic force models have been used in active suspension studies for decades, but few studies have investigated hydraulic effects, which are the core of system force generation. Accurate mathematical subsystem modelling is essential in representing physical subsystems and enhancing design estimation control. This thesis details the mathematical modelling of both passive and active suspension and controller design for a quarter-car test rig.

When using a conventional passive model, a significant difference between the experimental and simulation results was found for improved modelling of body movements. This led to an investigation in how to resolve this issue, accordingly, the consideration of a new term (friction force) was researched. Establishing a nonlinear friction force became a vital aspect of this work. In addition, emphasis was placed on hydraulic modelling and unknown model parameters that were experimentally identified. This experimental work is unique and helpful for advancing knowledge of any system. A new approach to implementing the friction force was used to identify the system through the transformation of a $\frac{1}{4}$ car model to one Degree of Freedom (DOF) and two-DOF models. This reduced the model complexity and allowed the parameters to be identified from a series of transfer functions linking vehicle parts and the hydraulic models. Simulation and experimental results were then compared.

The hydraulic component model is crucial to the formulation of accurate active control schemes. Full-state feedback controls were realised by Pole-Assignment (PA) and Linear Quadratic (LQ) optimal method. Simulation results suggest that even though the performance of active suspension designed by the PA method is superior to that of passive suspension, it still possesses a design constraint, similar to a passive system, as the design is a compromise between the effects of natural frequency and transmissibility. With a different design concept, the LQ method provided a better solution as it reduced energy consumption by 65% and effectively shifts the dominant natural frequency to a very low-frequency range. Thus, allowing the damping rate to be increased to its critical value with the smallest effect on transmissibility.

It was estimated for experimental work that the identified model with the LQ controller might be used to predict the dynamic responses of the actual system within a certain range of the design parameters due to the considerable difference between the initial condition of the test rig and the linearised operating design. The servovalve produced issues that did not allow validation of the controller.

Both simulation and experimental results, with several conditions, showed consistent agreement, between experimental and simulation output, consequently confirming the feasibility of the newly approved model for passive and active suspension systems that accounted for the actual configuration of the test rig system. These models, that subsequently implemented the nonlinear friction forces that affect the linear supported body bearings, are entirely accurate and useful. The nonlinear friction model captures most of the friction behaviours that have been observed experimentally. Additionally, the models of the nonlinear hydraulic actuators, covered by the dynamic equation for the servovalve, are moderately precise and practical. The suggested Proportional Integral (PI) control successfully guided the road hydraulic actuator and validated the control strategy. The suggested PA and LQ controllers for active systems successfully guided the system to achieve the targets. Ride comfort and handling response are close to that expected for the passive suspension system with road disturbances, whereas there were clear response enhancements for the active system.

ACKNOWLEDGEMENTS

First, I would like to give thanks to Allah the almighty, the all great without whom I could not have completed this educational endeavour.

I am deeply indebted to the Iraqi army and People's Mobilization (*Al-Hashd Al-Sha'abi*) for defending the homeland against the savage militants (ISIS). Without them, this work would not be possible.

The dissertation would not have been possible without the many people who took part in my life as a graduate student. They made this time unique and memorable for me.

I would like to express sincere gratitude to Dr Yiqin Xue, Dr Huw Davies, and Dr Roger Grosvenor, my immediate supervisors, for introducing me to this fascinating research area. They are generous and patient, guiding me in the research from the beginning to the end. Words cannot express my heartfelt gratitude for their efforts towards my development as a good researcher and a future academic.

I dedicate this work to the memory of my parents and brothers especially "Najem". Finally, this research would not have been possible without the unending support of my family. My lovely wife (Muna), I hope to make you proud and thanks for your patience, encouragement and support over the past difficult years. Many thanks to my brothers and friends for their continued support. Thanks as well to Allah for his gift, my beloved Dr Zaid and Dr Ahmed.

During my time at Cardiff University, I had the privilege of knowing and working with many great people. Extra special thanks go to my colleagues for continued scientific support, Ali Al-Khafaji, Raheem Al-Musawi, Adnan Al-Amili, Zinah Ahmed, and Haithem Elderrat.

I wish to express my sincere thanks to Cardiff University, especially the Manufacturing Engineering Centre (MEC) and electric workshop for the use of the facilities to pursue this research.

I also take this opportunity to thank my sponsors in Baghdad at the Ministry of higher education and scientific research, the University of Karbala in Karbala, Iraq and the Iraqi Cultural Attaché in London for their financial support but also for allowing me to gain a technical perspective in my work.

List of Acronym

A	System matrix
A/D	Analogue to Digital converter
APS	Auto Power Spectral function
ARX	Auto Regressive with an exogenous signal
ARMAX	Auto Regressive Moving Average with an exoger
ASLQ	Active Suspension designed by Linear Quadratic
ASPA	Active Suspension designed by Pole-Assignment
B	Input matrix
BJ	Box-Jenkins
C	Output matrix
CIT	Cranfield Institute of Technology
CPL	Contact Patch Load
CPS	Cross Power Spectral function
D	Disturbance matrix
D/A	Digital to Analogue converter
DAP	Data Acquisition Processor
DFT	Discrete Fourier Transform
DOF	Degree of Freedom
EHA	Electro Hydraulic Actuators
EUI	Engineering User Interface
FFT	Fast Fourier Transform
FRF	Frequency Response Function
IV	Instrument Variable method
Lotus	Lotus engineering
LQ	Linear Quadratic optimal control
LS	Least Square method
LVDT	Linear Variable Differential Transformer
OE	Output Error
PA	Pole-Assignment control
PC	Personal Computer
PEM	Prediction Error Method
PI	Proportional Integral controller

PID	Proportional Integral Derivative controller
PRBS	Pseudo Random Binary Sequence
PS	Passive Suspension
PSC	Programmable Servo Controller
PSCno.	Number used in programmable servo controller
Psi	Pound per Square Inch
RMS	Root Mean Square
SCU	Signal Conditioning Unit
s.d.	Standard Deviation
SV	Servo valve
SS	Steady State
X	State vector
Y	Output signal (scalar)

Nomenclature

- **Road input simulator for experiment**

A_{1r} :	Actuator cross-sectional area for side 1 = $1.96e - 3 \text{ m}^2$
A_{2r} :	Actuator cross-sectional area for side 2 = $0.94e - 3 \text{ m}^2$
B_{vr} :	Actuator viscous damping = 500 N/m s^{-1}
e_r :	Road control signal
F_{1r} :	Controller gain = 1
F_{2r} :	LVDT gain = 50.6 V/m
F_{hyder} :	Hydraulic road force (N)
g :	Gravitational constant (m/s^2)
G_r :	D/A gain = 0.0125 mA/m.c
$i_{max r}$:	Maximum applied current to servovalve = 100 mA
i_r :	Applied current to servovalve (mA)
i_{rss} :	Applied current to servovalve at steady-state (mA)
K_i :	Integral gain
k_{ir} :	Linearised flow gain of servovalve = $5.20e - 6 \text{ m}^3\text{s}^{-1}/\text{mA}$
K_p :	Proportional gain
k_{pr} :	Linearised pressure gain of servovalve ($\text{m}^3\text{s}^{-1}/\text{N m}^{-2}$)
k_{fr} :	Flow constant of servovalve = $0.99e - 4 (\text{m}^3 \cdot \text{s}^{-1}/\text{N}^{1/2})$
M_r :	Tyre mass = 5 kg
M_T :	Total mass = 285 kg
N :	A/D gain = 3276 m.c/V
P_{1r} :	Pressure for side 1 of actuator (N/m^2)
P_{2r} :	Pressure for side 2 of actuator (N/m^2)
P_{lr} :	Load pressure = 29.2 bar
P_{sr} :	Supply pressure = 200 bar
$P_{1r}(0)$:	Pressure for side 1 of actuator at SS = 74.2 bar
$P_{2r}(0)$:	Pressure for side 2 of actuator at SS = 125.8 bar
P_r :	Compensator gain
Q_{1r} :	Flow rate for side 1 of actuator (m^3/s)

Q_{2r} :	Flow rate for side 2 of actuator (m^3/s)
$Q_{\text{max } r}$:	Maximum flow rate obtained from servovalve = $5.20\text{e} - 4\text{m}^3/\text{s}$
Q_r :	Rated flow of servovalve = $3.33\text{e} - 4\text{m}^3/\text{s}$
R_{ir} :	Cross-port leakage resistance = $2.45\text{e}11$ ($\text{N}/\text{m}^5/\text{s}$)
T_s :	Sample time interval (ms)
u_r :	Servovalve control
V_{1r0} :	Actuator volume for side 1 = $80\text{e} - 6 \text{m}^3$
V_{2r0} :	Actuator volume for side 2 = $167\text{e} - 6 \text{m}^3$
V_{1r} :	Dynamic actuator volume side 1 (m^3)
V_{2r} :	Dynamic actuator volume side 2 (m^3)
X_r :	Measured road input displacement (m)
X_{rdf} :	Desired filter road input
X_{rd} :	Desired road input
X_{rf} :	Filter road input
x_{sr}	Spool movement (m)
β_{er} :	Effective bulk modulus = $1.43\text{e}9$ (N/m^2)
τ_r :	Time servovalve constant (s)
ξ :	Damping ratio
ω_n :	Undamped natural frequency (rad/s)

- **Passive suspension**

b_d :	Viscous damping = 260 ($\text{N}/\text{m} \cdot \text{s}^{-1}$)
b_t :	Tyre damping = 3886 ($\text{N}/\text{m} \cdot \text{s}^{-1}$)
C_e	Tracking parameter
D	Viscous coefficient ($\text{N}/\text{m}/\text{s}$)
$e1$	Curvature degree
F_{fric} :	Friction force (N)
F_{zd} :	Contact patch load (N)
g	Gravitational constant (m/s^2)
k_t :	Tyre stiffness = $9.2\text{e}5$ (N/m)
k_s :	Spring stiffness = $2.89\text{e}4$ (N/m)
L_d	Free length of viscous damping = 0.342 (m)

M_b :	Body mass = 240 (kg)
M_w :	Wheel mass = 40 (kg)
X_b :	Car body displacement (m)
X_w :	Wheel hub displacement (m)
X_r :	Road input displacement (m)
θ :	Actuator of viscous damper and spring angle=45°
$\Delta\theta$:	Dynamic change of (θ)
μ	Friction coefficient

- **Active suspension**

A:	5x5-system matrix
A_c :	Actuator cross-sectional area = $2.46e - 4 \text{ m}^2$
A_h :	Cross-sectional area of flexible hose = $9.08e - 5 \text{ m}^2$
B:	5x1-input vector
b_d :	Damping rate passive suspension (N/m. s^{-1})
b_t :	Tyre damping rate = $3886 (\text{N/m. s}^{-1})$
B_{va} :	Actuator viscous damping rate = 300 N/m s^{-1}
c:	3x3-output matrix
C_e	Tracking parameter
D	Viscous coefficient (N/m/s)
ea:	Active control signal
e1	Curvature degree
f:	Frequency (Hz)
F_d :	Unmeasured disturbance force (N)
F_{hyd} :	Hydraulic force (N)
g	Gravitational constant (m/s^2)
G_a :	D/A gain = 0.0125 mA/m. c
G_d :	5x1-disturbance vector
H_1 :	Controller gain
H_2 :	Load cell gain = $66.7e-6 \text{ V/N}$
i:	Applied current to servovalve (mA)
$i(0)$:	Applied current to servovalve at steady state (mA)

I:	5x5-identity matrix
I_1 :	Controller gain
I_2 :	Transducer gain for car body velocity = 0.2 V/m s^{-1}
J:	Cost function
J_1 :	Controller gain
J_2 :	Transducer gain for wheel hub velocity = 0.2 V/m s^{-1}
k_{ba} :	Forward gain for two-DIF model
k_e :	Servo valve linearised flow gain of extending case ($\text{m}^3\text{s}^{-1}/\text{mA}$)
k_{fa} :	Flow constant of servo valve = $7.38\text{e-}9 \text{ m}^3\text{s}^{-1}/\text{mA}(\text{N m}^{-2})^{1/2}$
k_i :	Linearised flow gain of servo valve = $2.3\text{e-}5 \text{ m}^3\text{s}^{-1}/\text{mA}$
k_{i1} :	Linearised flow gain for side 1 of servo valve ($\text{m}^3\text{s}^{-1}/\text{mA}$)
k_{i2} :	Linearised flow gain for side 2 of servo valve ($\text{m}^3\text{s}^{-1}/\text{mA}$)
k_{p1} :	Linearised pressure gain for side 1 of servo valve ($\text{m}^3\text{s}^{-1}/\text{mA}$)
k_{p2} :	Linearised pressure gain for side 2 of servo valve ($\text{m}^3\text{s}^{-1}/\text{mA}$)
k_r :	Servo valve linearised flow gain of retracting case ($\text{m}^3\text{s}^{-1}/\text{mA}$)
k_s :	Spring stiffness of passive suspension (N/m)
k_t :	Tyre stiffness = $2.8\text{e}5 \text{ N/m}$
K:	1x5-state feedback gain vector
k_1 :	1x5-state feedback gain vector for controller
k_1 :	1x5-state feedback gain vector for controller
k_2 :	5x5-transducer gain matrix
l :	Length of transmission line = 12.2 m
L_1 :	Controller gain
L_2 :	LVDT gain for tyre deflection = 18.2 v/m
L_d	Free length of viscous damping = 0.342 (m)
M_c :	5x5-controllability matrix
M_b :	Body mass = 240 (kg)
M_r	Tyre mass = 5 (kg)
M_T	Total mass = 285 (kg)
M_w :	Wheel mass = 40 (kg)
N:	A/D gain = 3276 m. c/V

P:	Forward gain for two – DOF model
P_{1a} :	Pressure for side 1 of actuator (N/m^2)
P_{2a} :	Pressure for side 2 of actuator (N/m^2)
P_{la} :	Load pressure = 96 bar
P_L :	Load pressure (bar)
P_{sa} :	Supply pressure = 200 bar
P_{1ass} :	Pressure for side 1 of actuator <i>at steady state</i> = 52 bar
P_{2ass} :	Pressure for side 2 of actuator <i>at steady state</i> = 148 bar
P_m :	5x5-positive definite real symmetric matrix
ΔP :	Change of pressure (N/m^2)
q_1 :	Weighting factor for car body acceleration
q_2 :	Weighting factor for suspension displacement
q_3 :	Weighting factor for tyre deflection
Q :	Flow rate (m^3/s)
Q_{1a} :	Flow rate for side 1 of actuator (m^3/s)
Q_{2a} :	Flow rate for side 2 of actuator (m^3/s)
Q_e :	Flow rate for extending case (m^3/s)
Q_i :	Input flow rate (m^3/s)
Q_m :	3x3-positive definite real symmetric matrix
Q_o :	Output flow rate (m^3/s)
Q_r :	Flow rate for retracting case (m^3/s)
R_{ir} :	Cross-port leakage resistance = $2.45e11$ ($\text{N/ m}^5/\text{s}$)
T:	5x5-transformation matrix
u_a :	Active control signal
V_{sa} :	Applied voltage
V:	Actuator chamber and hose volume= $7.13e-5$ m^3
V_{1a} :	Actuator chamber and hose volume for side 1 of actuator (m^3)
V_{2a} :	Actuator chamber and hose volume for side 2 of actuator (m^3)
V_e :	Effective control volume= $7.13e-5$ m^3
ΔV_e :	Change of control volume (m^3)
$\Delta V_e/l$:	Change of control volume per unit length (m^3/m)

W :	Forward gain for one-DOF model=0.40
W_e :	5x5-matrix
x :	5x1-state vector
y :	3x1-output vector
X_b :	Car body displacement (m)
X_{bf} :	Reference signal of X_b
X_w :	Wheel hub displacement (m)
X_r :	Road input displacement (m)
$X_b - X_w$	Suspension displacement (m)
$(X_b - X_w)_f$	Feedback signal of $X_b - X_w$
$X_r - X_w$	Tyre deflection (m)
β_{ea} :	Effective bulk modulus for active suspension system = $1.43e9$ (N/m ²)
ρ :	Hydraulic oil density = 860 kg/m ³
α :	Actuator angle= 27°
τ_a :	Time servovalve active constant (s)
ξ :	Damping ratio
ω_d :	Damped natural frequency (rad/s)
ω_n :	Undamped natural frequency (rad/s)
μ	Friction coefficient

Table of Contents

1 Introduction and Literature Review.....	1
1.1 Background and motivation	2
1.2 Scope of the research.....	3
1.3 Primary function of vehicle suspension	4
1.4 Mathematical modelling	5
1.5 Semi-active suspension system	13
1.6 The main differences between this study and that previously carried out using the same test rig .	16
1.7 Full-state feedback control.....	18
1.8 Research Aim and objectives.....	23
1.8.1 Aims.....	23
1.8.2 Objectives.....	24
1.9 Thesis organisation	25
2 Description and Development of Test Rig and System Components	27
2.1 Introduction	28
2.2 Road input simulator.....	34
2.2.1 Hydraulic actuator.....	34
2.2.2 Servovalve	35
2.2.3 Instrumentation and control system.....	35
2.3 Passive suspension system	37
2.4 Active suspension system.....	37
2.4.1 Lotus active actuator	37
2.4.2 Servovalve	39
2.4.2.1 Pressure and flow rate sensor tests	41
2.4.2.2 Servovalve test	42
2.4.3 Instrumentation and control system.....	43
2.5 Instrumentation	46
2.5.1 Linear Variable Differential Transformers (LVDTs).....	46

2.5.2 Load cell.....	48
2.5.2.1 Load cell for active actuator force.....	48
2.5.2.2 Load cell for CPL.....	49
2.5.3 Velocity sensors.....	52
2.5.4 CANAL data acquisition system.....	55
2.6 Moog Programmable Servo Controller (PSC).....	56
2.7 Data Acquisition Processor (DAP).....	58
2.7.1 Hardware organization.....	60
2.7.2 Software Organization.....	61
2.7.3 Applications overview.....	62
2.7.4 DAPview for Windows.....	63
2.7.4.1 Hardware and Software Requirements.....	64
2.7.5 Developer’s Toolkit for DAPL.....	64
2.7.5.1 Compatibility.....	65
2.8 Discussion.....	65
3 Road Input and a New Passive Suspension Model.....	67
3.1 Introduction.....	68
3.2 Road input simulator for the experiment.....	70
3.2.1 Nonlinear mathematical modelling.....	73
3.2.2 Design of PI controller.....	76
3.2.3 Filter and types of inputs.....	77
3.3 Passive suspension system: theoretical studies.....	78
3.3.1 Passive suspension system model.....	78
3.3.2 Friction forces and the relative dynamic angle.....	80
3.3.3 Mathematical model.....	81
3.3.4 Contact Patch Load (CPL).....	83
3.3.4.1 A mathematical model of contact patch load.....	84
3.4 Analysis of natural system frequencies.....	85
3.5 Physical test rig workpiece.....	88
3.6 Inflation pressure.....	89
3.6.1 Underinflated tyres.....	89
3.6.2 Over-inflated tyres.....	89
3.6.3 Correct tyre pressures.....	90

3.7 Experimental work	90
3.8 Identification of parameters	91
3.9 Comparing experimental and simulation results	96
➤ Amplitude = 70 mm	96
➤ Amplitude = 50 mm	101
➤ Amplitude = 30 mm	105
3.10 Discussion	110
4 Nonlinear Friction Model Identification and Effectiveness	114
4.1 Introduction	115
4.2 Why considering friction within this study?	117
4.3 The dynamic indicator	119
4.4 The static indicator	121
4.5 Conventional friction model	122
4.5.1 Stiction region	124
4.5.2 Stribeck effect	124
4.5.3 Viscous friction	126
4.6 How to account for the vertical force	126
4.6.1 Free body diagram of the test rig	126
4.6.2 Dynamic linkage angle expression.....	127
4.7 Nonlinear friction model	128
4.7.1 Mathematical friction model.....	130
4.7.2 Static friction model	130
4.7.3 Dynamic friction model	131
4.7.4 Steady-state friction	133
4.7.5 Simple friction model	134
4.8 Friction validation	136
4.8.1 System inputs	137
4.8.2 Validity of body velocity	137
4.8.3 Validity of relative wheel and body displacement	138
4.9 Friction hysteresis	139
4.10 Results	140
4.10.1 Friction results for general form (considering Coulomb friction).....	140

4.10.2 Friction results for simple form (without Coulomb friction)	142
4.11 Discussion	143
5 Mathematical Modelling for Nonlinear Active Suspension and System Linearity .	149
5.1 Introduction	150
5.2 The Lotus active suspension concept.....	152
5.3 Hydraulic nonlinear system modelling	156
5.3.1 Servovalve nonlinear model.....	157
5.3.2 Characteristic servovalve equation within the scope of linearization.....	162
5.3.3 Nonlinear actuator model and hydraulic force	166
5.4 Nonlinear friction forces model for AS	170
5.5 Comparison between one-DOF and Lotus model	172
5.6 Two-DOF model	174
5.6.1 Open-loop state-space model	176
5.6.2 Closed-loop system	180
5.7 Discussion	181
6 Design PA and LQ Controllers	186
6.1 Introduction	187
6.2 Road simulator input.....	189
6.3 Physical Modelling	190
6.4 Control issue and multivariable feedback control	190
6.5 Pole-Assignment control (PA).....	197
6.5.1 Design example	202
6.6 Simulation results for passive and active suspension designed by pole-assignment.....	207
6.7 State observers	210
6.8 Linear Quadratic optimal control (LQ)	212
6.9 Application to the active suspension system	214
6.10 LQR algorithm	215
6.10.1 Determination of weighting factors	223

6.11 Design example	224
6.12 A new active suspension model	226
6.13 Dynamic performance and optimum design of an active suspension system designed by pole-assignment and linear quadratic optimal control.....	228
6.14 Comparison between passive suspension and active suspension designed by pole-assignment and by linear quadratic optimal control.....	231
6.15 System bump input exceeds the limit of the test rig.....	237
6.16 Random system input for simulation.....	241
6.17 Discussion	247
7 Conclusion and Future Work	252
7.1 Introduction	253
7.2 Most vital aspects of this study	253
7.3 The main contribution of this study	258
7.4 Recommendations for future work	260
8 REFERENCES.....	261
9 APPENDIX.....	I

List of figures

Fig. 1.1. Skyhook damping model for a semi-active suspension system.	7
Fig. 1.2. The Lotus active model.	9
Fig. 1.3. Schematic of the chain-like structure created under an applied field (Preumont 2011).	14
Fig. 1.4. a) Magneto-Rheological composite damper RD 1097-01, b) Its characteristic damping force versus piston velocity (Warminski et al. 2012).	14
Fig. 1.5. System responses under random input (Du et al. 2005).	15
Fig. 1.6. Different controller performances for bump (impulse-type) road disturbances.....	16
Fig. 2.1. Overall layout of the passive experimental test rig.	30
Fig. 2.2. Overall layout of the active experimental test rig.	31
Fig. 2.3. Photograph of the passive test rig (front view)	31
Fig. 2.4. Photograph of the active test rig (front view)	32
Fig. 2.5. Drawing showing the arrangement and angle position of active actuator	34
Fig. 2.6. Side view photograph of the test rig	36
Fig. 2.7. Louts active actuator.	37
Fig. 2.8. Physical movements of active actuator.	38
Fig. 2.9. Photograph of the active Moog servovalve.	39
Fig. 2.10. Photograph of the hydraulic connection.	40
Fig. 2.11. Pressure and flow rate sensors test.	41
Fig. 2.12. Servovalve pressures on boths side as a function of applied voltage	43
Fig. 2.13. Servovalve flow rates on both side as a function of applied voltage	43
Fig. 2.14. Schematic diagram of the active suspension control system	45
Fig. 2.15. The LVDT used for the measurement of tyre deflection.	47
Fig. 2.16. Load cell [measuring hydraulic force]	47
Fig. 2.17. Load cell [measuring contact patch load] from left to right: top and side view.	50
Fig. 2.18. Measured CPL through the LabVIEW program	50
Fig. 2.19. Test rig used for the calibration of the load cell	51
Fig. 2.20. Calibration curve of load cell used for the measurement of CPL	52
Fig. 2.21. Cross-sectional view of the cable actuated sensor (velocity and displacement sensor) (Surawattanawan 2000)	52
Fig. 2.22. Photograph of the installation of the velocity sensor for the measurement of car body velocity and displacement.	53
Fig. 2.23. Photograph of the installation of the velocity sensor for the measurement of wheel hub velocity and displacement.	54
Fig. 2.24. Calibration graph for the body velocity sensor.	54
Fig. 2.25. Calibration graph for the wheel velocity sensor.	55
Fig. 2.26. Terminal box of the CANAL data acquisition system.	56
Fig. 2.27. Moog Programmable Servo controller (PSC)	57

Fig. 2.28. Data Acquisition Processor (DAP) card.....	58
Fig. 2.29. System supervisory PC (left) and CPL LabVIEW display PC (right)	60
Fig. 2.30. Hardware organisation	61
Fig. 2.31. Software organisation	62
Fig. 3.1. Performance compromise of passive suspension systems (Mouleeswaran 2012).	69
Fig. 3.2. Schematic diagram of road simulator system.	71
Fig. 3.3. Schematic diagram of the test rig and road simulator.	71
Fig. 3.4. Free body diagram of a quarter car (test rig) passive suspension model.....	79
Fig. 3.5. Free body diagram of a quarter car passive suspension model.	82
Fig. 3.6. A ¼ car passive suspension system model including external forces.	83
Fig. 3.7. Passive suspension model without damping elements or external forces.	85
Fig. 3.8. Free body diagram of a ¼ car test rig with passive suspension.	86
Fig. 3.9. Car body and wheel natural frequency as a function of suspension stiffness.	88
Fig. 3.10. Inflation pressure (Gordons-tyres 2018).	89
Fig. 3.11. Experimental body velocity as a function of time.....	92
Fig. 3.12. Experimental wheel velocity as a function of time.	93
Fig. 3.13. Experimental road displacement as a function of time.	93
Fig. 3.14. Schematic for the servovalve including upper and lower pipes.	94
Fig. 3.15. Comparing both of step, X_{rd} , and road, X_r , input results.....	96
Fig. 3.16. Control force supposed to be the system.	97
Fig. 3.17. Comparing X_w , X_b , (m), experimental and simulation results.	97
Fig. 3.18. Comparison between body velocity, \dot{X}_b , (m/s) results	98
Fig. 3.19. Comparison between wheel velocity, \dot{X}_w , (m/s) results	98
Fig. 3.20. Comparison between relative movement, X_w-X_b (m) results	99
Fig. 3.21. Comparing chamber 1 flow rates.....	99
Fig. 3.22. Comparing chamber 2 flow rates	107
Fig. 3.23. Comparing CPL (N) experiment and simulation results.....	108
Fig. 3.24. Effect of inflation pressure on CPL for $X_r=70\text{mm}$	109
Fig. 3.25. Comparing both step, X_{rd} and road, X_r (m) input results.....	102
Fig. 3.26. Control force supposed to be the system	102
Fig. 3.27. Comparison of X_w , X_b , (m) experimental and simulation results.....	102
Fig. 3.28. Comparison between body velocity, \dot{X}_b , (m/s) results.....	103
Fig. 3.29. Comparison between wheel velocity, \dot{X}_w , (m/s) results.....	103
Fig. 3.30. Comparison between relative movement, X_w-X_b (m) results	103
Fig. 3.31. Comparing chamber 1 flow rates.....	104
Fig. 3.32. Comparing chamber 2 flow rates.....	104
Fig. 3.33. Comparing CPL (N) experimental and simulation results.....	104
Fig. 3.34. Effect of inflation pressure on CPL for $X_r=50\text{mm}$	105
Fig. 3.35. Comparing both step, X_{rd} and road X_r input results.....	106
Fig. 3.36. Control force supposed to be the system	106

Fig. 3.37. Comparing $X_w, X_b, (m)$ experimental and simulation results.....	107
Fig. 3.38. Comparison between body velocity, $\dot{X}_b, (m/s)$ results.....	107
Fig. 3.39. Comparison between wheel velocity, $\dot{X}_w, (m/s)$ results.....	107
Fig. 3.40. Comparison between relative movement, $X_w - X_b (m)$ results.....	108
Fig. 3.41. Comparing chamber 1 flow rates.....	108
Fig. 3.42. Comparing chamber 2 flow rates.....	108
Fig. 3.43. Comparing CPL (N) experimental and simulation results.....	109
Fig. 3.44. Effect of inflation pressure on CPL for $X_i=30mm$	109
Fig. 4.1. Schematic diagram of the test rig.....	118
Fig. 4.2. Typical 1 DOF test result (Watton 2005).....	119
Fig. 4.3. Simulation results for X_r, X_w and $X_b (m)$	120
Fig. 4.4. Experimental results for X_r, X_w and $X_b (m)$	120
Fig. 4.5. Measurements of pure delay of X_b from X_w at three positions.....	121
Fig. 4.6. Experimental results of difference displacements between X_w and X_b	122
Fig. 4.7. Conventional Friction Model (Tsurata et al. 2000).....	124
Fig. 4.8. Friction force versus velocity (Kinetic / static model).....	125
Fig. 4.9. Schematic representation of the friction force F_f on a moving object M.....	125
Fig. 4.10. Free body diagram of the test rig.....	126
Fig. 4.11. Engineering geometry of passive units.....	127
Fig. 4.12. Body displacement (X_b) with time.....	134
Fig. 4.13. Experimental step input to the system.....	137
Fig. 4.14. Experimental results for body velocity.....	138
Fig. 4.15. Simulation results for body velocity with time.....	138
Fig. 4.16. Simulation results of the difference between ($X_w - X_b$).....	139
Fig. 4.17. Friction as function of the body velocity.....	141
Fig. 4.18. Damping friction as function of the body velocity.....	142
Fig. 4.19 Damping and Coulomb friction as function of the body velocity.....	142
Fig. 5.1. Influence of vehicle parameters, quarter-car simulation (Fischer and Isermann 2004).	150
Fig. 5.2. Schematic representation of passive, adaptive, semi-active and active systems.....	152
Fig. 5.3. Comparison between ideal passive suspension and Lotus active suspension.	153
Fig. 5.4. Control block diagram of the Lotus active suspension in servo controller format.	155
Fig. 5.5. Control block diagram of the Lotus active suspension in regulator controller format.	156
Fig. 5.6. Electrohydraulic servovalve (Watton 2007).	158
Fig. 5.7. Servovalve schematic diagram.	158
Fig. 5.8. Extending case of the active actuator.	160
Fig. 5.9. Retracting case of the active actuator.....	161
Fig. 5.10. Flow rate/voltage characteristics for servovalve side one.	164
Fig. 5.11. Flow rate/voltage characteristics for servovalves side two.	164
Fig. 5.12. Flows entering and leaving a control volume.....	166

Fig. 5.13. Schematic diagram of the AS test rig.....	169
Fig. 5.14. Free body diagram of the ¼ car and active suspension models.	170
Fig. 5.15. Block diagram representing the interaction between the system and its environment.	176
Fig. 5.16. Block diagram of the open-loop state-space model.....	180
Fig. 5.17. Full-state feedback control applied to the state-space model.	180
Fig. 6.1. Block diagram of single position feedback control.....	192
Fig. 6.2. Pole-Zero closed system map for $(X_b - X_w)$ feedback.	193
Fig. 6.3. Block diagram of full-state feedback control.	194
Fig. 6.4. Block diagram of full-state feedback PA controller.	195
Fig. 6.5. Pole-Zero closed system map for $(X_b - X_w)$, $(X_w - X_r)$ and F_{hyd} feedbacks.....	196
Fig. 6.6. Location of the five suggested closed-loop poles for the PA controller in pole-zero map.	201
Fig. 6.7. Comparing the road inputs (system inputs) for both systems.....	207
Fig. 6.8. Comparison between the wheel and body travel for both PS and ASPA systems.....	208
Fig. 6.9. The wheel velocity for PS in comparison with ASPA wheel velocity.	208
Fig. 6.10. Comparison between the body velocities for both system.....	209
Fig. 6.11. The suspension movement comparison for PS and ASPA.	209
Fig. 6.12. Damping friction force for PA and ASPA as a function of body velocity.	210
Fig. 6.13. Contact patch load (N) for both systems.	210
Fig. 6.14. Block diagram of system and full-order state observer (Ogata 2010).	212
Fig. 6.15. Block diagram of full-state feedback control (linear quadratic optimal control).	216
Fig. 6.16. Simulation model for active suspension designed by full-state feedback.....	229
Fig. 6.17. Experiment setup for the validation of PA and LQ controllers.	230
Fig. 6.18. Simulated body acceleration for PS, ASLQ and ASPA under step road excitation..	233
Fig. 6.19. Comparison of body velocity for PS, ASLQ and ASPA under step road excitation $(X_b = V_b)$	233
Fig. 6.20. Comparison of PA and LQ controller under step road excitation.	234
Fig. 6.21. Location of the dominant closed-loop poles of the two suspension designs.	236
Fig. 6.22. Mixed ramp and bump road inputs for three vehicle speed values, 50, 100 and 150 km/h, with an amplitude of 0.1 m.	238
Fig. 6.23. Comparison of the body velocity for PS, ASLQ and ASPA for three vehicle speed values, 50, 100, and 150 km/h under bump road excitation.	238
Fig. 6.24. Comparison of the body acceleration for PS, ASLQ, and ASPA for three vehicle speed values, 50, 100, and 150 km/h, under bump road excitation.	239
Fig. 6.25. Comparison of suspension travels for PS, ASLQ, and ASPA for three vehicle speed values, 50, 100, and 150 km/h, under bump road excitation.	240
Fig. 6.26. Random road inputs relative to three vehicle speed values, 50, 100, and 150 Km/h.	244

Fig. 6.27. Comparison of the body velocity for PS, ASLQ, and ASPA for three vehicle speed values, 50, 100, and 150 km/h, under random road excitation.....	245
Fig. 6.28. Comparison of suspension travel for PS, ASLQ and ASPA for three vehicle speed values, 50, 100, and 150 km/h, under random road excitation.....	246
Fig. A1.1. Block diagram of the road measured feedback control.....	VII
Fig. A1.2. Pole-zero map of the closed system when used X_r as feedback.....	VIII
Fig. A1.3 Location of the two suggested closed-loop poles for PI controller in pole-zero map.....	VIII

List of tables

Table I: A comparison between the advantages and disadvantages of using PSC versus DAP hardware.....	58
Table II: RMS results.....	136
Table III: Comparison of state feedback signals	174
Table IV: Performance comparisons for PS and active suspension PA & LQ control.....	232
Table V: Comparisons of natural frequencies, damping ratios and hydraulic force for passive and active suspension designs.....	234
Table VI: Road roughness values (Tyan et al. 2009).....	242

Introduction and Literature Review

1.1 Background and motivation

The suspension system is a critical component of any vehicle system. There are three types of suspension systems, namely: passive, semi-active and active that have been widely investigated by many researchers who have investigated different design techniques and control algorithms (Ghazaly and Moaaz 2014). Simple passive suspension systems lack performance in vehicle stability compared with semi-active and active suspension systems. The dynamic behaviour of passive automotive suspension systems is in effect fixed once spring and viscous damper characteristics have been specified. The fixed damper and spring component of the passive system has been reported to not perform sufficiently well in energy absorption under sustained load or road disturbances (Alkhatib et al. 2004) and (Segla and Reich 2007). Semi-active suspension systems use variable dampers or other variable energy dissipator components in the automotive suspension. An example of semi-active dissipator is Magneto-Rheological (MR) damper, which uses MR fluid (Giua et al. 2004), (Cho et al. 2005). MR fluids are materials that respond to an applied magnetic field with a change in rheological behaviour. Typically, this change manifests as the development of yield stress which increases with the applied magnetic field. Thus, the dissipative force provided by the damper can be controlled by adjusting the electromagnetic field. Semi-active suspension systems that have been investigated in the research literature aim to achieve lower energy consumption and as good performance as full-active suspension systems (Sohn et al. 2004), (Do et al. 2010). Semi-active systems are not considered further in the research reported in this thesis, other than via literature review reported in Section 1.5. Active suspension systems are equipped with electronic control systems which control the suspension elements. Unlike a passive suspension system, active systems do not have limited performance and are a new advancement in removing the drawbacks and inevitable design compromise present in passive systems. Active suspension systems reduce car body accelerations by allowing the suspension to absorb wheel accelerations via a controlled actuator (Gysen et al. 2009), (Sam and Hudha 2006).

Suspension design has been extensively explored over the past few decades, with the aim of improving the ride comfort, handling and safety of road

vehicles. The next generation of road vehicles will employ alternative powertrains by harnessing hybrid and electric technology to offer viable solutions for reducing fossil fuel consumption and meeting more stringent emission and safety standards. This poses a significant challenge in the design of chassis in term of materials layout, and system integration, which, also have a considerable impact on vehicle suspension dynamics and suspension design. Therefore, further insight into the fundamentals of vehicle systems and precise practical study of them could assist vehicle development. In this respect, the current research acknowledges the urgent need to re-evaluate suspension system models, in particular, where the typical $\frac{1}{4}$ -car experimental configuration are used with consideration of the friction terms. Hydraulic systems have been used in active suspension studies for decades; they are the core of system force generation. However, only a small number of studies have investigated the hydraulic effects. The modelling in this study also places an emphasis on studying the nonlinearities of the hydraulic elements. The modelling of the hydraulic system, through implementation of a servovalve equation, aims to provide advances in suspension design, dynamics, and control in order to address the challenges associated with the stated development of road vehicles.

1.2 Scope of the research

Practical modelling of passive and active suspension systems that considers the real construction of these systems, by considering friction forces, in contrast to earlier research, presents a significant challenge. The problem of controlling suspension systems is very complicated due to the relationship between the system's components and their associated parameters. Previous research conducted on suspension control systems covers a broad range of design issues and challenges. Developments have been taxing the ingenuity of engineers for many years; this has led to the evaluation of a wide range of design proposals and practical implementations, including fully active. The control strategies of fully active suspension have been studied to describe and improve ride comfort and handling. For example, (Hrovat 1990) explored the connection between linear-quadratic Gaussian optimal one- and two-DOF models and (Türkay and Akçay

2008) used a quarter car active suspension system using vertical acceleration and suspension travel measurements for feedback.

This chapter introduces on the following topics, which are central to this research project:

- A new $\frac{1}{4}$ -car simulation model, including friction forces, is developed to align with an experiential test rig.
- An extended fully active suspension model including nonlinear hydraulic actuator terms.
- The main difference between the current study and previous ones, particularly those conducted on the same experimental test rig, as demonstrated in Section 1.6.
- Full-state feedback control, pole assignment and linear quadratic optimal control, designs for active suspension systems, as demonstrated in Section 1.7.

1.3 Primary function of vehicle suspension

As a rule, the principal purpose of vehicle suspension is to provide excellent ride comfort for occupants together with vehicle handling and stability. The main indicator of ride comfort is car body acceleration, in the sense that as much as a slight acceleration level of the vehicle body leads to better ride comfort. Vehicle's handling capability can be identified by tyre deflection, in the sense that a similar tyre deflection, measured from an equilibrium state, results in a better vehicle-handling characteristic. A contact patch load determines vehicle stability in a laboratory environment, in the sense that a high capacity measured from load cells beneath the tyre provides better vehicle stability and safety. It is well known that ride comfort is a primary concern for passenger cars, while vehicle handling is more desirable for off-road, high-speed vehicles, such as racing cars. In order to focus on passenger cars, the emphasis of this work was ride comfort, i.e. to minimise car body acceleration.

Vehicle dynamic model type and performance criteria are dependent upon each other, if a more complex model is used, then more choice of performance

criteria may be established. The purpose of this study is to analyse and develop passive and active suspension designs, with new insight for a $\frac{1}{4}$ car test rig model. The latter is considered by categorising the test rig as a two-DOF $\frac{1}{4}$ car model. The model composes of a car body and wheel unit, with only vertical motion (bounce mode) to be addressed. Even though the two-DOF model cannot be used to investigate other modes of movement (pitch and roll), which must be performed on higher DOF models (half and full car models), it was still useful, since it contains essential features of the suspension design problem. The two-DOF model provides correct indicators of performance benchmarks associated with car body acceleration and physical constraints, namely suspension displacement and tyre deflection, which is the displacement of wheel hub relative to the road surface.

In both the real world and the laboratory environment, suspension displacement is limited by the working space available for the car body and wheel hub. Tyre deflection is limited as the tyre should stay in contact with the road surface at all times to provide a link between the car body and the road surface. Tyre deflection can be theoretically represented by a linear spring and a viscous damper connecting the wheel hub and road. If a tyre contact point departs from the road surface, the linear theory applied to the system will no longer be valid.

According to the above performance criteria, the primary function of vehicle suspension applied to the two-DOF $\frac{1}{4}$ car model used in this work is:

To minimise the car body acceleration within the available suspension displacement and tyre deflection.

This statement is the assumed design objective and was used to study the characteristic system responses of passive and active suspensions.

1.4 Mathematical modelling

A scientific model is characterised by an arrangement of conditions that represent the dynamic behaviour of a system. The model may be described in a wide range of routes; contingent upon the application of the system and circumstances, one mathematical model might be more qualified than other models. In modelling, a compromise between the simplicity of the design and the precision of

investigation results must be made. It is generally satisfied if the model is adequate for the problem under consideration.

The system responses investigated and tested in this work are presented in two stages. For the **passive case**, the first stage tests were carried out on the test rig platform to evaluate the behaviours of the real system. The second stage tests were performed by establishing a nonlinear mathematical model of each subsystem, and making a simulation using a C++ compiler and MATLAB Control System Toolboxes. Furthermore, to discover the extent of any agreement existing between both; in the case of the **active system**, a simulated model was used to evaluate the performance of the mathematical approach, in order to validate the results and enable algorithm control. This was conducted in-conjunction with experimental work that investigated the extent of improvement in comparison with the inherent trade-off between ride comfort, suspension travel and road-holding abilities.

System modelling is one of the required assignments for active suspension design because even the best controller cannot be expected to achieve anything if the scientific model utilised does not adequately represent the physical system. In fact, the developed model is central in determining the complexity of the control law necessary to govern system dynamics. Thus, focusing on the modelling of all sub-systems and the whole test rig system is one of the main aspects of this study. Many researchers have proposed various active suspension configurations. Significant developments can be traced to two sources: Skyhook damping (Karnopp 1983) and the Lotus dynamic model (Williams and Wright 1984), (Williams and Wright 1986; Thompson and Davis 1991).

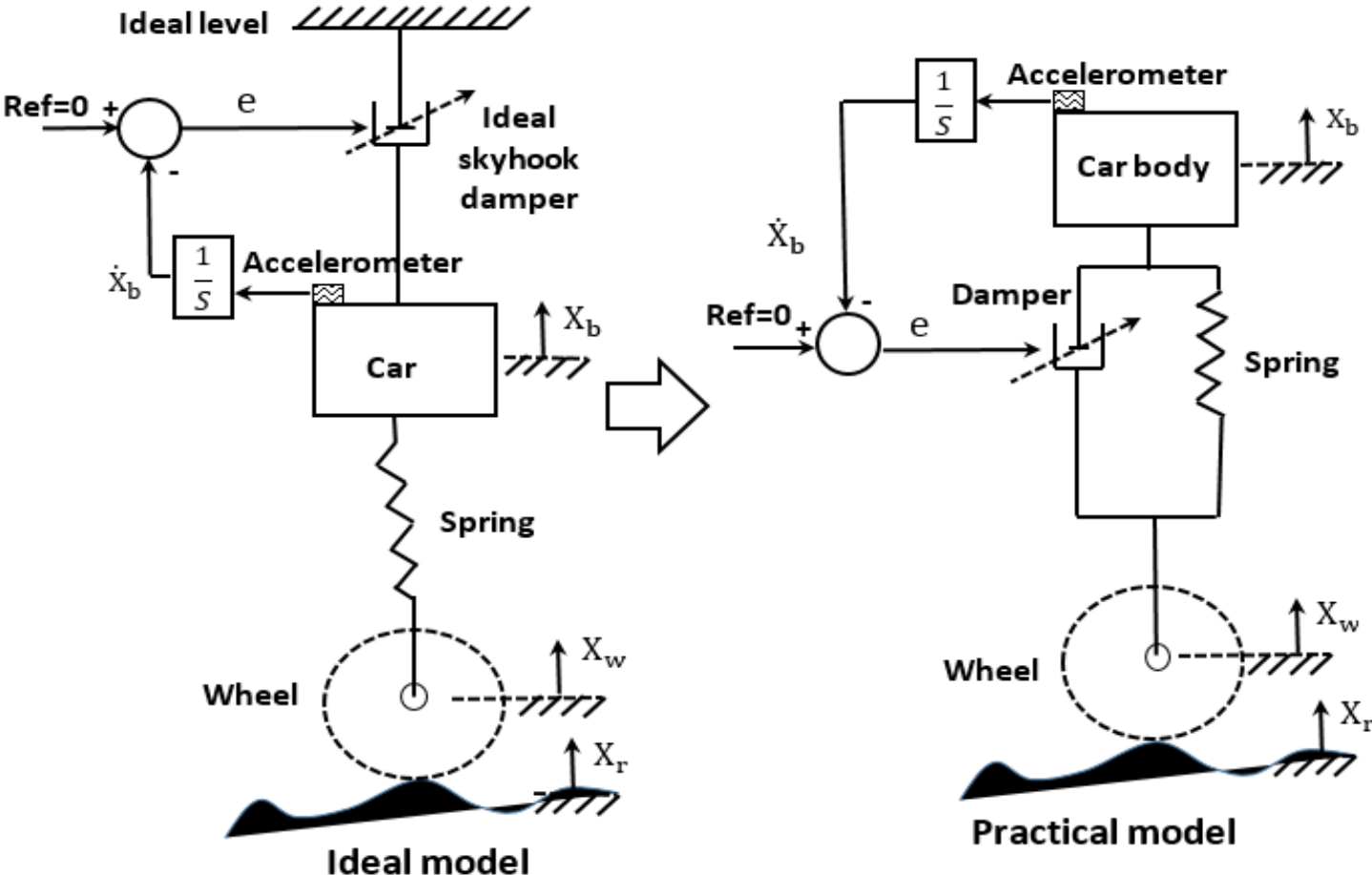


Fig. 1.1. Skyhook damping model for a semi-active suspension system.

Karnopp offered the concept of skyhook damping model, type of semi-active suspension, as shown in Fig.1.1. In this example, forces are excited within the adaptable shock absorber to imitate the ideal, hypothetical, damper that is connected to the vehicle body and an inertial reference. It is assumed that the perfect body is suspended via the damper. Therefore, the damping force does not oppose vehicle wheel movement, but road surface inputs are not transmitted to the body via this damper. A damping force conflicting and proportional to the vehicle body velocity is applied to the car body. This type of control requires measurement of relative velocity across the damper, an assessment of absolute vehicle vertical velocity and a relatively fast value to control the damper force independent of its initial velocity. In practice though, a spring is used in addition to the damper to support the vehicle body weight and maintain the position of the car body. It should be noted that the active suspension system configured by the skyhook-damping model is stable because of the support spring placed in parallel with the damper; without this spring the system cannot be used. In addition, the actuator can only mimic the hypothetical skyhook damper to a certain extent and there are times when the actuator force acts in the wrong direction. To remove this limitation of semi-active suspensions, fully active suspension was developed.

Lotus active suspension was designed, in the early 1980's by Lotus Engineering in collaboration with the Cranfield Institute of Technology (CIT). The system was conceived to solve aerodynamic problems of controlling massive down-forces without compromising driver conditions or vehicle handling. It comprises a high-pressure hydraulic actuator, in place of a conventional spring and damper, and a servovalve which is used to control the hydraulic flow rate to the actuator. Hydraulic systems are employed in the realisation of active suspension hardware because of their outstanding advantages (Merritt 1967a), (McCloy and Martin 1980).

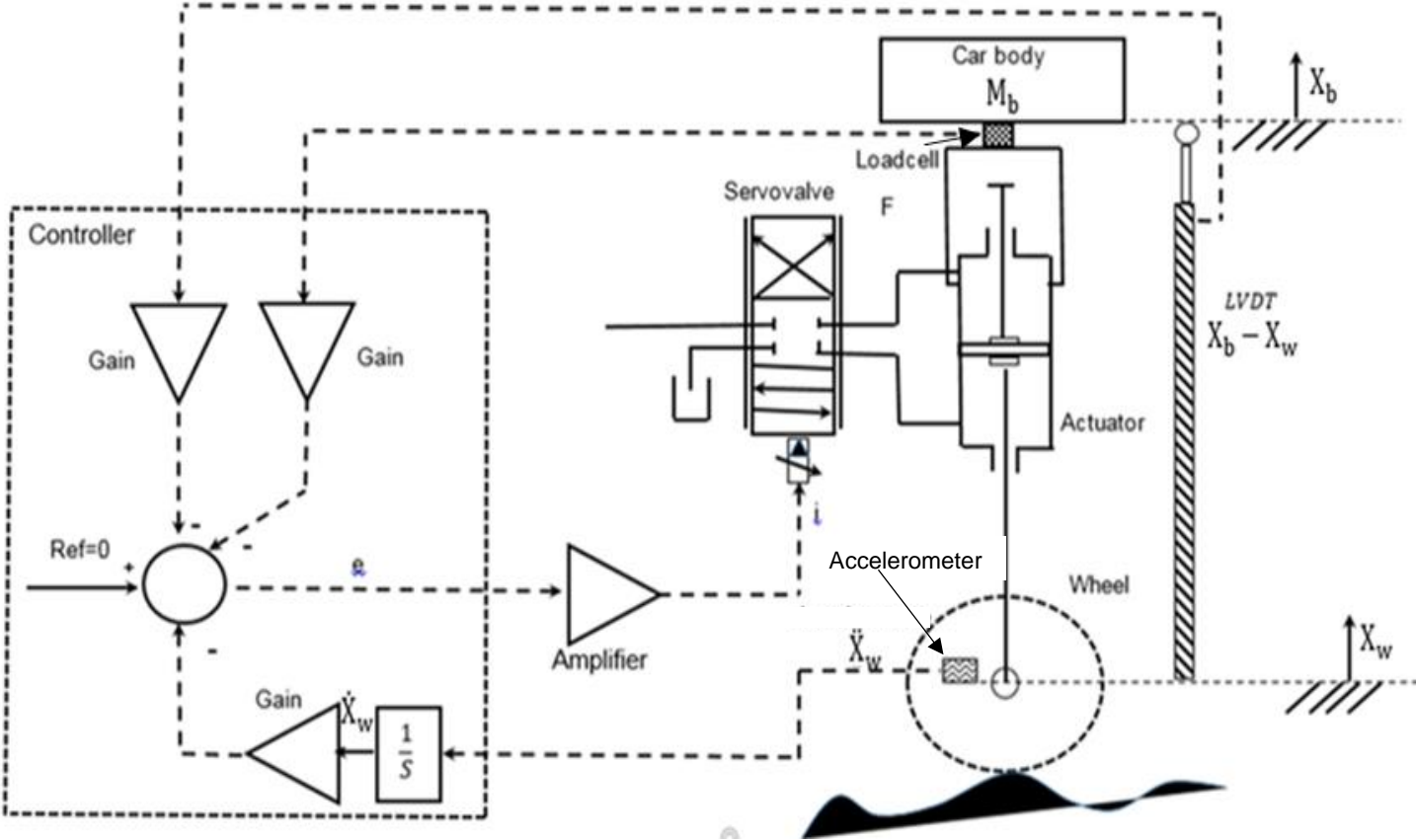


Fig.1.2. The Lotus active model.

Fig.1.2 shows a schematic of an existing Lotus model. The required signals to produce a control force from the hydraulic actuator are:

- Applied force (from the load cell)
- Suspension displacement (from an LVTD)
- The velocity of the wheel hub (from an accelerometer)

The hardware configuration, mathematical model and control law developed by Lotus and CIT were patented in 1984 and 1986 (Williams and Wright 1984) (Williams and Wright 1986). Wright and Williams, the Lotus engineers who invented the system, published their work describing the system in principle and the hardware configuration (Wright 1984), (Wright and Williams 1989). (Thompson and Davis 1991) pointed out mistakes in the Lotus patent, which they then corrected, and expanded on some of the technical descriptions.

The Lotus active model is mathematically simple yet it contains considerable thought and is a smart idea. The model attempts to simulate an active suspension capable of adapting its characteristics, i.e. stiffness and damping rate, via feedback gains. In comparison to the skyhook-damping model, a support spring is unnecessary for system stability. However, if a spring is added in parallel with the Lotus hydraulic actuator, it would assist in supporting the weight of the car body. Thus, if the hydraulic power supply fails, the car body is still supported by the spring. The suspension stiffness may be generated within a closed-loop control using feedback signals from a force sensor and a displacement sensor according to the car body mass placed on the force sensor. The suspension dynamic response may be damped down by feedback from the velocity signal. The mathematical model was developed on the basis of a one-DOF model without the wheel unit. System disturbances were from aerodynamic down-forces acting on the car body because the Lotus active suspension was initially designed for racing car applications. This differs from general passenger cars where system disturbances are mainly caused by the road input acting at the wheel unit.

The patent details and research publications relating to the Lotus active suspension are primarily qualitative. A specific account of system operation and

performance appears to be lacking. More importantly, the mathematical model of the hydraulic system was not included in the design. The control law was proposed according to an ideal hydraulic force generator. In addition, details of how to set the feedback gains, i.e. how to design its controller, were not given. It is believed that practical implementation of the Lotus active suspension would be exceedingly time-consuming due to the need to tune the feedback gains by trial and error.

The first attempt at hydraulic modelling was investigated by (Ben Mrad et al. 1991). A nonlinear model of hydraulic components was presented together with several simulation results. However, the configuration of the model differed from the Lotus active suspension. The most important point relating to this work is that there was no discussion regarding how to utilise the nonlinear model for the controller design. According to physical modelling, the nonlinear model was elaborately proposed making it difficult to extend the analysis beyond this work.

(Engelman and Rizzoni 1993) started with a model that included nonlinear servovalve equations and proposed a linearization technique to obtain linear equations. However, two questions arose from this paper:

- Assumptions about the operating conditions (supply pressure, pressures at both servovalve ports, and tank return pressure) were not defined. As a result, linearised gains cannot be found and linear model analysis does not sufficiently reflect the real case.
- There was no information on the constant parameters used for simulation, bringing into question the simulation results and discussion.

Three further points can be made about the modelling:

- The spring was placed in parallel with the actuator, negating any stability issue.
- The model neglected viscous actuator damping and actuator oil leakage.
- A mistake was found in the linearization process of the model.

In hydraulic closed-loop position control, the current to the servovalve in the hypothetical model operating under conditions for linearisation, or a steady state, is equal to zero. If this statement is applied in this work, the derived linearised equations would be altered. Even though this work contains some errors, the main ideas provide useful guidance for subsequent development. In particular, the linearisation technique was revisited and applied to control the purpose of the design, as shown in **Chapter 5**.

(Thompson and Chaplin 1996) also proposed a hydraulic actuator placed in parallel with a support spring. Their model ignored tyre damping, viscous actuator damping, and actuator oil leakage. Their analysis started with nonlinear servovalve equations, which were processed into two separate cases: extending and retracting. Numerical constants were given based on an assumption. The system operating conditions were defined. The analysis concluded with two nonlinear equations representing both directional movements of the actuator. The nonlinear model was inserted into a linear $\frac{1}{4}$ car model using block diagram analysis. The simulation was used to demonstrate the different responses of active suspensions with and without the hydraulic model to varying road input.

Three interesting points can be made as a result of Thompson and Chaplin's work:

- Firstly, the time domain simulation of the nonlinear model coupling with the linear model was performed via block diagram analysis. This is acceptable from the viewpoint of modelling; however, it becomes a more laborious task for controller design, which must deal with the nonlinear components. It should be noted that because of this, Thompson and Chaplin were not able to include the nonlinear hydraulic model during the controller design stage.
- Secondly, the nonlinear model is limited to only time domain analysis. A broader analysis of the frequency domain could have been made if a model had been derived. Specifically, a Bode plot could have been obtained from the system transfer functions.
- Thirdly, the work was conducted on the basis of purely theoretical models without any experimental validation and with assumed constant parameters. Thus, raising the question of the reliability of the model and the validity of constant parameters.

It is interesting that, although active suspension has been researched for decades, most studies tend to concentrate on the aspects of theoretical control without developing an accurate and practical model and without consideration of the friction forces. It can be concluded that there is a gap between the modelling and the controller design in this area. This is likely caused by two reasons: firstly, developing an accurate and practical model requires verification by experimentation, which necessitate many facilities, i.e. test rig, hydraulic system, instrumentation, and controller. Secondly, there are notably few accounts of the development of successful experimental test rigs because of particular difficulties that have been encountered in the application of the theory. This current work attempts to overcome this difficult task by using and developing the $\frac{1}{4}$ car test rig.

1.5 Semi-active suspension system

Stiffening, damping and isolation are considered the main methods used to suppress vibration passively. A damper can be added to a structure in order to reduce structural resonance peaks by dissipating the vibration energy through the damper itself. Damping can be achieved passively with fluid dampers, eddy currents, elastomer elements or by diverting dynamic energy from the main structure to the dynamic vibration absorber. Vibration energy can also be converted to electrical energy using a transducer and dissipated into an electrical network or stored as harvested energy (Preumont and Seto 2008).

Recently, semi-active (also called semi-passive) devices have been developed which essentially consist of passive devices with controllable properties. Notable examples include Magneto-Rheological (MR) fluids and piezoelectric transducers with switched electric networks. A large change in the viscosity effect (rheological) was first observed in electro-rheological fluids when subjected to electric fields by Winslow in 1947. An Electro-Rheological fluid (ER) is insulating oil containing micro-sized particles. MR fluid was discovered by Rabinowin, 1951, who observed the same rheological effects through the application of a magnetic field to a fluid containing magnetized particles. The particles make columnar chain-like structures parallel to the magnetic field in fluids, as shown in Fig.1.3. These structures limit fluid flow and require the

minimum shear stress of the flow to be initiated. This phenomenon consumes very little power, is reversible and leads to a rapid response within milliseconds (Preumont 2011).

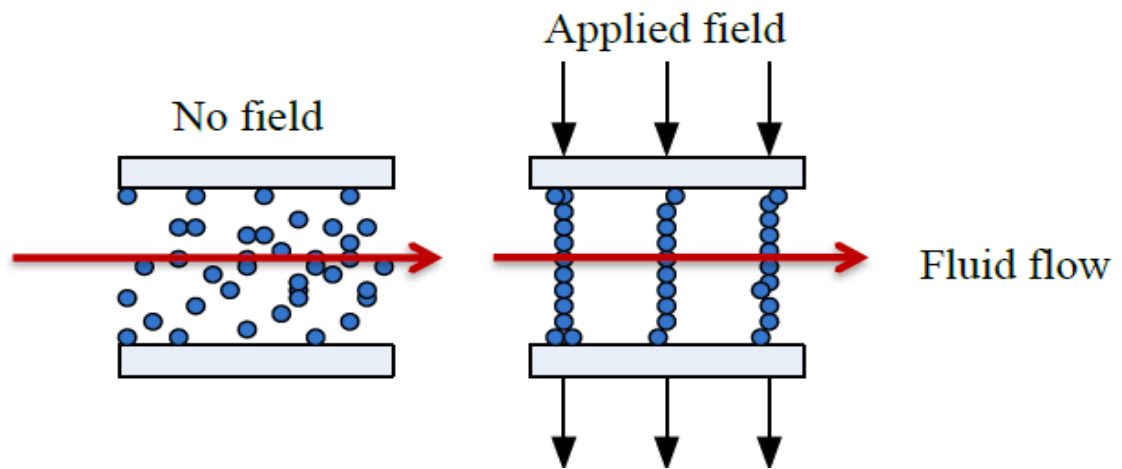


Fig. 1.3. Schematic of the chain-like structure created under an applied field (Preumont 2011).

The application of MR fluid is already part of the design of many structures such as automotive vehicles, tall buildings, robotic manipulator arms and spacecraft. MR dampers are highly nonlinear devices and their force-velocity relationship can be difficult to define. Such dampers have two recognised modes, or states: off and active. MR dampers are a good solution to dissipate energy in mechanical systems and structures. They are available in three types; the monotube is the most common of which due to its compact size and capacity to be mounted in any direction. It is mounted between the mass of the oscillator and the base. Fig.1.4 shows a mono tube MR damper and its characteristic curve of damping force against speed for several values of magnetic field. More information about MR dampers can be found in the reference book (Warminski et al. 2012).

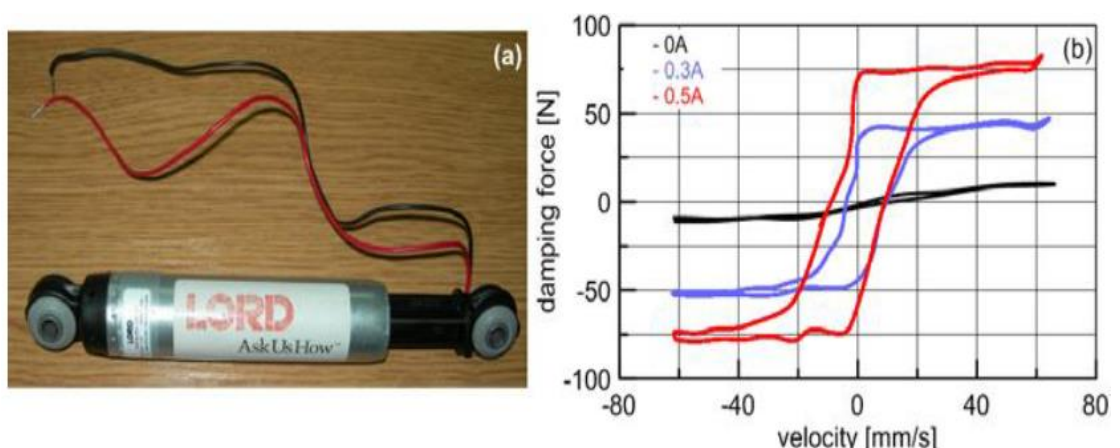


Fig.1. 4. a) Magneto-Rheological composite damper RD 1097-01, b) Its characteristic damping force versus piston velocity (Warminski et al. 2012).

(Du et al. 2005) showed that the active control force for $\frac{1}{4}$ -car suspension model with an MR damper under random excitation could be found using derived polynomial model, the results of which are shown in Fig.1.5

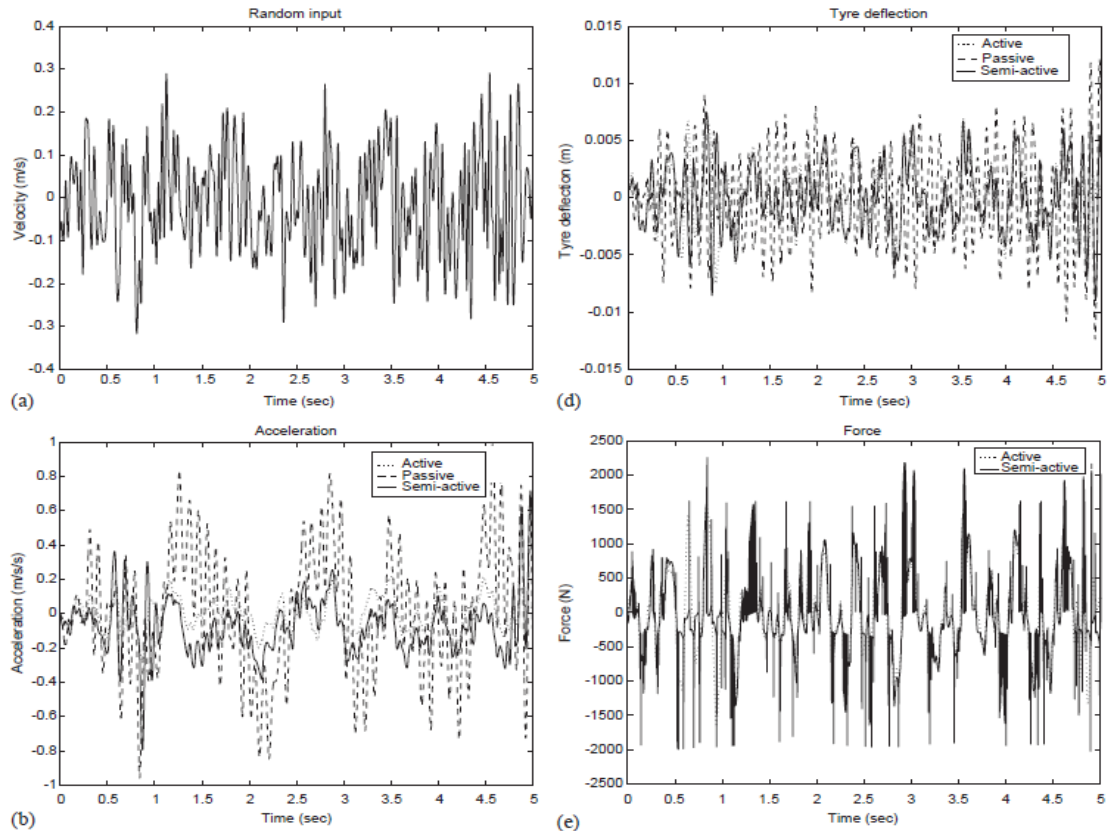


Fig.1.5. System responses under random input (Du et al. 2005).

(Rashid et al. 2011) presented a laboratory study of several fuzzy and hybrid fuzzy-based controllers to experimentally control a semi-active suspension control system. The experimental investigations included an MR damper which utilized MR fields to improve the adjustable damping effects. Fig.1.6 shows the results for several controllers where minimisation of body acceleration relative to 'bump road' disturbance inputs occurred.

As previously stated, semi-active models are not further investigated in this research.

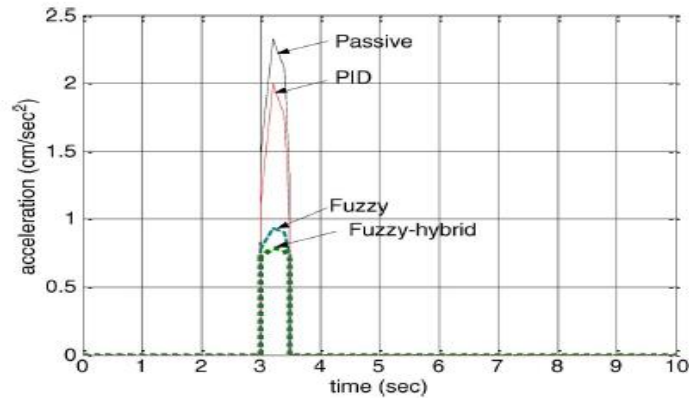


Fig.1.6. Different controller performances for bump (impulse-type) road disturbances
(Rashid et al. 2011).

1.6 The main differences between this study and that previously carried out using the same test rig

In 2000, Surawattanawan studied passive and active suspension using the same test rig (Surawattanawan 2000). Although his study covered good points certain vital elements were not reflected. First of all, the real angular inclinations of the passive suspension system units such as spring, damper and linkage, were not considered. Accordingly, the effect of friction forces arising from the resolved normal force at the bearings for the $\frac{1}{4}$ -car test rig body were ignored. Secondly, Surawattanawan's study considered linear models for road and active hydraulic actuators without implementation of servovalve equations for both, bringing into question the consistency of the experimental results. Thirdly, use of a linear control to drive a linear system is a perfect situation; therefore, comparison with a practical situation is debatable, raising the question of reliability of the linear control model.

From this point of view, a new investigation of the test rig is conducted, considering the actual orientation of the suspension units with the inclusion of the friction forces at the body lubricant bearings (into the equations of motion), leading to establishment of a new quarter car model for passive and active suspension. Further findings are an accurate nonlinear friction model, which is one of the essential positive factors of this study. This study considers nonlinear hydraulic actuator models of both road and active actuators with regard to the servovalve dynamic equations.

The suspension study, as mentioned, deals with ride comfort and automotive stability. Reducing acceleration is a sign for enhanced driver and passengers pleasure, which is the primary target of this investigation. However, there were limitations with the test rig for studying vehicle handling and stability. With regard to this point, **modification were made to the test rig** in this study. Including: replacement of the Programmable Servo Controller (PSC) hardware with a Data Acquisition Processor (DAP) and adding load cells beneath the tyre in order to measure the Contact Patch Load (CPL) between the road, a sign of stability, represented by a base, and the tyre.

Further to the limitations outlined above, (Al-Zughaibi A. and Davies 2015) investigated a further crucial limitation of the test rig by considering a constant car body mass. In contrast this is consistently a variable in the real world due to various reasons such as: a change in the number of passengers; the amount of luggage; and fuel weight due to fuel consumption. In this research, the designed controller overcomes this issue and simultaneously deals with the problems of time-delay and road disturbance.

To summarise, the absolute, critical differences between the current study and the previous one is that the present research covers some essential points, as follows:

- Consideration of a nonlinear hydraulic actuator model to create road disturbance inputs (system inputs), referenced by a dynamic servovalve equation, is illustrated.
- Consideration and design of a PI controller for achieving road simulator.
- The real inclined position of the passive and active suspension subsystem units are considered.
- A new implementation of the friction forces within the equation of motions for passive and active suspension systems for $\frac{1}{4}$ -car models is investigated.
- Modelling the nonlinear friction forces at the body supported lubricant bearings is conducted.
- Modelling a nonlinear hydraulic actuator for active suspension system by advancing the servovalve equation is investigated.

- Design and implementation of Pole Assignment (PA) controller to drive the nonlinear active suspension system by compensating the friction forces using a state-space system representation is investigated.
- Design and implementation of Linear Quadratic (LQ) optimal controller to drive the suspension system by implementing the friction forces, also using state-space system representation, is investigated.
- Use of DAP card converter from Analogue to Digital (A/D) and vice-versa connected with supervisory PC to help the design of a digital controller instead of using PSC hardware controllers is considered.
- Experimental validation of system parameters is conducted.
- Load cells are used beneath the tyre to measure the CPL.

Although there are many differences between this study and Surawattanawan's work, their thesis remains a very important reference for the current research. It was helpful for obtaining test rig data and informing about the test rig before modification. Therefore, most of this information will be used.

1.7 Full-state feedback control

Another important task in active suspension design is to determine the control law parameters in order to provide good system performance. The hydraulic actuator (control core) replaces the spring stiffness and damper coefficients, and in general, more parameters are required and with less constraints than in a passive system. Although there are many different forms of control design, for example, (Yoshimura et al. 2001) considered the construction of an active suspension system for a quarter car model using the concept of sliding mode control, while the practical viability of a hybrid control technique applied to a vehicle active suspension system of a quarter car model using skyhook and adaptive neuro active force control was conducted by (Priyandoko et al. 2009). (Rajamani and Hedrick 1995) presented an adaptive observer for a class of nonlinear systems included the conditions for convergence of state and parameter estimates. The developed theory was used for observer-based parameter identification in the active suspension system of an automobile. Due

to the specific dynamics, active suspension usually requires a compromise in control policy, such as Linear Quadratic Regulation (LQR) or linear quadratic gaussian to determine the feedback gains of the controller (Ting et al. 1995). (Shieh and Li 1998) conducted the design and implementation of an integrated fuzzy logic controller for a DC-servomotor system. The proposed strategy was intended to improve the performance of the original control system through the use of a fuzzy logic controller as the motor load changed. However, the attention here will be confined to fixed-gain full-state feedback control schemes, specifically, PA and LQ have been proposed. Conceptually, the current study will focus on the modelling of the control force (hydraulic force) relative to the existing $\frac{1}{4}$ -car test rig. Therefore, suggesting fundamental (advances) controls such as PA and LQ controls, could be helped to clearly understand the system concept. In another perspective, and it is important to point out that these controls were used in a previous study of the same test rig by (Surawattanawan 2000) where the linear behaviour of the hydraulic system were considered in contrast to reality. Therefore, testing these controls with a nonlinear hydraulic system gains sufficient system knowledge and helps to correctly validate the system parameters. This leads to push the knowledge in this field.

Despite PA being the standard method used to obtain a full-state feedback controller with different aspects, few studies (Hall and Gill 1987) have applied this approach to active suspension. For example, an optimal pole-placement control that combines LQ control and the pole-placement technique was used in the model of the Macpherson type suspension system (Hong et al. 1999). The current research has found only one distinguished publication, that of Hall and Gill (Hall and Gill 1987) included the following aspects:

- A Skyhook system arrangement was applied to predict the best pole locations.
- An idealised control force model was used without details on how to generate it, thus, neglecting some of the hydraulic effects.
- Tyre damping was neglected.
- Absolute displacements of the car body and wheel unit were used for state feedback; this was not possible in the physical realisation.

The study by Hall and Gill (1987) examined the effect of closed-loop pole locations have on the performance of active suspension systems and tried to find an optimum design solution. The closed-loop poles were varied according to their position in the s-plane and each configuration was used to plot transmissibility in relation to changes in road input. The efforts by Hall and Gill (1987) stimulated much additional research in this area, as described in **Chapter 6**.

The most well-known approach of deriving the control law for active suspension is LQ theory (Hrovat 1997a). This method requires that the system is linear, the performance index (cost function) is quadratic, and all state variables are measurable. An optimal feedback gain vector is calculated by solving an algebraic Riccati equation to minimise the performance index.

(Thompson 1976) deserves credit for being a pioneer in the application of LQ theory to active suspension. Some aspects of his work are as follows:

- Ideal force model was used; hydraulic model was neglected.
- Tyre damping was neglected.

Thompson used LQ theory to derive the control law for active suspension and indicated that there was significant potential for performance improvements over passive systems. Controller assessment was performed by modifying two state variables: car body and wheel displacements. The amendment was executed by changing the absolute values of the two state variables to those relative to the ground. Thus, allowing a disturbance step input to be applied to the system on the assumption that the initial states of the car body and wheel displacements are relative to ground change because of the step input. However, this is not a convenient method because modification of the state variables involves complex mathematical procedures, for example, a cost function must be modified according to new state variables. In addition, the controller assessment is only valid for the step input.

One reason for the complexity in Thompson's derivation is the selection of state variables in the mathematical modelling stage. Two of the state variables chosen were absolute displacements of the car body and wheel, which cannot be measured in practice. Thus, becoming a problem for the following controller assessment: the defined cost function, and measurement realisation. Many analytical procedures are needed to transform the original state variables and the

specified cost function into new ones for controller assessment. In fact, the complicated derivation made by Thompson can be dramatically reduced if appropriate state variables (measurable variables) are chosen in the modelling process. Examination of Thompson's work provides awareness for the active suspension modelling in this research work.

(Wilson et al. 1986) derived for the LQ law and extended it to the case of limited state feedback control. It is well known that even if the system is stable and state feedback is detectable, a minimising solution may not exist in the limited state feedback case. Therefore, a gradient search technique can be applied to find the optimum solution. Although the work proposed a numerical example of a controller design, their model still used the same state variables as Thompson. In addition, no controller assessment or simulation results were presented in this paper.

(Sharp and Hassan 1986) compared an active design, with Thompson derived LQ controller, to passive and semi-active suspension for one road surface roughness and vehicle speed. Simulation results were generated in a form that allowed comparison between different types of suspension with equal suspension working spaces. However, the results did not clearly show the benefit of the LQ design. Although they did present the relationships between the performance index, feedback gain value and suspension displacement.

(Hrovat 1997a), (Hrovat 1988) performed the first global study of LQ theory applied to active suspension. Simulation results were shown in the form of carpet plots of normalised Root-Mean Squared (RMS) acceleration against RMS suspension displacement and RMS tyre deflection, respectively. This gives a very useful guideline for design in which the influence of weighting factors on system performance (i.e. car body acceleration) and design constraints (i.e. suspension displacement and tyre deflection) can be graphically determined. However, the mathematical model used was relatively straightforward and neglected tyre viscous damping and hydraulic effects.

(Kumar 2008) conducted a comparison between passive and active systems for a $\frac{1}{4}$ car model using PID controller and employing hydraulic or pneumatic actuators, which provide the desired force in the suspension system. Some aspects of their work are as follows:

- An idealised force model was used, ignoring how it was generated, thus, neglecting some of the hydraulic effects.
- Representing the tyre by only the spring neglected damping.
- Zeigler and Nichols tuning rules were used for tuning PID gains.
- There was no control validation.

(Darus and Enzai 2010) performed an enhanced performance of active suspension for quarter-car model by implementing the LQ and PID controllers with two types of road inputs. Some aspects of their work are as follows:

- An idealised force model was used, thus neglecting some of the hydraulic effects.
- Using a linear model raises questions about the model validity.
- Representing the tyre by only the spring neglected damping.
- There was no mention of how to tune the PID gains.
- The inputs did not represent reality.

(Brezas et al. 2015) designed and performed experimentation of a clipped-optimized Linear Quadratic (LQ) with a semi-active suspension system. They used a more realistic road disturbance excitation, offering optimal semi-active treatment suspension control for the quarter car model. This study included a deterministic load interference on the suspended mass and rolling angle and used roll velocity weights to be as tuning parameters for handling behaviour. Some relevant points from this work:

- An idealistic control force model was used, thus neglecting some of the hydraulic effects.
- Assumptions were made that the adjustable damper could deliver the requested (admissible) damping instantaneously.
- The tyre was only represented by a linear spring, thus, ignoring damping.

It should be noted that there are many publications in this topic area. This review has attempted to narrow the scope of the area by providing a framework at the

beginning and throughout this chapter, notable publications relating to this work were selected, summarised and discussed.

In conclusion, most previous practices have developed active suspension controls on the basis of an idealised hydraulic actuator capable of delivering force infinitely fast. However, in practice, obtaining high fidelity actuation is very challenging and requires a fuller understanding of hydraulic system dynamics. Therefore, the issue of actuator dynamics is an important aspect of practical significance in active suspension control. As far as this research work is concerned, few studies have been performed on hydraulic modelling and experimental validation. In addition, different assumptions were used in various cases and it is difficult to determine which hypotheses provide the best practical solution for hydraulic modelling without experimental validation. Therefore, the primary objective of this study is to provide a rigorous theoretical analysis, together with experimental validation, for nonlinear model of a hydraulic system of a real $\frac{1}{4}$ -car test rig.

All unknown parameters in the mathematical model were identified experimentally. System identification, a useful tool to create a model from experimental data, was applied, together with the derived mathematical model, to determine unknown parameters as shown in **Chapter 3**. More surprisingly, as far as this research is concerned, the quarter-car electrohydraulic active suspension has never been studied by system identification.

The identified model was then used to develop an active suspension controller. The fixed-gain state-feedback controllers, namely PA and LQ, were used. The performance of the two controllers was theoretically compared with a passive suspension system.

1.8 Research Aim and objectives

Bearing in mind the problems stated in the preceding sections, the overall goal and objectives of the research project are listed below.

1.8.1 Aims

The suspension system remains a popular focus of research owing to the extensive industrial production of automotive, vehicles, and mainly cars, for more

than a century. At the same time, the primary target for the suspension system is to develop ride comfort and stability. Therefore, experimentally studying this system leads to significant knowledge of system modelling and control that will assist suspension modification. A passive suspension model should take into account the real position of suspension units in the test rig; accordingly, a new term implementation, the friction force, within the equation of motion for a quarter-car model is investigated and developed. In addition, a nonlinear hydraulic actuator is considered, with a suitable controller to create system inputs, such as road disturbance. A nonlinear friction model is proposed, covering all the observed measurements that occur at body supported lubricant bearings. Active suspension is investigated by altering suspension characteristics to optimise the system, providing the comfort and stability appropriate to our requirements, through designing of PA and LQ controllers. Improving performance in the active suspension system by controlling system responses, demonstrated through simulation, which depend on physical tests for passive suspension with amended step inputs and inflation pressures. CPL is an indicative measure of stability which is investigated. Therefore, load cells are used to measure CPL with both the passive and active systems.

1.8.2 Objectives

The following targets must be met to achieve the aims:

- i. Finding the knowledge gap in the modelling and control of suspension systems in terms of realistic system representation [literature review].
- ii. Developing a nonlinear mathematical model for a hydraulic actuator, with road input as system input and the active system as a control force, through implementation of a dynamic servovalve equation.
- iii. Investigating the influence of implementing new terms within the passive and active suspension models, by developing new nonlinear mathematical suspension models and considering friction forces within the equations of motion.
- iv. Establishing and investigating the nonlinear friction forces at supported body lubricant bearings.

- v. Identifying the parameters and validating the model experimentally.
- vi. Applying the full-state feedback control scheme (PA and LQ) to drive the nonlinear active suspension system.
- vii. Making comparisons and assessments between the passive and active suspension systems designed by PA and LQ.
- viii. Validating the controller design.
- ix. Applying and using load cells beneath the tyre to measure the CPL in both passive and active systems.

1.9 Thesis organisation

Chapter 2: Details the development of the $\frac{1}{4}$ -car test rig, consisting of two main parts; the passive and active suspension system, involving the road simulator. Describes the instrumentation, some practical problems found during this research and solutions to the issues are explained. Useful techniques for using DAP process instead of PSC hardware control and their benefits are also described in this chapter.

Chapter 3: On the experimental side, the nonlinear mathematical modelling of the road simulator is investigated and validated. This model includes the nonlinear mathematical model of a hydraulic actuator covered by the dynamic servovalve equation, which was driven by Proportional Integral (PI) control. This obtained model will be used for comparison between the simulation and experiment for both the passive and active suspension systems.

The passive suspension mathematical model, taking into account the test rig configuration, is derived and validated. The novelty of this model is the implementation of the friction forces within the equation of motion for a $\frac{1}{4}$ -car. The mathematical model of CPL is investigated and validated; setting the benchmark for the subsequent development and assessment of an active suspension system.

All unknown model parameters are experimentally identified. The method of system identification is applied with guidance from the physical model results.

Chapter 4: Develops the nonlinear mathematical model for friction forces occurring at the body bearings. Emphasises the fact that this model is dependent

on the experimental observations and dynamic system analysis. Investigates and validates what the indicators of this friction are, how to account for such friction, the types of friction and their effects on system responses.

Chapter 5: Improves the nonlinear active suspension mathematical model, highlighting the modelling of the nonlinear hydraulic actuator by covering the servovalve equation. Considering, for the first time, the different aspects of friction forces within the $\frac{1}{4}$ -car test rig. Comparisons between the developed model and the original Lotus active control are made. The model is derived in state-space format, as used in controller design, and a series of disturbance transfer functions are used for controlled assessments. Finally, five state variables are validated before the controller design is processed.

Chapter 6: Concerns the application of controller design to the developed active suspension model. Two types of controller design, namely PA and LQ, are proposed. These advance controllers are used to drive the nonlinear hydraulic active system. Comparison of system responses between the active and passive on one side and between these two controllers on the other, are conducted and investigated.

Chapter 7: Provides the conclusions of this study and makes recommendations for future work.

Description and Development of Test Rig and System Components

2.1 Introduction

The automotive industry has been identified as having the fastest growth amongst industries in the current industrial climate. Jumping directly to the research topic area reported in this thesis, it has been further stated that continuing developments in suspension systems will largely influence the future of vehicle design and manufacture. Indeed, the application of suitable analysis methods and applied research is portrayed as a necessity. Improvements to suspension systems directly impact passenger ride comfort and safer driving handling capability, with a need to address the balance between achieving these aims. (Chikhale and Deshmukh 2013) discuss that analysis of vehicle suspension systems is essential to improving passenger comfort is to be improved.

Through new designs of suspension system designs would ultimately be tested and validated on vehicles, for example on test tracks, during research and development, $\frac{1}{4}$ car model are often used. Such models are used in analysis and simulations, as well as for experimental validation. As implied from the terminology, a quarter car model has $\frac{1}{4}$ the mass of a car and a single wheel. This mass is usually constrained to only vertical motion. Such an approach simplifies the ultimate application to a vehicle, for example, it simplifies any vibration-based analysis methods and enables in-lab experimental testing. It does rely upon the argued case that if the control of the vertical motion is well considered and implemented then overall system performance should also be stable. One such $\frac{1}{4}$ car model is used in the research reported in this thesis for modelling, simulation and experimental testing of both passive and active suspension systems and later extended to include more advanced control techniques inherent to active suspension systems.

This section introduces the $\frac{1}{4}$ car experimental model. The implementation of a road input simulator to provide realistic scenarios within which to evaluate the suspension performance is an important element to consider when using such models. The introduction then confirms the passive suspension system used in this study. Collectively, the road input simulator and passive suspension system are reported in full detail in **Chapter 3**. The friction model scope and methods used in this study are presented in **Chapter 4** and an active suspension system appears in **Chapter 5**. The remainder of this introduction presents the

instrumentation, hydraulic servo control and data acquisition information for the $\frac{1}{4}$ car model.

The general layout of both passive and active suspension configuration are presented in schematic, as shown by Figs. 2.1 and 2.2 respectively, and in pictorial form, as shown by Figs. 2.3 and 2.4 respectively. Fig. 2.1 also includes the aforementioned road input simulator and its servo control, as well as the overall instrumentation and data acquisition elements. Fig. 2.2 also shows the common elements of both suspension systems, such as the road input simulator and its servo control, but this time for active suspension system. The action elements of the active suspension configuration can be observed. From a comparison of Figs. 2.3 and 2.4 to Figs 2.1 and 2.2. As shown in Fig. 2.2, the active suspension element has its own hydraulic servo control, controlled via an SCU unit. The dashed lines feeding into the SCU represent the system states that are utilised in the controller designs and their subsequent implementations. For the purpose of this introduction the system states are a hydraulic force, two velocity signals and two (relative) displacements.

Other salient information for the $\frac{1}{4}$ car model is introduced here and referred to in more detail in later chapters. A 240 kg mass plate represents the $\frac{1}{4}$ car body and is constrained to move vertically via two 1 m long rail type linear bearings (THK type HSR 35CCA).

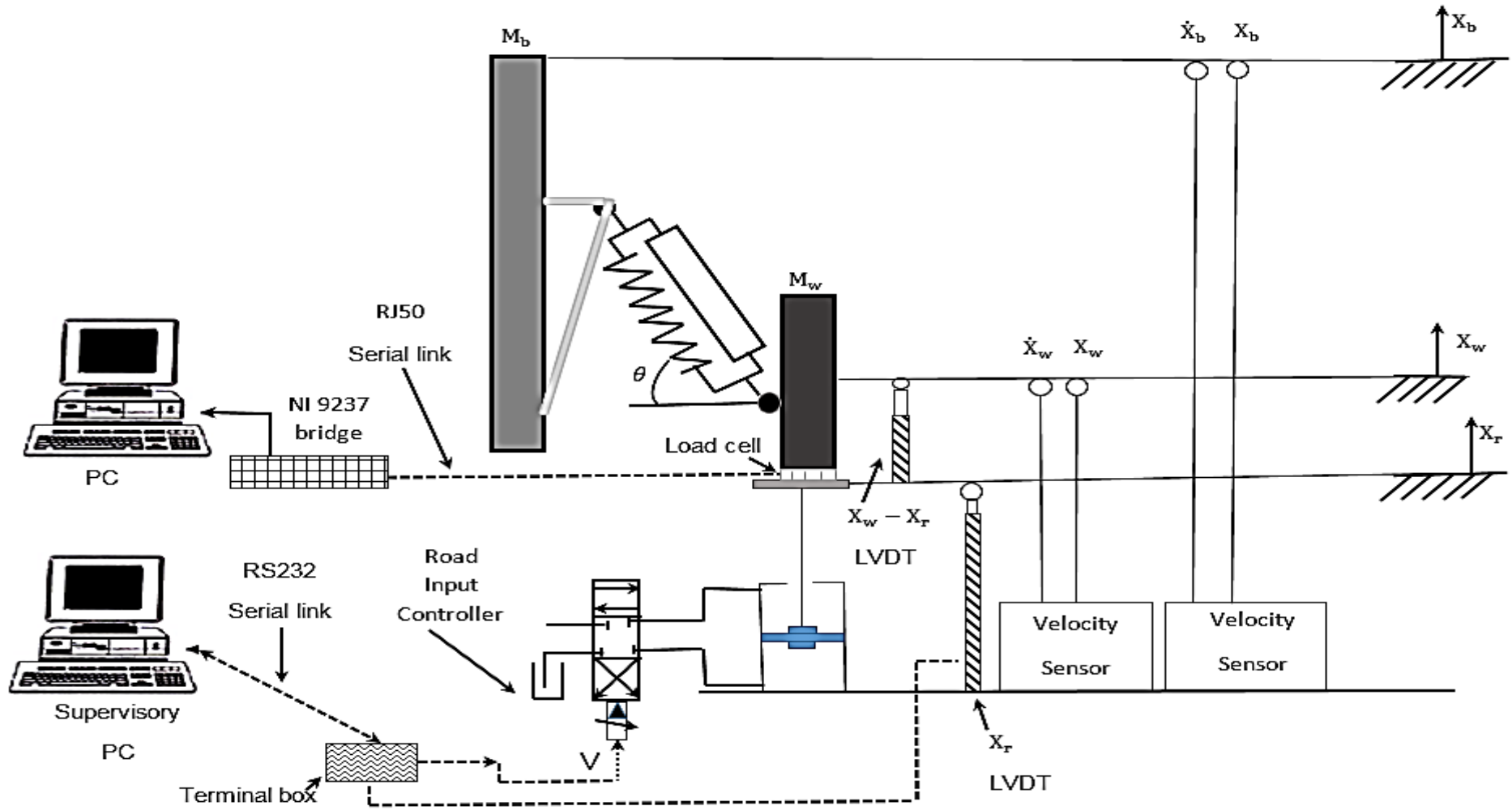


Fig. 2.1. Overall layout of the passive experimental test rig.

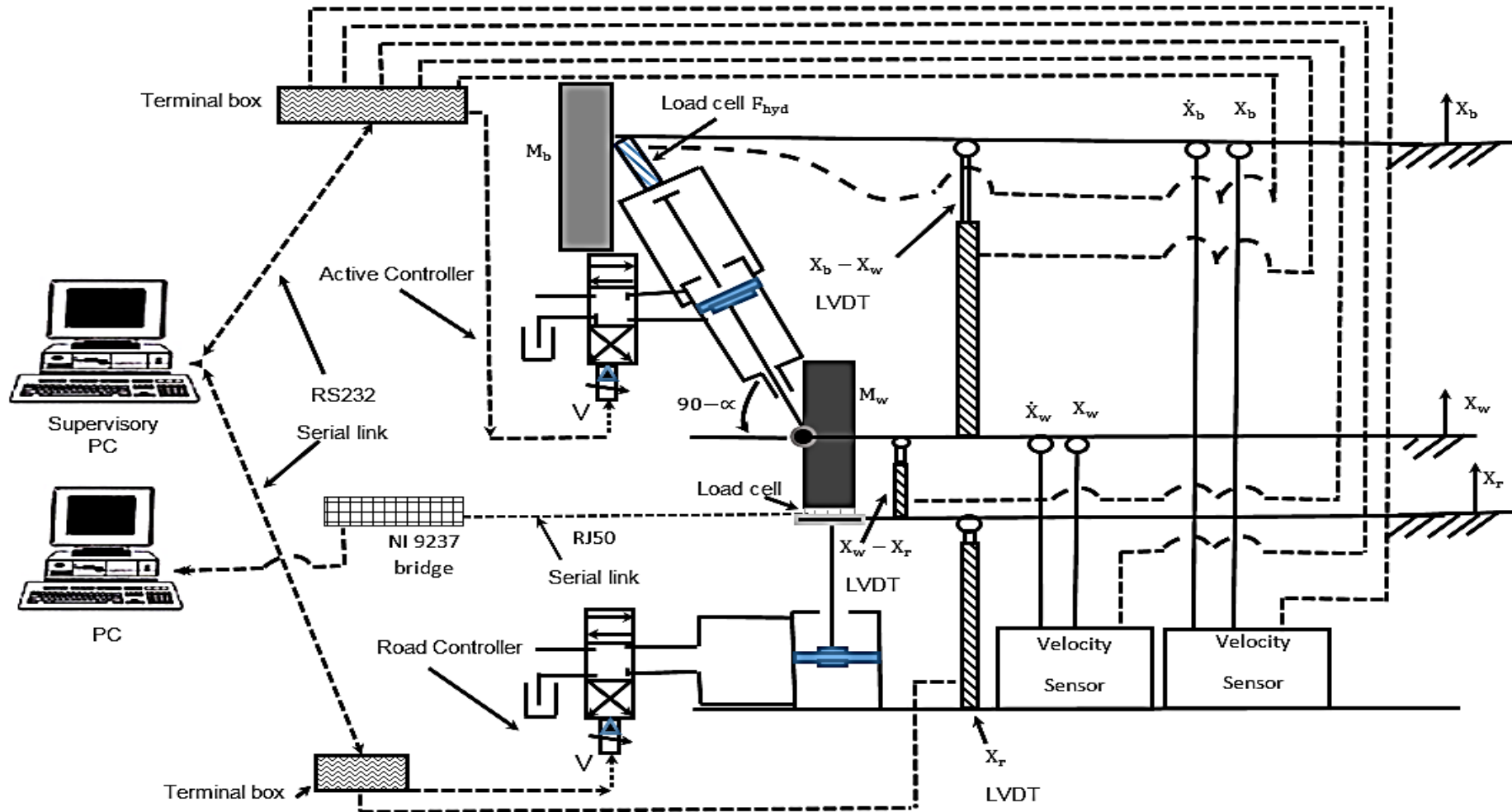


Fig. 2.2. Overall layout of the active experimental test rig.

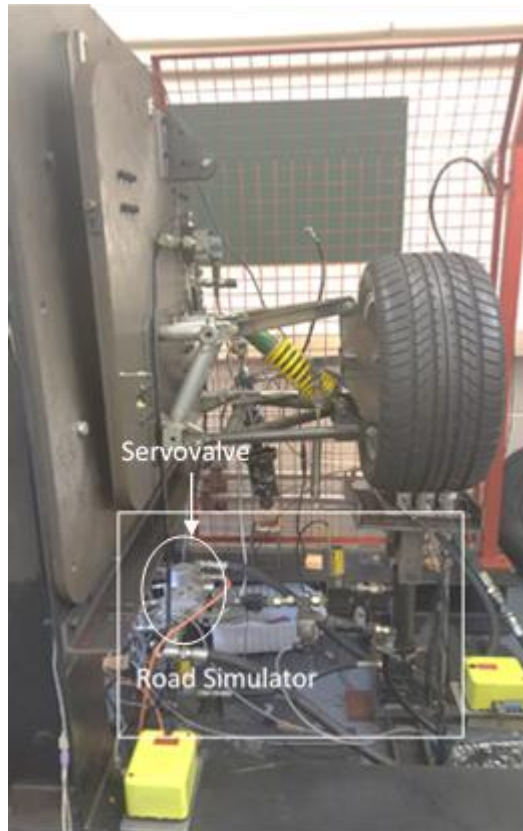


Fig. 2.3. Photograph of the passive test rig (front view).

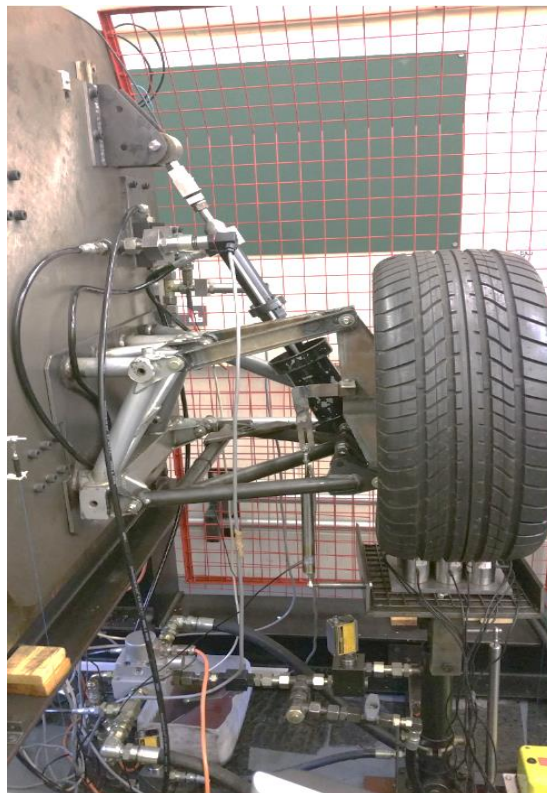


Fig. 2.4. Photograph of the active test rig (front view).

There are aspects to be considered when $\frac{1}{4}$ car models are used. For instance: the linear bearings will introduce frictional effects, in addition to those prevalent elsewhere in the entire system. This study deems that such dynamic frictional effects were to be included in the analysis and simulation efforts. It is well known that these 'extra' effects would not be in operation on a car or test track testing scenarios, as discussed earlier. It was deemed that these would allow more complete modeling and validation and would better inform the active suspension controller design activities.

The $\frac{1}{4}$ car experimental test rig was inherited from previous studies, primarily as reported by (Surawattanawan 2000). It is also noteworthy that a, now retired, Cardiff University academic, Watton, was heavily involved with such fluid power applications (Watton 1989). This textbook produced by Watton includes modelling information that is pertinent to the $\frac{1}{4}$ car model. These are referenced more fully in **Chapters 3, 4 and 5**. The basic configuration is as largely as those previous studies. The upgrades made in the current research, mainly to the data acquisition and related systems, are reported later in this introduction.

The existing suspension linkage design was utilised. It is a double wishbone configuration and its selection was re-confirmed on the basis of it maintaining the upright geometry of the wheel. For the current study a more appropriate and detailed account of the real positions was included. As steering mechanisms were not required for the $\frac{1}{4}$ -car model the suspension linkages were assembled from modified rear chassis components. Upper and lower wishbones were custom fabricated from welded steel sections and steel tube sections. These connected the wheel hub to the chassis, which in turn was connected to the $\frac{1}{4}$ -car body.

Fig. 2.5 more specifically shows the suspension linkage arrangements. The Lotus active actuator position is also shown and is positioned at an angle (α) relative to the vertical plane of the wheel unit. For the active suspension actuator, a Dowty servovalve installed at the car body was attached to the actuator via flexible hoses. The load cell, shown in Fig. 2.5, was placed between the base plate of the road input simulator and the tyre (the wheel and tyre were supplied by TVR). This load cell was actually a group of 9 load cells, detailed later in Section 2.5.2.2, and was used to measure the CPL between those elements. The road simulator actuator was controlled via a Moog servovalve. Another load cell,

shown in Figs. 2.2 and 2.7 that appears later, was used to measure the hydraulically generated forces between the active suspension actuator and the car body at the pivot point. A common, existing, hydraulic power supply was used with 200-bar rated supply pressure, as previously reported by Watton (1989).

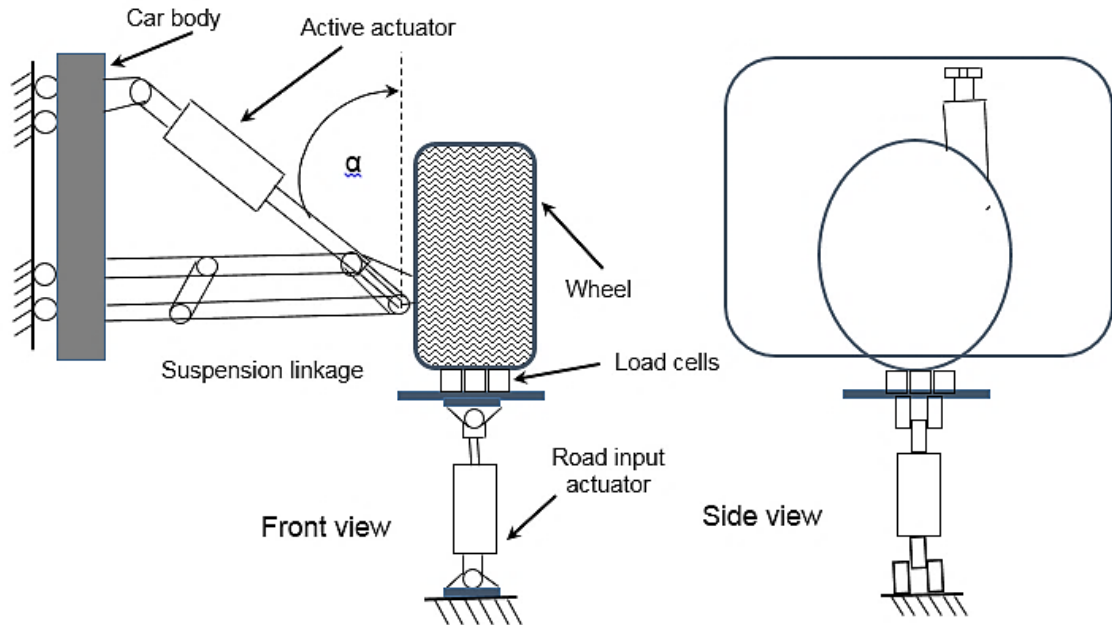


Fig. 2.5. Drawing showing the arrangement and angle position of the active actuator.

2.2 Road input simulator

The previously mentioned road input simulator consists of a Titan hydraulic actuator, a Moog servovalve, an LVDT (to provide a road displacement signal, X_r , as shown in Figs 2.1 and 2.2) and a control system. Road input actuators are typically used to provide a range of time varying conditions, often to reflect the more extreme changes in road surface that a suspension would need to deal with. The time varying conditions can include, whilst not being limited to, step changes, ramp changes and randomly varying conditions.

2.2.1 Hydraulic actuator

The fixing arrangement for single rod actuators, such as the Titan actuator require consideration. The arrangement may lead to non-vertical movement being generated. In this study, any lateral movements are worthy of documentation and are included in the modelling of some of the frictional effects. (Pincott 1996) investigated the fixing arrangement of the type used in ¼-car test rigs and

determined that the hydraulic force of the actuator would be applied at an angle 1° from vertical. Thus, for the maximum travel of 80mm the maximum lateral force would then be 1.7% of the maximum vertical force (Pincott 1996). Two clevis eye mountings were used in the test rig of this study. The lower spherical eye fixed to the base structure needed to accommodate small lateral movements resulting from the wheel unit moving vertically across the fixed radius of the suspension linkage. The upper spherical eye was attached to a support dish under the wheel unit and accommodated small lateral movements due to wheel scrub. Such mounting prevents any off-centre loading of the actuator, and piston bearing friction is minimised. Compared to Pincott's (1996) finding, the test rig has a maximum travel of 70mm. In summary the designer aimed to maximize vertical motion and minimize any lateral movement. It was deemed however that the lateral forces cannot be ignored as they will undoubtedly introduce Coulomb frictional forces at the $\frac{1}{4}$ -car body. As such, these and other frictional effects are included in this study and are described in detail in **Chapter 4**.

2.2.2 Servovalve

The Moog servovalve (type E671 with 20 l.min⁻¹ flow and 100 mA rating) used is a two-stage mechanical feedback valve (Moog 1991). The dynamic performance of such servovalves is often specified via a quoted bandwidth. The higher the bandwidth value the faster the achievable response will be. For the Moog E671 a 20Hz bandwidth is quoted at $\pm 100\%$ current input and 50 bar supply pressure; equating to a step response rise time of 8ms. The control signal for the servovalve was configured in parallel connection mode and passed via a data I/O card (designated SCU in Fig. 2.1) and, to provide sufficient power, a Moog buffer amplifier (G122-824). A block wiring diagram is provided in **APPENDIX D**. With the stated configuration, the directed maximum flows through the servovalve were achievable with a control signal that generated $\pm 100\text{mA}$ at the servovalve inputs.

2.2.3 Instrumentation and control system

The data I/O card was configured for real-time operation using embedded software written and compiled in C++. The input to the positional control of the

road input actuator was from an analogue signal generated by an LVDT measuring the road displacement. The LVDT shaft moved in parallel with the actuator, the position of the LVDT is shown in Fig. 2.6. The control output was an analog signal which, as previously stated, was then routed via a power amplifier to drive the Moog servovalve. The fuller details of the PI based positional control algorithm for the road input actuator are provided in **Chapter 3**. Details of all of the LVDTs used are follow in Section 2.5.1.

The next sections describe any further differences between the configurations of the passive and active suspension systems prior to describing the latter in greater detail.



Fig. 2.6. Side view photographs of the test rig.

2.3 Passive suspension system

As shown schematically in Fig. 2.1, a conventional passive suspension system consisting of a parallel spring, to provide support, and a viscous damper was used in this study. The particular damper used was a Bilstein (B46-17 16-W000).

2.4 Active suspension system

The following provide additional information about the active actuator, a brief review of the operating principles of active suspension systems, details for the Dowty servovalve and report on the initial servovalve validation tests. An description of the extended instrumentation and control system elements that were required in comparison to passive suspension concludes the sub-sections.

2.4.1 Lotus active actuator

Fig. 2.7 shows the Lotus actuator used to convert hydraulically derived forces into controlled relative displacements. The actuator connection points are at the centre of the wheel hub and at the car body pivot. The latter is via an in-line load cell, which is highlighted in Fig. 2.7.

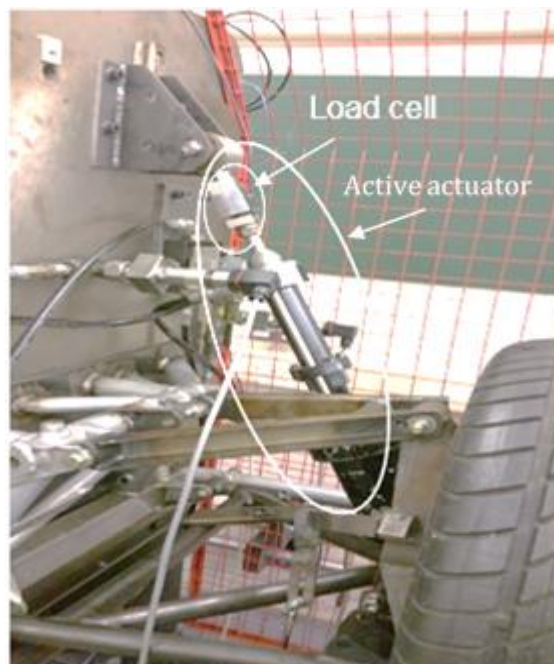


Fig. 2.7. Lotus active actuator.

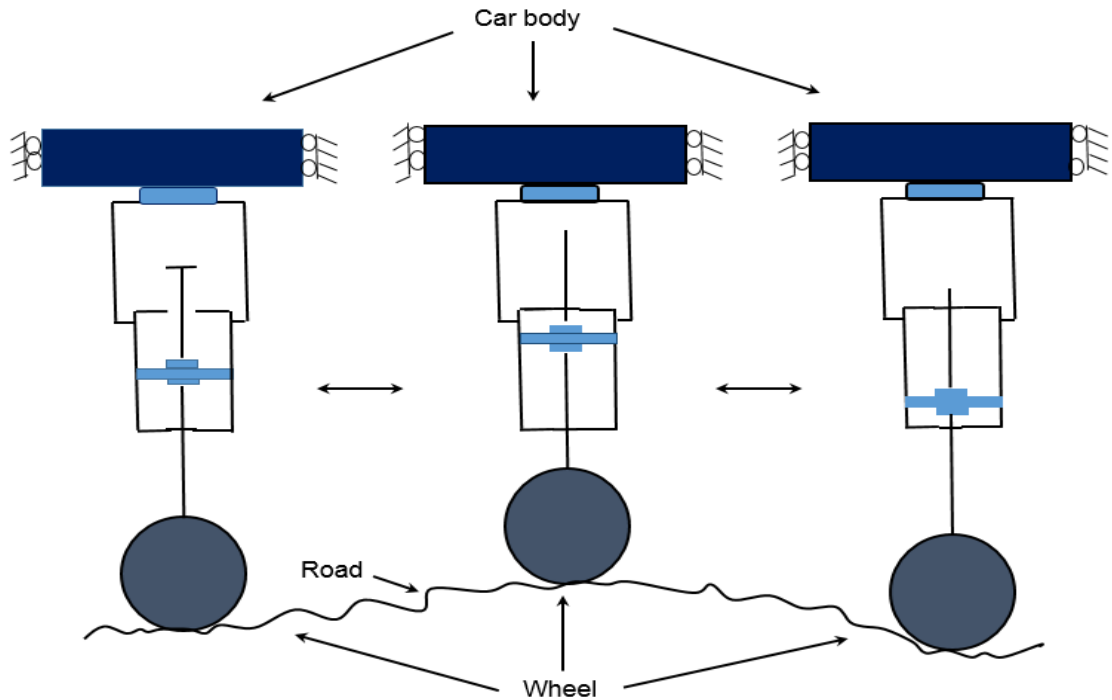


Fig. 2.8. Physical movements of active actuator.

The physical actuator movements and the overall principle of active suspension system are summarised in Fig. 2.8. It can be seen that the controlled movement of the actuator rod within the actuator casing, if applied in the correct manner, will reduce the amount of vertical body displacement as the road input changes in a generalised time-varying pattern. This principle is shown for the double-rod type actuator, which used a built in LVDT. This configuration is transferrable to other actuators. A single-rod type actuator could be used, offering a more compact option at lower cost and greater reliability. The internal LVDT provides an actuator displacement signal for use as a feedback signal in the deployed active suspension control systems.

According to the previous literature, Electro-Hydraulic Actuators (EHA) are highly nonlinear systems with uncertain dynamics in which the mathematical representation of the system cannot sufficiently represent the practical system (Wang et al. 2009), as investigated in the next chapter. The actuator plays a vital role in manoeuvring industrial processes and manufacturing lines. An EHA can be used with either a proportional valve or a servovalve, like that employed in this study. A servovalve converts an electrical signal to hydraulic power (Zulfatman and Rahmat 2009). There are different types of electro-hydraulic valve actuators, which move rotating movement valves; for example, ball, fitting and butterfly

valves through a quarter-turn or more, from open to closed. There are additional valve actuators, which travel straight, valves such as a gate, globe, diaphragm, and squeeze valves operated by sliding a stem that controls the component. For the most part, valve actuators are added to throttling valves which can be moved to any position as a significant aspect of a control loop (Rahmat et al. 2010).

Relevant specifications for EHA include actuation time, hydraulic fluid supply pressure range and acting type. Other features of these actuators that should be identified before use include over-torque protection, local position indication and integral push buttons and controls. The application of EHA's is critical in the field of robotics, suspension systems, and industrial processes as they can provide precise movement, high power capability, fast response characteristics and excellent positioning capability.

2.4.2 Servovalve

In electrohydraulic systems, a control valve, either a proportional valve or servovalve, is required to regulate the hydraulic flow rate variably controlled via an electrical input signal. The original prototype Lotus active suspension was fitted with a Dowty servovalve (type 4551, 38 l/min) (Wright and Williams 1984). This arrangement was used as the standard for selection of the Dowty servovalve (type 4551, 19 l/min, 40 mA rating) (Dowty 2000) used in this study, as shown in Fig. 2.9.



Fig. 2.9. Photograph of the active Moog servovalve.

Even though the maximum flow rate of the servovalves used in this study is different to that used by Wright and Williams (1984), is sufficient to provide the required maximum flow rate of 19 l/min. The hydraulic connections between the servovalve and actuator are shown in Fig. 2.10.

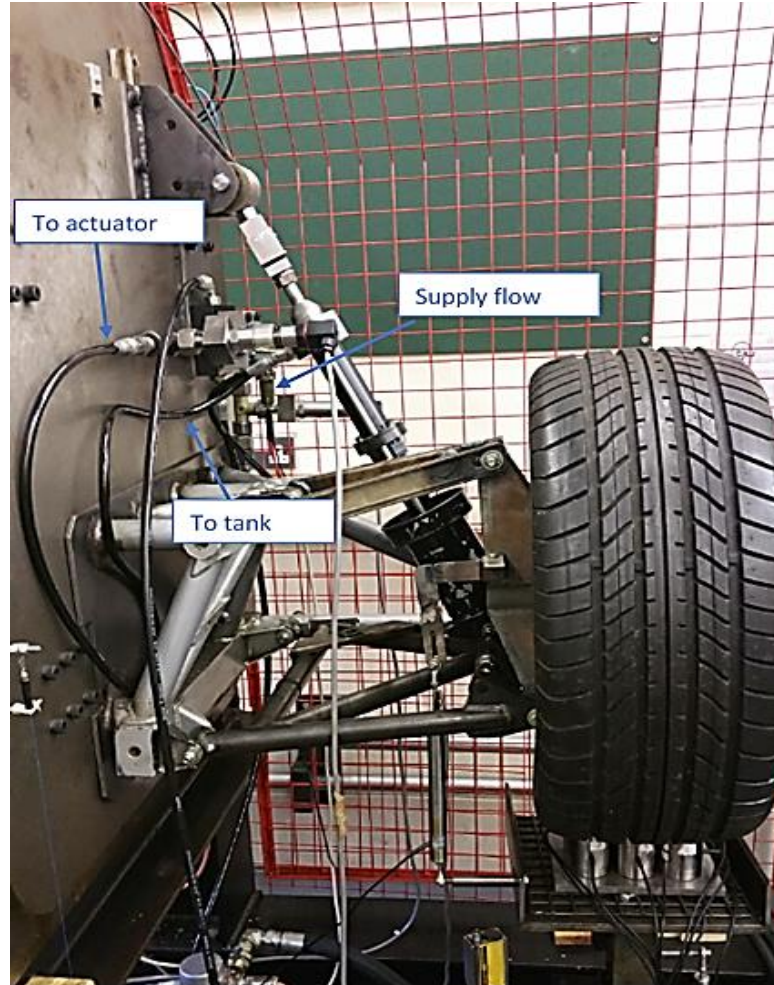


Fig. 2.10. Photograph of the hydraulic connection.

In general, the frequency response of a servovalve is measured from a transfer function relating flow rate output to applied current input. More specifically, the frequency range in which amplitudes are between 0 dB and -3 dB (the cut-off frequency) is called system bandwidth. A 45 Hz bandwidth is stated for the servovalve. This also infers how fast the flow rate output responds to a step input as it is inversely proportional to bandwidth. The servovalve specification (at $\mp 100\%$ current and 210-bar supply pressure) accordingly indicates that the valve can generate a flow step response with a 3.5 ms rise time. The flow gain of a servovalve depends upon the maximum flow rate, rated current or voltage, and the type of electrical connection (series or parallel). If a series

type is chosen, the measured voltage will be half that of the differential rate voltage. However, if a parallel is chosen, the rated voltage will be equal to the differential rated voltage. The parallel type was selected for this work as it provides the maximum flow rate. In addition, the parallel type has the advantage that if one coil fails, the second can continue to operate.

As previously mentioned, this study used a parallel electrical connection. The control signal sent from the data I/O within the PC to the servovalve was passed through an amplifier, a Moog buffer amplifier (G123-825). The block wiring diagram for the active servovalve is shown in **APPENDIX D**.

The legacy elements of the test rig were re-commissioned and the operational characteristics of the servovalve were experimentally validated by conducting the following two tests.

2.4.2.1 Pressure and flow rate sensor tests

In order to check the servovalve validation, pressure and flow rate sensors were incorporated into a specific, purpose-built test rig, as shown in Fig. 2.11. This test rig consisted of pressure and flow rate sensors mounted onto manifolds either side of the servovalve. The primary supply flow was adjusted to generate load pressures which were then measured with both a pressure gauge and a pressure sensor.

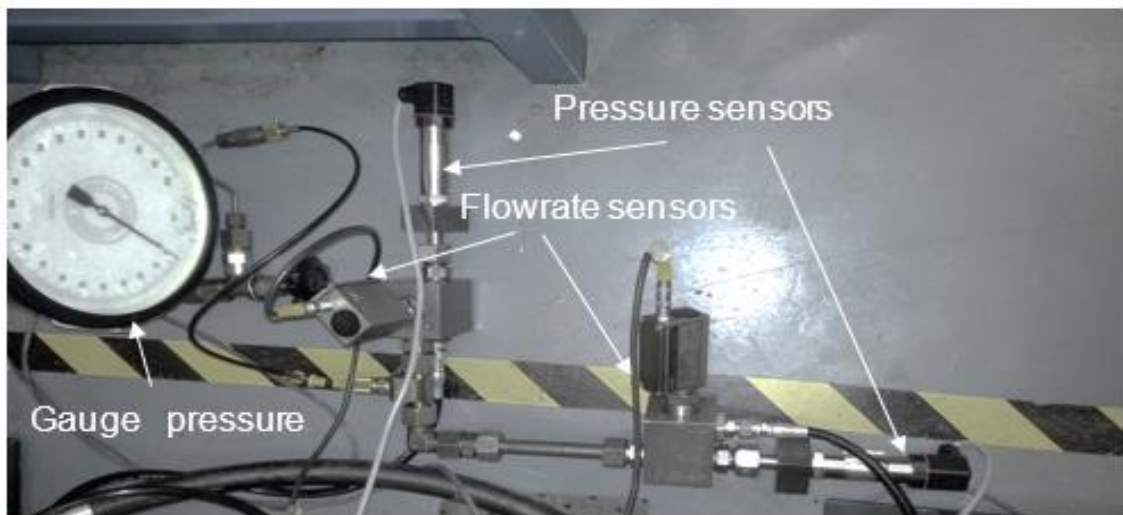


Fig. 2.11. Pressure and flow rate sensors test.

2.4.2.2 Servovalve test

As previously mentioned, the servovalve is a fundamental element of the active suspension system controller. Therefore, it is imperative that the servovalve be assessed separately from the primary test rig using a similar purpose-built test rig to that used for the testing of the pressure and flow rate sensors, as described in Section 2.4.2.1. The servovalve consists of two pressure and two flowrate sensors on both sides, as well as a restructure, which is connected to a computer through a data acquisition to supply the voltage and monitor the measured pressure and flowrate. It is essential to show the characteristics of the servovalve by defining the relationship between the top (P_{2a}) and bottom (P_{1a}) pressures as a function of the applied voltage, as shown in Fig.2.12. It became apparent that the intersection between both pressure sides (pressure load) was shifted from an original point; this is regarding to an offset issue, as shown in Fig. 2.12.

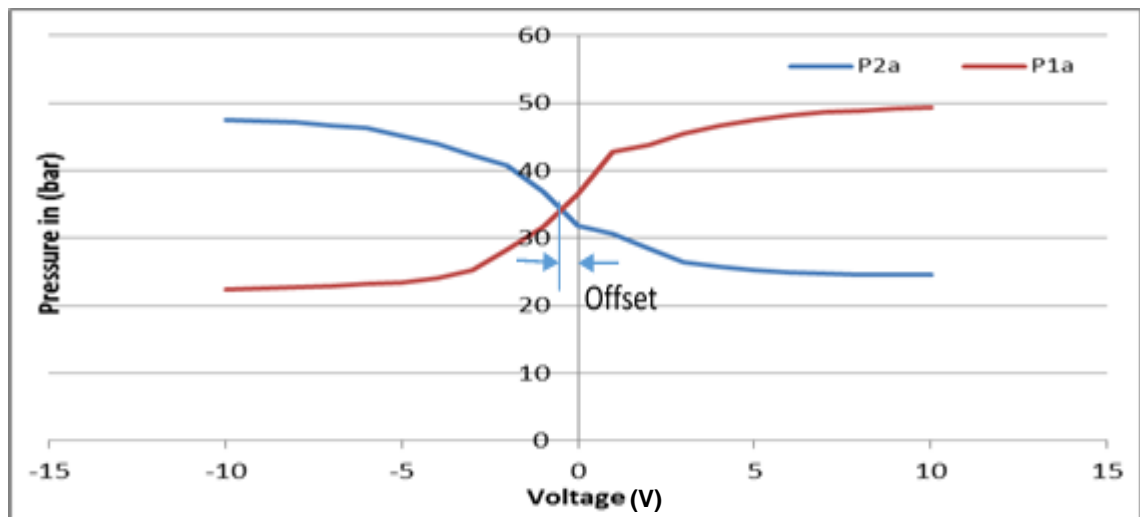


Fig. 2.12. Servovalve pressures on both sides as a function of applied voltage.

Fig. 2.13 shows the relationship between the flow rates for both sides, according to the applied voltage. Although the overall behaviour of both flow rates is close to an S-shape and is quite similar to the ideal characteristics of the servovalve given by the data sheet, by indicating the offset servovalve problem, it is clearly observed that here is a shift from zero position.

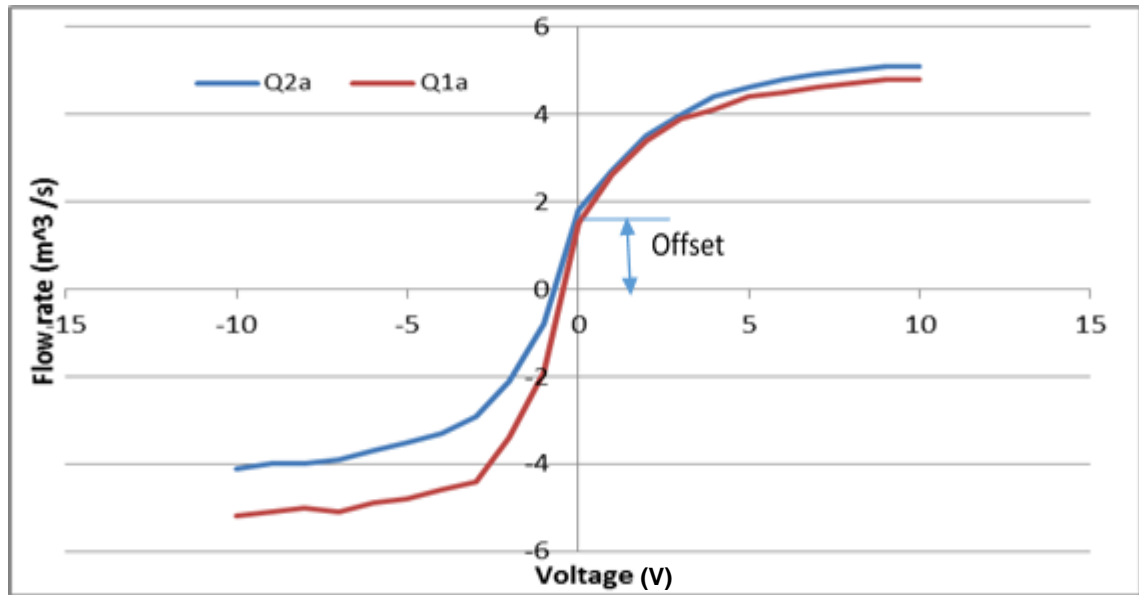


Fig. 2.13. Servo valve flow rates on both sides as a function of applied voltage.

Even though there is a slight deviation in the behaviour of the servovalve, the servovalve can still be used in this study with some manipulation. It is likely that this minor fault is due to the spool crawling position which was established to generate oil leakage due to the degradation of the servovalve's characteristics.

2.4.3 Instrumentation and control system

Further to that as previously shown in Fig. 2.2, Fig. 2.14 shows a schematic of the control system including the five system state feedback signals. The use of these states in active control design is explained further in **Chapters 5** and **6**. The states are as follows:

- Load cells to measure the force transfer from actuator to car body.
- Velocity transducers to measure the car body velocity.
- Velocity sensors to measure the wheel hub velocity.
- LVDT to measure the suspension movement, or relative displacement between the car body and the wheel hub.
- LVTD to measure the tyre deflection, or relative displacement between the wheel hub and the road.

Following the signal conditioning processes, the five states feedback measured signals which are fed into an Analogue to Digital converter (A/D) for

collection by a PC's data acquisition card. C++ was then used with a dedicated DAP card programme to calculate and generate the control output in real-time. The control output was then fed to a Digital to Analogue converter (D/A) within same data acquisition card and amplified to the conditional electrical current or voltage, used to drive the servovalve. The feedback gains, which were obtained by applying PA and LQ, govern the control output as displayed by the control algorithm in **Chapters 5 and 6**.

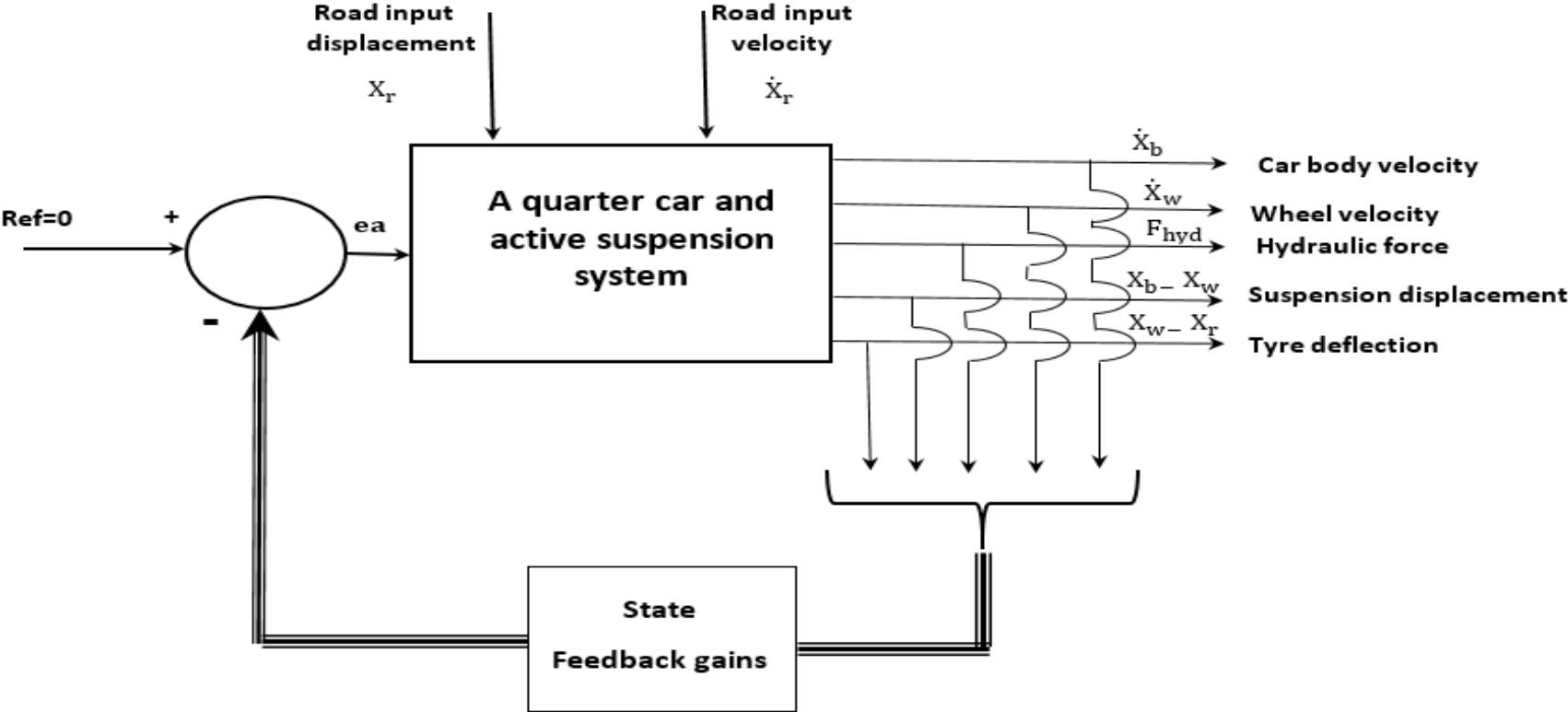


Fig. 2.14. Schematic diagram of the active suspension control system.

2.5 Instrumentation

Having introduced the specific aspects relating to the road simulator and the passive and active suspension systems, the overall instrumentation elements of the test rig can now be discussed.

2.5.1 Linear Variable Differential Transformers (LVDTs)

For direct measurement of displacement from a few micro-millimetres to several meters, an LVDT is ordinarily used as a position sensor. The fundamental design of an LVDT comprises a primary coil winding and two identical secondary windings on a common pulley with, a movable magnetic core, or a push rod. The primary coil winding is excited with a low voltage AC supply, whereas the two secondary windings are connected so that their combined output represents the difference in electrical voltage induced into them. With the rod in a central position, the output is zero. The movement of the rod from this central position produces output, which varies in magnitude and phase according to rod displacement. All the LVDTs used in this work, with the exception of the Lotus actuator integral LVDT, were supplied by RDP Electronics Limited (LVDT 1994). Three LVDTs are used to measure:

- Suspension displacement, existing inside the active actuator.
- Displacement of the road simulator actuator, as shown in Fig. 2.6.
- Tyre deflection, as shown in Fig. 2.15.



Fig. 2.15. The LVDT used for the measurement of tyre deflection.

It should be noted that the displacement of the car body and road simulator were not used for the control of the active suspension system. The LVDT used to measure suspension displacement is a built-in LVDT installed inside the Lotus actuator. The displacement of the car body was used for the validation of the mathematical model, which as described in **Chapters 3** and **5**, also helped to discover and validate the friction force. While it would have been very easy to include the displacement of the road simulator in the simulation of the test rig, which is correctly used as feedback for the road simulator controller, at present, use in the real world would be impossible to measure. That said, researchers have recently included sensors within tyres and wheels which could be helpful in measuring the road variation input (Wang and Winner 2015).

The LVDTs were calibrated to check their gain values and linearity. The calibration test results were obtained from several tests of each LVDT. The gain values of the suspension, road simulator and tyre deflection LVDTs were found to be 25.386 m-code/mm, 167 m-code/mm and 88.775 m-code/mm, respectively.

Voltage outputs from the signal conditioning units were adjusted to within a range of ± 5 V, equal to the range of the A/D within the data acquisition card. Adjustment of the voltage outputs required an understanding of tuning offsets and gains in the signal-conditioning unit (Technical 1994). The output was optimised

in order to utilise the full range of the A/D. Thus, reducing the quantization effect that occurs in the digitising process (Franklin and Powel 1981). It is well-known that a digital signal is composed of a finite number of bits, or binary digits. Thus, in using an A/D, the digital signal is truncated to a fixed length where its accuracy is dependent upon how many binary digits are used to convert the analogue signal.

From the specification of the data acquisition card the A/D used in this study is 12-bit processing (equivalent to= 4096 binary digits) and based on a ± 5 V working range. Using the following two system example:

System 1: If an LVDT and a signal conditioning unit are set to ± 1 V / ± 100 mm it follows that 819 binary digits would be used, and the accuracy would be = 0.120 mm/digit.

System 2: If an LVDT and a signal conditioning unit are set to ± 5 V / ± 100 mm it follows that 4096 binary digits would be used, and the accuracy would be 0.024 mm/digit.

It is therefore apparent that the efficiency of **System 2**, which utilises the full working range of the A/D, is five times more accurate than **System 1**.

2.5.2 Load cell

A load cell transducer relies upon strain gauges, which are manufactured from metal foil or semiconductor materials (Bolton 2003), to measure forces. Any applied force causes the load cell to stretch or compress, i.e. a strain is invoked within the strain gauges, which is proportional to the force within the load cell structure and results in a change in electrical resistance. Strain gauges experience a fractional change in resistance under strain, which cannot easily be measured directly. Therefore, the strain gauges used in load cell, are typically configured in a Wheatstone bridge circuit. This circuit can be used to convert the resistance change to a voltage change which is much easier to measure. The two types of load cells used in this study for different purposes are detailed in this section.

2.5.2.1 Load cell for active actuator force

The U4000 load cell (Loadcell 2000) supplied by Maywood Instruments Limited was used to measure the force transferred from the active hydraulic actuator to

the car body (hydraulic force), as shown in Fig. 2.16. Input and output signals from the load cell are conditioned via a D2000 signal conditioning unit (D2000 2000). The maximum applied load to the load cell is 1500 kgf. The analogue output from the conditioning unit was set, at ± 2 V by the supplier.

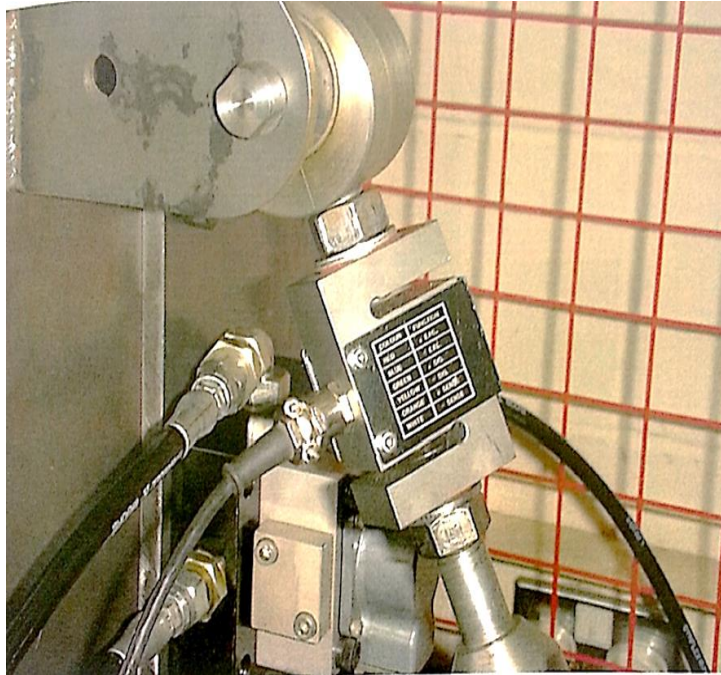


Fig. 2.16. Load cell [measuring hydraulic force].

2.5.2.2 Load cell for CPL

Further facility was added to the test rig enabling CPL to be measured. This was achieved by designing and manufacturing, a multi-cell load cell wall using nine F218z load cells, each with a maximum load limit of 30 KN, which were made by Novatech, as shown in Fig. 2.17. The load cells were fixed to the base of the test rig using bolts beneath the tyre, as was shown in Fig. 2.4. Data acquisition was achieved using a NI 9237 bridge module with a NI 9172 compact DAQ chassis, which, can sample all nine-load cells at once.

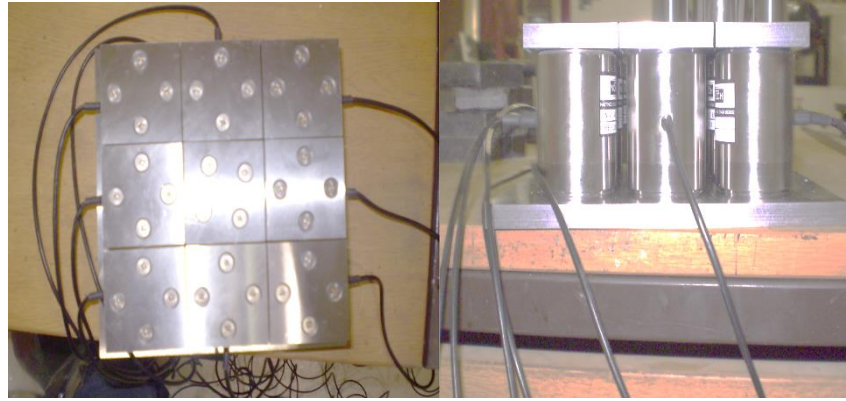


Fig. 2.17. Load cells [measuring CPL] from left to right: top and side view.

The NI 9237 bridge module can take 50000 samples per second. There are four inputs to the bridge module using RJ50 female terminals. There are currently three bridge modules available at Cardiff University meaning there are twelve inputs for all 9-load cells to be used together. The bridge module can also provide the excitation voltage to the load cells. LabVIEW is the recommended software for use with this data acquisition equipment, as shown by Fig. 2.18.



Fig. 2.18. Measured CPL through the LabVIEW program.

National Instruments recommend that the NI 9237 goes with the NI 9172 compact DAQ chassis. The NI cDAQ 9172 can receive data from up to eight I/O

modules at once, thus, it will quickly take the three bridge modules. The output from the chassis is a USB cable, which can plug directly into any computer.

These load cells were calibrated using a compression/tension universal test machine (Avery Denison, with a maximum load of 600 kN) in Cardiff University's Light Structures Test laboratory. For the purpose of calibration, a variety of weights, [5, 10, 15, 20 and 25 kN] were used. The maximum load for each load cell is 30 kN, as shown by Fig. 2.19. All load cell calibration results are similar to the calibration curve results shown in Fig. 2.20 for one load cell.



Fig 2.19. Test rig used for the calibration of the load cells.

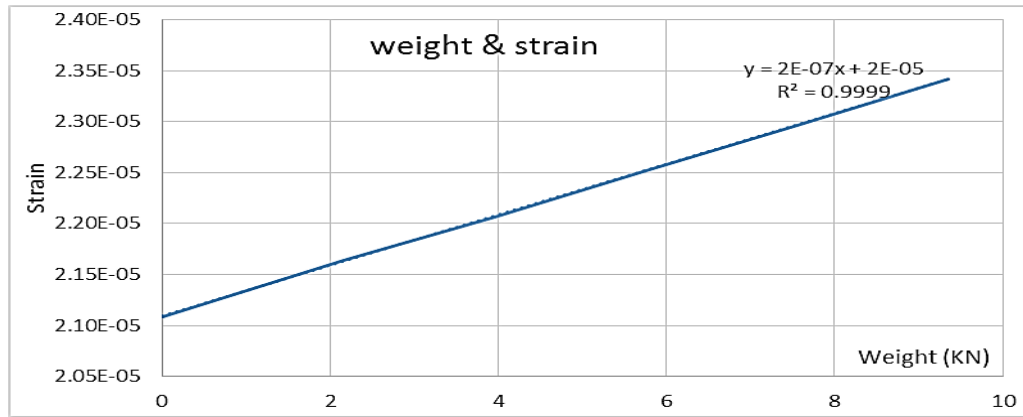


Fig. 2. 20 Calibration curve of one load cell used for the measurement of CPL.

2.5.3 Velocity sensors

For the purpose of the modelling undertaken in this study, it is considered that using a velocity sensor to directly obtain a velocity signal is no different to using a high-quality accelerometer. Equally, in using a velocity sensor, difficulties caused by the filtering and integration of the real-time signal can be reduced.

Two cable actuated sensors (type WGS2) supplied by ASM were used. Fig. 2.21 shows a cross-sectional view of the sensor. A cable-actuated sensor is an electromechanical device that translates linear motion into a proportional electrical voltage. The sensor can be used to measure both velocity and displacement. This type of sensor consists of a measuring cable, a machined cable drum, a shaft, a coil spring, and an electronic circuit board. The cable winds onto the drum mounted on the shaft, which is tensioned by the spring. The spring provides a constant pull-in force to control the cable and maintain the cable's tension.

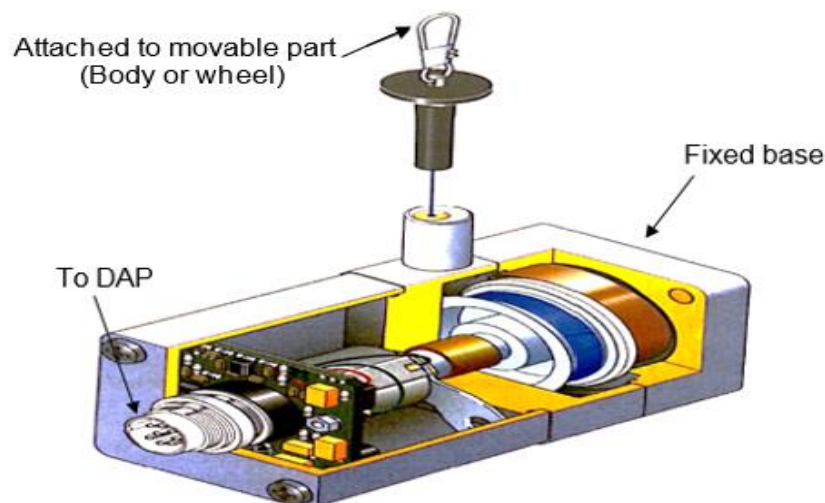


Fig. 2.21. Cross-sectional view of the cable actuated sensor (velocity and displacement sensor) (Surawattanawan 2000).

The free ends of the cable were attached to the moving parts being measured, the car body and the wheel hub, as shown in Figs. 2.22 and 2.23. The sensor converts the linear cable movement into rotary motion and then to electrical output voltage as it winds on and off the drum. As already mentioned, the sensor can be used to measure both velocity and displacement simultaneously. The electrical circuits of both signals are entirely separate. The measurement of velocity is a self-generating process and does not require any power supply, whereas the measurement of displacement requires a power supply (+18 to +27 VDC and 20 mA maximum current). Following trial runs, as previously used, it was found that the velocity signals obtained from both sensors were satisfactory.

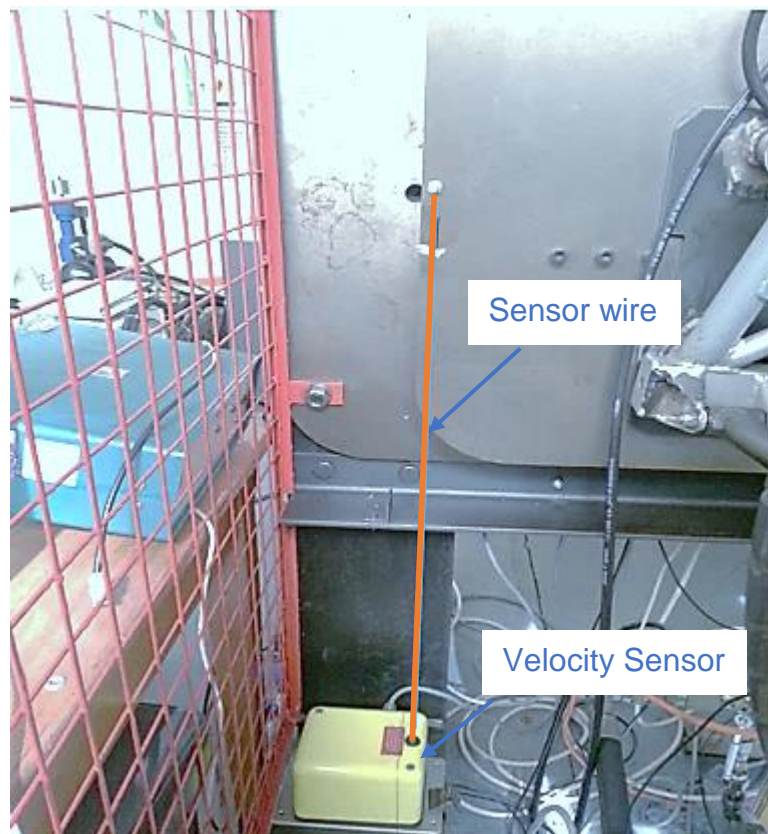


Fig. 2.22. Photograph of the installation of the velocity sensor for the measurement of car body velocity and displacement.

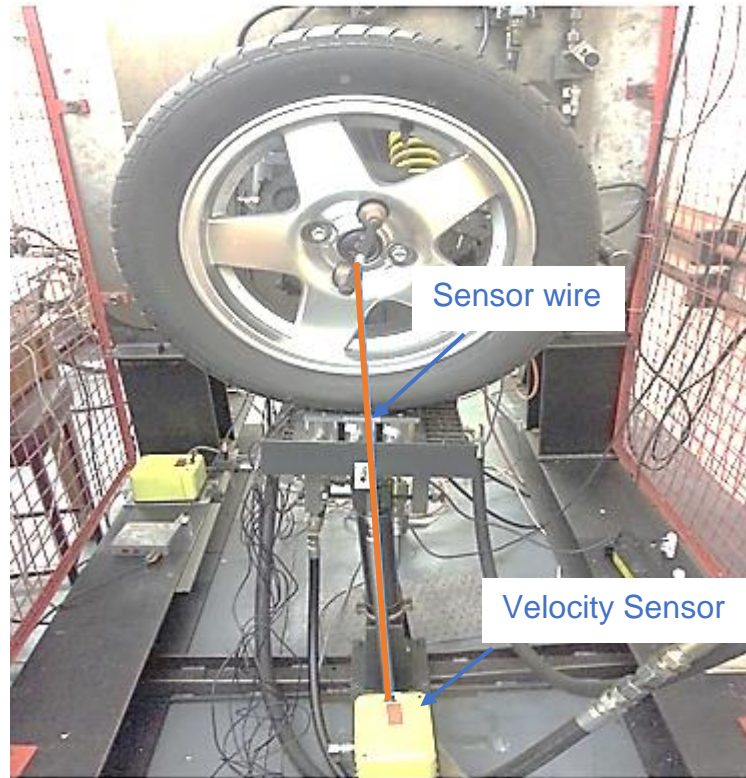


Fig. 2.23. Photograph of the installation of the velocity sensor for the measurement of wheel hub velocity and displacement.

Fig. 2.24 shows the calibration graph for the body velocity sensor, while Fig. 2.25 shows the calibration graph for the wheel velocity sensor. It is clearly shown in Figs. 2.24 and 2.25 that the relationship between voltage output with either body or wheel velocity is linear. Thus, the sensors are sensitive to both velocities and the reading reliable.

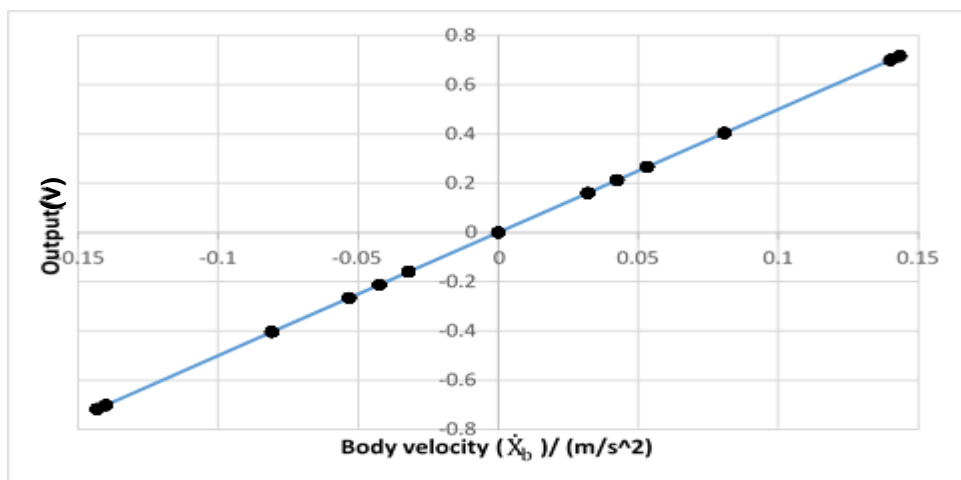


Fig. 2.24. Calibration graph for the body velocity sensor.

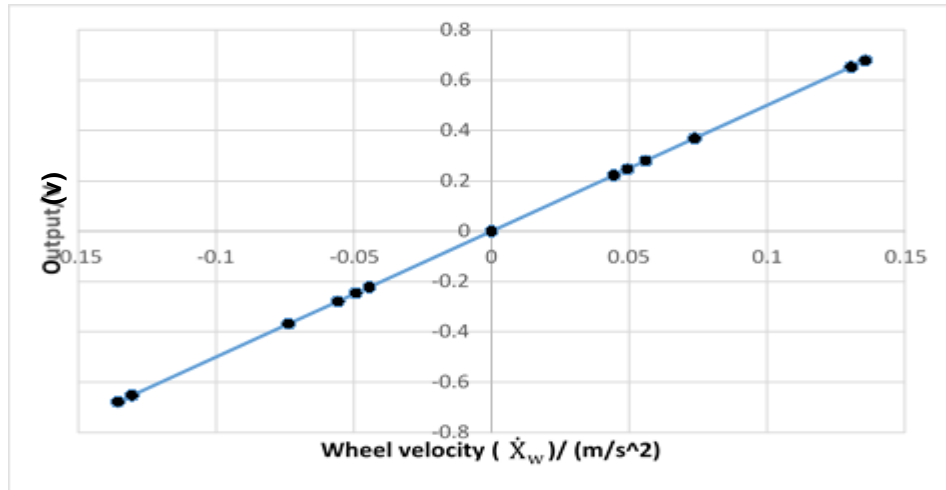


Fig. 2.25. Calibration graph for the wheel velocity sensor.

The WGS2 sensors gave dual displacement and velocity signals and, as stated, were applied to both body and wheel motions. **Chapter 3** presents a comparison between experimental and simulation results. The results show good agreement with the displacement values and are aligned with the calibration results reported here. However, it was subsequently discovered that for the velocity values a different conversion factor had been used. This conversion factor was obtained from the manufacturer's data sheet, as provided in **APPENDIX D**. A scaling factor of 2 results from a 'T5' values of 5 V/m/s being used opposed to a 'TA' values of 10 V/m/s being used. These sensors were legacy elements and information about the specific model numbers and wiring were not available. This anomaly is further discussed in **Chapter 3** when comparing the obtained velocity profiles and validating the simulation. The simulation information allowed derivatives to be taken giving the correct displacement information to pinpoint the conversion factor anomaly.

2.5.4 CANAL data acquisition system

The data acquisition system previously used by Surawattanawan (2000) with the test rig also used in this study, is the CANA system supplied by Thoroughbred Digital Systems Limited. CANAL is a high-speed data acquisition system with four parallel input channels, Fig. 2.26 shows the terminal box and connection used for both the previous and current studies. The CANAL system consists of both

analogue and digital processing cards installed in a PC. In the previous work, the CANAL system was mainly used for data acquisition in a transient mode.

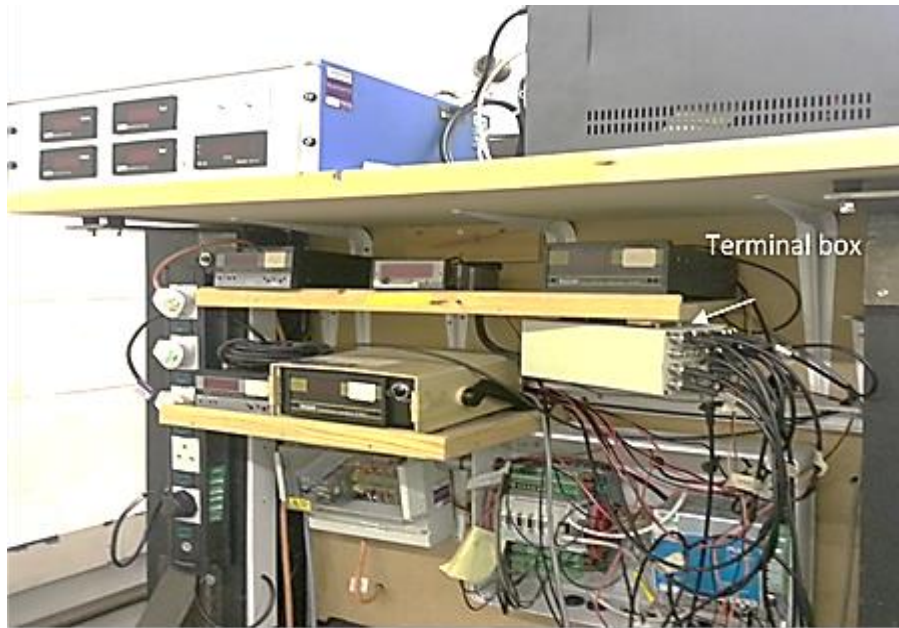


Fig. 2.26. Terminal box of the CANAL data acquisition system.

CANAL's interface software was used to set up the hardware configuration, such as the sampling rate and the duration of the transient capture. The graphic user interface allowed the measured signals to be verified before being saved in ASCII format for further processing. The sampling rate can be automatically varied from 500 Hz to 32 kHz using analogue anti-aliasing filters of the input signals. A sampling frequency of 500 Hz was used in both the previous work by Surawattanawan (2000) and the current study, which is sufficient for the system dynamics. A trigger mechanism was used for the capture of transient data, allowing the user to precisely specify the starting point and delay time for data capture. The trigger mechanism was set based on the level and slope of the input signals. Using such a mechanism helped in drawing comparisons between each set of experimental and simulation data.

2.6 Moog Programmable Servo Controller (PSC)

The PSC, supplied by Moog Controls Limited, as shown in Fig. 2.27, was used by Surawattanawan (2000) and is a real-time digital controller containing an inbuilt microprocessor (M2000). The PSC has six 12-bit analogue input (A/D) channels and two 12-bit analogue output (D/A) channels. The number of bits

represents the resolution of the A/D or D/A and effects the signal quantization and the resolution of the digital signals. Therefore, the working ranges of the interface analogue signals from the transducers and servovalve, should employ the full working range of the input/output channels of the PSC in order to minimise the quantization effect. The output channels may be configured to operate in either current or voltage mode depending on the hardware setting.



Fig. 2.27. Moog Programmable Servo Controller (PSC).

The PSC connects to a supervisory PC via an RS232 serial link. The serial connection gives access to low-level parameter commands of the PSC through a software interface. The PSC can work standalone without any supervisory PC following a programme transfer due to its built-in microprocessor. A sampling rate of 500 Hz was used as it was sufficient to encompass the significant dynamics of both the hydraulic and active suspension systems. Two PSCs were used in the previous work by Surawattanawan (2000); one to control the active suspension, and the other to monitor the road simulator.

In the current research, some modification was necessary to upgrade the data acquisition system. The previous CANAL system and its PSC hardware were replaced with a new Data Acquisition Process (DAP). Significant advantage was gained by removing the PSC hardware as the new DAP allows improved control system design options and the direct implementation of digital control algorithms. Table I provides a more detailed comparison before and after the new DAP hardware installed.

Table I: A comparison between the advantages and disadvantages of using PSC versus DAP hardware.

<u>PSC</u>	<u>DAP</u>
The PSC is a real-time digital controller. It has an A/D and a D/A converter. It can work standalone without any supervisory PC.	There is scope to design the digital control using the DAP card more flexibly. It is easy to convert the A/D using the card itself.
It needs several hardware accessories, such as analogue low pass Butterworth filter and an Engineering Use Interface (EUI).	It does not require any accessories.
Time delay and amplitude reduction of the output are a critical problem.	The delay time within the time interval is negligible.
Works with separate data acquisition, including a data logger, with a limited number of samples.	Uses the PC data acquisition card to design a controller without needing data logger.
Significant interface issues.	Reduced interface issues.
Using function blocks, such as analogue input and output, summing junction, PID filter, wave generator, data logger, flag generator, handler, and a limiter.	No need to use function blocks.
Energy loses.	Reduced energy loses.
High-cost.	Relatively low cost.

2.7 Data Acquisition Processor (DAP)

The Data Acquisition Processor (DAP) used in this study is from Microstar Laboratories and is a complete data acquisition system that occupies one expansion slot of a PC as shown by Fig. 2.28. To set up an application, the DAP requires a series of commands. Typical commands set DAP options, define variables and define start stop procedures. Commands can be entered interactively from the keyboard using DAPview for Windows or can be sent to the

DAP from a program running on the host PC. A text file of DAP commands is a file that can be created using the integrated editor in DAPview plus or using any text editor on the host PC. Sample command files are also provided on the DAP diskette. Both the DAP and DAPview have help and error messaging facilities.



Fig. 2.28. Data Acquisition Processor (DAP) card.

A network interface card is a circuit board, or card, that is installed into a computer's motherboard to connect it to a network and provides Digital to Analog (D/A) or Analog to Digital (D/A) conversions allowing data to be sent to the computer's display. The DAP connects to a supervisory PC's network interface card via a serial link. A sampling rate of 500 Hz was used because it is sufficient to encompass the significant dynamics of the hydraulic and active suspension systems. The DAP has six 12-bit analogue input A/D channels and two 12-bit analogue output D/A channels. The number of bits represents the resolution of the A/D or D/A and effects the signal quantization and the resolution of the digital signals. The output channels may be configured to operate in either current or voltage mode depending on the hardware setting. For this study, the configuration was voltage mode. Two PCs were used in this work, one to control the active suspension and road simulator, the other to display the LabVIEW program to show the CPL results. The arrangement of the two PCs is shown in Fig. 2.29.

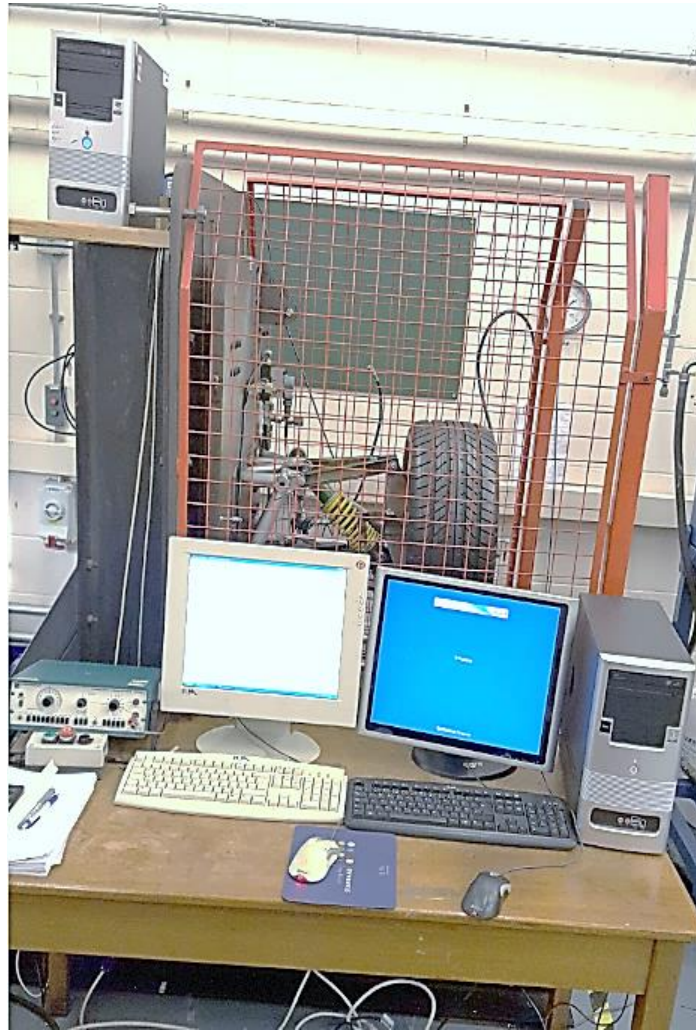


Fig. 2.29. System supervisory PC (left) and CPL LabVIEW display PC (right).

2.7.1 Hardware organization

Fig. 2.30 shows the hardware organisation of the DAP. The DAP is a complete microcomputer with the following features: it has a microprocessor, random access memory (RAM) and read-only memory (ROM), analog and digital inputs, analog and digital outputs, input/output control and timing circuits, timers, and direct memory access controllers (DMA), or first-in-first-out buffers (FIFO), for high-speed data transfer. Some DAP models also have a digital signal processor with static RAM, and other models also have a serial interface. The DAP is connected to the PC through special FIFO interface hardware.

The DAP provides analogue and digital expansion signals for external multiplexing of analogue and digital inputs. The DAP accepts up to 512 analogue inputs and up to 128 digital inputs using external multiplexers (Microstar 1998).

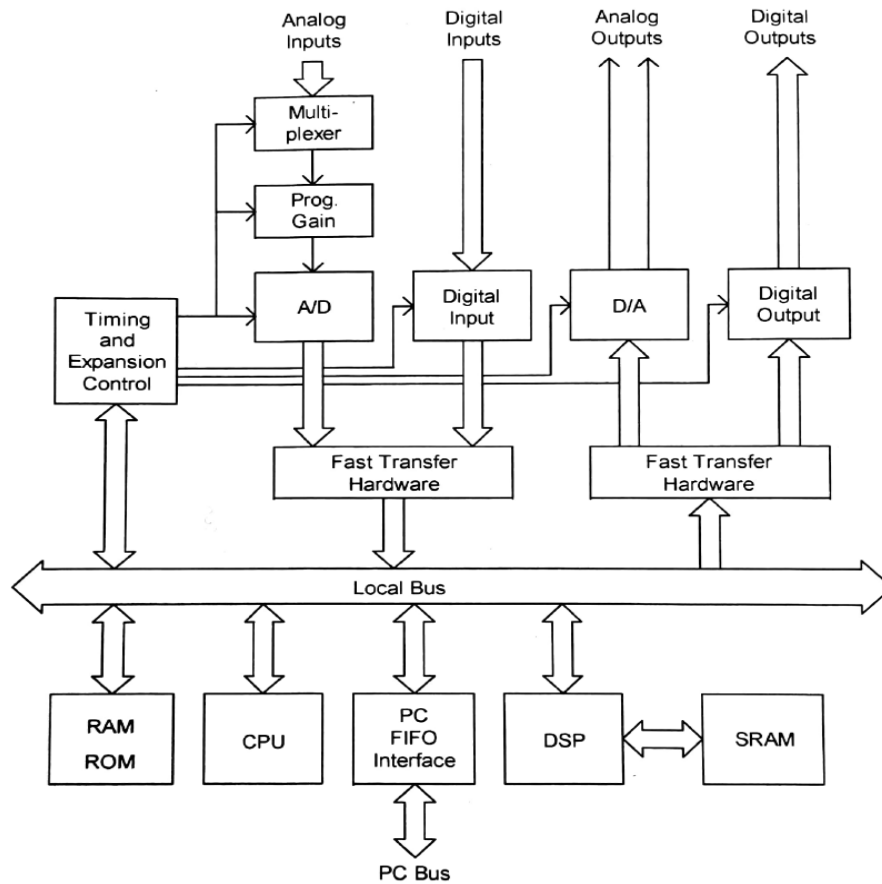


Fig. 2.30. Hardware organisations.

2.7.2 Software Organization

A procedure is a group of commands that together perform some function. A DAP manual operating system (DPAL) allows the user to define input, processing and output procedures for a DAP. Processing procedures are made up of task commands which can be executed concurrently when a procedure is active. A task command can be used several times over to define distinct functions within a procedure definition. A processing procedure, for example, might contain several task commands for the calculation of an average which, the DAP executes concurrently on different input channel pipes.

It is easy to create a DAPL application, simply:

- Name all constants, variables, pipes and triggers
- Define one or more procedures
- Start one or more processes.

Fig 2.31 shows the software organisation of a typical application.

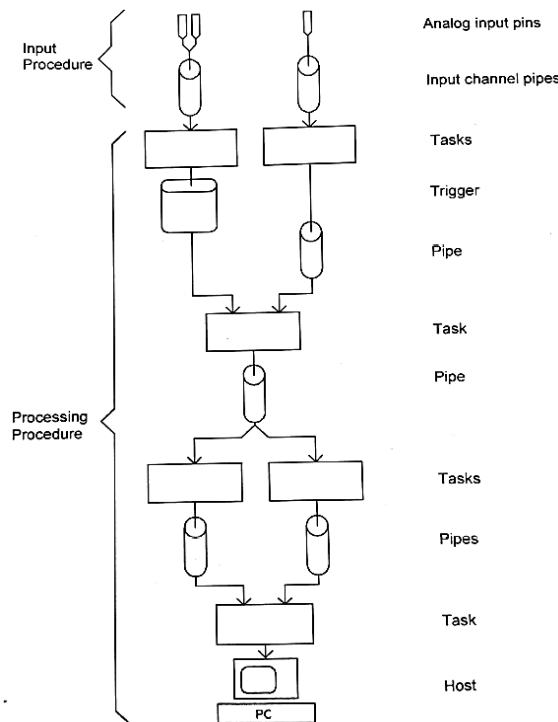


Fig. 2.31. Software organisations.

2.7.3 Applications overview

A brief outline of the applications follows (Microstar 1998):

Input:

There were three input applications: sampling three inputs, sampling 5000 values and digital input.

Basic Real-time Processing:

There were six applications for the necessary real-time processing: averaging, peak detection, real-time data analysis, DAPL expressions, extracting a bit from a digital input and finding histograms.

Output:

There were eight output applications: asynchronous output, synchronous output, generating waveforms, generating arbitrary periodic waveforms, generating arbitrary periodic waveforms by copying, generating arbitrary periodic waveforms by interpolation, generating one-shot pulses and using analogue output expansion.

Soft Triggers:

There were ten applications for soft triggers: soft triggers, peak detection using the PEAK command, implementing a digital oscilloscope, using hysteresis, triggering on two conditions, retriggering, spike detection, time stamping pulses, detecting bit transitions and using triggers to calculate the frequency.

Further Real-time Processing:

There were nine applications for further real-time processing: finding deviations between inputs, thermocouple linearisation, interpolation, autoranging, identifying maxima and minima, almost simultaneous sampling, mixing fast inputs and slow inputs, multiple rate data transfer and observing the timing of rotating machinery.

Digital Signal Processing:

There were three applications for digital signal processing: digital filtering, spectral analysis and calculating transfer functions.

Process Control:

There were three applications for process control: alarms, PID control and pulse width modulation.

Communications:

There were six applications for communications: test communication, text communication from several tasks, simultaneous transfer of text data and binary data; sending data to DAP, synchronising several DAP and serial interface.

2.7.4 DAPview for Windows

DAPview for Windows provides a robust environment for creating DAP applications for Windows. DAPL command files that configure a DAP can be developed and quickly tested using this interactive environment. Any acquired data can be displayed in an attractive format with graph, table, indicator, and digital panel meter windows (Microstar 1995).

DAPview takes advantage of the onboard intelligence of the DAP for real-time processing, freeing the PC to display data and multitask with other applications.

2.7.4.1 Hardware and Software Requirements

To use DAPview, the target computer must meet the following minimum requirements (Microstar 1995):

- PC Hardware Requirements:
 - A 386 PC with a 1.2-MB or 1.44 MB floppy drive
 - A hard drive or a network drive with 3 MB of free space
 - 4 MB of RAM
 - A monitor with VGA resolution
 - Mouse device recommended
- PC Software Requirements:
 - Microsoft Windows version 3.1 running in enhanced mode
 - DOS 3.3 or newer
- Data Acquisition Processor and Software Requirements:
 - DAPL 3.0 or newer (DAPL 4.0 is recommended)

2.7.5 Developer's Toolkit for DAPL

The Developer's Toolkit for DAPL contains the software tools required for creating custom commands for Microstar Laboratories Data Acquisition Processors. Custom commands are user-defined processing task commands that extend the DAPL or DAPL 2000 operating system. Most applications only require the data processing functions, which are available as predefined DAPL commands, so the Developer's Toolkit for DAPL is primarily designed for advanced users (Microstar 1997).

Custom commands are written in C, compiled and stored on the host PC, and downloaded from the PC to a DAP. Once custom commands are downloaded, they are used in DAPL processing procedures in the same manner as predefined DAPL commands.

Pipes provide the connections for data to move between tasks. The pipes specified in a custom command parameter list can be communication pipes, input

channel pipes, user-defined pipes, or other piped of other types. It makes no difference within the custom command as all pipes are treated uniformly.

2.7.5.1 Compatibility

The Developer's Toolkit for DAPL supports DAPL versions 4.0 and above and DAPL 2000 versions 1.0 and above. Some DAPL features supported by the Developer's Toolkit for DAPL are not available in DAPL versions prior to version 4.3. The waveform, Fast Fourier Transform (FFT) and FIR filter functions are only available in DAPL 2000. For all supported compiler versions, the custom commands are compiled as DOS applications written in C.

The Developer's Toolkit for DAPL supports the following compilers:

- Microsoft C compiler version 6
- Microsoft C/C++ compiler version 7
- Microsoft Visual C++ version 1.0 and 1.5 Professional Edition
- Borland C++ compiler versions 4.0 and 4.5

The Developer's Toolkit for DAPL supplies two versions of its runtime library. The SMALL library supports all Data Acquisition Processors, DAPL and supported compiler types. This library provides no floating-point features but generates the smallest and most efficient code modules. The FP library uses more code and system memory space, but provides access to the floating point emulator and other hardware services integrated into the DAPL operating system (Microstar 1997).

2.8 Discussion

The servovalve electrical connection must be carefully chosen (series or parallel types) as it significantly affects the servovalve flow gain.

The interface between the analogue signals and the DAP requires the quantization effect of the A/D to be determined because the resolution/accuracy of the signal depends upon the digitising process of the converter. A basic understanding of the offset and gain adjustments of the signal conditioning unit are also required.

The DAP was investigated in some detail. And some of the useful features of the digital controller used in this work can be summarised as follows:

- The controller is suitable for fast-response hydraulic servo-control because the card contains a built-in servo amplifier.
- The card also includes a microprocessor. After download of the configuration program, the card can work independently without any supervisory PC. With respect to mobility, this development could be easily transferred to a real vehicle in practice.
- Using a WGS2 velocity transducer has proved to be the best solution for measuring the velocity signal in this work. Nevertheless, the measured signal had a problem with offset level and small amplitude.
- The controller allows the user/designer complete access to every internal parameter. Hence, even complicated configurations can be set up within the system.
- Regarding system analysis, it is vital to understand the numerical scheme used within the controller as directly affects the gain value used inside the closed-loop and hence the stability/performance of the system response.

Road Input and New Passive Suspension Model

3.1 Introduction

The suspension system is critical in determining the handling capability, and thus, the functional safety of vehicles. The suspension system is responsible for the transmission of forces between the vehicle and the road. A typical vehicle suspension system consists of springs, which provide stiffness and shock absorbers, which provide both damping and stiffness, and a combination of linkages that connect the structure of the vehicle to the road wheels. In other words, the suspension system is a mechanism that physically separates the vehicle body from the car wheel. The primary purpose of the vehicle suspension system is to minimise the vertical acceleration transmitted to the passengers, which directly provides road comfort and maintains contact between the vehicle and the road surface. In recent decades many researchers have paid considerable attention to the issues of enhancing comfort, guaranteeing the stability of suspension systems and to improving suspension performance for sufficient, required safety. Many vehicle suspension system models have been proposed (Elbeheiry and Karnopp 1996), (Soliman et al. 2014), and (Al-Holou et al. 2002).

Today's market demands safer automobiles which include passive and active safety devices. Passive safety systems are designed to protect occupants involved a crash and includes airbags, seat belts and side-impact beams (Mokhiamar and Abe 2002). Active safety systems are the control techniques that keep a vehicle under control and prevent a crash from occurring. Thus, even though ride comfort and handling performance are essential characteristics of suspension performance evaluation (Yagiz et al. 2008), design performance in term of safety is also highly necessary. The main factors that have attracted research attention in the area of suspension systems are durability, stability, road holding and ride comfort under various operating conditions (Avesh and Srivastava 2012). It should be noted that there will be some conflict, or compromise, between ride comfort and handling performance (Biglarbegian et al. 2006). The design aims and demands are now discussed. Suspension systems are exposed to extreme working conditions. Vehicles must be able to traverse both rough and smooth terrains. A major challenge in developing suspension systems is dealing with the highly changeable damping forces required for

vehicles crossing rough terrain. The fixed characteristics of a passive suspension system, i.e. the quasi-linear damping characteristic of conventional dampers, prevent the damper from generating high damping forces and from varying the damping according to the operating conditions. It is typically accepted that passive suspension systems have limited performance as their components can only store or dissipate energy, whereas active suspension components can both add and consume energy within the system. This will be demonstrated in detail in the following chapters.

Passive suspension design is a compromise between ride comfort and vehicle handling, as depicted in Fig. 3.1. Overall, a compromise between these two conflicting criteria can only be obtained if the suspension has been developed using passive springs and dampers (Mouleeswaran 2012). The answer to this issue appears to have been found in the development of active suspension systems.

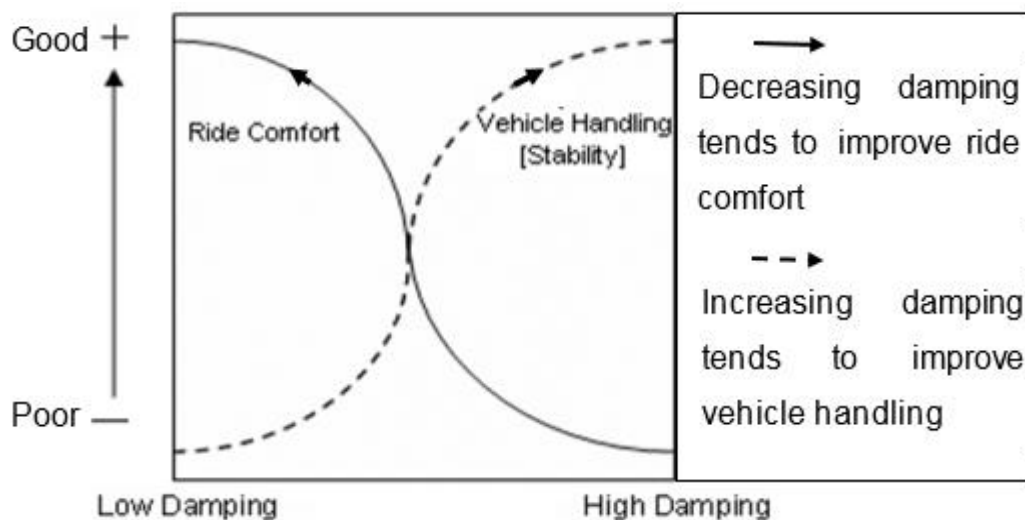


Fig. 3.1. Performance compromise of passive suspension systems (Mouleeswaran 2012).

Ride safety suspension should have hard damping with minor stiffness, while a comfort-oriented suspension should have as little damping of the chassis mass as to still provide sufficient isolation or smooth stiffness, especially within a specific frequency range. It has been reported (Baillie 1999) that ride comfort correlates to human sensitivity towards vertical vibrations within the frequency range 4 to 8 Hz.

Although active suspension may lead to better performance regarding vibration suppression, which will be robustly discussed in the next chapters, passive suspension still has the most significant market share due to their

acceptable performance and simple structure (Yim et al. 2010). The main fault of passive suspension is that it is unable to improve both ride comfort and safety simultaneously. The mechanical model of a conventional vehicle's passive suspension system may be regarded as the parallel combination of a damper and spring. Mass is one of three essential components of vibration, it is therefore tricky to directly isolate in a passive system where two masses are necessary to connect the body and the wheel respectively.

This chapter considers the use of experimental results to generate a new mathematical model of a passive suspension system and explores system responses, such as: road, wheel and body velocities and displacements, through simulation by amending the system step inputs, such as: uneven road inputs and changing tyre inflation pressures.

To account for the actual configuration of the test rig system, in contrast to previous studies using $\frac{1}{4}$ car model test rigs, the current study considered a new passive suspension system model by implementing a new term for nonlinear friction forces that effects the elongated lubricant supported body bearings. Such a friction model captures most of the experimentally observed friction, as shown in **Chapter 4**.

One of the other essential points of this study is how to experimentally generate the system inputs. Therefore, an active actuator is used to produce the system inputs, as detailed in the next section. Modifying the test rig to allow measurement of the CPL is a secondary target of the study. Consequently, load cells were fixed beneath the tyre using a National Instruments (NI) 9172 Compact DAQ chassis corresponding with the LabVIEW software, CPL will be measured through two adjustable parameters, Step Inputs (SI) and Inflation Pressures (IP), as will be explained later. Finally, a C++ compiler environment was selected to simulate the mathematical models. This helped to develop a complete picture of the features of this system for enhancing performance.

3.2 Road input simulator for the experiment

The road simulator system, proposed for this study, was developed using a hydraulic actuator to provide road inputs to both the passive and active suspension systems via a wheel unit. The road simulator system was described

in **Chapter 2**. A schematic diagram of the road simulator system is shown in Fig. 3.2.

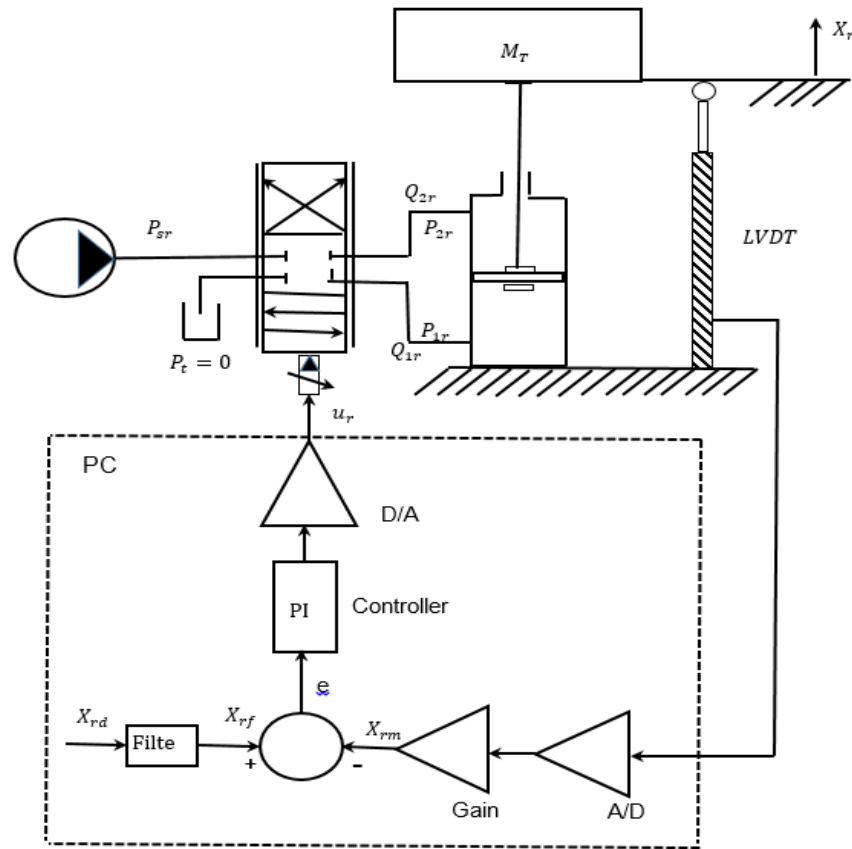


Fig. 3.2. Schematic diagram of road simulator system.

The road simulator system was designed to generate mixed ramp, step and sine wave road inputs. The mixed ramp inputs were used to move the hydraulic piston from zero position to the mid-point of the actuator, at which point the step inputs were then used as the primary inputs. These inputs are individually applied to the passive system, as demonstrated in this chapter, and to the active suspension system, as presented in **Chapter 6**. The mixed ramp and step road inputs are applied to the test rig as previously discussed, while random inputs are used for the simulation. This study focuses on the step inputs which are intended for use in time domain studies. Displacement and velocity outputs of the road simulator system are the disturbance inputs for the active suspension system. Therefore, all the systems are dynamically related and the dynamic behaviour of the road simulator system is thus, an essential factor in this study and should be investigated.

In general, Electro-Hydraulic Servo Systems (EHSS) are widely used in many industrial applications and mobile systems because of their high power-to-weight ratio, high stiffness, fast response, self-cooling, excellent positioning capabilities, etc. However, the dynamical models of the EHSS contain many uncertainties, which are the consequence of the physical characteristics, disturbances and load variations (FitzSimons and Palazzolo 1996). The dynamic behaviour of these systems is highly nonlinear due to phenomena such as: pressure-flow characteristics, hysteresis in flow gain characteristics, oil leakage, oil temperature variations, characteristics of valves near null, etc. In practice, determining an exact dynamic model that contains all the physical phenomena of EHSS represents a highly difficult task. Nonlinear static performance characteristics occur due to fluid flow forces, as mentioned by an old, but still excellent, textbook by (Merritt 1967b) and (Arafa and Rizk 1987). (Maneetham and Afzulpurkar 2010) presented a Proportional-Derivative (PD) controller for high-speed nonlinear hydraulic servo systems, but did not consider effects of the actuator leakage, bringing into question the validity of the results. (Alleyne and Hedrick 1995) examined the nonlinear dynamics of an electro-hydraulic actuator in a $\frac{1}{4}$ car active suspension model and used these dynamics to formulate a nonlinear control law. However, this study fails to reflect the influence of the tyre damper and neglects details about the test rig. Therefore, the researcher should keep in his mind this previously referenced work before starting to investigate hydraulic systems.

In the current study, the hydraulic piston is assumed to support a vertical load acting such that it always endeavours to retract the piston back in the same direction. For open-loop control systems, a critically lapped servovalve spool is acceptable; for closed-loop control systems, an asymmetrically underlapped servovalve spool is consistently assumed. The latter assumption is useful for closed-loop analysis since a small amount of spool underlaps often occur in practice (Surawattanawan 2000). Should it be desirable, it is an easy matter to reduce the underlap to zero to simulate a critically lapped spool.

3.2.1 Nonlinear mathematical modelling

The modelling of a single rod actuator with closed loop position control and known actuator seal leakage presents an exciting variation from that usually published literature. (Surawattanawan 2000) conducted a previous study using the same test rig and involving some good points, but the study considered linear models for the road and active hydraulic actuator, without implementing servovalve equation for both actuators, leading to questions about the consistency of the experimental results. Therefore, the current study will theoretically show that such a system results in four position offsets due to:

1. The servovalve dynamic equation.
2. The actuator volume of both side chambers is changeable.
3. The seal leakage term.
4. Both side flow rates are adaptable.

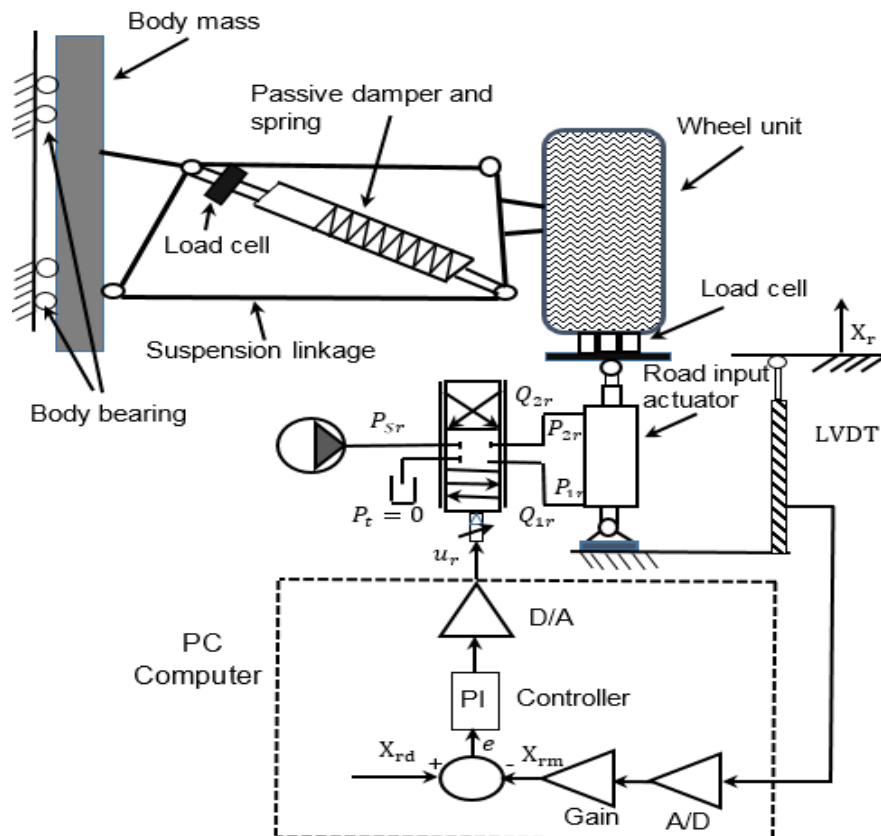


Fig. 3.3. Schematic diagram of the test rig and road simulator.

Considering Fig. 3.3, the test rig and road simulator schematic diagram and conventional modelling undertaken by (Alleyne and Hedrick 1995) and

(Watton 2007); spool valve displacement, x_{sr} is related to the voltage input, u_r , by a first-order system given by:

$$\dot{x}_{sr} = \frac{1}{\tau_r} (u_r - x_{sr}) \quad (3.1)$$

where, $\tau_r(s)$ is a time servovalve constant, u_r is servovalve control, or applied voltage, x_{sr} (m) is servovalve spool displacement and \dot{x}_{sr} (m/s) is servovalve velocity. Note that the symbol “r” means relative to the road.

Therefore, depending on the direction of the servovalve spool movement, we have two cases:

Case 1: If $x_{sr} \geq 0$ when extending, the sign of the pressure or the pressure differences under the square root of the actuator flow rate equation, should be checked.

$$\text{if } P_{sr} - P_{1r} \geq 0 \quad (3.2)$$

$$Q_{1r} = K_{fr} x_{sr} \sqrt{P_{sr} - P_{1r}} \quad (3.3)$$

$$\text{if } P_{sr} - P_{1r} < 0 \quad (3.4)$$

$$Q_{1r} = -K_{fr} x_{sr} \sqrt{P_{1r} - P_{sr}} \quad (3.5)$$

$$\text{if } P_{2r} \geq 0 \quad (3.6)$$

$$Q_{2r} = K_{fr} x_{sr} \sqrt{P_{2r}} \quad (3.7)$$

$$\text{if } P_{2r} < 0 \quad (3.8)$$

$$Q_{2r} = -K_{fr} x_{sr} \sqrt{-P_{2r}} \quad (3.9)$$

Case 2: If $x_{sr} < 0$ when retracting

$$\text{if } P_{sr} - P_{2r} \geq 0 \quad (3.10)$$

$$Q_{2r} = K_{fr} x_{sr} \sqrt{P_{sr} - P_{2r}} \quad (3.11)$$

$$\text{if } P_{sr} - P_{2r} < 0 \quad (3.12)$$

$$Q_{2r} = -K_{fr} x_{sr} \sqrt{P_{2r} - P_{sr}} \quad (3.13)$$

$$\text{if } P_{1r} \geq 0 \quad (3.14)$$

$$Q_{1r} = K_{fr} x_{sr} \sqrt{P_{1r}} \quad (3.15)$$

$$\text{if } P_{1r} < 0 \quad (3.16)$$

$$Q_{1r} = -K_{fr} x_{sr} \sqrt{-P_{1r}} \quad (3.17)$$

The actuator flow rate equations, including compressibility and cross-line leakage effects for both sides may be written as:

$$\frac{V_{1r}}{\beta_{er}} \dot{P}_{1r} = Q_{1r} - A_{1r} \dot{X}_r - \frac{(P_{1r} - P_{2r})}{R_{ir}} \quad (3.18)$$

$$\frac{V_{2r}}{\beta_{er}} \dot{P}_{2r} = A_{2r} \dot{X}_r + \frac{(P_{1r} - P_{2r})}{R_{ir}} - Q_{2r} \quad (3.19)$$

$$V_{1r} = V_{1r0} + A_{1r} X_r \quad (3.20)$$

$$V_{2r} = V_{2r0} - A_{2r} X_r \quad (3.21)$$

$$F_{hydr} = (P_{1r} A_{1r} - P_{2r} A_{2r}) \quad (3.22)$$

Also, Newton's 2nd law of motion gives the following for the tyre motion:

$$\ddot{X}_r M_r = (P_{1r} A_{1r} - P_{2r} A_{2r}) - B_{vr} \dot{X}_r - k_t (X_r - X_w) - b_t (\dot{X}_r - \dot{X}_w) - M_T g \quad (3.23)$$

where, M_r is tyre mass, the displacements of the tyre and wheel are X_r and X_w respectively, the velocity of the tyre and wheel are \dot{X}_r and \dot{X}_w respectively, \ddot{X}_r is the acceleration of the tyre mass, M_T is the total test rig mass, g is ground acceleration, the spring coefficient are k_s and k_t and the damping coefficient are B_{vr} and b_t .

A low voltage is used to control the servovalve. The control voltage is passed through an amplifier that provides a specific spool movement resulting in the power to alter the valve's position being achieved. The valve then delivers a measured amount of fluid power to an actuator. The use of a feedback transducer on the actuator returns an electrical signal to the amplifier to condition the strength of the voltage for the servovalve. The main drawback of state feedback law using a static-state controller is that it cannot eliminate the steady-state errors due to hydraulic leakages and constant disturbances or reference input commands. It is therefore necessary for the structure of the controller to contain an integral action to overcome this drawback.

The suggested PI controller is:

$$u_r(t) = K_p e_r(t) + K_i \int_0^t e_r(t) dt \quad (3.24)$$

The error signal is:

$$er(t) = X_{rdf}(t) - X_r(t) \quad (3.25)$$

where, K_p is proportional gain, K_i is integral gain, er is the error, X_{rdf} and $X_r(m)$ are the desired filtered signal input and the measured road displacement respectively.

From Equations 3.1 and 3.24, it is evident that the PI control can be used to drive the road actuator to achieve the control scheme, since it eliminates steady-state errors by increasing the system type, without appreciably changing the dominant roots of the characteristic equation. This is in agreement with the author's supposition; good agreement would be found between the experimental and simulation results. This will later be revealed as indubitable proof that this control is precisely appropriate for this system.

3.2.2 Design of PI controller

Although the servovalve equations are non-linear equations whose flow rate outputs are functions of two inputs, spool movement, or voltage signal, and pressure, as shown in the previous equations, for the purpose of control design, linearised models of the power system around an equilibrium point are adequate. Therefore, in the current study, the PI controller is designed in two ways: the first is through trial and error, where the final system must meet performance specifications and should be reliable and economical; while the second method for designing a controller used the following steps:

1. Assuming a linearisation technique for the servovalve equation.
2. Using the flow rate continuity equation for both sides of the chamber, as mentioned in Equations 3.18 and 3.19.
3. Using Equation 3.22 to account for the hydraulic force.
4. Using Equation 3.23, derived from Newton's 2nd law of motion, for tyre motion.
5. Using Equation 3.1 for to calculate the applied voltage, or control force.
6. Establishing the state space representation for the system by choosing the state vector to generate A, B, C and D matrices.

7. The open-loop transfer function and closed-loop poles were identified.
8. Using a second order system by suggesting a suitable damping (ξ) and un-damped natural frequency (ω_n) to drive the system.
9. Finding the suitable K_P and K_I gains for the controller.

Note: for further details of the design of PI see **APPENDIX A**.

3.2.3 Filter and types of inputs

In this study, as previously mentioned, both mixed ramp and step inputs were used for three cases and were influenced by the amplitude values; the results of which will be displayed in this chapter. These inputs, despite being more difficult than sine wave inputs, helped show the system response, and any shortcoming that could damage the test rig. The digital first order filter should be considered as a low pass filter, which was designed and coded in C++ compiler through the DAP card within the PC. Thus, the input signals were passed through the filter and then sent to the test rig.

The first order filter can be expressed as:

$$X_{rdf} = \left(\frac{\tau_r}{T_s} X_{rd} + X_{rd} \right) / \left(1 + \frac{\tau_r}{T_s} \right) \quad (3.26)$$

where, X_{rdf} and X_{rd} are the filter obtained and desired inputs respectively, τ_r is a time constant and T_s is the sampling time interval.

For a precise and repeatable experimental investigation, three amplitude settings, 30, 50 and 70 mm, were used in this study. For each case, the hydraulic actuator piston started from the zero position and moved through ramp inputs to reach the mid-point of the actuator first Steady-State (SS), followed by step inputs filtered with specific amplitude values to give the highest positive values second SS, before returning to the lowest amplitude with twice the displacement value third SS.

3.3 Passive suspension system: theoretical studies

3.3.1 Passive suspension system model

To understand the characteristics of a passive suspension system and allow a comparison between passive and active suspension systems, a passive suspension system was theoretically investigated, modelled and designed using the suspension working space from the $\frac{1}{4}$ car test rig. Vehicle suspension systems have developed over the last 135 years to a very high level of sophistication (Peng et al. 1997). Development of active suspension systems began in the 1930's, but the most significant developmental work has been conducted since 1950. Semi-active suspensions systems were first proposed in the early 1970's and showed that performance comparable to that of fully active suspension systems was possible (Karnopp et al. 1974).

However, most manufacturers today use passive suspension systems which employ different types of spring in combination with hydraulic or pneumatic shock absorbers. Despite a large range of designs currently available, passive suspension systems will always be a compromise between passenger ride comfort, handling, and suspension stroke over the operating range, because they can only store and dissipate energy in a pre-determined manner (Nekoui and Hadavi 2010) and (Hanafi 2010). The passive suspension system model clearly needs revision.

$\frac{1}{4}$ car models can be successfully used to analyse a suspension system's response to road inputs. However, the accuracy of the results will depend on how accurately and effectively the system parameters such as: sprung mass, unsprung mass, stiffness and damping, have been measured. In this study, the system responses were obtained under different road excitations using established the model (Pathare 2014).

Most previous research, (Hanafi et al. 2009), (Jamei et al. 2000), (Tan and Bradshaw 1997), (Westwick et al. 1999), (Buckner et al. 2015), and (Hardier 1998) involving $\frac{1}{4}$ car modelling generally assumed that the damper and spring move vertically, ignoring any effects of inclination. In contrast, in the real world the damper and spring are mostly inclined. Therefore, there is no reason to make this assumption now. Also, when using the vertical model to simulate the

experimental passive test rig results in this study, significant differences between the experimental and simulation results, as Figs. 4.3 and 4.4 show, were found. Bearing this in-mind and given the practical viewpoint that a suspension designer must optimise the system within a limited working space, it was decided that the passive suspension test rig model must be modified to take into account the actual organisation of the damper and spring systems. Therefore, the nonlinear friction forces that affect the body bearing should be considered.

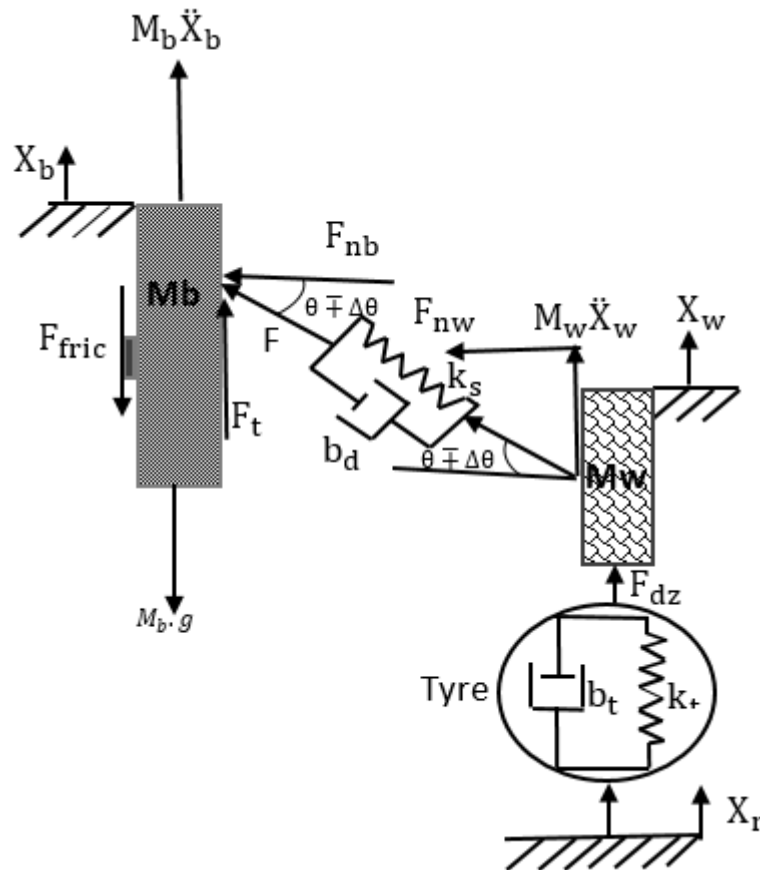


Fig. 3.4. Free body diagram of a quarter car (test rig) passive suspension model.

Fig. 3.4 shows the free body diagram of both the body M_b and wheel M_w masses where the displacements of wheel and car body are X_w and X_b respectively. It should be noted that X_r , X_w and X_b are relative to mathematically calculated ideal ground level, which does not exist in the real world, but does exist in the laboratory environment. In addition, it is assumed that the tyre behaves as a point-contact follower that is in continuous contact with the road surface. Thus, to establish the model it was necessary to consider the friction forces.

3.3.2 Friction forces and the relative dynamic angle

The mathematical expression for the nonlinear friction model, which will be investigated in detail in **Chapter 4**, is relatively complicated and consists of several different terms that are used to accurately represent the observed phenomena. The nonlinear friction model provides real insight and functional information in cases such as that shown in Equation 3.27.

$$F_{\text{fric}} = \begin{cases} k_s(X_w - X_b) + b_d(\dot{X}_w - \dot{X}_b) & \dot{X}_b = 0.0 \\ C_e e^{(|\dot{X}_b|/e_1)} + \left[\frac{\mu(k_s(X_w - X_b) + b_d(\dot{X}_w - \dot{X}_b))}{\tan(\theta \mp \Delta\theta)} \right] + \sigma_v \dot{X}_b & \dot{X}_b > 0.0 \\ -C_e e^{(|\dot{X}_b|/e_1)} - \left[\frac{\mu(k_s(X_w - X_b) + b_d(\dot{X}_w - \dot{X}_b))}{\tan(\theta \mp \Delta\theta)} \right] + \sigma_v \dot{X}_b & \dot{X}_b < 0.0 \end{cases} \quad (3.27)$$

where, \dot{X}_w and \dot{X}_b are the wheel and body velocities respectively, C_e is a tracking parameter, e_1 is the degree of curvature, μ is a friction coefficient, σ_v is a viscous coefficient. θ is the construction angle and $(\theta \mp \Delta\theta)$ is the dynamic construction angle.

Equation 3.27 shows the nonlinear frictions model, which depends on the body velocity and the relative historical movements between wheel and body travel. This model includes two main parts: static and dynamic frictions. The former occurs when $\dot{X}_b = 0.0$. The latter, with two expressions, depends on the velocity acceleration, deceleration and direction: first, the transition behaviour from the stiction to slide regime including the Stribeck effect; second, the Coulomb friction accounted for the dynamic force normal to the bearing body; third, and finally, viscous friction relative to the surface of the lubricant. The most crucial results from this model are highlighted by the hysteresis behaviours of friction relative to velocity and body displacement history behaviours, as shown by the results in **Chapter 4**.

In addition, the construction linkage angle can be dynamically changed by $\mp \Delta\theta$ as follows:

$$\Delta\theta = \sin^{-1} \left[\frac{(X_w - X_b) \sin 60}{L_d - (X_w - X_b) \sin 30} \right] \quad (3.28)$$

where, L_d is the free length of damper and spring.

Why consider a friction force within this study? How to build up the nonlinear friction model? Why does this model consist of both static and dynamic friction? Why consider the Stribeck effect, Coulomb and viscous friction? How to account for the force normal to the bearing body, responsible for generating Coulomb friction? How to determine the dynamic construction angle values and how does vary? How to explain the hysteresis behaviour of the friction? All these questions will be answered in greater detail in **Chapter 4**.

3.3.3 Mathematical model

As mentioned in **Chapter 1**, vehicle suspensions are designed to minimise car body acceleration \ddot{X}_b , which is the central aspect of our requirements, within the limits of suspension displacement $X_w - X_b$ and tyre deflection $X_r - X_w$. Monitoring the CPL between the tyre and the road is vital to actively linking with stability, a secondary target. Hence, the vehicle response variables that need to be examined are:

1. Car body acceleration, \ddot{X}_b
2. Suspension displacement, $X_w - X_b$
3. Tyre deflection, $X_r - X_w$
4. Contact Patch Load (CPL), F_{zd}

The previous study (Surawattanawan 2000) using the same test rig did not consider the real positions of the spring and damper, so; consequently, the friction effects were ignored. (Ali Al-Zughaibi et al. 2018) implemented, for the first time, the friction force within Newton's 2nd law of motion when applied to a ¼ car model. Therefore, using Fig. 3.4, the new dynamic equation of motion for the mass body of the passive system becomes:

$$M_b \cdot \ddot{X}_b = [k_s(X_w - X_b) + b_d(\dot{X}_w - \dot{X}_b)] - F_{fric} \quad (3.29)$$

While the dynamic equation of motion for the mass wheel is:

$$M_w \cdot \ddot{X}_w = -[k_s(X_w - X_b) + b_d(\dot{X}_w - \dot{X}_b)] + k_t(X_r - X_w) + b_t(\dot{X}_r - \dot{X}_w) \quad (3.30)$$

The constant parameters taken from the test rig are as follows:

Car body mass, $M_b = 240$ kg

Wheel unit mass, $M_w = 40$ kg

Tyre stiffness, $k_t = 920000$ N/m

Tyre damping rate, $b_t = 3886$ N/ms⁻¹

Suspension stiffness, $k_s = 28900$ N/m

Suspension damping, $b_d = 260$ N/ms⁻¹

A $\frac{1}{4}$ car passive suspension system was developed using C++ which incorporated sufficient DOFs to capture all the translational motions of the un-sprung masses in space, alongside an adequate representation of the different sub-systems, such as the wheel and tyre system, as shown in Figs. 3.5 and 3.6.

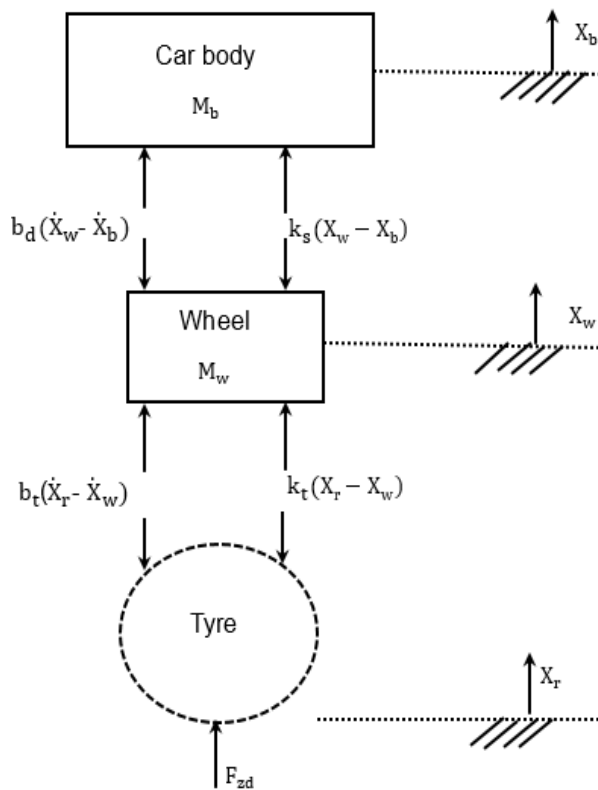


Fig. 3.5. Free body diagram of a quarter car passive suspension model.

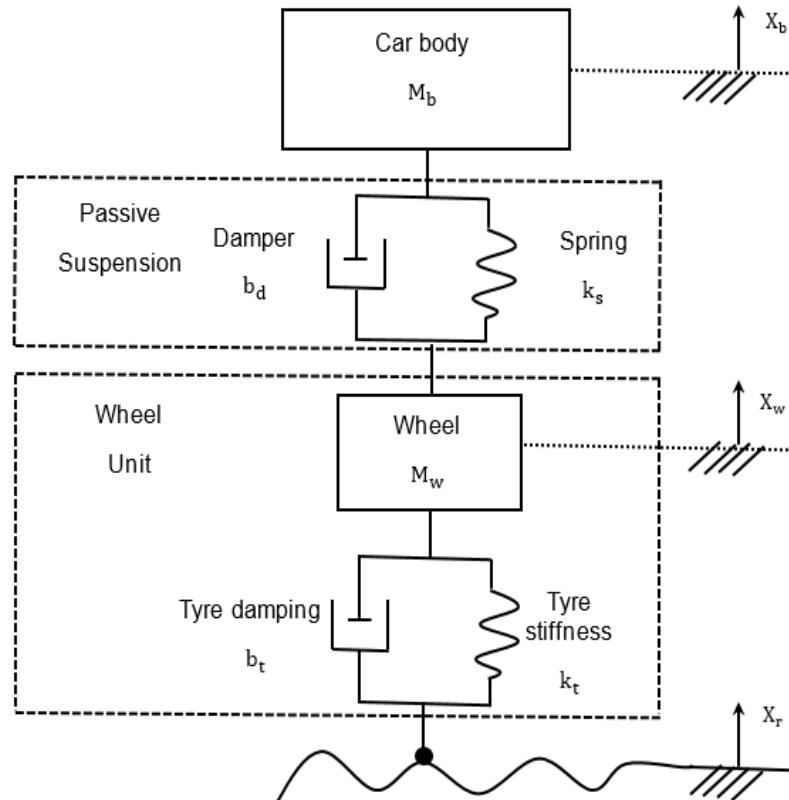


Fig. 3.6. A 1/4-car passive suspension system model including external forces.

3.3.4 Contact Patch Load (CPL)

The function of the automotive suspension system is to not only isolate the effect of road surface irregularities to improve the ride comfort for passengers, but it must also control the dynamic tyre load within the acceptable working space of the system to enhance vehicle stability and safety. Therefore, the CPL between the tyre and road is crucial to this investigation. Dynamic tyre load is the primary effect of the tyre/road friction forces which control lateral vehicle stability during handling manoeuvres and braking, in terms of stopping distance and traction forces, as well as tyre rolling resistance (Wong 2001).

Many intelligent suspension systems, such as semi-active and active suspension systems, are developed for both handling performance and ride comfort. Since the suspension system plays a vital role in standard loading, they can be used to adjust the amounts of normal loading and improve the potential of normal loading. As the parameters of conventional suspension systems cannot be changed, as in the current case, it cannot be used for further control of conventional forces. However, semi-active or active suspension systems are

capable of changing their parameters such as stiffness and damping coefficient (Xu and Ahmadian 2013).

Tyre loads and the road/tyre interface coefficient of friction govern all aspects of vehicle motion and are essential to vehicle simulation, handling evaluation, control system design, and safety measures. Nevertheless, tyre load and road friction depend on uncontrollable environmental characteristics, such as: temperature, wear, normal load, tyre pressure, amongst other factors, that are difficult to measure directly. As the tyre is the only link between the road surface and vehicle, it plays a highly significant role in accident mitigation and prevention. Thus, road safety is of great interest to research and development divisions within the vehicle industry. It is therefore clear that the CPL should be deeply investigated.

This study conducted an experimental investigation into the influence of road step inputs and inflation pressures on the CPL. Both the CPL and the impacts of these two parameters were monitored to obtain knowledge about their dynamic behaviour and for comparison with values determined from the active suspension system setup. The test rig was modified to allow the CPL to be measured using a set of none F218z load cells fixed beneath the tyre, as shown in Figs. 2.3 and 2.4 in **Chapter 2**. These load cells were calibrated as mentioned in **Chapter 2**, and are used for measuring these contact loads using the programme LABVIEW. A theoretical derivation of the CPL is now discussed.

3.3.4.1 A mathematical model of contact patch load

Given Fig. 3.5, the dynamic equation of CPL is:

$$F_{zd} = k_t(X_r - X_w) + b_t(\dot{X}_r - \dot{X}_w) \quad (3.31)$$

From Equations 3.29, 3.30 and 3.31, the CPL under steady-state condition is:

$$k_s(X_w - X_b) = M_b g + F_{fric} \quad (3.32)$$

$$k_t(X_r - X_w) = k_s(X_w - X_b) + M_w g \quad (3.33)$$

$$F_{zs} = k_t(X_r - X_w) \quad (3.34)$$

Substituting Equations 3.32, 3.33 into 3.34 yields:

$$F_{zs} = M_b g + M_w g + F_{fric} \quad (3.35)$$

Thus, CPL can be monitored and studied as a function of variation in step system inputs and the inflation pressure. This was achieved experimentally using the load cells and simulated through implementation of the CPL mathematical equation within a developed C++ program.

3.4 Analysis of natural system frequencies

The natural frequency of a system can be determined from the solution of the equations of motion, assuming the mass in the system moves with harmonic motion and without any damping (Ljung and Glad 1994).

Fig. 3.7 shows the $\frac{1}{4}$ car model without any damping, or external force acting on either mass, meaning the system vibrates freely. Assuming the masses move in a vertical direction and $X_b > X_w$ then, the only internal forces acting on the masses are spring forces.

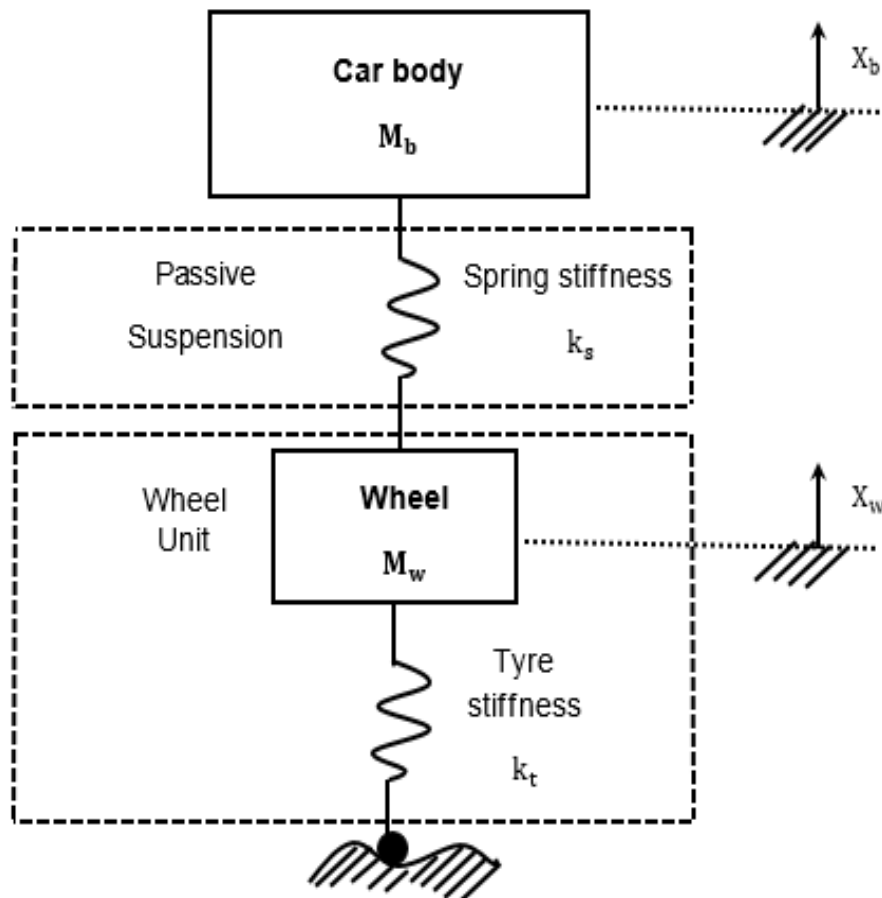


Fig. 3.7. Passive suspension model without damping elements or external forces.

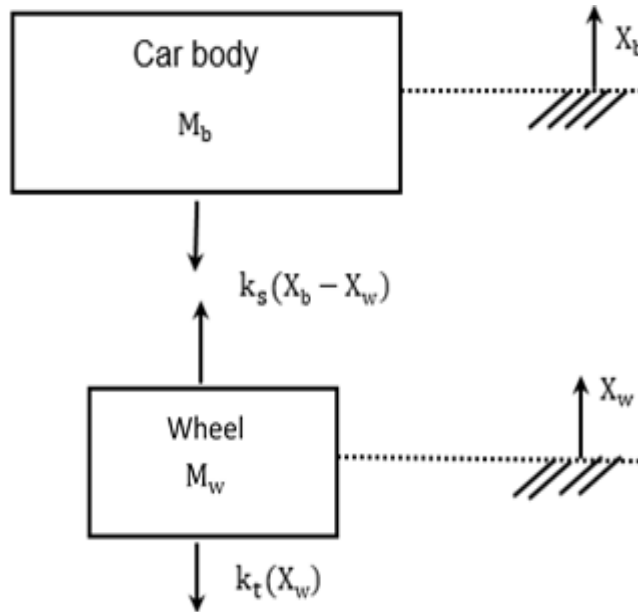


Fig. 3.8. Free body diagram of a $\frac{1}{4}$ -car test rig with passive suspension.

The free body diagrams of the two masses were also shown in Fig 3.8. By applying Newton's 2nd law to each mass, the equations of motion are:

$$M_b \ddot{X}_b = -k_s(X_b - X_w) \quad (3.36)$$

$$M_w \ddot{X}_w = k_s(X_b - X_w) - k_t X_w \quad (3.37)$$

Equations 3.36 and 3.37 can therefore be written in matrix form as:

$$\begin{bmatrix} M_b & 0 \\ 0 & M_w \end{bmatrix} \begin{bmatrix} \ddot{X}_b \\ \ddot{X}_w \end{bmatrix} + \begin{bmatrix} -k_s & k_s \\ k_s & -(k_s + k_t) \end{bmatrix} \begin{bmatrix} X_b \\ X_w \end{bmatrix} = \begin{bmatrix} 0 \\ 0 \end{bmatrix} \quad (3.38)$$

The mass and stiffness matrices have the unique property of being symmetric, meaning they are equal to their transpose. Each motion is assumed to be in a principal mode where only one coordinate varies. There are two principle modes in this work. A set of coordinates, X_b and X_w are called generalised coordinates and are used to describe general motions and recognise motion constraints. There is no manner of motion that can be described completely by X_b or X_w without involving the other coordinates. Therefore, both generalised coordinates are assumed to have a harmonic of the same frequency, (ω) .

$$X_b = X_B \sin \omega t \quad (3.39)$$

$$X_w = X_W \sin \omega t \quad (3.40)$$

Substituting these harmonic expressions into Equations 3.36 and 3.37 results in two algebraic equations with X_B , X_W and ω^2 as unknowns.

$$(-M_b\omega^2 + k_s)X_B + (-k_s)X_W = 0 \quad (3.41)$$

$$(-k_s)X_B + (-M_w\omega^2 + k_s + k_t)X_W = 0 \quad (3.42)$$

These equations can be written as a model fraction, λ , to eliminate the constants X_B and X_W :

$$\lambda = \frac{X_B}{X_W} = \frac{k_s}{-M_b\omega^2 + k_s} = \frac{M_w\omega^2 - k_s - k_t}{-k_s} \quad (3.43)$$

Cross-multiplying gives a quadratic in ω^2 :

$$(M_w\omega^2 - k_s - k_t)(-M_b\omega^2 + k_s) = -k_s^2 \quad (3.44)$$

$$(M_bM_w)\omega^4 - (M_b(k_s + k_t) + M_wk_b)\omega^2 + k_s k_t = 0 \quad (3.45)$$

where, the following constants were used:

Car body mass, $M_b = 240$ kg

Wheel unit mass, $M_w = 40$ kg

Tyre stiffness, $k_t = 280000$ N/m

Suspension stiffness, $k_s = 19600$ to 117600 N/m

The relationship between suspension stiffness and the two natural frequencies for the car body and the wheel are plotted in Fig. 3.9, illustrating that both vary proportionally with suspension stiffness. The test rig car body natural frequency is in the range of 1.4-2.9 Hz, which is outside of the undesired frequency ranges of 4-8 Hz, as mentioned earlier, while the wheel natural frequency varies from 8.75 Hz to 17.7 Hz. For dynamic analysis, the low-frequency range, which is of greatest concern in vehicle suspension design, is mainly influenced by the car body natural frequency.

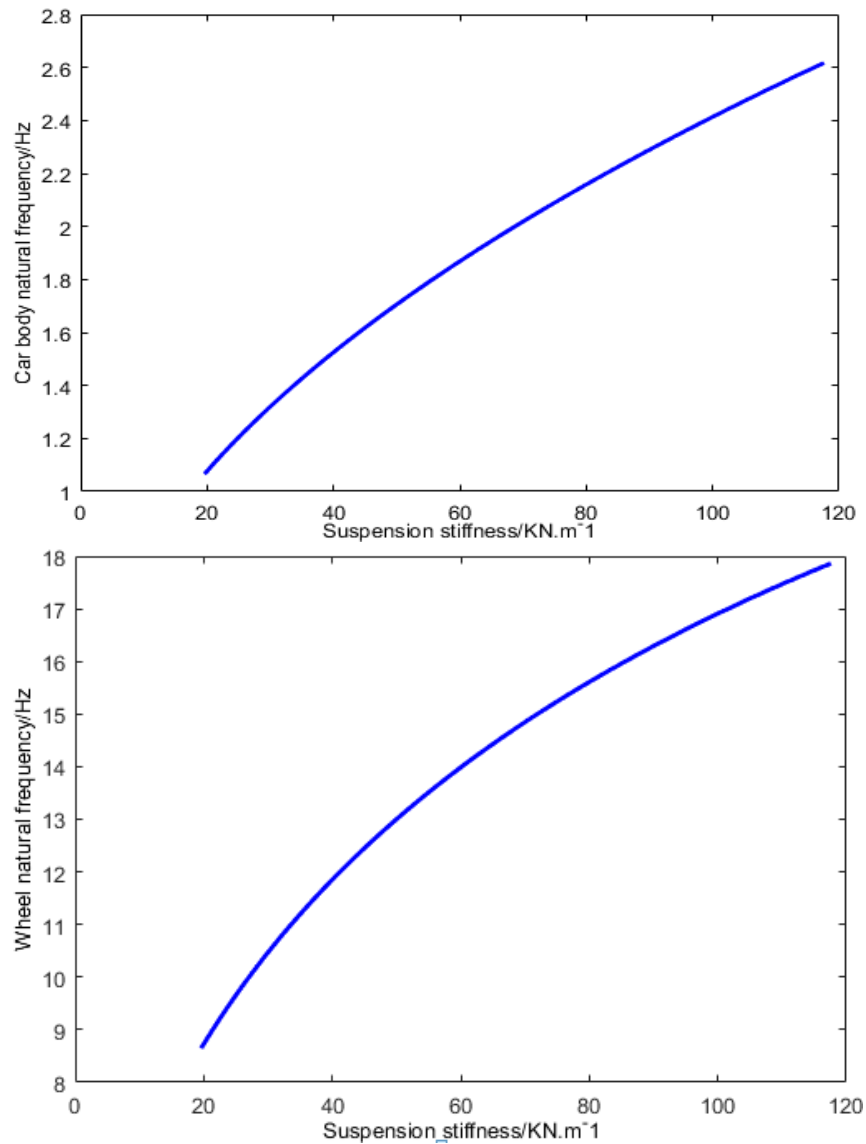


Fig. 3.9. Car body and wheel natural frequency as a function of suspension stiffness.

3.5 Physical test rig workpiece

According to the test rig constraints, the maximum physical ranges of $X_w - X_b$ and $X_r - X_w$ are ± 73 mm and ± 20 mm respectively. Therefore, the maximum values of $X_w - X_b$ and $X_r - X_w$, are be ± 25 mm and ± 6.8 mm. In addition, to generalise the results, $X_w - X_b$ and $X_r - X_w$ can be presented as a percentage of the maximum range, or:

$$\% \text{ of rms } X_w - X_b = \frac{\text{rms } X_w - X_b}{25} * 100 \quad (3.46)$$

$$\% \text{ of rms } X_r - X_w = \frac{\text{rms } X_r - X_w}{6.8} * 100 \quad (3.47)$$

3.6 Inflation pressure

Maintaining the correct tyre pressure helps to extend tyre life, improve vehicle safety and maintain fuel efficiency. Tyre pressure is measured by calculating the amount of air that has been pumped into the inner lining of the tyre in Pounds per Square Inch (psi) or bar pressure. Vehicle manufacturers specify the correct tyre pressure and it is crucial, as the driver, to ensure that the pressure is checked and corrected on a regular basis. All tyres lose air, typically at a rate of around 0.69 bars or 1 psi, per month (KwikFit 2015); this can be accelerated by frequent long-distance driving, uneven road surfaces and heavy loads. Air loss also increases in warmer temperatures. There are three categories of inflation pressure (Gordons-tyres 2018) as shown in Fig. 3.10.

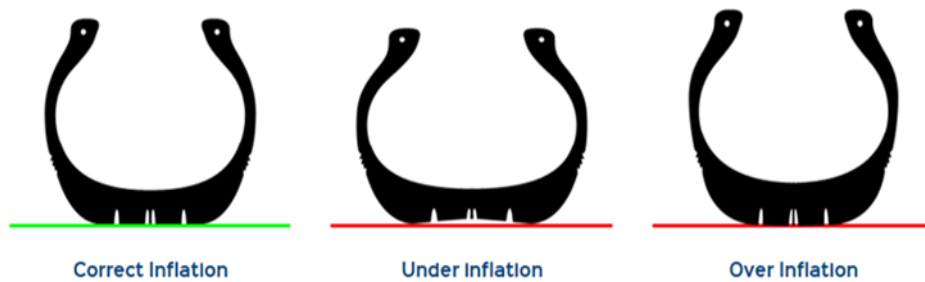


Fig. 3.10. Inflation pressure (Gordons-tyres 2018).

3.6.1 Underinflated tyres

Tyres can quickly become underinflated if not checked regularly. Underinflated tyres will have uneven contact with the road and will exhibit excessive wear on the inside and outside edges of the tread if left underinflated for a period of time. Not only does low tyre pressure wear tyres out quicker, but it may also lead to increased road rolling resistance, resulting in reduced fuel efficiency and increased CO₂ emissions.

3.6.2 Over-inflated tyres

Putting too much air into tyres can be just as damaging and costly as underinflation. Over-inflated tyres will have a smaller contact patch, the part of the tyre that contacts the road, compared to correctly inflated tyres. This can lead to a loss of traction and reduced braking distance. Overinflated tyres will also

wear heavily and unevenly across the central part of the tyre, leading to shorter tyre lifespans than if the tyre was correctly inflated.

3.6.3 Correct tyre pressures

It is not always apparent that air is being lost from tyres, but it escapes at a rate of up to two psi of air every month. This rate of loss increases during warm weather, requiring more checks, when temperatures rise.

From the information above, it is clear that the impact of inflation pressures on vehicle stability and safety must be investigated. Therefore, in this study, three different tyre pressure values, 15, 25 and 35 psi, were used during experiments. The tyre pressure was changed using a laboratory air pipe source that controls pressure using gauge device. Due to the limitations of the test rig, it would have been difficult to measure changes in the contact patch area as well as the force distribution across that area, both of which are directly related to inflation pressure. Thus, only CPL could be used, through application of nine load cells placed underneath the tyre, to explore the force distribution.

3.7 Experimental work

At this stage, to prepare the test rig ready to conduct the experiment tests, several processes had to be followed to ensure all sensors worked correctly and the load cells were fixed correctly beneath the tyre. Consequently, the following steps were carried out:

1. The CANAL data acquisition card within the PC was replaced with a DAP card and the PSC hardware was removed as explained in **Chapter 2** and in line with the primary modification of the test rig. A digital control programmed was written in C++ to generate suitable system step inputs that represent road inputs and was then compiled.
2. The test rig sensors, such as: displacement and velocity sensors for the road, wheel and body, were checked. The servovalve pressure and flow rate sensors for the road simulator were also tested. In addition, all the sensors were calibrated, as previously shown in **Chapter 2** in Figs. 2.16 to 2.19.

3. The 9 Novatech F218z load cells were checked. These load cells had already been calibrated using a compression/tension universal test machine, an Avery Denison with a maximum load of 600 KN in Cardiff University's Light Structures Test Laboratory, as mentioned in Section 2.4.2.2 in **Chapter 2**.
4. The load cells were correctly fixed to the test rig, beneath the tyre, allowing the CPL to be measured between the tyre and the base, as shown in Figs. 2.3 and 2.4 in **Chapter 2**.
5. The supply pressure was checked and value determined; a small value for the road simulator actuator and 200 bar for the active suspension actuator.
6. A pressure gauge and the laboratory source air were used to adjust the tyre inflation pressure.

In this study, to clarify and validate the experimental results, all tests were repeated. Accordingly, three different cases were considered in this study with three different amplitudes, 30, 50 and 70 mm, to investigate the system response. Meanwhile, the CPL was studied and monitored as a function of the variation of two parameters; the road step system inputs, and the tyre inflation pressures.

3.8 Identification of parameters

According to the mathematical models for the passive suspension system and the road simulator, which were developed in this study, the following parameters can be identified as:

Spring stiffness k_s , viscous damping b_d , tyre stiffness k_t , viscous tyre damping b_t , actuator viscous damping B_{vr} , effective bulk modulus β_{re} , and cross-port leakage resistance R_{ir} .

- Identify [k_s , b_d , k_t , and b_t]

The four parameters, k_s , b_d , k_t , and b_t , can be directly determined from the experimental test data using Newton's 2nd law of motion for the body and wheel masses separately, as described by Equations 3.36 and 3.37. Depending on the experimental results, finding the accelerations of the body and wheel masses

using the equations of motion also helped to obtain the previously identified parameters values as follows:

Fig. 3.11 shows the body velocity results within the period $t = 19.9\text{-}20.4$ s at an amplitude of 50mm.

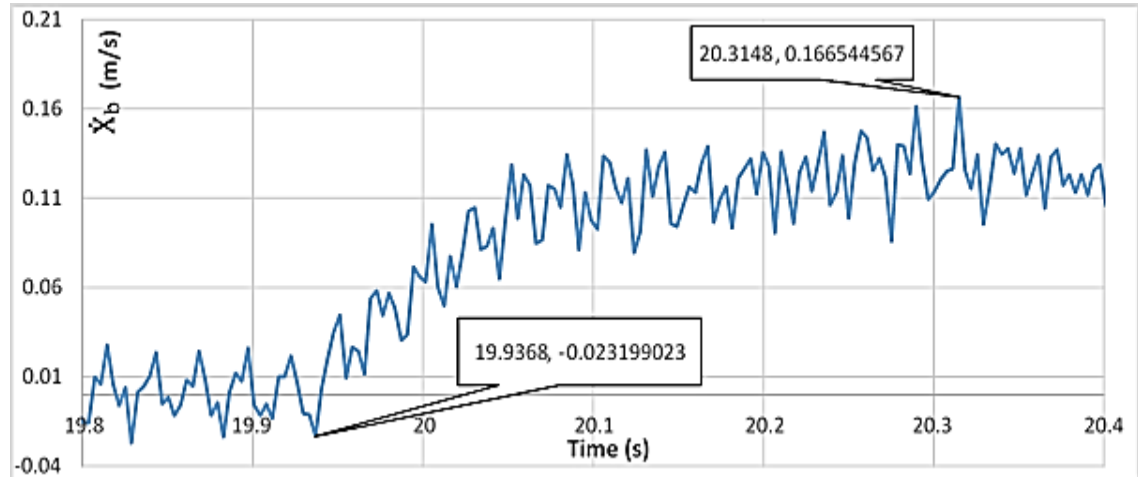


Fig. 3.11. Experimental body velocity as a function of time.

From this experimental data, the body acceleration can be calculated as:

$$\ddot{X}_b = \frac{0.1665 - (-0.0231)}{20.3148 - 19.9368} = \frac{0.1896}{0.378} = 0.5 \text{ m/s}^2 \quad (3.48)$$

The relative displacement and velocity for the wheel and body values at $t = 20.314$ s, are:

$$X_w = 0.0777 \text{ m}, \quad X_b = 0.0725 \text{ m}, \quad \dot{X}_w = 0.0493 \text{ m/s}, \quad \dot{X}_b = 0.1665 \text{ m/s}$$

From the mathematical simulation model, the difference in the friction values at the two steady-states (F_{fricS}), is equal to zero.

By applying Equation 3.36 using the detailed values when $t = 20.3184$ s, the following was found:

$$k_s = 2.89 \times 10^4 \text{ N/m} \quad \& \quad b_d = 260 \text{ N/m/s}. \quad (3.49)$$

Similarly, Fig. 3.12 shows the wheel velocity results at $t = 19.9404$ s at an amplitude of 50mm.

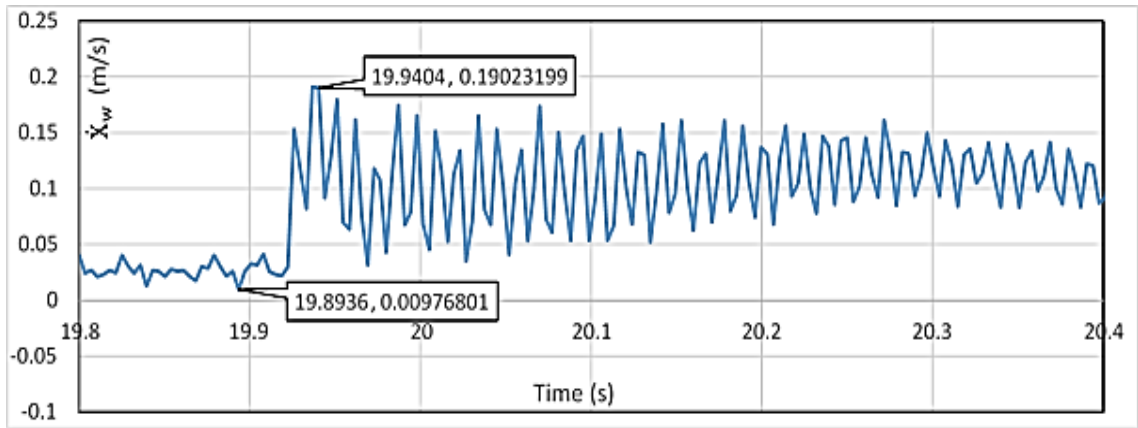


Fig. 3.12. Experimental wheel velocity as a function of time.

It can therefore be calculated from this experimental data that the wheel acceleration is:

$$\ddot{x}_w = \frac{0.1902 - 0.0097}{19.9404 - 19.8936} = \frac{0.1805}{0.0468} = 3.85 \text{ m/s}^2 \quad (3.50)$$

Again, in a similar fashion, Fig. 3.13 shows the road experimental displacement input from 19.8 to 20.4 s, Therefore, using this experimental data, the road velocity was found at $t=19.9404$ s as:

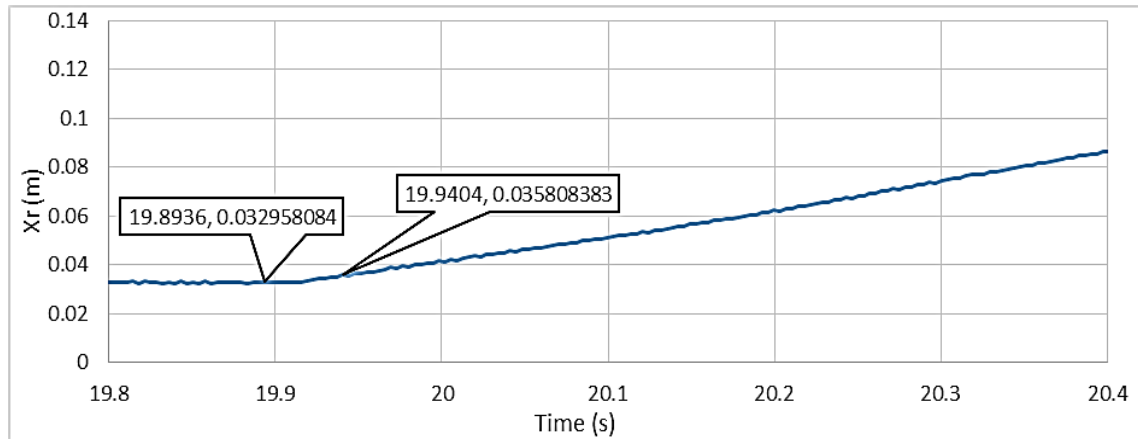


Fig. 3.13. Experimental road displacement as a function of time.

$$\dot{x}_r = \frac{0.0358 - 0.0329}{19.9404 - 19.8936} = 0.0619 \text{ m/s} \quad (3.51)$$

and the relative displacements and wheel and body velocity values are:

$$X_w = 0.0777 \text{ m}, \quad X_b = 0.0725 \text{ m}, \quad \dot{X}_w = 0.0493 \text{ m/s}, \quad \dot{X}_b = 0.1682 \text{ m/s}$$

Using Equation 3.36 with the experimental data when $t = 19.9404$ s and the values from Equations 3.49 and 3.50, the following values were obtained:

$$k_t = 9.2 \times 10^5 \text{ N/m} \text{ and } b_t = 3886 \text{ N/m/s} \quad (3.52)$$

- Identify bulk modulus [β_{re}]

To identify the compressibility of a fluid, β_{re} , it is necessary to calculate the hydraulic undamped natural frequencies in the system. Perhaps, this one fluid parameter causes concern in its numerical evaluation due to other effects. To elaborate, the types and lengths of pipes that the oil passes through must be known to measure β_{re} . The road servovalve has two lines, as schematically shown in Fig. 3.14, of steel and hosepipe of specific length and diameter, also shown in Fig. 3.14.

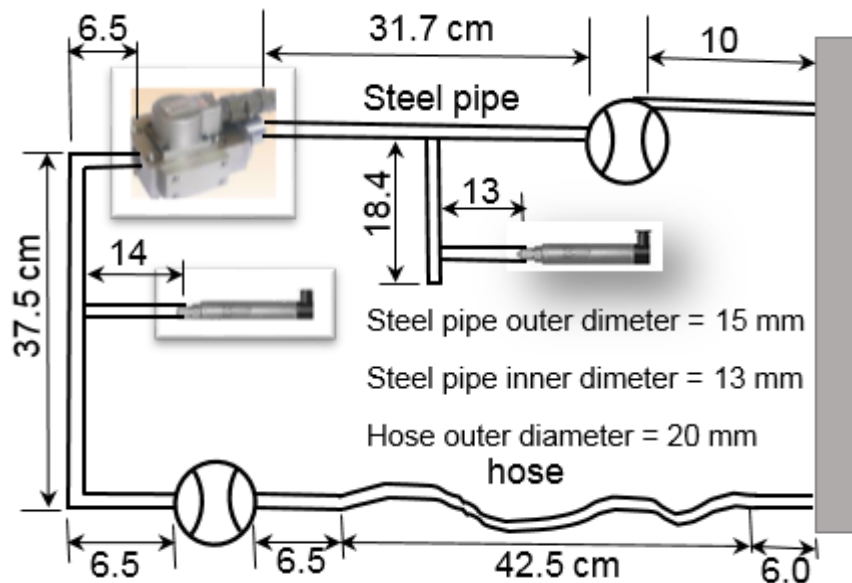


Fig. 3.14. Schematic for the servovalve including upper and lower pipes.

For the upper steel pipes, the following formula can be used to calculate the effective bulk modulus (Watton 2009):

$$\frac{1}{\beta_{es}} = \frac{1}{\beta_o} + \frac{1}{\beta_s} \quad (3.53)$$

where, β_{es} is the effective bulk modulus for steel pipe, β_o is the oil bulk modulus equal to $1.6e9 \text{ N/m}^2$ and β_s is the steel pipe bulk modulus.

According to (Watton 2009), the following equation can be used to find β_s as follows:

$$\frac{1}{\beta_s} = \frac{2}{E} \left[\frac{d_o^2 + d_i^2}{d_o^2 - d_i^2} + \nu \right] \quad (3.54)$$

where, E is the modulus of elasticity equal to $2e11 \text{ N/m}^2$, d_o is the outer steel pipe diameter equal to 15 mm , d_i is the inner steel pipe diameter equal to 13 mm and ν is the Poisson's ratio equal to 0.25.

Therefore, the bulk modulus was found to be:

$$\frac{1}{\beta_s} = \frac{2}{2e11} \left[\frac{0.015^2 + 0.013^2}{0.015^2 - 0.013^2} + 0.25 \right]$$

$$\frac{1}{\beta_s} = 7.2857e - 11 \quad \rightarrow \quad \beta_s = 1.372e10 \text{ N/m}^2 \quad (3.55)$$

and the effective bulk modulus was found to be:

$$\frac{1}{\beta_{es}} = \frac{1}{2e11} + \frac{1}{1.372e10} \quad \rightarrow \quad \beta_{es} = 1.43e9 \text{ N/m}^2 \quad (3.56)$$

Meanwhile, the bottom line is mixed and consists of both steel pipe and hose. For the steel pipe part, the effective bulk modulus remains equal to $1.43e9 \text{ N/m}^2$. While the effective bulk modulus for hose, β_h , part is quite complex to calculate. From the previous study, the hose bulk modulus is significantly lower than that for oil since in this study it was used the estimated hose bulk modulus from a transient test conducted by (Watton and Xue 1994), the values of it being around 30% from oil bulk modulus.

Therefore, hose bulk modulus can be approximately calculated using:

$$\beta_h = 30\% * \beta_o \quad (3.57)$$

giving:

$$\beta_h = 30\% * 1.6e9 = 0.48e9 \text{ N/m}^2 \quad (3.58)$$

By comparing between β_s and β_h it is clear that $\beta_s \gg \beta_h$, thus, β_s is the dominant bulk modulus and the hose effective bulk modulus is:

$$\frac{1}{\beta_{eh}} = \frac{1}{\beta_o} + \frac{1}{\beta_p} \quad (3.59)$$

giving:

$$\beta_{eh} = 1.43e9 \text{ N/m}^2 \quad (3.60)$$

in conclusion then, a β_{re} of $1.43e9 \text{ N/m}^2$ can be used for both lines.

The other two parameters, B_{vr} and R_{ir} , were found using the same approach as (Surawattanawan 2000) to give:

$$B_{vr} = 500 \text{ N/ms}^{-1} \text{ and } R_{ir} = 2.45e11 \text{ Nm}^{-2}/\text{m}^3\text{s}^{-1}$$

3.9 Comparing experimental and simulation results

At this stage of the current passive suspension system investigation, the results were collected for all the different parameters: the displacement's and velocity's of the road, wheel and car body, as well as the relative movements between the wheel and body, together with the proposed controller and flow rate signals for both side of the chamber, in addition to monitoring of the CPL experimentally captured from load cells. A developed and compiled C++ script was used to compare the experimental and mathematical simulation model results. In this study, results were collected by varying the step inputs and inflation pressures, which could be more important for this state. Three step input values of 30, 50 and 70 mm and three inflation pressures of 15, 25 and 35 psi were used.

The experimental and simulation results are displayed in two columns; the left-hand side representing the experimental data and, in comparison with, the right-hand side shows the simulation results. The results for the three different test cases are as follows:

➤ **Amplitude = 70 mm**

Fig. 3.15 shows the experimental step inputs, $X_r = \mp 70$ mm which consists of the original square signal inputs and the measured road inputs, in comparison with the mathematical model simulation results. It is evident that the behaviour is identical in terms of the magnitude of values between the experimental and simulation results, this is a necessary condition to make a satisfactory comparison between experimental and simulation results.

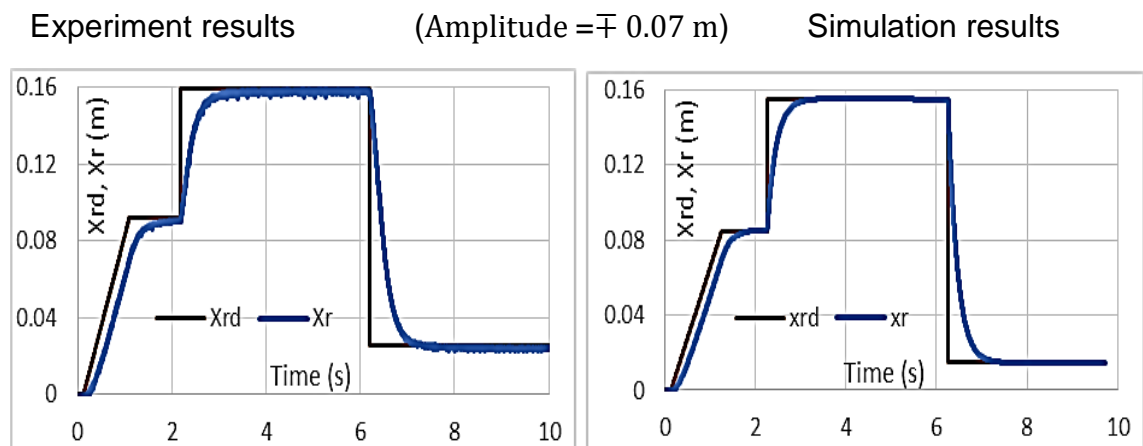


Fig. 3.15. Comparing both step, X_{rd} and road, X_r input results.

Fig. 3.16 shows the results of the proposed PI controller. The experimental and simulation controllers having the same behaviour, but with different magnitudes of the voltage representing the control forces with a scaling factor close to 3. This could be because of an incorrect conversion factor for sensor.

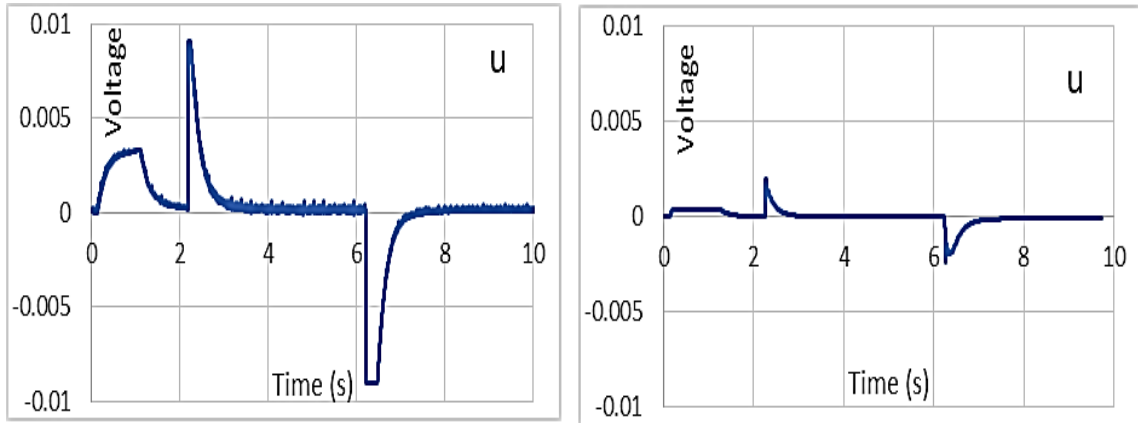


Fig. 3.16. Control force supposed to be the system.

Fig 3.17 shows the experimental validation of wheel and body displacement, with good agreement between the model and experimental results. It is clear that at the beginning of the test, the body travel was delayed compared to the wheel movement and that any sudden input changes relate to the stiction region or static friction effects. In addition, there are differences between them at any changes in the dynamic input, this could be because of dynamic friction, as mentioned in Section 3.3.1.1.

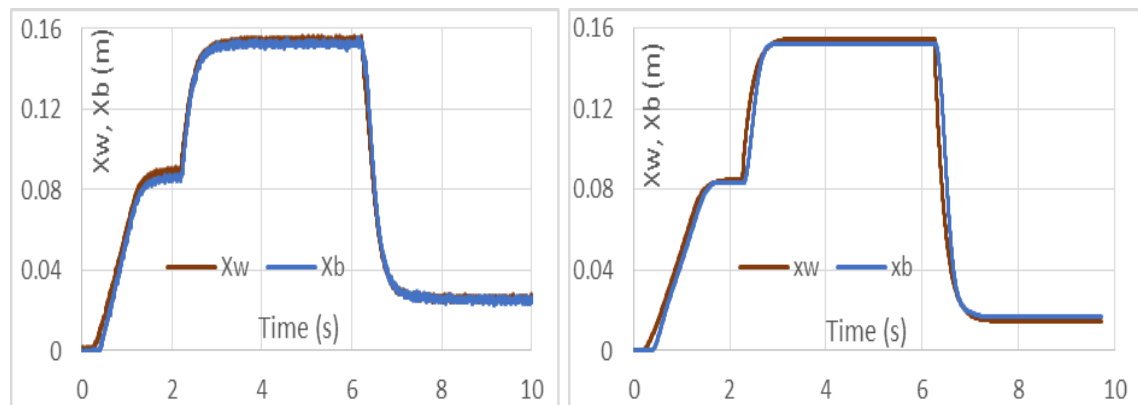


Fig. 3.17. Comparing X_w , X_b , (m), experimental and simulation results.

A comparison between experimental and simulation body and wheel velocity shown in Figs. 3.18 and 3.19 respectively.

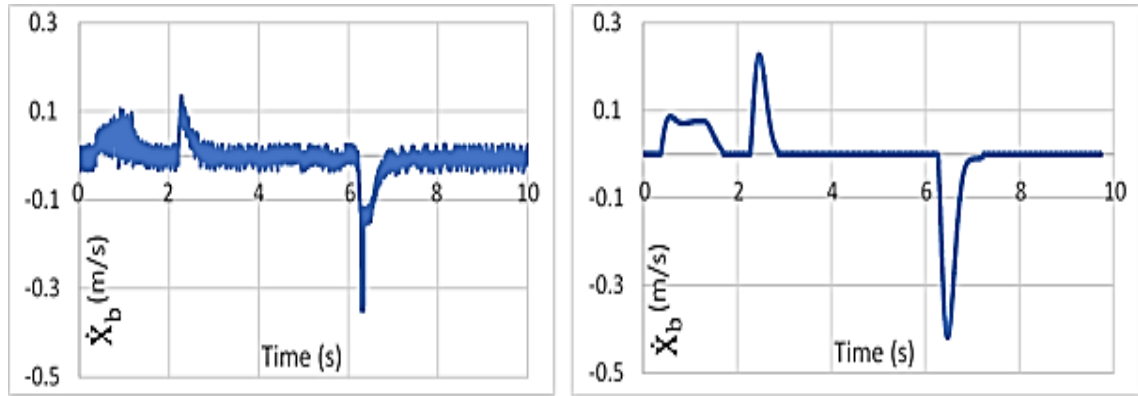


Fig. 3.18. Comparison between body velocity, \dot{X}_b , (m/s) results.

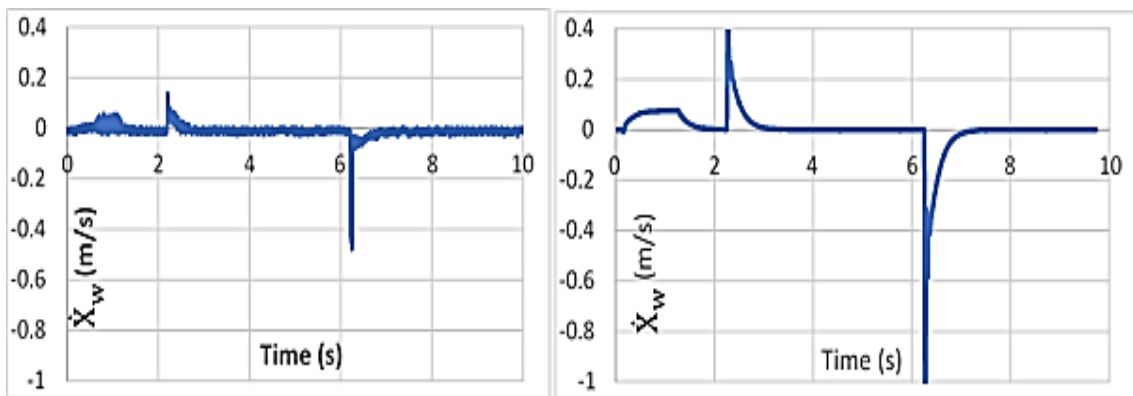


Fig. 3.19. Comparison between wheel velocity, \dot{X}_w , (m/s) results.

It can be observed that although they have the same behaviour, there are insufficient values in agreement between the experimental and simulation results for both body and wheel velocity. This could be related to using the incorrect gain sensor (WGS2). The agreement between the experimental and simulation results could be enhanced using a 10 V/m/s gain sensor as mentioned in **Chapter 2**. In general, there is a difference in the values whereby the body and wheel velocity's in the simulation are higher than the experimental data. A scaling factor of approx. 2 was used.

Fig. 3.20 shows the relative movement of the wheel and body mass for the experimental and simulation results. It is evident that at the beginning of the test, there are significant differences between the wheel and body movements relative to stiction effects. This signal helped to reveal the friction effects, as displayed in **Chapter 4**. The high noise levels in some of the experimental results might come from the sensory characteristics. In general, behaviours can be

identified, but there is insufficient agreement between the experimental and model results.

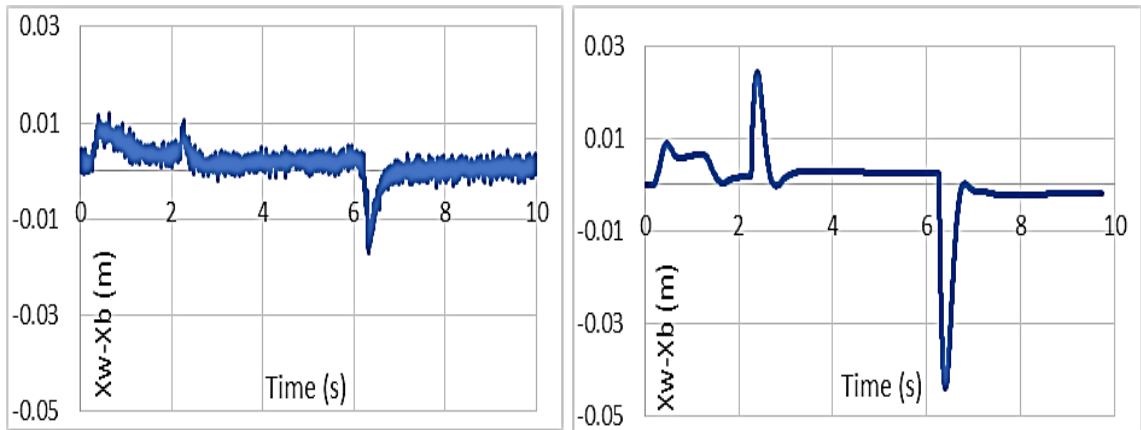


Fig. 3.20. Comparison between relative movement, $X_w - X_b$ (m) results.

Figs. 3.21 and 3.22 show a comparison between experimental and simulation results for flow rates in both sides of the road actuator chambers. Behaviours can be identified, but there insufficient agreement in the values between the experimental and simulation results. A scaling factor of approx. 2 was used which could have caused inaccuracy in the gain sensor in addition to high noise level experienced due to the characteristics of the sensor.

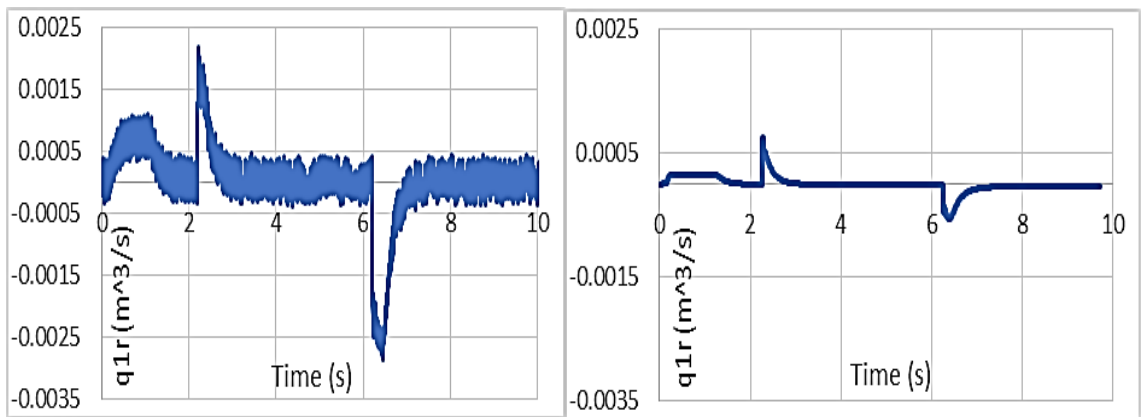


Fig 3.21. Comparing chamber 1 flow rate.

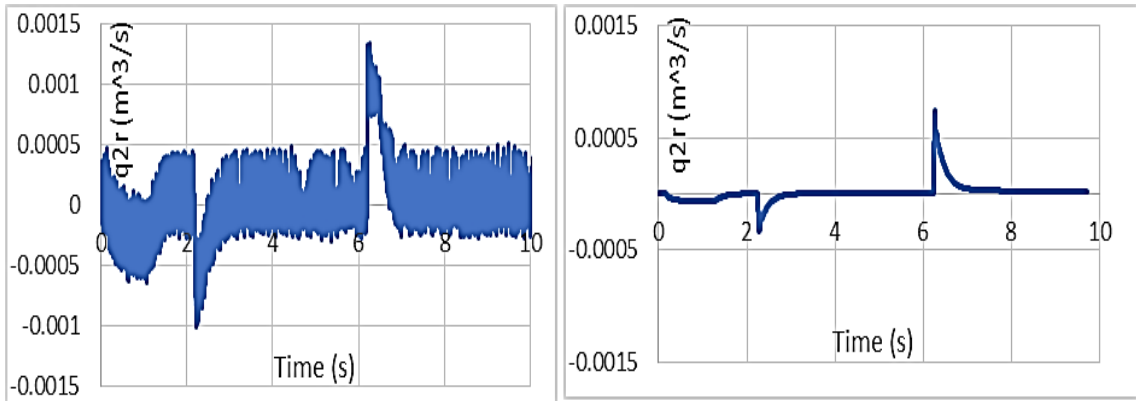


Fig 3.22. Comparing chamber 2 flow rate.

Fig. 3.23 shows the CPLs collected from the nine load cells, which were put beneath the tyre, in comparison with the results acquired from the simulation model using a developed and compiled C++ script.

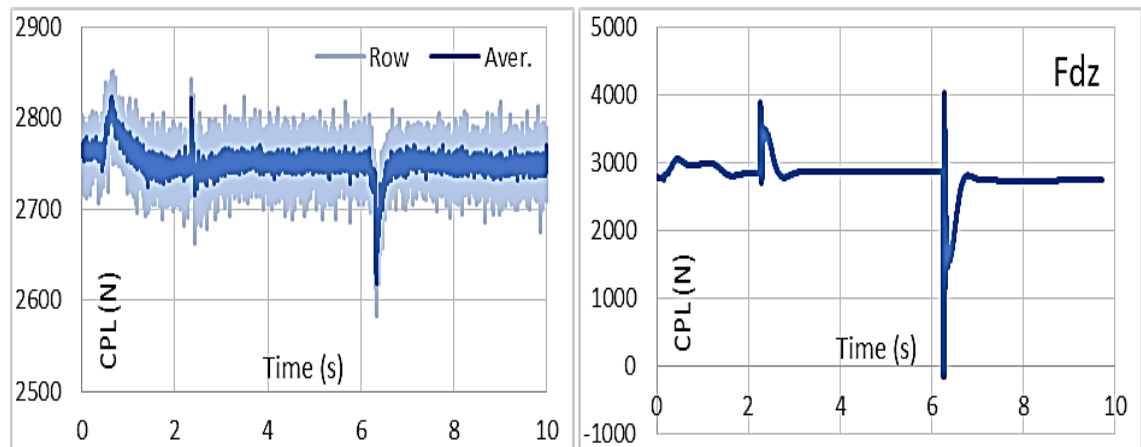


Fig. 3.23. Comparing CPL (N) experimental and simulation results.

It is evident that only dynamic CPL will be changed, attached to the system inputs and dynamism to follow the road input forces, i.e. for the steady-state condition, loads will be reduced to a static load including the relative friction values. In general, the behaviour can be identified, but there is inadequate agreement between the experimental and simulation results. This could be because the load cells were not sensitive enough, as evidenced by the experimental results containing high noise levels. Therefore, to make the behaviour of CPL clearer, the readings are shown in two shapes in Fig. 3.23: one as the original (row) reading, the other an average (20:1) which is brighter and more precise, which was acceptable for comparison purposes.

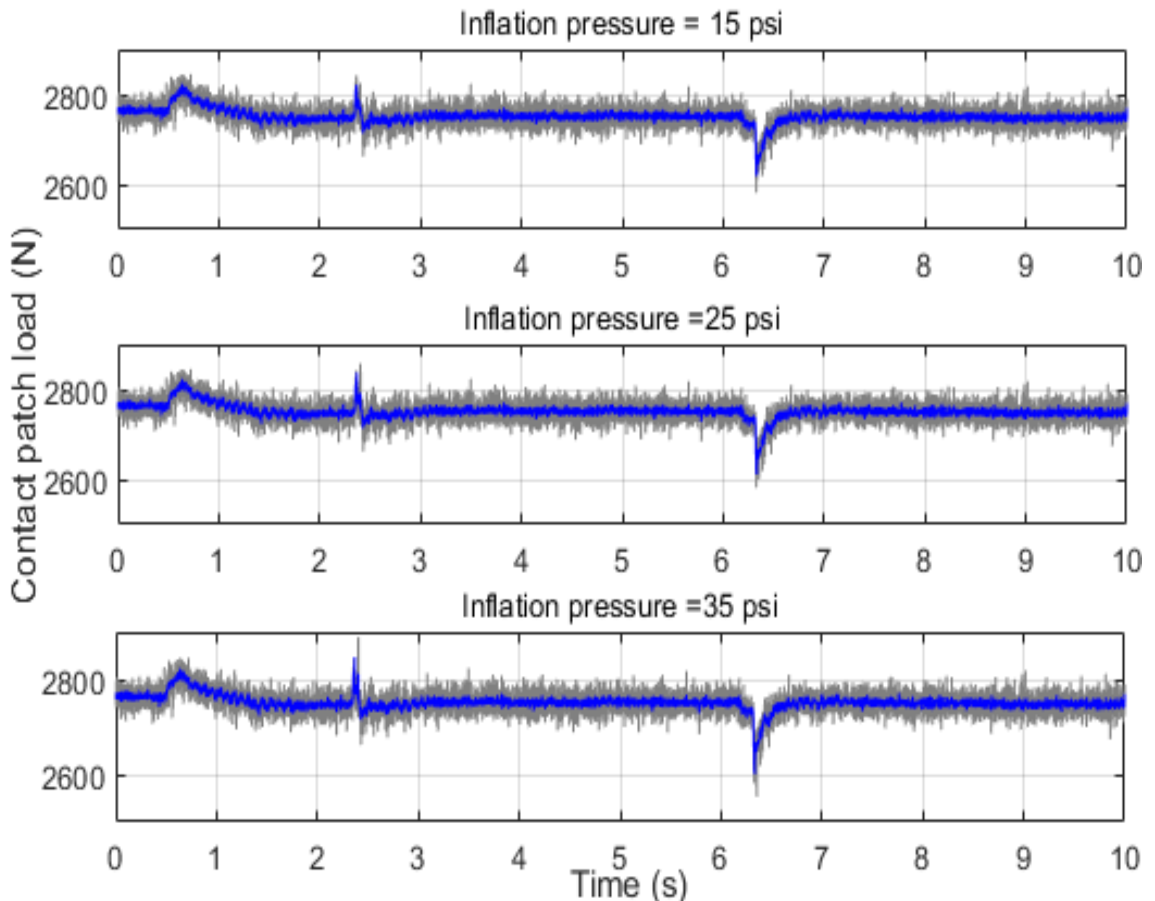


Fig. 3.24. Effect of inflation pressure on CPL for $X_r=70\text{mm}$.

In this study, the influence of inflation pressure on CPL is smaller compared with the change in the contact area. This is possibly due to the limitations of the test rig as there is no way to measure it. It is essential to study the effect of inflation pressure on the variation in the contact area, rather than the contact load. This is because in real life, car stability and safety, particularly when cornering or manoeuvring, is directly influenced by the tyre contact area. However, studying the impact of inflation pressure on CPL helps to open-up opportunities for further in-depth research in this field. Three different inflation pressures were used to demonstrate their effect on CPL, as shown in Fig. 3.24. It is clear that for dynamic forces, if the inflation pressure increases, there is a slight increase in the contact load without changes in the step inputs.

➤ **Amplitude = 50 mm**

For this case, the consistent processes to account for the system response behaviour of parameters, such as: wheel and body displacement and velocity, were followed as for stage one as mentioned in Section 4.7. There is good performance agreement between the experimental and simulation results for all

response signals. Overall, displacement and velocity are lower than those for case one with an amplitude of 70 mm. This could be because the force inputs to the system were less. Comparisons between the system responses were shown in Figs. 3.25 to 3.32.

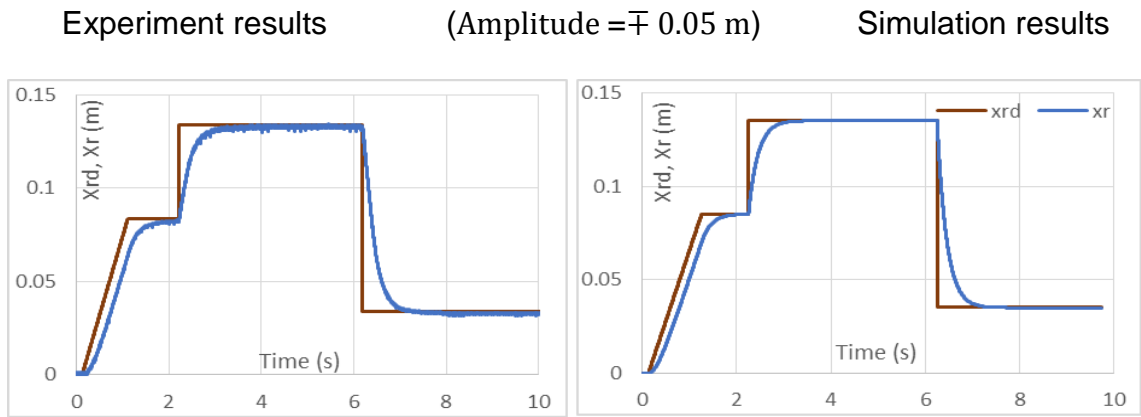


Fig. 3.25. Comparing both steps, X_{rd} and road, X_r (m) input results.

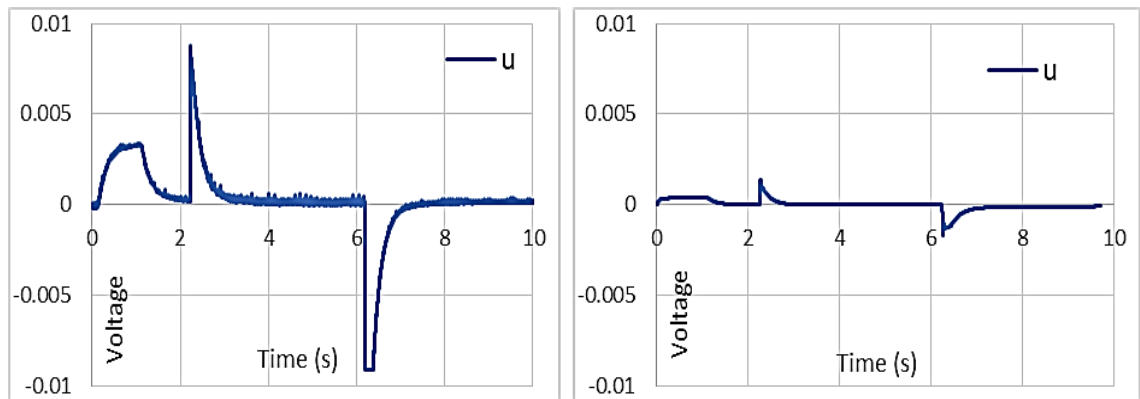


Fig. 3.26. Control force supposed to be the system.

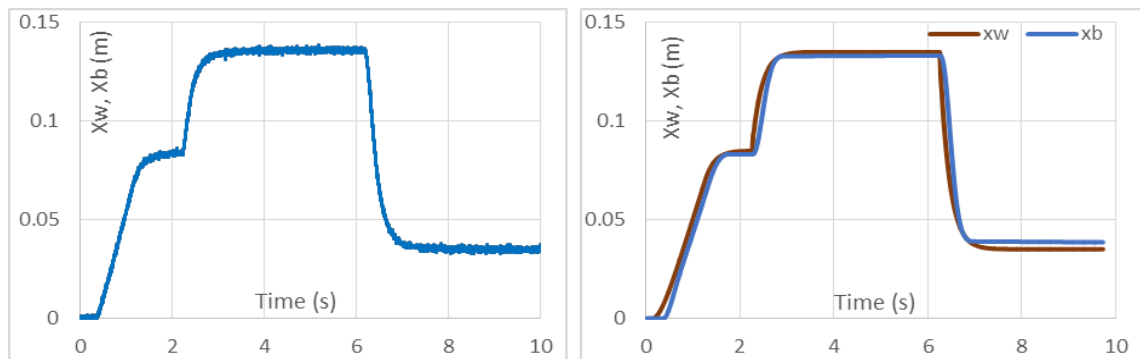


Fig. 3.27. Comparing X_w , X_b , (m) experimental and simulation results.

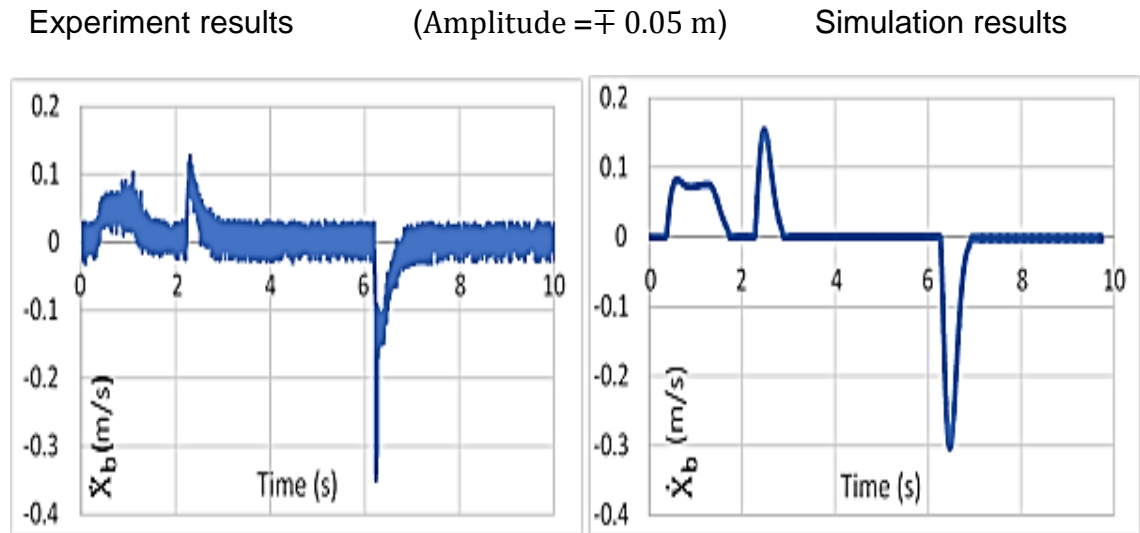


Fig .3.28. Comparison between body velocities, \dot{X}_b , (m/s) results.

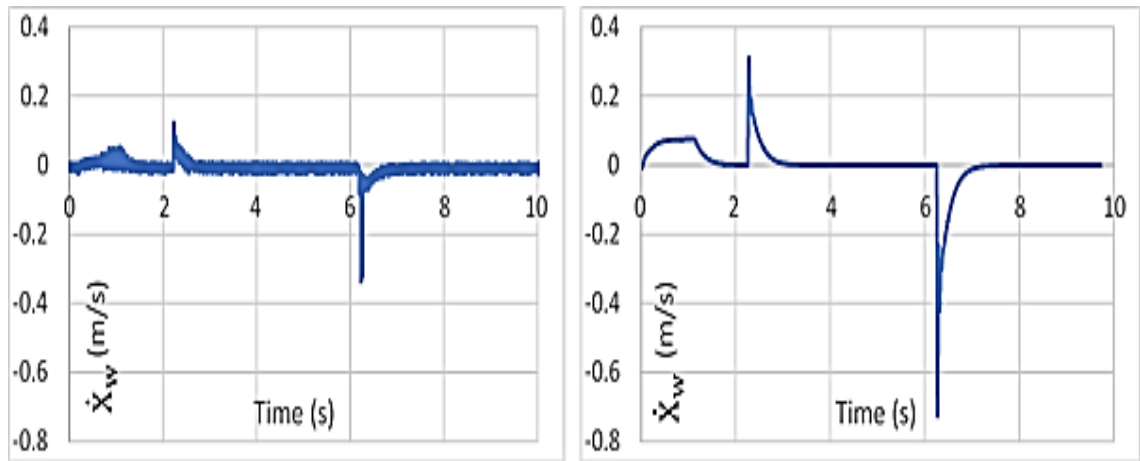


Fig. 3.29. Comparison between wheel velocities, \dot{X}_w , (m/s) results.

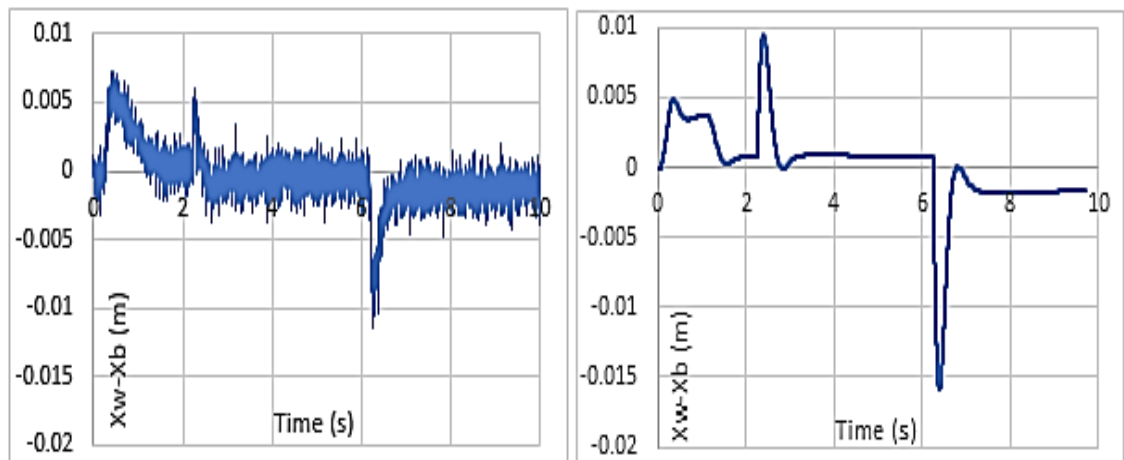


Fig. 3.30. Comparison between relative movement, $X_w - X_b$ (m) results.

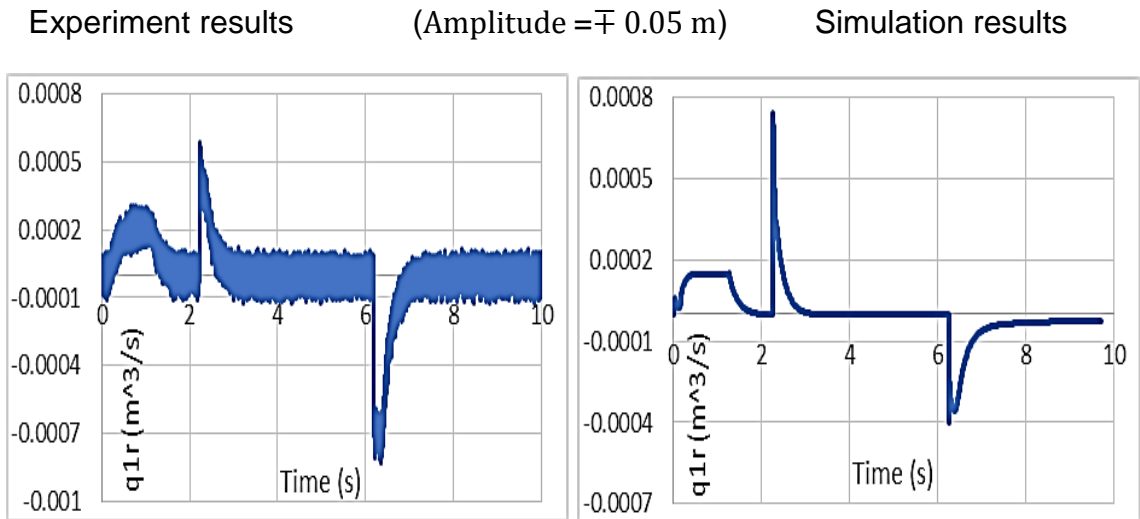


Fig. 3.31. Comparing chamber 1 flow rates.

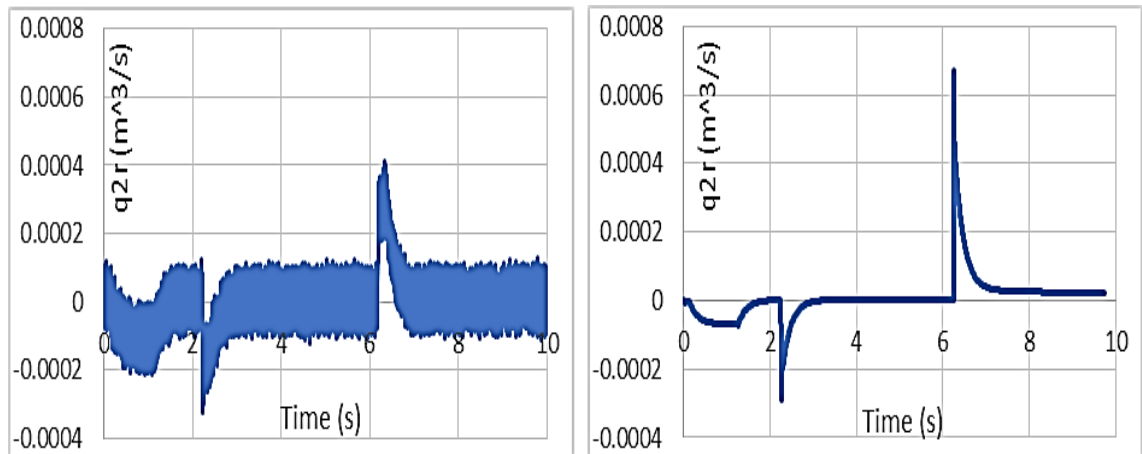


Fig. 3.32. Comparing chamber 2 flow rates.

On the other hand, Fig. 3.33 indicates that the amount of contact load is less than in case one; the reason for this is that the CPL proportional to the input forces applied to the tyre at the contact point.

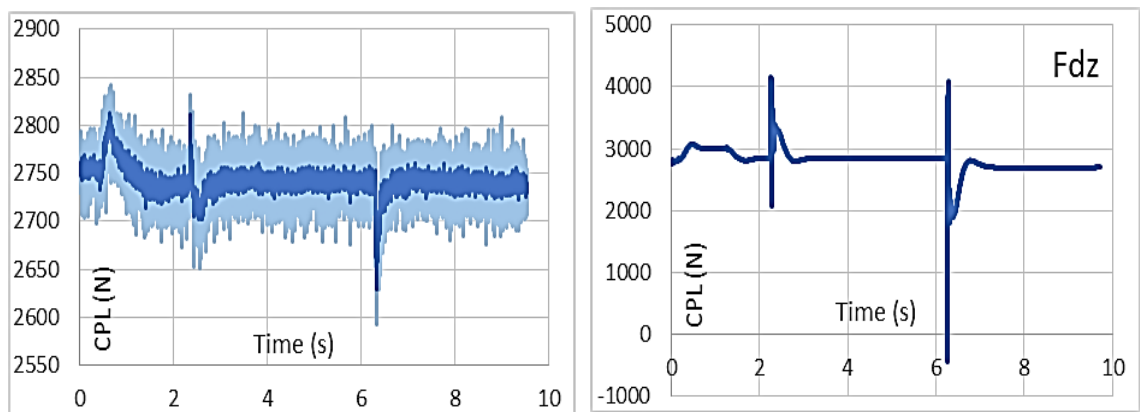


Fig. 3.33. Comparing CPL (N) experiment and simulation results.

In addition, the direct relationship between inflation pressure and CPL can be seen in Fig. 3.34, as well as the reduction in total CPL due to lower input forces.

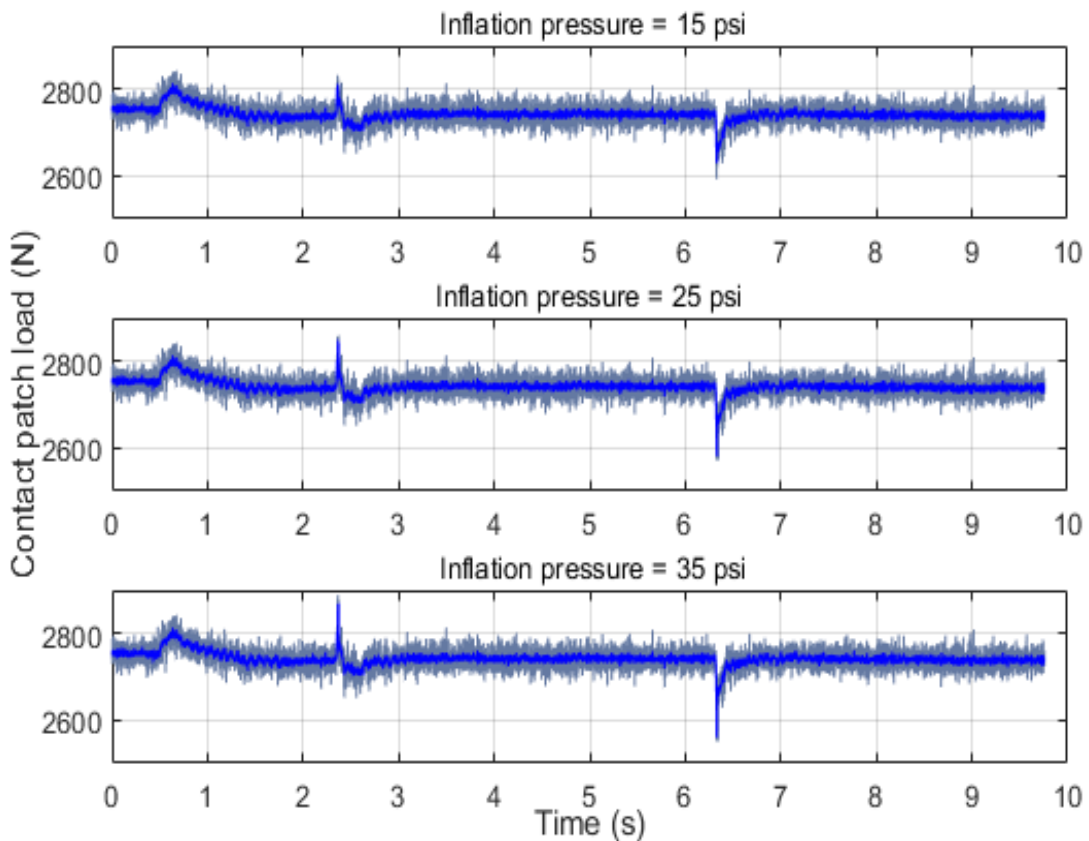


Fig. 3.34. Effect of the inflation pressure on CPL for $X_r=50\text{mm}$.

➤ **Amplitude = 30 mm**

For this case, the test was run in a similar way to the two previous cases with amplitudes of 70 mm and 50 mm. The results of the system responses and comparison between the experimental and simulation data are shown in Figs. 3.35 to 3.44.

From Figs. 3.38 and 3.39 it is evident that there more noise for the body and wheel velocities compared to previous stages with amplitudes of 70 mm and 50 mm. This is likely due to the force input being reduced to a small value resulting in the sensor readings indicating noise. Nevertheless, the agreement between the experimental and modelling results was not affected by the remaining noise, as mentioned with the two cases of amplitude = 50 mm and 70 mm.

Fig. 3.40 shows the relative travels displacement between the wheel and body; it is apparent that at the start if the test the difference was high, but smaller

than the previous two cases because of the stiction region. The position of the dynamic inputs was slightly changed, probably because the system inputs to the suspension system are lower, also resulting in sensor readings with high noise levels.

Formerly, if the applied forces reduced by decreasing the amplitude level then CPL would also decrease. Fig. 3.43 demonstrates the comparative CPL for the experimental and simulation model results when the amplitude = 30 mm.

Finally, the CPL functions corresponding to the three inflation pressures, 15, 25 and 35 psi, are shown in Fig. 3.44. It is evident that a direct relationship exists between CPL and inflation pressure, but for this case, the total forces are lower than those in the two previous cases.

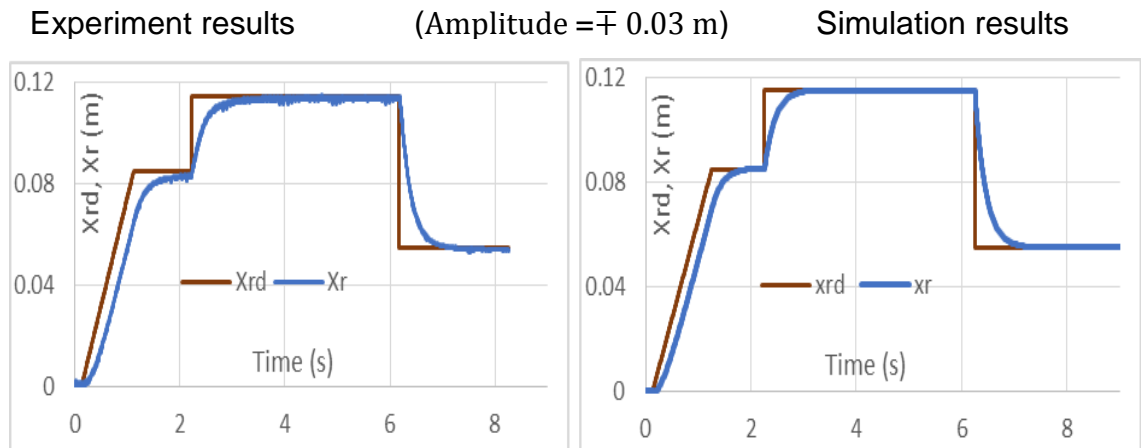


Fig. 3.35. Comparing both steps, X_{rd} and road, X_r (m) input results.

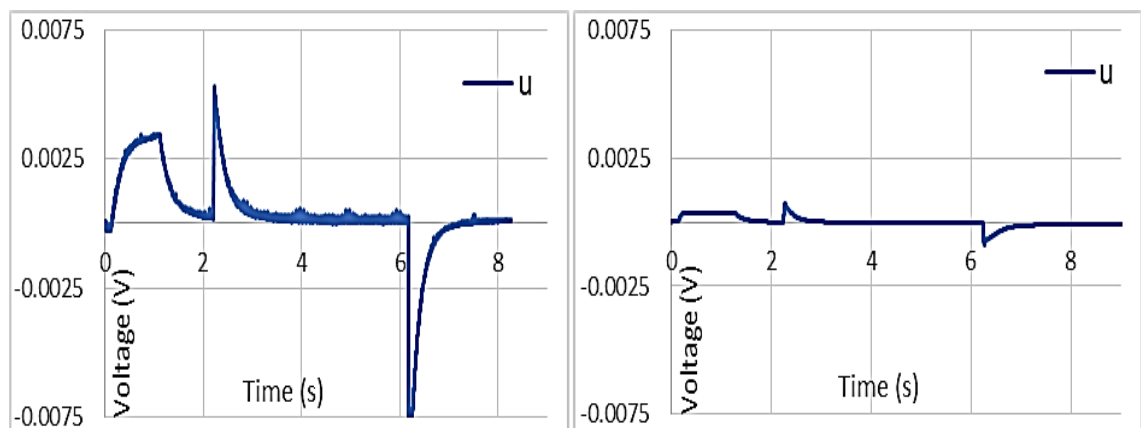


Fig. 3.36. Control force supposed to be the system.

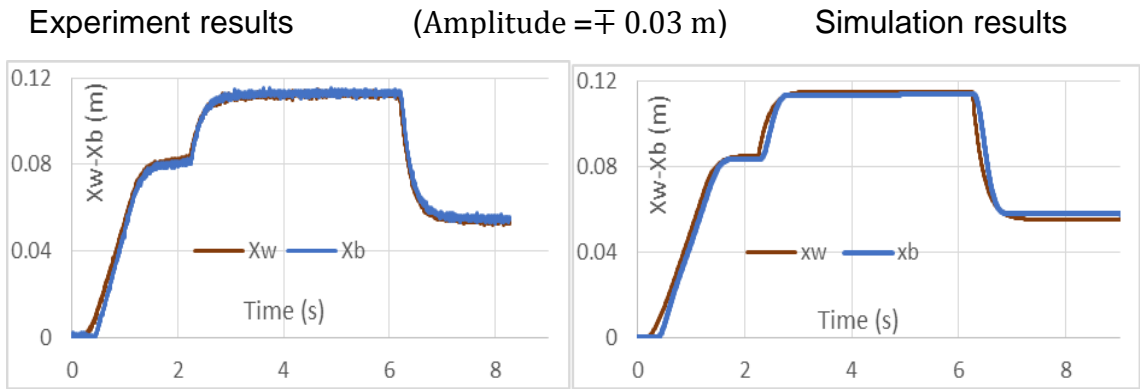


Fig. 3.37. Comparing X_w , X_b , (m) experimental and simulation results.

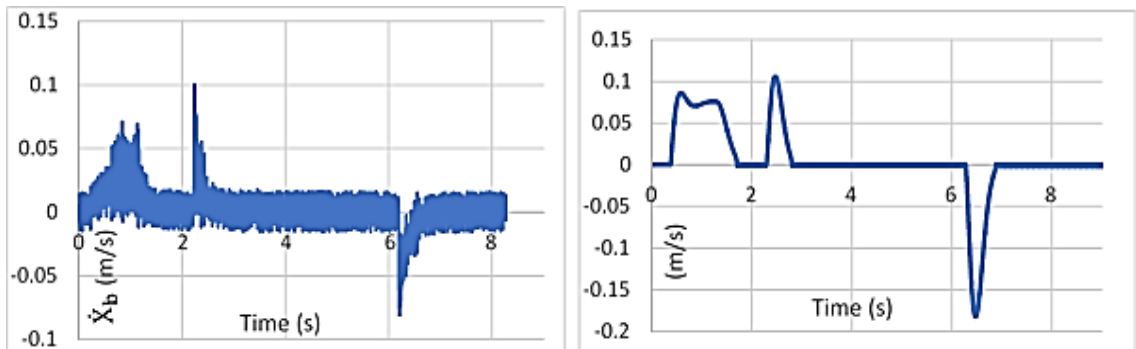


Fig. 3.38. Comparison between body velocity, \dot{X}_b (m/s) results.

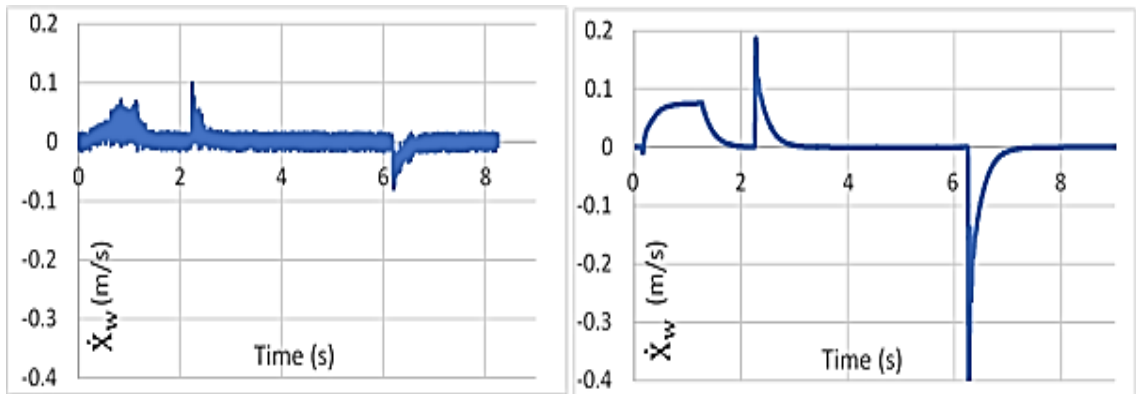


Fig. 3.39. Comparison between wheel velocity, \dot{X}_w (m/s), results.

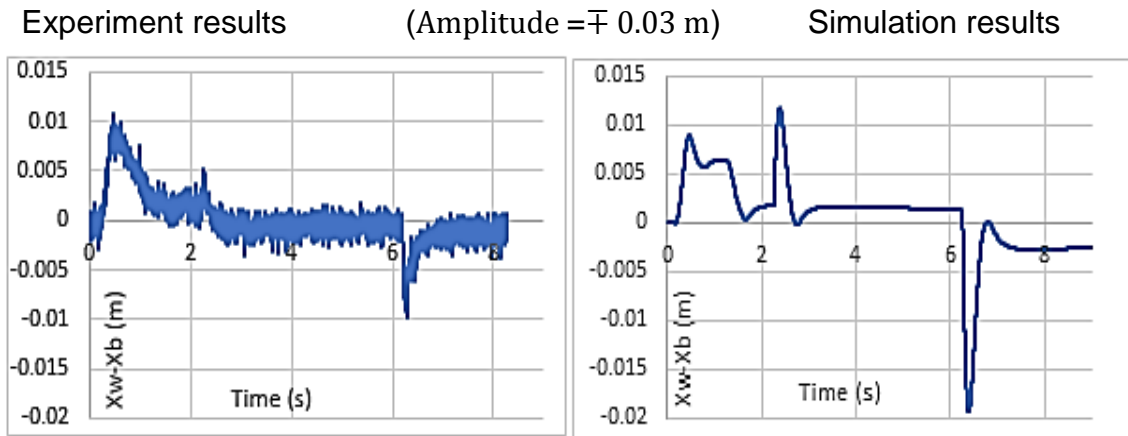


Fig. 3.40. Comparison between relative movement, $X_w - X_b$ (m) results.

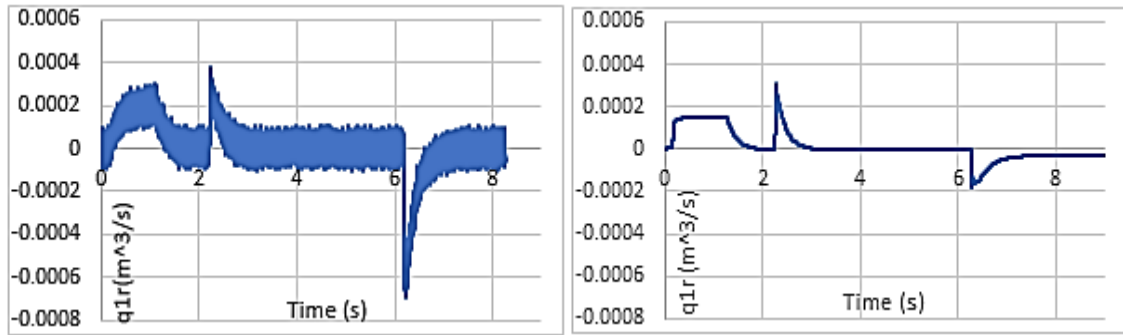


Fig. 3.41. Comparing chamber 1 flow rates.

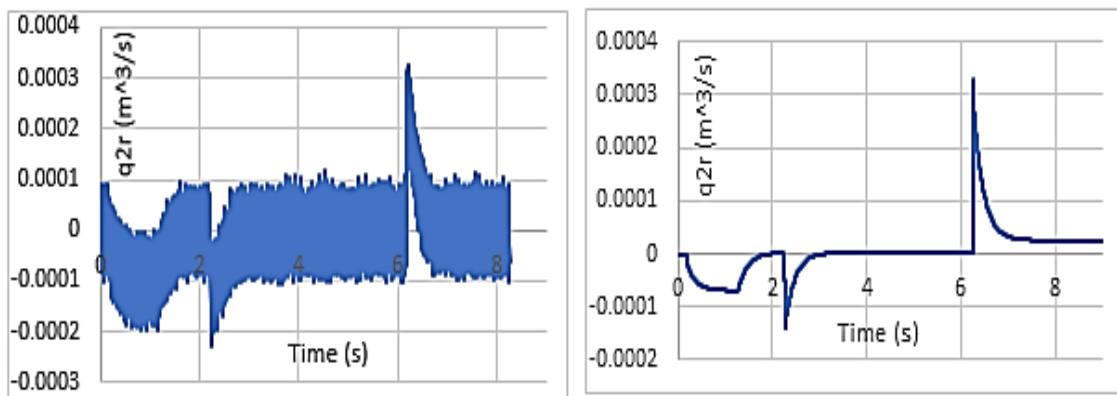


Fig. 3.42. Comparing chamber 2 flow rates.

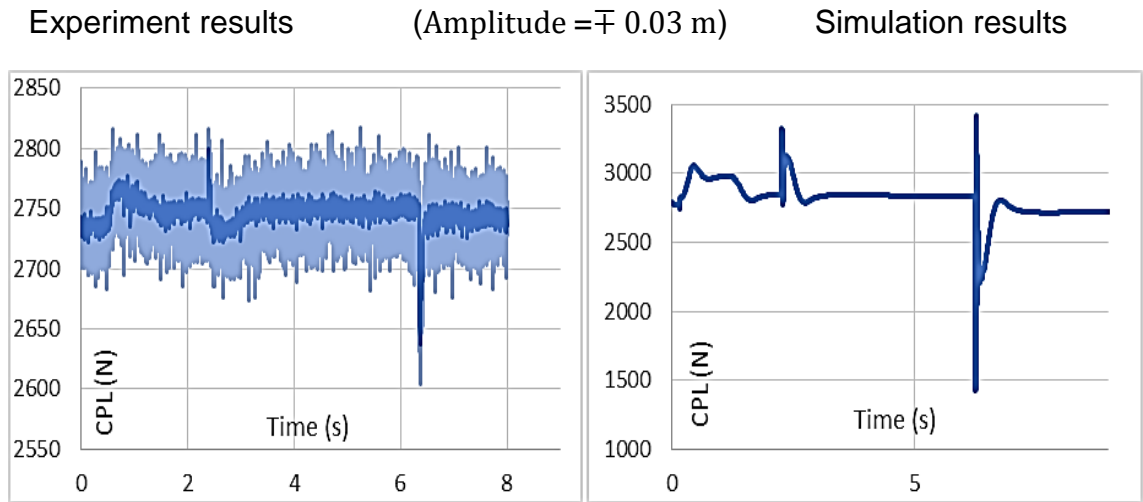


Fig. 3.43. Comparing CPL (N) experiment and simulation results.

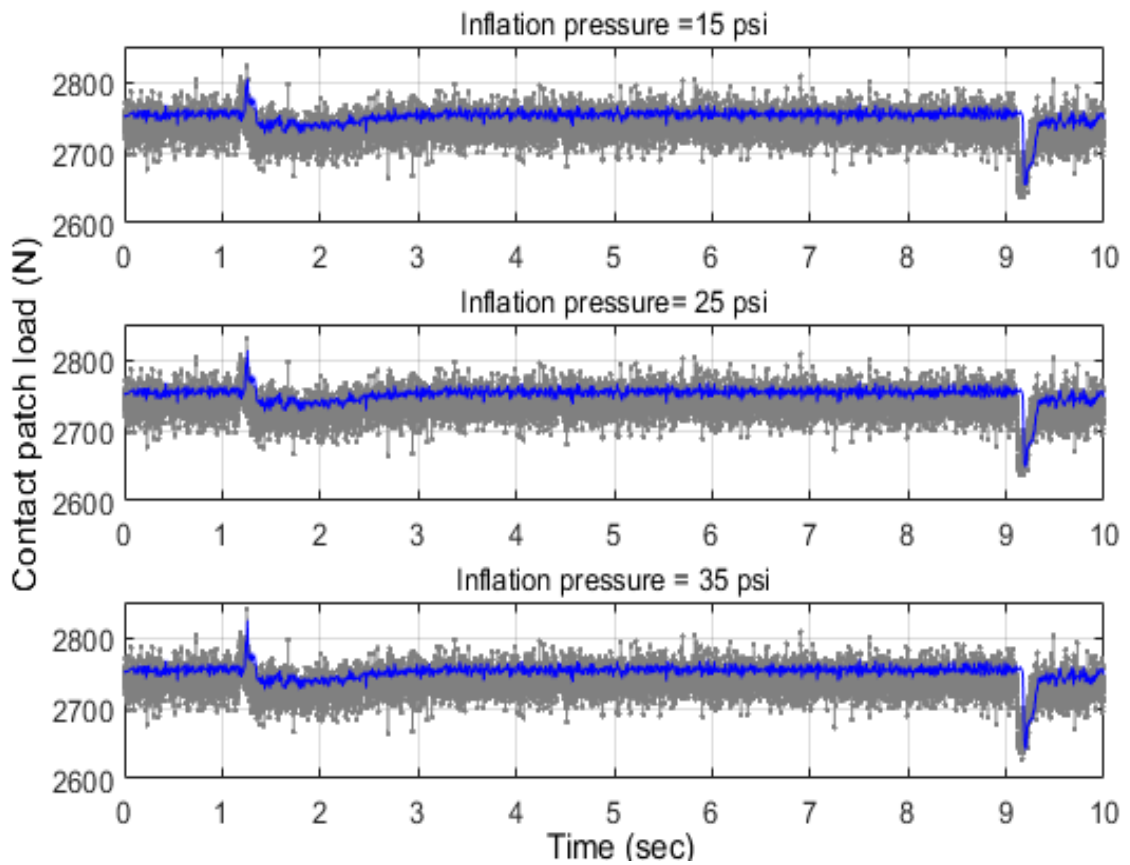


Fig. 3.44. Effect of the inflation pressure on the CPL for $X_r=30$ mm.

3.10 Discussion

This chapter was set-up to question the aspects of modelling of the passive suspension that merit inclusion within the $\frac{1}{4}$ car by considering a new term, friction force, depending on conducting experimental work and the system inputs. After a brief re-stating of the general model consideration, test rig limitations and CPL simulation model, this discussion will review and summarise the findings.

- **Road simulator for the experiment**

The road simulator system was developed to provide the mixed ramp with step or sine wave road inputs; the former should be considered for moving the hydraulic piston from the ground to the mid-point, while the latter provides the primary input, as was shown in Section 3.2. These inputs were used when testing both passive and active suspension systems for time domain studies. The bump and random inputs are used within simulations for the passive and active systems to show the control action effectiveness, as will be shown in **Chapter 6**. Displacement and velocity outputs from the road simulator system act as disturbance inputs for the active suspension system. The nonlinear mathematical model of the road simulator was investigated to utilise the model for improvement of the desired response within the stability and subsequent analyses of the passive and active suspension systems.

It was analytically found that including the leakage resistance parameter effects system stability according to the dynamic equation relating the output spool displacement of the actuator to the electrical voltage of the servovalve. It has been shown that the use of a control structure that contains an integral action is crucial to overcoming this problem. Therefore, the recommended controller is PI control.

In agreeing to the type of input, the necessary task of establishing clear system responses led to the consideration of a low pass filter, as shown in Section 3.2.3. Three amplitude rates settings of 30, 50, and 70 mm, were utilised for a precise and repeatable test examination in this review.

- **Passive suspension: theoretical studies**

In Section 3.4, the natural frequencies of the system were determined by solving the frequency equation. It was found that both natural frequencies increased as

the suspension stiffness increased, but with different gradients, by using the constant parameters from the test rig and varying the suspension stiffness within the possible suspension working space of the test rig. The natural frequency of the car body was within the range of 1.1-2.6 Hz, i.e. outside of the undesired frequency range, while the natural frequency of the wheel was within the range of 8.6-17.7 Hz.

In effect, the use of the vertical model to simulate the passive test rig was attempted. It was generally assumed that in $\frac{1}{4}$ car modelling, the damper and spring move vertically, discounting the inclination effects, which led to confronting of the issue that there were significant differences between the experimental and simulation results, as shown in **Chapter 4**. Based on this point, and the practical viewpoint that a suspension designer must optimise the system within the limited working space, the passive suspension test rig model was modified to consider the actual organisation of the damper and spring systems. Therefore, the nonlinear friction forces that affected the body bearings have been considered.

The nonlinear friction model was relatively complicated due to the involvement of different terms that were built to signify the practical phenomena as was illustrated in Section 3.3.2. This model includes two main parts: static and dynamic frictions. The latter, with two expressions, depends on the velocity, acceleration, deceleration and direction, which comprises: the Stribeck effect, Coulomb, and viscous friction. In addition, the new dynamic construction linkage angle has been accounted for, which was dynamically changed by $\mp\Delta\theta$.

- **Contact patch load (CPL)**

The CPL between tyre and road was investigated theoretically and experimentally, as shown in Section 3.3.4. Consequently, the CPL was studied as a function of varying step system inputs and inflation pressure, achieved experimentally using load cells and for the stimulation by implementing the CPL mathematical equation within the C++ program. The three classes of inflation pressure were undertaken to gain information about the effects of these categories on the CPL as illustrated in Section 3.6.

- **Experimental work**

The test rig was prepared for experimental work depending on several processes that were made and these processes including testing the sensors work, and

checking the load cells correctly fixed underneath the tyre, as demonstrated in Section 3.7.

- **Parameters identification**

At this stage, validation parameters was made in Section 3.8. Seven parameters were identified, including spring stiffness, k_s , viscous damping, b_d , tyre stiffness, k_t , viscous tyre damping, b_t , actuator viscous damping, B_{vr} , effective bulk modulus, β_{re} , and cross-port leakage resistance, R_{ir} .

- **Comparing experimental and simulation results**

In the current stage, Section 3.9, results were collected from the preliminary tests for different response parameters, as well as the proposed controller and the flow rate signal for both sides of the chamber. Additionally, monitoring of the CPL was conducted, which was experimentally captured from the load cells. A satisfactory comparison was determined between the experimental results gathered from the test rig tests and those results obtained from the mathematical simulation on the $\frac{1}{4}$ car model through C++ compiler environment. In this study, results were expanded by changing two parameters: the step inputs and the inflation pressures. The former was altered using three values, 30, 50 and 70 mm, whereas the latter was varied in the scope of three values, 15, 25 and 35 psi.

- **In summary**

With several conditions having been made, both simulation and experimental results, revealed a consistent agreement in behaviour and magnitude, when considering the correct sensor conversion factor between the experimental and simulation output. This consequently confirmed the feasibility of the new relay model for the passive suspension system which took account of the actual configuration of the test rig system and is entirely accurate and useful. This model, subsequently implemented the nonlinearity friction forces that affect the linear body bearings. The nonlinear friction model captures most of the friction behaviour that has been observed experimentally, such as the stiction region, Stribeck effect and viscous friction. These friction effects could be individually responsible for causing the relative delay difference between the wheel and body travels at the beginning of the test and the other dynamism values changing. In

addition, the nonlinear hydraulic actuator, which was covered by the dynamic equation of the servovalve, and the CPL models are moderately precise and practical. The suggested PI controller successfully derived the hydraulic actuator to validate the control strategy.

Although the CPL was studied, the effect is very miniscule in consequence of variations in the step inputs and the inflation pressures owing to the limitations of the current test rig. Nevertheless, this contribution is essential to opening up the possibility of further research into the CPL, vehicle stability, safety and road handling which are directly influenced by CPL.

Nonlinear Friction Model Identification and Effectiveness

4.1 Introduction

Friction occurs almost everywhere. Many things, including human acts, depend on it. It is usually present in machines. Usually, friction is not required, so a great deal is done to reduce it by design, or by control.

Friction is the force resisting the relative displacement between contact surfaces. Derived from the electromagnetic forces between atoms, as well as adhesion, deformation forces and the mechanical contact of asperities, friction dissipates the kinetic energy of relative motion into heat. Friction is often quantified by a coefficient of friction (μ), expressing the ratio of the friction force to the applied load (Nichols 2007).

The spearheading work of Amontons, Coulomb, and Euler, who attempted to clarify the friction phenomenon regarding the mechanics of relative movement of rough surfaces in contact with one another, is mentioned by (Al-Bender et al. 2004). From that point forward, only sporadic consideration has been paid to the vital question of friction as a dynamic process that changes on contact. Instead, the most significant proportion of the investigation has concentrated on describing and evaluating complex mechanisms, such as adhesion and deformation that contribute to development of frictional resistance, while frequently ignoring the dynamic aspects of the issue. Consequently, despite those mechanisms being relatively well researched, characterised and understood, no efficient and comprehensive model has emerged for the evolution of the friction force as a function of the states of the system; namely time, displacement and velocity. The requirement for such a model is now becoming more urgent, since the consideration of the friction force dynamics proves essential to understanding and control of systems, including rubbing elements, from machines to earthquakes. Therefore, if it were possible to qualify and quantify this friction force dynamic, it would be a relatively simple step to treat the dynamics of a whole system comprising friction; thus, our results are consistent with their findings.

Friction is a very complicated phenomenon arising from the contact of surfaces. Experiments indicate a functional dependence upon a large variety of parameters, including sliding speed, acceleration, critical sliding distance, normal

load, surface preparation and, of course, material combination. In many engineering applications, the success of models in predicting experimental results remains strongly sensitive to the friction model.

A fundamental, unresolved question in system simulation remains: what is the most appropriate way to include friction in an analytical or numerical model and what are the implications of the chosen friction model?

From a control point of view, friction is an essential aspect of many control systems for both high quality, servomechanisms and hydraulic systems. Friction can lead to tracking errors, limit cycles, and undesired stick-slip motion. Control strategies that attempt to compensate for the effects of friction, without resorting to high gain control loops, inherently require a suitable friction model to predict and compensate for the friction. Even though no exact formula for the friction force is available, friction is commonly described in an empirical model. Nevertheless, for precision/accuracy requirement, a good friction model is also necessary to analyse stability, predict limit cycles, find controller gains, perform simulations, etc. Most existing model-based friction compensation schemes use classical friction models, such as Coulomb and viscous friction. In applications with high precision positioning and with little velocity tracking, the results are not always satisfactory. A better description of the friction phenomena for small velocities, especially when crossing zero velocity, is necessary. Friction is a natural phenomenon that is quite difficult to model and is not yet completely understood (De Wit et al. 1995).

From a friction type point of view, in fluid or grease lubricated mechanisms, friction decreases as the velocity increases away from zero. In general terms, this effect is understood. It is due to the transition from boundary lubrication to fluid lubrication. In boundary lubrication, extremely thin, perhaps monomolecular, layers of boundary lubricants that adhere to the metal surfaces separate metal parts. These lubricant additives are chosen to have low shear strength, so as to reduce friction, proper bonding and a variety of other properties such as stability, corrosion resistance or solubility in the bulk lubricant. Boundary lubricants are standard in greases and oils specified for precision machine applications. It should be noted that in virtually all the requests, it is the prevention of wear during start and stop that dominates the choice of boundary lubricant. With the exception of when lubricants and the friction properties of boundary lubricants are a

secondary consideration (Rabinowicz 1965) (Horst 1978). Therefore, this study considers transition friction.

This study found that friction helps to remove a vibration, or oscillation, from mass body displacement as the damping contributes in the test rig. That was unexpected because it always caused the system to deteriorate and friction to be incorporated with the primary target of suspension system performance, the primary study objective. However, unfortunately, while that clearly occurs with the test rig, in real life, the connection between the suspension system and the car body does not allow the body to slide in anywhere, despite existing joint frictions. Therefore, it is vital to consider friction in this study and this novel contribution takes into account the friction with the test rig and implements with a $\frac{1}{4}$ car suspension model (Al-Zughaibi 2018). In addition, the author hopes to contribute towards a reconsideration of friction with conventional car suspension models.

4.2 Why considering friction within this study?

In our test rig, a $\frac{1}{4}$ - race car, to achieve the primary target of this test rig and the design requirements, the designer had to force the mass body to move in vertical lines as described in **Chapter 2**. Therefore, a 240 kg mass plate, used to represent a $\frac{1}{4}$ car body, is organised to move vertically via two linear bearings. Two rails, THK type HSR 35CA, 1000 mm long and parallel to each other, are used with each linear bearing. A double wishbone suspension linkage was chosen because it preserves the geometry of a wheel in an upright position independent of the suspension type used. The wheel hub is connected to the chassis, which is attached to the car body. The test rig passive suspension photograph was shown in Fig. 2.3 in **Chapter 2**, while the schematic diagram is shown here in Fig. 4.1.

(Surawattanawan 2000) conducted simulation and experimental study for the same test rig without consideration of the real position for the Spring and Viscous Damper (S and VD); as a result, the friction effects were ignored. However, in the author's opinion, the real inclined position of S and VD should be considered. Accordingly, the test rig design and the input type help to generate a normal force at the body bearings and a vertical force relative to body movement, as will be demonstrated by the free body diagram of test rig later. This force is

responsible for generating Coulomb friction at body lubricant bearings. In addition, the mass body has been slipped on lubricant bearings; this will undoubtedly generate viscous friction. Therefore, it is essential to consider these frictions in the current study, qualified by the critical effects of friction in any system, as well as their effects on results. The explanation of friction models and their effects will be described later.

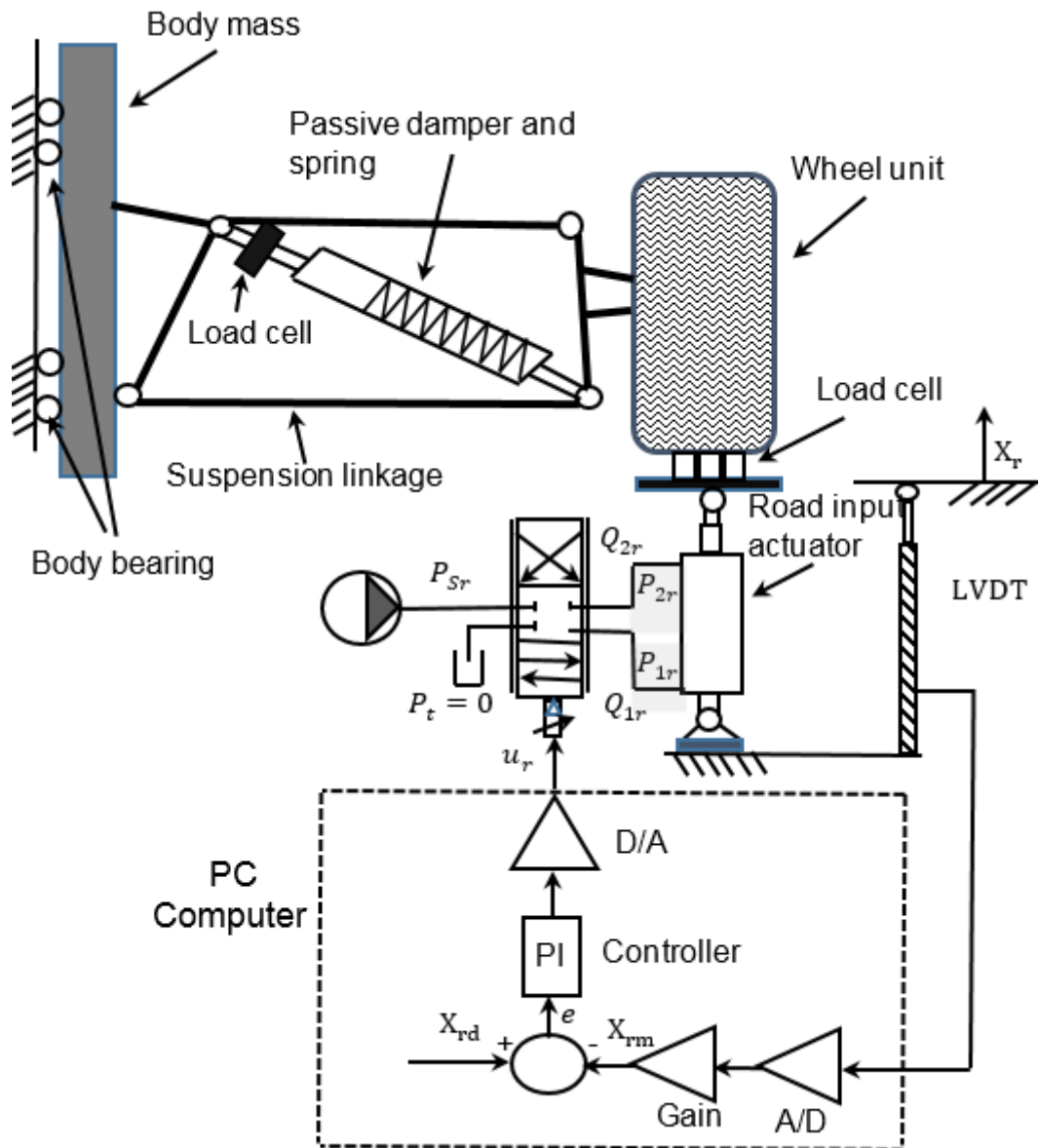


Fig. 4.1. Schematic diagram of the test rig.

Following completion of the passive suspension experimental work, an attempt to model these experimental tests by developing a passive suspension model, as mentioned in **Chapter 3**, was pursued. The simulation was achieved through developing code in C++. An issue arose in that a considerable difference was found between the body displacement observed in experiments and in the simulation results. From this aspect, the idea of considering friction force emerged. In the remainder of this study, algorithm control to enhance suspension performance is examined, it was deemed that identification of friction in the test rig is crucial to achieving accurate tracking. There were two clear indicators from observation measurements, which helped to quantify the friction effects, these are discussed in the following sections.

4.3 The dynamic indicator

From the simulation results, it was found there are definite fluctuations in body displacement, as generally expected from a quarter-car suspension model, regarding our experience and references. Watton (2005) mentioned in his book “Modelling, Monitoring and Diagnostic Techniques for Fluid Power Systems” on pages (182 -186), regarding the same test rig, there was an oscillation at the car body in both experimental and simulation results, as shown in Fig. 4.2.

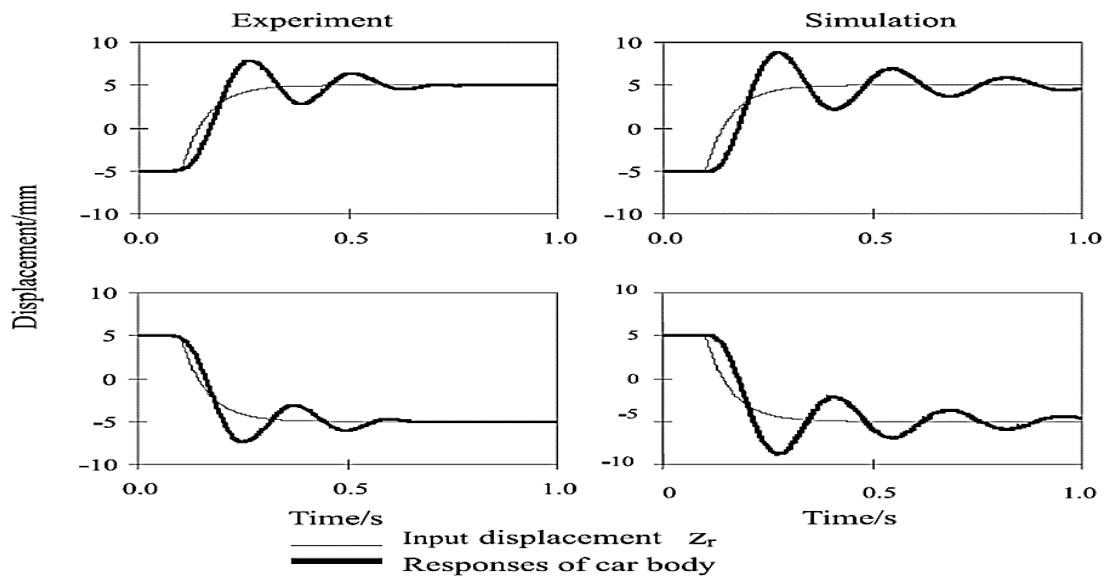


Fig. 4.2. Typical 1 DOF test result (Watton 2005).

It is clearly seen that the body displacement oscillates in the current simulation results, without implementing friction forces, as shown in Fig. 4.3. There were different in the periods of oscillation between Figs. 4.2 and 4.3. This is relative to the different models and parameters used.

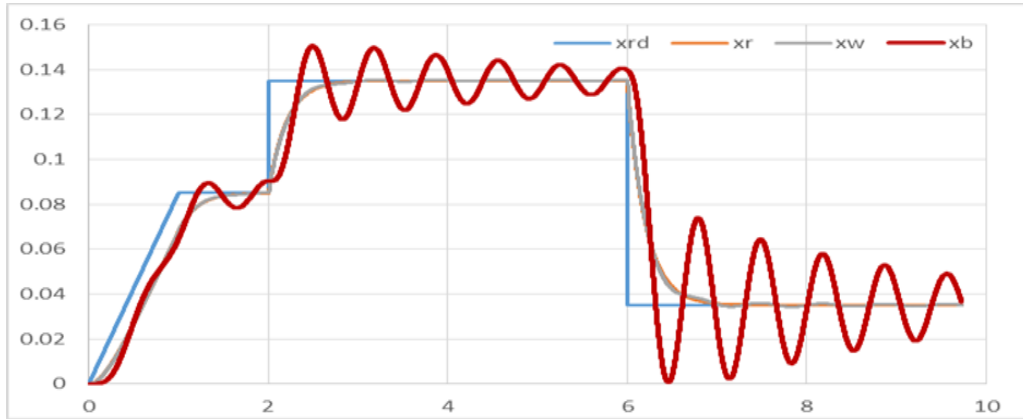


Fig. 4.3. Simulation results for X_r , X_w and X_b (m).

There were no such fluctuations in the experimental results, as shown, for example, in Fig. 4.4.

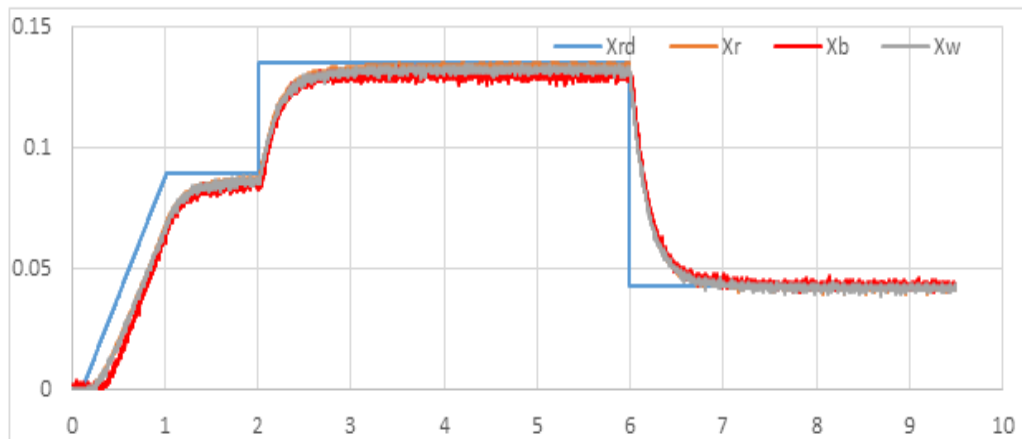


Fig. 4.4. Experimental results for X_r , X_w and X_b (m).

Figs. 4.3 and 4.4 display the desired input, without filter, for the road and the responses of the wheel and body for the present simulation and experimental results respectively. It is clearly seen that the wheel displacement follows the road displacement in both experiment and simulation results. While the body travel follows the wheel with a pure delay, which will be shown in more detail in Section 4.4, and fluctuates in the simulation results. The author named this disparity ‘a dynamic friction indicator’. This name was not unique, having been used by several authors before.

From this point of view, it could be said that for the experimental work, the friction forces at body lubricant bearings are responsible for eliminating the oscillation from the body travels.

4.4 The static indicator

In demonstrating the measured body and wheel movements, a delay is illustrated between them when the wheel rises up or falls, the body similarly travels after pure delay. The early and later stages of the wheel rise and fall respectively, the results to system input and the body delay are shown in Fig. 4.5.

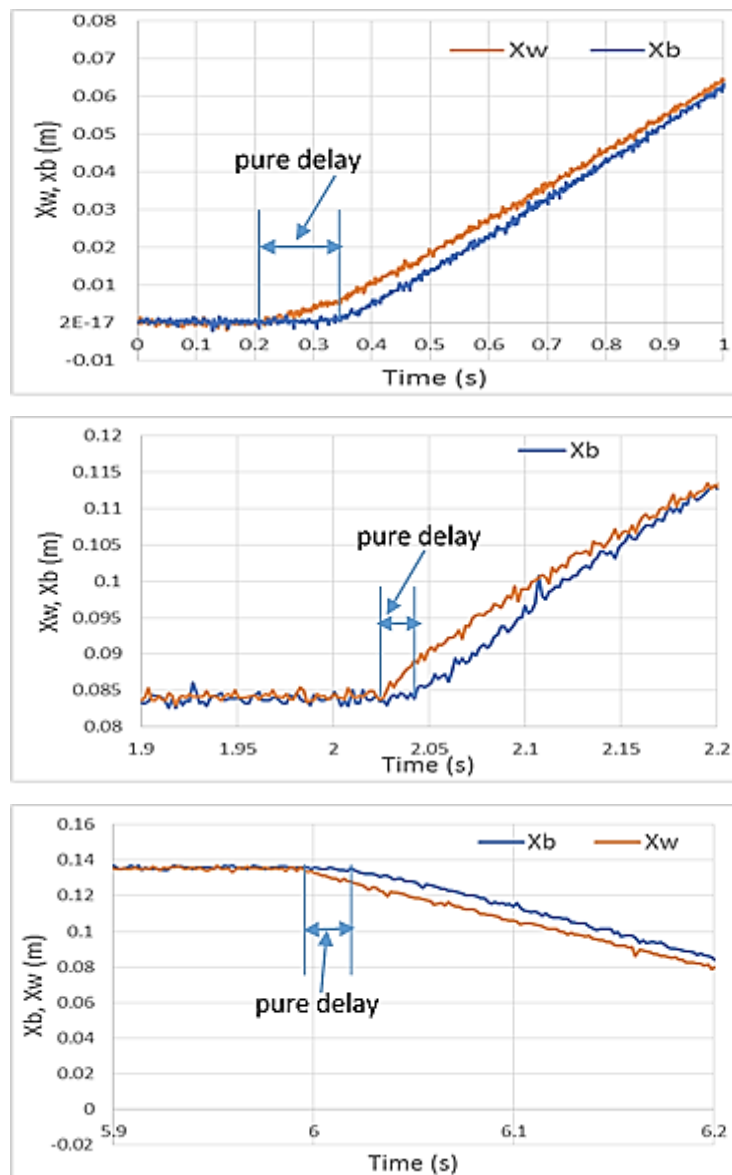


Fig. 4.5. Measurements of pure delay of X_b from X_w at three positions.

For more convenience, the experimental data of the relative travel between the wheel and body ($X_w - X_b$) was used. These are available from test rig LVTD sensors and the result is shown in Fig. 4.6. The evident noise is attribute to sensor and experimental characteristics. From this figure, it is clearly seen that there is zero difference between X_w and X_b at start of the test or for a short period, approx. 0.3 s. This is believed to be due to data acquisition delays. The differences gradually increase while the wheel starts to move up, the differences between X_w and X_b steadily increase until reaching the maximum. During this period the body sticks without movement ($X_b = 0.0$), when the resulting force overcomes the static friction, the body will start to move. The relative travel difference between them slowly reduces, approx 0.5-1.5 s, until reaching zero or near zero at Steady State (SS), after 1.5 s.

This observation, which the author named ‘static friction indicator’, leads to an investigation of the body stiction. It was found that this could be regarded as the effect of static friction force.

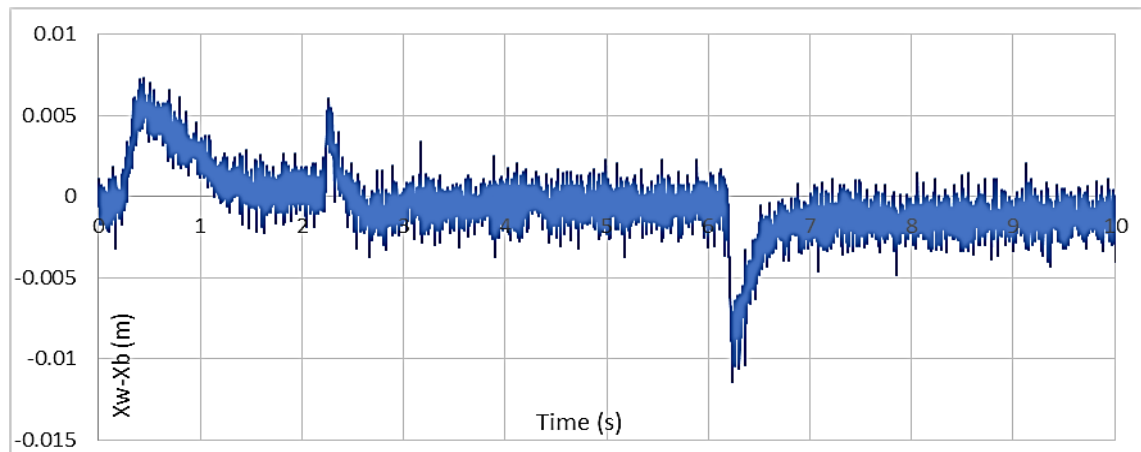


Fig. 4.6. Experimental results of difference displacements between X_w and X_b .

To include knowledge about friction in the simulation model, consideration of conventional friction was pursued, drawing upon published information. The following section reviews the approach.

4.5 Conventional friction model

The traditional friction model considered the construction of a more comprehensive friction prediction model that accounts for the various aspects of this particular phenomenon so that mechanical systems with friction can be more

accurately identified and, consequently, better controlled. Most of the existing model-based friction compensation schemes use classical friction models, such as Coulomb and viscous friction. In applications with high precision positioning and with little velocity tracking, the results are not always satisfactory. A better description of the friction phenomena for small speeds, especially when crossing zero velocity, is necessary. Friction is a natural phenomenon that is quite difficult to model and is usually modeled as a discontinuous static map between velocity and friction torque that depends on the velocity's sign. Typical examples are different combinations of Coulomb friction, viscous friction, and Stribeck effect, as mentioned in (Armstrong-Helouvry 2012), (De Wit et al. 1995) and (Lischinsky et al. 1999). However, there are several exciting properties observed in systems with friction that cannot be explained by static models. This is necessarily due to the fact that friction does not have an instantaneous response to a change in velocity, i.e. it has internal dynamics. Examples of these dynamic properties (Armstrong-Hélouvry et al. 1994) (De Wit et al. 1995) are:

- Stick-slip motion, which consists of limit cycle oscillation at low velocities, caused by the fact that friction is more significant at rest than during motion.
- Presiding displacement which shows that friction behaves like a spring when the applied force is less than the static friction break-away force.
- Frictional lag which means that there is some hysteresis in the relationship between friction and velocity.

The general description of friction is a kind of relation between velocity and friction force, depending on the velocity situations, described in several types of research. For example, Tustin's model consists of Coulomb and viscous friction (Tsurata et al. 2000). The inclusion of the Stribeck effect, with one or more breakpoints, gives a better approximation at low velocities, as shown in Fig. 4.7.

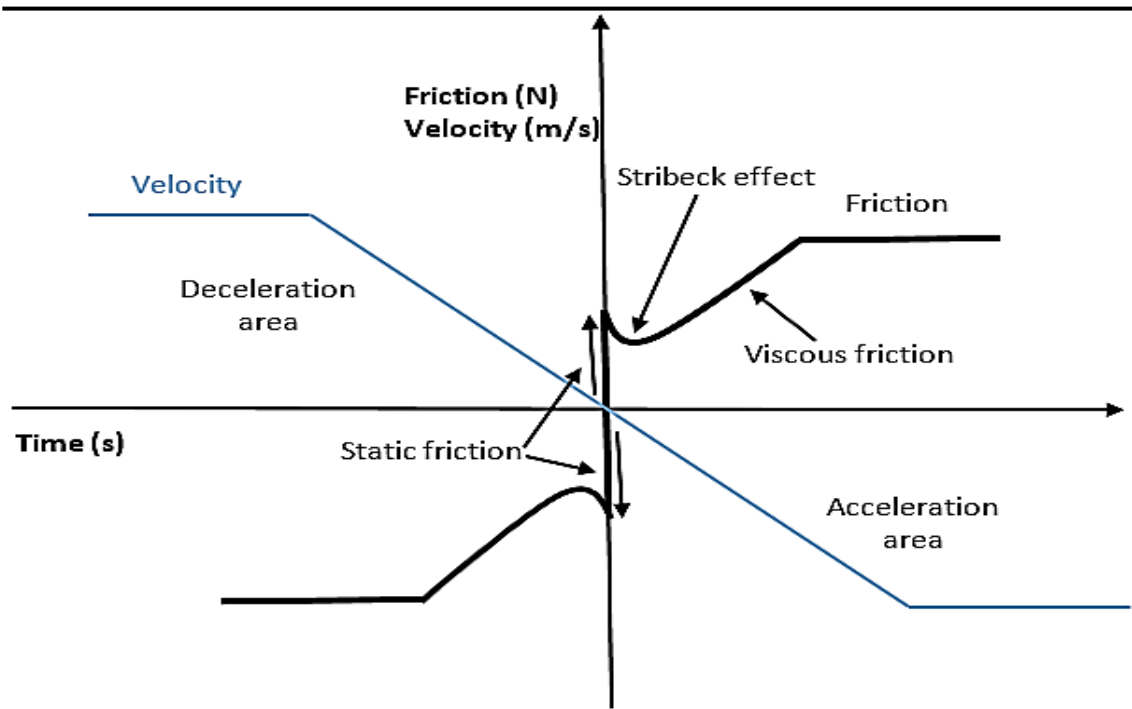


Fig. 4.7. Conventional Friction Model (Tsurata et al. 2000).

A summary of these friction types, is provided as follows:

4.5.1 Stiction region

The most basic friction model is static, which behaves like a spring when the applied force is less than the static friction breakaway force. This friction could be counted from the force balance ($\sum F = 0.0$), because of body stick or motionless. The direction of this friction depends on what the following body velocity direction will be. For this situation, static, stiction effect or pre-sliding friction occurs only as the total force is lower or equal to the breakaway force, as can be clearly distinguished in Fig. 4.7. When the system breaks away and starts to slide, the friction force reaches a maximum force, called the breakaway force.

4.5.2 Stribeck effect

(Dupont 1994) conducted the characteristic friction velocity curve for hard materials separated by liquid lubricants, which was contrasted with the static-kinetic model in Fig. 4.8. For liquid lubricants effect. it is clear that the Stribeck effect curve as was shown in Fig. 4.7, the reason for its shape was accepted, behaved exponentially. At very low velocities, the liquid is squeezed from between the bodies and the shearing of solid-to-solid contacts plays a dominant

role. At slightly higher velocities, pockets of lubricant under high pressure bear part of the load. At sufficiently high speeds, a fluid film separates the solids and bears the entire weight. The friction curve is positively sloped in this region. It is the negative slope of Stribeck region in Fig. 4.7 that promotes instability.

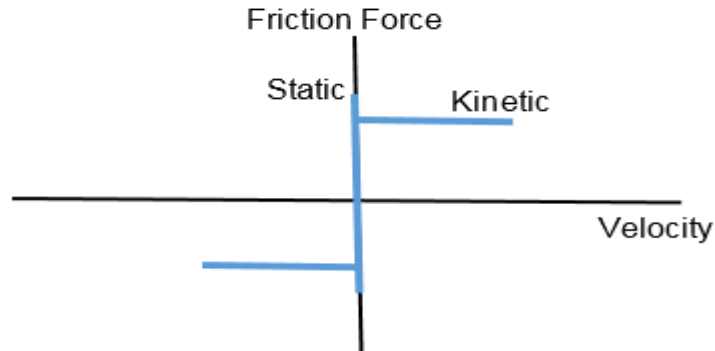


Fig. 4.8. Friction force versus velocity (Kinetic / static model).

Mathematical models of the friction velocity curve at the Stribeck effect often represent the transition from static to kinetic friction by an exponential velocity term (Armstrong-Helouvy 2012), (Canudas de Wit et al. 1991).

From another perspective, the general friction model is the Coulomb model (Harnoy et al. 2008) where the friction force is given by:

$$F_f = \mu F_n \text{sign}(v) \quad (4.1)$$

where, F_f is Coulomb friction force, μ is the friction coefficient, F_n is the normal force component and v the relative velocity of the moving object, which, for our purposes, is represented by the body mass with velocity equal to the body velocity, \dot{X}_b . The schematic representation of Coulomb friction is shown in Fig. 4.9.

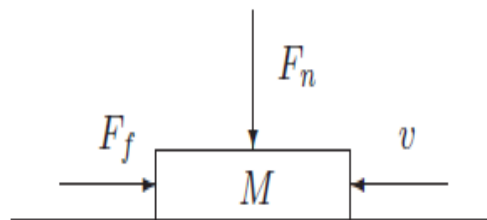


Fig. 4.9. Schematic representation of the friction force F_f on a moving object M .

4.5.3 Viscous friction

The viscous friction force is linear with regard to the velocity as previously shown in Fig 4.7, and can be expressed as:

$$F_{\text{fric}V} = \sigma_v v \quad (4.2)$$

where, $F_{\text{fric}V}$ is viscous friction, σ_v is the viscous friction coefficient and v is the velocity. As oil viscosity is somewhat slimy and insensitive to changes in pressure and the temperature is virtually constant, in this study, the oil viscosity was assumed to be constant. Now, in order to start establishing the real bearing friction model, it should involve the dynamic analysis of the test rig as follows:

4.6 How to account for the vertical force

The following explains in detail the main features of the friction model and will be begin with how to account for the vertical force that is responsible for generating Coulomb friction by drawing a free body diagram of the test rig.

4.6.1 Free body diagram of the test rig

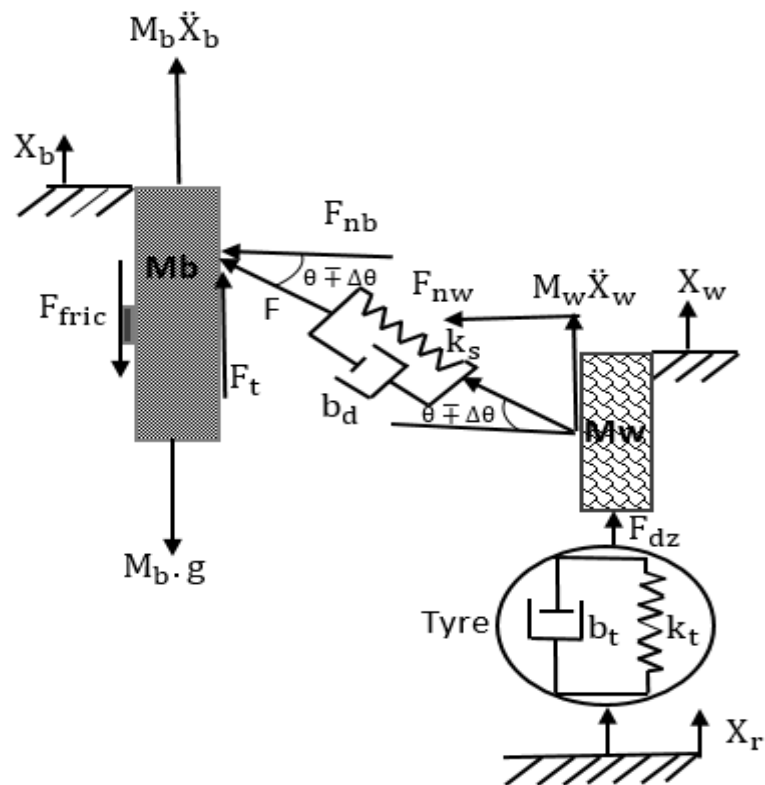


Fig. 4.10. Free body diagram of the test rig.

Fig. 4.10 shows the free body diagram of the test rig; the friction force acts as an internal force in the tangential direction of the contacting surfaces. This force obeys a constitutive equation, such as Coulomb's law, and acts in a direction opposite to the relative velocity. Therefore, the inclination position of S and VD and the system type inputs help to generate the kinematic bearings body friction relative to this normal force component. From Fig 4.10, the following analysis should be conducted to account for this friction force:

$$F = k_s(X_w - X_b) + b_d(\dot{X}_w - \dot{X}_b)/\sin(\theta \mp \Delta\theta) \quad (4.3)$$

$$F_{nb} = F \cos(\theta \mp \Delta\theta) \quad (4.4)$$

$$F_{nb} = k_s(X_w - X_b) + b_d(\dot{X}_w - \dot{X}_b)/\tan(\theta \mp \Delta\theta) \quad (4.5)$$

$$F_{fricC} = \mu F_{nb} \quad (4.6)$$

where, F_{fricC} is Coulomb friction, μ is the friction coefficient, F_{nb} is the body normal force component and F is the spring and damping forces.

4.6.2 Dynamic linkage angle expression

The construction linkage angle is dynamically changed by $\mp \Delta\theta$.

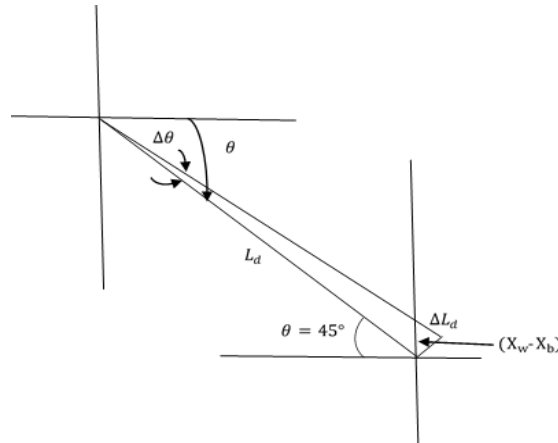


Fig. 4.11. Engineering geometry of passive units.

From engineering geometry of passive units, as shown in Fig. 4.11, it can be found that:

$$\frac{L_d - \Delta L_d}{\sin(90 - \theta)} = \frac{X_w - X_b}{\sin(\Delta\theta)}, \quad \theta = 45^\circ \quad (4.7)$$

$$\sin(\theta) = \frac{\Delta L_d}{X_w - X_b} \quad (4.8)$$

$\Delta L_d = (X_w - X_b) \sin(\theta)$, where, ΔL_d is the dynamic change in S and VD length.

Then,

$$\frac{L_d - (X_w - X_b) \sin(\theta)}{\sin(\theta)} = \frac{X_w - X_b}{\sin(\Delta\theta)} \quad (4.9)$$

$$\sin \Delta\theta = \frac{(X_w - X_b) \sin(\theta)}{L_d - (X_w - X_b) \sin(\theta)} \quad (4.10)$$

$$\Delta\theta = \sin^{-1} \left[\frac{(X_w - X_b) \sin(\theta)}{L_d - (X_w - X_b) \sin(\theta)} \right] \quad (4.11)$$

4.7 Nonlinear friction model

To achieve a high level of performance, frictional effects have to be addressed by considering an accurate friction model, such that the resulting model faithfully simulates all observed types of friction behaviour.

A nonlinear friction model is developed based on observed measurement results and dynamic system analysis. The model includes a stiction effect, a linear term (viscous friction), a non-linear term (Coulomb friction) and an extra component at low velocities (Stribeck effect). During acceleration, the magnitude of the frictional force at just beyond zero velocity decreases due to the Stribeck effect, which means the influence of friction reduces from direct contact with bearings and body into the mixed lubrication mode at low velocity. This could be due to lubricant film behaviour.

In respect of acceleration and deceleration when the direction changes for the mass body, friction almost depends on this direction, while the static frictional force exhibits spring-like characteristics. However, friction is not determined by current velocity alone, it also depends on the history of the relative wheel and body velocities and movements, which are responsible for friction hysteresis behaviour.

This model, which has now become well established, has provided a more satisfactory explanation of observed dynamic fluctuations of body mass. It will be attempted to heuristically “fit” a dynamic model to experimentally observed results. The resulting model is not only reasonably valid for the ¼ car test rig

behaviour but, is also reasonably suitable for most general friction lubricant cases.

The model simulates the symmetric hysteresis loops observed in the bearings body undergoing small amplitude ramp and step forcing inputs. As might be expected, they are capable of reproducing the more sophisticated pre-sliding behaviour in particular hysteresis. The influence of hysteresis phenomena on the dynamic response of machine elements with moving parts is not yet thoroughly examined in the literature. In other fields of engineering, where hysteretic phenomena manifest themselves, more research has been conducted. In reference (Smyth et al. 2002), for example, adaptive modelling techniques were proposed for dynamic systems with hysteretic elements. The methods are general, but no insight into the influence of the hysteresis on the dynamics is given. Furthermore, no experimental verification is provided. (Altpeter 1999) made a simplified analysis of the dynamic behaviour of the moving parts of a machine tool where hysteretic friction was present.

In this study, the friction model, despite its simplicity, can simulate all experimentally observed properties and facets of low-velocity friction force dynamics. Because of the test rig schematic and the system input signal, with historic travel, there are three circumstances depending on whether the body velocity is accelerating or decelerating. Firstly, the velocity values start from zero and just after velocity reversals, reach the highest and are restored to zero, or close to zero at SS. Secondly, the velocity starts from SS with a sharper increase than in the first stage and will extend to peak before returning to zero or near to zero at second SS. Thirdly, it starts from the second SS and after velocity reversals will touch a maximum value, twice rather than at case two, and go back down at a third SS. In the all these velocity cases, the velocity behaviours will make friction hysteretic loops, possibly because of increases in body velocity differing from decreases. The historical action of relative travels of wheel and body contributes to friction hysteresis.

In general, this friction model considers the static, stiction region, and dynamic friction, which consists of the Stribeck effect, viscous friction and Coulomb friction. The mathematical model and summary for each part will be demonstrated in the next step.

4.7.1 Mathematical friction model

The mathematical expression for establishing the friction model gave the constituent terms described in order to accurately represent the observed phenomena, as shown in Equation 4.12.

$$F_{\text{fric}} = \begin{cases} k_s(X_w - X_b) + b_d(\dot{X}_w - \dot{X}_b) & \dot{X}_b = 0.0 \\ C_e e^{(|\dot{X}_b|/e_1)} + \left[\frac{\mu(k_s(X_w - X_b) + b_d(\dot{X}_w - \dot{X}_b))}{\tan(\theta \mp \Delta\theta)} \right] + \sigma_v \dot{X}_b & \dot{X}_b > 0.0 \\ -C_e e^{(|\dot{X}_b|/e_1)} + \left[\frac{\mu(k_s(X_w - X_b) + b_d(\dot{X}_w - \dot{X}_b))}{\tan(\theta \mp \Delta\theta)} \right] + \sigma_v \dot{X}_b & \dot{X}_b < 0.0 \end{cases} \quad (4.12)$$

Equation 4.12 shows the friction model, which includes the two main parts of friction: static when, $\dot{X}_b = 0.0$, and dynamic, when $\dot{X}_b > 0.0$. The latter is presented by two expressions, depending on the velocity direction, and is discussed in detail later. In static friction, the stiction area is solely dependent on the velocity because the body velocity should be close to zero velocity, or frequently just beyond zero velocity. The static model is accounted by the force balance of the test rig when the body was motionless while the wheel was moved and describes the static friction sufficiently accurately. However, a dynamic model is necessary which introduces an extra state which can be regarded as transition, Coulomb and viscous friction. In addition to these friction models, steady physics state is also briefly discussed in this study. It will be shown in the following **Chapters 5** and **6** that this model is useful for various control tasks.

4.7.2 Static friction model

After a test starts, the wheel begins to move respective to the road inputs and initially the body remains motionless. This results from the static bearing friction and is undoubtedly a stick region-body, $X_b = 0.0$. This friction component can be considered via the test rig vertical forces balance $\sum F_v = 0.0$.

For the test rig, the following conventional model represents a 1/4 racing car without considering body friction:

$$M_b \cdot \ddot{X}_b = [k_s(X_w - X_b) + b_d(\dot{X}_w - \dot{X}_b)] \quad (4.13)$$

The first reported implementation of friction forces within Newton's 2nd law for a ¼ car model (Ali Al-Zughaibi et al. 2018) leads to a new dynamic equation of motion for the mass body:

$$M_b \cdot \ddot{X}_b = [k_s(X_w - X_b) + b_d(\dot{X}_w - \dot{X}_b)] - F_{fric} \quad (4.14)$$

As described in the short period where the body remains motionless $X_b = 0.0$ and $\ddot{X}_b = 0.0$, Equation 4.14 becomes:

$$0.0 = [k_s(X_w - X_b) + b_d(\dot{X}_w - \dot{X}_b)] - F_{fricS} \quad (4.15)$$

then,

$$F_{fricS} = [k_s(X_w - X_b) + b_d(\dot{X}_w - \dot{X}_b)] \quad (4.16)$$

where, F_{fricS} is the static friction, which is a function of the relative displacements and relative velocities between the wheel and body multiplied by spring stiffness and viscous damper coefficients, with direction totally dependent on the next stage \dot{X}_b direction. This is considered as pre-sliding displacement, which exhibits how friction characteristics behave like a spring when the applied force is less than the static friction breakaway force.

From the experimental work, Amplitude input = 50 mm, it was found that the maximum stick friction force occasionally occurs at $(X_w - X_b) \leq 0.0069$ and $X_b \cong 0.0$.

4.7.3 Dynamic friction model

Earlier studies, see for example: (Armstrong-Hélouvy et al. 1994); (Armstrong-Hélouvy 2012) and (Dupont 1994), have shown that a friction model involving dynamics is necessary to describe the friction phenomena accurately. A dynamic model describing the spring-like behaviour during stiction was proposed by (Dahl 1968). The Dahl model is essentially Coulomb friction with a lag in the change of friction force when the direction of motion is changed. The model has many commendable features and is theoretically well understood. Questions, such as the existence and uniqueness of solutions and hysteresis effects, were studied in an interesting paper by (Bliman 1992). The Dahl model does not include the Stribeck effect. An attempt to incorporate this into the Dahl model was made by (Bliman and Sorine 1993) where the authors introduced a second-order Dahl model using linear space invariant descriptions. The Stribeck effect in this model

is only transient, however, following a velocity reversal it is not present in the steady-state friction characteristics. The Dahl model has been used for adaptive friction compensation (Walrath 1984) and (Leonard and Krishnaprasad 1992), with improved performance as a result. There are also other models for dynamic friction, Armstrong-Helouvry proposed a seven-parameter model (Armstrong-Helouvry 2012). This model does not combine the different friction phenomena but is, in fact, one model for stiction and another for sliding friction. Another dynamic model suggested by (Ruina and Rice 1983) had been used in connection with control by (Dupont 1994). This model is not defined at zero velocity.

In this study, it was proposed that a nonlinear dynamic friction model combines: The transition behaviour from stiction to the slide regime including the Stribeck effect, the Coulomb friction with consideration of the normal dynamic force at body bearings with suitable friction coefficient and the viscous friction dependent on the body velocity and appropriate viscous coefficient. This model involves arbitrary steady-state friction characteristics. The most crucial results of this model are to highlight precisely the hysteresis behaviours of friction relative to body velocity behaviour.

Referring to Equation 4.12, there are two forms of dynamic friction, depending on the body velocity direction, it will be shown in detail as follows:

For $\dot{X}_b > 0.0$ the dynamic friction form is:

$$F_{\text{fricD}} = \left\{ C_e e^{(|\dot{X}_b|/e_1)} + \left[\frac{\mu(k_s(X_w - X_b) + b_d(\dot{X}_w - \dot{X}_b))}{\tan(\theta \mp \Delta\theta)} \right] + \sigma_v \dot{X}_b \right\} \quad (4.17)$$

From Equation 4.17, it is clearly seen that dynamic friction consists of three parts. A summary is given for each: part one form is:

$$F_{\text{fricT}} = C_e e^{(|\dot{X}_b|/e_1)} \quad (4.18)$$

where, F_{fricT} is transition friction, C_e is attracting parameter and e_1 is the curvature degree, the absolute body velocity value meaning the direction of velocity is not affected. The transition friction has exponential behaviour with degrees identified experimentally and completely agrees with the literature review of most research studies regarding lubricant friction, which begins from the maximum value at the sticky region and quickly dips when the body just begins to move, or the body velocity is increased.

Secondly, F_{fricC} represents Coulomb friction, which is equal to the normal bearings force times the friction coefficient (μ), as follows:

$$F_{\text{fricC}} = \left\{ \frac{\mu(k_s(X_w - X_b) + b_d(\dot{X}_w - \dot{X}_b))}{\tan(\theta \mp \Delta\theta)} \right\} \quad (4.19)$$

where, F_{fricC} is Coulomb friction with the opposite sign to velocity direction.

Finally, F_{fricV} represents viscous friction, which, because there is a lubricant contact between bearing and body, is counted by multiplying the body velocity with an appropriate viscous coefficient (σ_v).

$$F_{\text{fricV}} = \sigma_v \dot{X}_b \quad (4.20)$$

when $\dot{X}_b < 0.0$, the overall dynamic friction expression becomes:

$$F_{\text{fricD}} = \left\{ -C_e e^{(|\dot{X}_b|/e1)} + \left[\frac{\mu(k_s(X_w - X_b) + b_d(\dot{X}_w - \dot{X}_b))}{\tan(\theta \mp \Delta\theta)} \right] + \sigma_v \dot{X}_b \right\} \quad (4.21)$$

Equation 4.21 is similar to Equation 4.17 as they have the same three terms, but with a negative sign added in just for the transition friction term. This is because these values will describe the development friction in the opposite direction in the negative friction region.

The underlying motivation is that when the dynamic behaviour of the ¼ car model is thoroughly understood, the knowledge can be used to design appropriate feedback controllers for active suspension systems with compensation for the friction forces, as will be verified in the following **Chapters 5 and 6**.

4.7.4 Steady-state friction

It is vital to consider the friction behaviour within a steady-state (SS) period. From Fig. 4.12 of body displacement as function of time, it is clear that the historical movement demeanour, which starts to move from the stiction region, $X_b = 0.0$ and $\dot{X}_b \cong 0.0$, is the first SS, stage (A), then reaches the second SS, stage (B) at the mid-point of the road hydraulic actuator $X_b = 0.085$ m and $\dot{X}_b \cong 0.0$. Secondly, the body starts moving from the second SS and will reach the highest with a total amplitude $X_b = 0.135$ m and $\dot{X}_b \cong 0.0$ at the third SS, stage (C). Finally, it will start to move from the third SS stage and reach the lowest value of

amplitude $X_b = 0.035$ m, travelling twice the distance compared with the second stage. Thus, it will finally achieve the four SS (D) at $X_b = 0.035$ m and $\dot{X}_b \cong 0.0$.

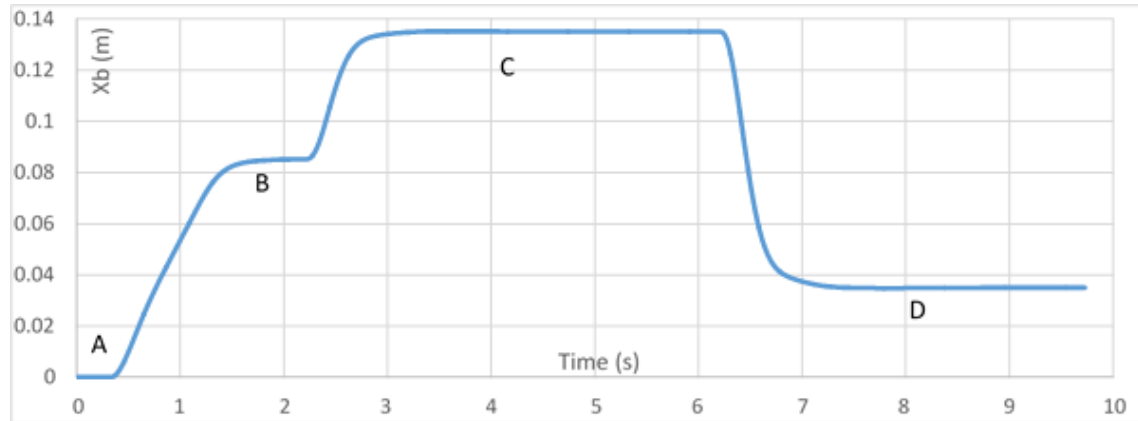


Fig. 4.12. Body displacement (X_b) with time.

At body stiction and SS station, \ddot{X}_b is equal to zero. Therefore, the friction at steady-state should be similar to static friction as mentioned in Section 4.7.2.

4.7.5 Simple friction model

Equation 4.12 gives a general form for nonlinear friction occurring at the body supported lubricant bearings. This model could be studied from a different point of view, whereby it can be returned to two dominant parameters, the body velocity and the normal body force, that could be termed damping friction relative to the body velocity and Coulomb friction qualified to normal body force.

For simplicity, even though the friction model, Equation 4.12, reflected most of the observations measured using the system dynamics analysis and was used with the passive suspension model, it can still be employed in simple form through overlooking Coulomb friction. Therefore, the simple expression of friction without Coulomb friction is:

$$F_{\text{fric}} = \begin{cases} k_s(X_w - X_b) + b_d(\dot{X}_w - \dot{X}_b) & \dot{X}_b = 0.0 \\ C_e e^{(|\dot{X}_b|/e1)} + \sigma_v \dot{X}_b & \dot{X}_b > 0.0 \\ -C_e e^{(|\dot{X}_b|/e1)} + \sigma_v \dot{X}_b & \dot{X}_b < 0.0 \end{cases} \quad (4.23)$$

In Equation 4.23, this model has the same three various forms dependent on \dot{X}_b , value and direction. Part one is the static friction, which has precisely the same shape for general friction, while the dynamic formula, damping friction,

depending only on the body velocity in a different form by ignoring the Coulomb term. The interesting point is that, by implementing these simple friction forms, the simulation results also acquire a good agreement in comparison with the experimental results regarding system response parameters, which encouraged its use with the active suspension system, as shown in **Chapter 5**. The question arises as to which one is more suitable for our case? Although the general friction model system, Equation 4.12, gives more detail, depending on the system dynamics, and has the ability to highlight the hysteresis phenomenon that should occur with this system type, the simple friction model has lost this hysteresis.

However, the simple form also provides a real accord between the experimental and simulation results for system response, with little variation relative to that gained from considering general friction. From this point of view, a mathematical analysis is used, by using the Residual Mean Square (RMS). The RMS is defined as “a measure of the difference between data and a model of that data”. Therefore, two measured signals X_b and $X_w - X_b$, will be used to show the accuracy of considering the general or simple friction forms.

RMS accounts for the measurement and simulation with and without Coulomb friction for relative movements between the wheel and body, as illustrated:

$$(\text{RMS})_c = \sqrt{\frac{1}{N} \sum ((X_w - X_b)_m - (X_w - X_b)_{Sc})^2} \quad (4.24)$$

And,

$$(\text{RMS}) = \sqrt{\frac{1}{N} \sum ((X_w - X_b)_m - (X_w - X_b)_S)^2} \quad (4.25)$$

where, $(\text{RMS})_c$ and (RMS) are the RMS between the measured and simulation values with and without considering Coulomb friction respectively, $(X_w - X_b)_m$ is the measured relative displacement, $(X_w - X_b)_{Sc}$ and $(X_w - X_b)_S$ are the simulation data with and without implementing Coulomb friction, N is the total number of sample. The RMS results are shown in Table II.

Table II RMS results

Signal	(RMS) _c	(RMS)
$(X_w - X_b)$	0.006362	0.006366
X_b	0.096267	0.096386

From Table II, the RMS results show that using the friction model considering Coulomb friction is more accurate.

4.8 Friction validation

This study, builds and implements a friction model within the body motion equation; showing how much the friction affects the simulation results from one side and how these agree with the experiment results. For example: comparing the relative displacement between (X_w and X_b) and the body velocity behaviours for both simulation and experiment results. Therefore, this model suggests considering the static and dynamic friction dependent on the historical body velocity and displacement.

The friction model is based on the experimental observations that have to be performed to determine the friction characteristics of the bearings body. Various methods exist for the identification of friction. For example: (Johnson and Lorenz 1992) mentioned that friction was determined iteratively in experiments by successively tuning the feed-forward parameters of the static, sliding and viscous friction until the position error was below specified limits. Dynamic effects caused by the mass and the damping of the system were compensated for in advance. Meanwhile, the friction was identified by (Kermani et al. 2005) through application of a sine to the system as constant velocity experiments could not be conducted. An often used and distinct method to identify friction as a function of the velocity is to perform constant velocity experiments. The system is moved at constant velocity and the mean control output is a measure of the friction.

In this study, in contrast to literature references, the test rig does not have friction sensors. Therefore, other experimental signals were used to identify the friction. The inputs were filtered to be compatible with test rig operation and to avoid abrupt changes that could cause damage, as mentioned in **Chapter 3**. The input amplitude of 50 mm is shown in Fig. 4.13. The body moves at a velocity

relative to wheel travel. The body and wheel velocities follow the input forces and the LVDT sensors and type WGS2 velocity sensors are considered to be a measure of the displacements and velocities for road, wheel and body, which have to be overcome.

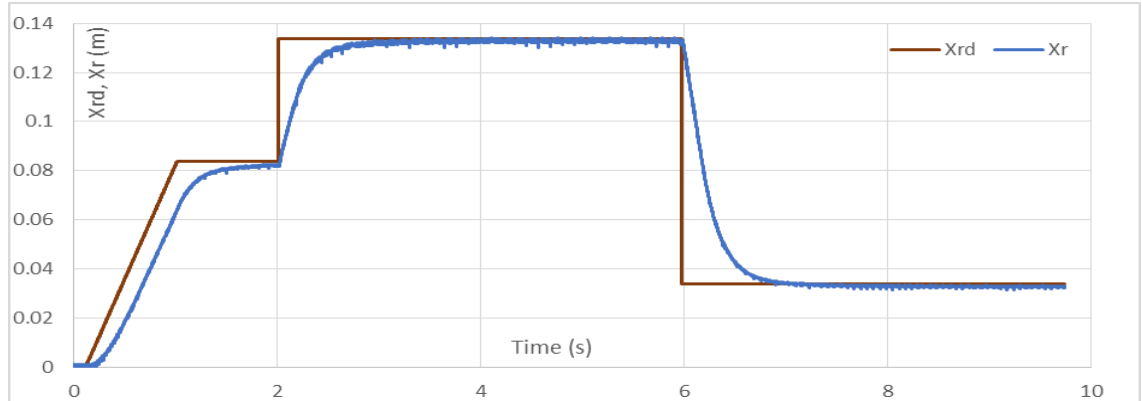


Fig. 4.13. Experimental step input to the system.

4.8.1 System inputs

In the laboratory tests, although the test rig setup allows the application of both sine and step inputs, a step input was chosen since it clearly shows the system response. The simulation of random inputs is shown later in **Chapter 6**. Firstly, the system input profiles moves the hydraulic actuator piston from ground to a mid-point position. Then, it was possible to give further level input change, depending on the selected amplitude. In reality, a mixed input, or a truncated ramp, input were applied in practical work to avoid the hard edge of signals that could cause damage. The input was also passed through a first-order filter. Eventually, the desired, X_{rd} (red colour) and measured inputs, X_r (blue colour) were displayed in Fig. 4.13.

4.8.2 Validity of body velocity

As previously mentioned, there was no sensor to directly measure friction. The body velocity signal was used to verify the friction model by expanding the comparison between the body velocity measured from experimental work, as shown in Fig. 4.14, and with those values from the simulation model, as shown in Fig. 4.15. It is clearly seen that there is good agreement between both. The simulation values were identified from the simulated mathematical model for body motion after considering the friction as exclusively accurate. In other words, there

is a direct relationship between the friction behaviour and the body velocity variations that lead to providing further evidence that the friction model is entirely correct.

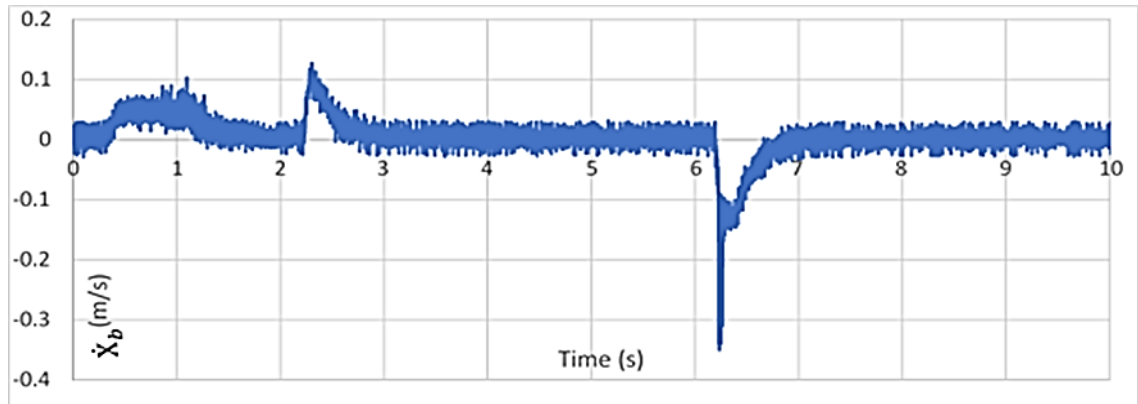


Fig. 4.14. Experimental results for body velocity.

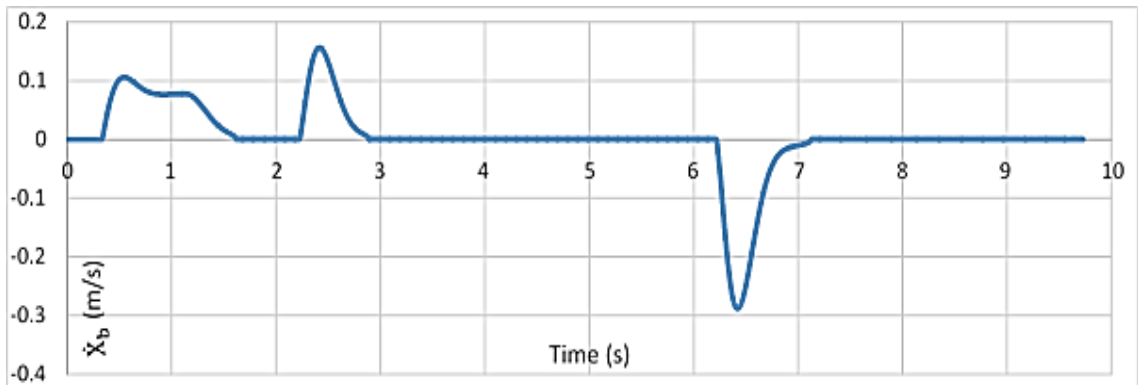


Fig. 4.15. Simulation results for body velocity with time.

4.8.3 Validity of relative wheel and body displacement

Returning to the corresponding difference in signal between X_w and X_b , it is a significant measured signal that helps to show the friction effects by creating comparison between the experimental results, as shown in Fig. 4.6, and those obtained from the simulation model, as shown in Fig. 4.16. It is evident that there is a reasonable settlement between the experimental and simulation results and every variation change is shown; meaning the considered friction model is reasonably accurate.

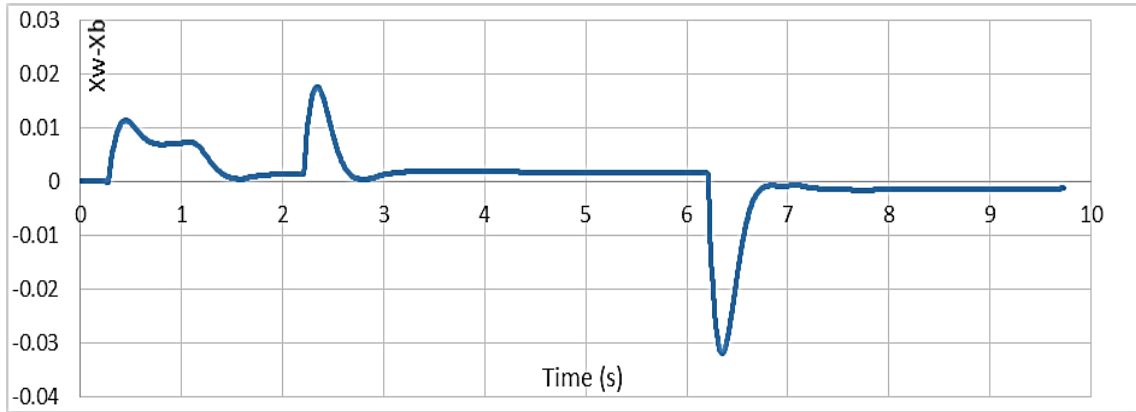


Fig. 4.16. Simulation results of the difference between $(X_w - X_b)$.

4.9 Friction hysteresis

The Concise Oxford Dictionary gives a general definition of hysteresis as “the phenomenon in which the value of a physical property lags behind changes in the effect causing it”.

This study proposes a friction model that includes all the various aspects mentioned above, while overcoming the shortcomings of the previous survey for this test rig and verifies its essential aspects experimentally. The friction identification results in the next chapter are a successful way to design an accurate control.

This section describes hysteresis as experienced in the friction force versus velocity behaviour of a moving body relative to a bearing’s body. The hysteretic friction is, moreover, not a unique function of the velocity, but depends on the displacement and previous history of the movement. Thus, referring to Fig. 4.17 for altered input force with an amplitude of 50 mm, if there has never been a relative movement before, the friction force follows a static line independent of time, as shown in Figs. 4.18 and 4.19, for the same force inputs. However, the remaining hysteretic friction is comparable to the dynamic behaviour of the body mass that is connected to a variable reference frame through a hysteretic movement. It is essential to have a thorough understanding of these dynamics if the mass is to be position controlled to a very accurate level. Since the hysteretic friction force depends on the position and the past velocity reversals, the force is described by Equation 4.17, the position signal is chosen such that there is one loop inside the outer hysteresis loop when $\dot{X}_b > 0.0$. Meanwhile, Equation 4.21

displays the friction force in a negative direction when $\dot{X}_b < 0.0$. The input is chosen such that there is the most massive hysteresis loop; it is a double in comparison with the larger loop when $\dot{X}_b > 0.0$.

The resulting hysteresis curve is quasi-independent of the time scale of the applied position signal. When an inner loop is closed, the curve of the outer loop is followed again, showing the non-local memory character of the hysteresis. This is followed later by the most considerable circle curve on the other side.

4.10 Results

4.10.1 Friction results for general form (considering Coulomb friction)

Fig. 4.17 shows friction force as a function of body velocity for the input force when amplitude = 50 mm, while the other cases when amplitude is = 30 or 70 mm, are mentioned in **Chapter 3**. Accordingly, with the same friction behaviour, the same friction model can be used. It is apparent that the friction behaves as a hysteresis loop. Therefore, both sets of curves form a circle, enclosing a nonzero area, which is typical of dynamic friction besides the starting static friction. The loops enclosed three areas relating to velocity increases, decreases and directions. This is similar to expectations from the results of a dynamic friction model discussed in Sections 4.8.1 and 4.8.3. The upper portion of the curve shows the behaviour for increasing velocity when $\dot{X}_b > 0.0$ in two circumstances, while the lower portion shows the behaviour for decreasing velocity when $\dot{X}_b < 0.0$. This phenomenon may be a consequence of the dynamics of the process rather than of the nonlinearity, this phenomenon is often referred to as hysteresis. The hysteretic friction is, moreover, not a unique function of the velocity, but depends on the previous hysteresis of the movements.

In fact, there are two urgent situations that should be highlighted: the first is when the velocity equals zero, the body is motionless and the friction values are similar to static friction values, as discussed in Section 4.8.2; while the second important situation is when the values of friction are within the SS situation, which has already been specified in the previous analysis in Section 4.8.4.

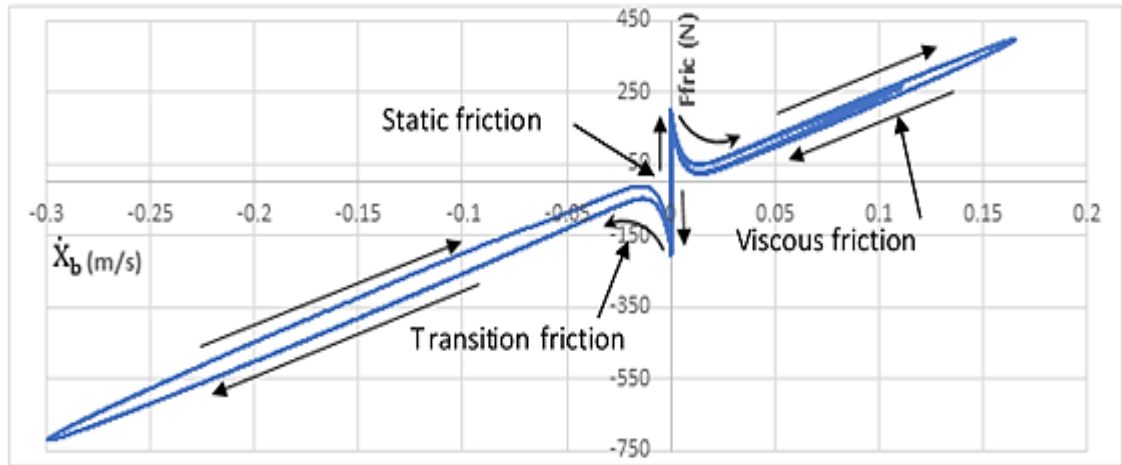


Fig. 4.17. Friction as function of the body velocity.

However, Fig. 4.17 shows the behaviour of friction relative to the body velocity. It is evident that the reaction in the stick region, or static friction at $X_b=0.0$, friction values start from zero and reach a maximum at the breakaway threshold force. From the experimental test, the breakaway force at the maximum relative displacement between X_w and X_b and the corresponding values for wheel and body velocity, accounted for by Equation 4.16, could be estimated. As a result, it was found to be equal to 193.8 N. Therefore, after the first positive position of static friction, because the direction of displacement moves up, whenever the body starts to move, when $X_b > 0.0$, the friction hardly dips relative to the transition area from direct contact between body and bearings to mixed hydraulic contact. This clearly shows the Stribeck effects relative to hydraulic layer behaviour; a squeeze-film effect. Following the system inputs and velocity value when $\dot{X}_b > 0.0$, the friction firstly draws a small, enclosed, positive cycle. After that, the body velocity returns to the second SS and increases to reach a maximum value before returning to the third SS with friction drawing a larger enclosed cycle in a positive direction. When $\dot{X}_b < 0.0$, the static values are equal to those for $\dot{X}_b > 0.0$ in the opposite direction, while the friction draws the most massive enclosed nonzero cycle with a value twice that of the larger enclosed cycle in the positive direction. This is because of the friction value and guidance following the road input and velocity values.

4.10.2 Friction results for simple form (without Coulomb friction)

In considering friction, while disregarding the Coulomb effects relative to the vertical force from the force inputs and the construction of the test rig, the inclination of the spring and damper from one side and the distance between the wheel unit and body mass from another side allows a promotion friction formula, damping friction, to be obtained. Although some features of friction characteristics, the hysteresis behaviour, will have been lost in considering this friction model with the passive suspension system design, success also has been achieved close to the experimental data. Fig. 4.18 shows the damping friction as a function of the body velocity when amplitude = 50 mm. It is approved that there is no hysteresis performance.

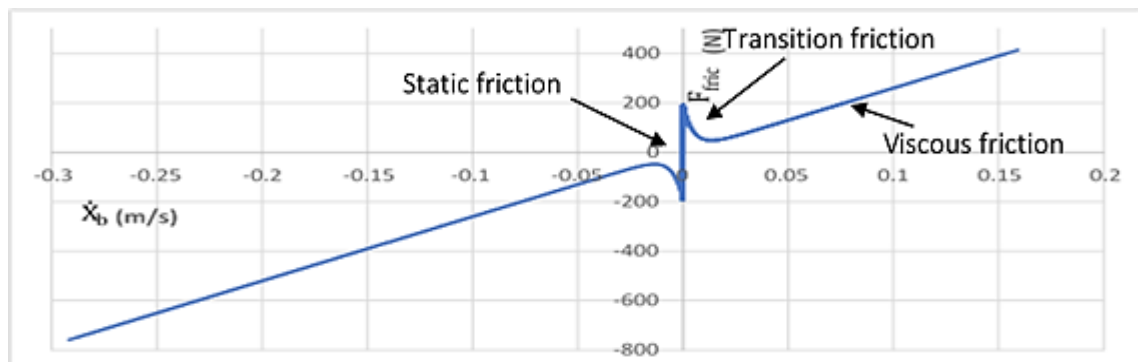


Fig. 4.18. Damping friction as a function of the body velocity.

Meanwhile, Fig. 4.19 illustrates the association between damping and Coulomb friction. Although the damping friction is dominant, it remains vital to reflect the Coulomb friction in the general friction model, because it is responsible for bringing hysteresis performance to the model and, as mentioned, this is quite essential to our system type.

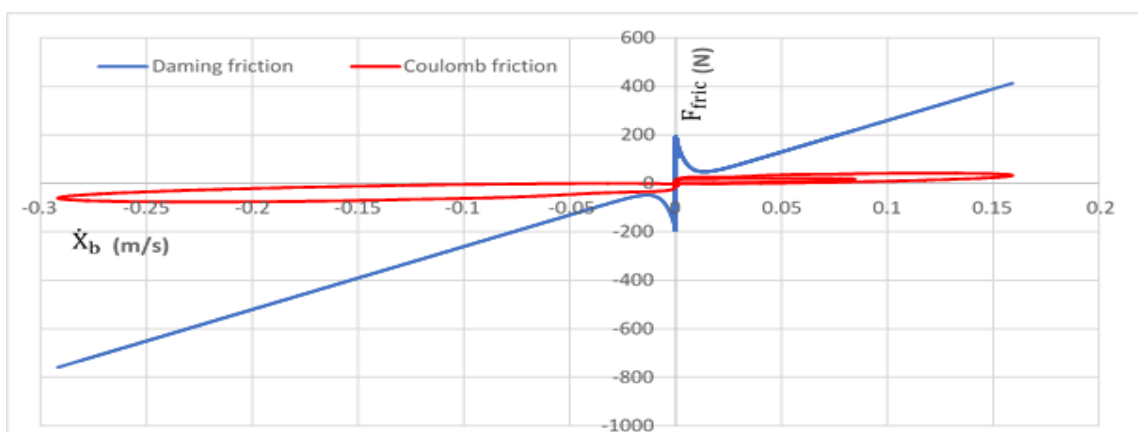


Fig. 4.19. Damping and Coulomb friction as a function of the body velocity.

4.11 Discussion

This Chapter was set up to question the aspects of friction that merit inclusion with the $\frac{1}{4}$ car model. After a brief stating of the general frictional considerations, this discussion will review and summarise the findings.

Friction is a highly complex phenomenon, evolving at the contact of surfaces. Experiments demonstrate a functional addiction upon a significant change in parameters, including sliding speed, acceleration, critical sliding distance, normal load, surface preparation, and material combination. In many engineering applications, the success of models in predicting experimental results remains strongly sensitive to the friction model. Friction is a natural phenomenon that is quite difficult to model and is not yet completely understood.

The principal question investigated to inform the simulation framework was: what is the most suitable technique for including friction in an analytical or numerical model, and what are the inferences of friction model superiority? The constituent elements are discussed in turn as follows:

- **The main reasons for considering friction**

In this study, as shown in Section 4.3, considering and implementing the friction model within the equation of motion for the mass body is qualified for the following reasons:

1. Friction itself is crucial to find in any mechanical system. Friction exists everywhere, since degradation, precision, monitoring and the control system are strongly affected by friction.
2. From the experiment test, it is clearly seen that there is no oscillation of mass body travels, while that was found with simulation model results. Therefore, a new term should be considered to overcome the issue, that is to say, a friction term.
3. In addition, from experimental measurements in Section 4.4, it is apparent that at the start of the test, while the wheel began to move in relation to road inputs, the body remained motionless for a period.

- **Conventional friction model**

The majority of current model-based friction compensation schemes utilise classical friction models, such as Coulomb and viscous friction. In applications with high precision positioning and with low-velocity following, the outcomes are not generally acceptable. Typical types are different combinations of Coulomb friction, viscous friction and the Stribeck effect, as has been mentioned in several researchers' works as shown in Section 4.5.

- **How to account for the normal force**

In accounting for Coulomb friction, it is necessary to find the normal applied force to the surface contact between the body and bearings that is responsible for generating this friction. The free body diagram for the test rig, as shown in Fig. 4.10 in Section 4.6, helps to find the suitable form for an account of this normal force, as displayed in Equation 4.5. Also, for the dynamic case, the inclined position angle of S and VD will dynamically change. Therefore, it should be very precisely measured, from Fig. 4.11 and applying Equation 4.11, it should be possible to calculate the variation for the dynamic position.

- **Why consider transition friction in this study?**

The frictional change force is attributable to the viscosity of oil and is proportional to the shear rate of the oil film, as was illustrated in Section 4.7. In this area, the pressure produced in the oil film supports the bearing load. Since the two surfaces do not directly contact, friction reduction hardly takes place. If the circumferential speed is increased, in this starting state, the frictional resistance will diminish smoothly toward the base point, following the exponential behaviour with a particular degree curve. The oil film appears to become progressively thinner and at an appropriate body speed, the oil film becomes so thin that the movement projections of the two surfaces finally start to crash into each other at that point. In this manner, the frictional resistance no longer diminishes, moreover, increments quickly, producing a minimum point. With further increases in the body velocity, collision of the projections of the two surfaces becomes more severe and the frictional coefficient will further increase.

- **Nonlinear friction model**

To accomplish the abnormal state of execution, frictional impacts must be attended to by considering an accurate friction model, with the end goal that the

subsequent model would accurately simulate all observed kinds of friction behaviour as was accurately investigated in Section 4.8. Based on observed measurement results, a promising friction model was developed. The model incorporates a stiction effect, a linear term (viscous friction), a non-linear term (Coulomb friction), which relies upon the ordinary dynamic constraint whose sign depends on the course of the body speed and an additional segment at low speeds (Stribeck effect).

In respect to accelerating and decelerating when the course changes for the mass body, the static frictional force shows spring-like qualities. In addition, alternate friction largely depends on the body velocity direction. Nevertheless, friction is not dictated by current velocity alone, it relies additionally upon the historical backdrop of relative negotiated speed and movement, which is in charge of friction hysteresis conduct.

In this review, the established friction model, irrespective of its extreme effortlessness, can recreate all, that we are aware of, conditionally watched properties and features of low-velocity friction force dynamics. Considering the test rig schematic and the force information, there are three conditions, depending upon whether the body speed is speeding up or decelerating. Firstly, the velocity qualities start from zero and soon after, velocity reversals reach the most elevated level and are maintained at zero, or close to zero, at SS. Secondly, the velocity begins from SS with a sharper increment than in the first stage and will be stretched to the ultimate before it returns to zero, or near to zero, at SS. Thirdly, it will begin from SS and, after velocity reversals, will reach the highest estimate, twice the time as for case two, and spine to SS. In every one of these velocity cases, the velocity behaviour will make friction hysteretic loops that could account for the increments of body speed in a variety of paths from reductions.

In general, this friction model deliberates the static, stiction region and dynamic friction, which consists of the Stribeck effect, viscous friction and Coulomb friction, which rely on the dynamic tangential force, which evolves in the test rig contact bearings. Therefore, there are general and simple friction forms as follows:

- **Mathematical friction model**

$$F_{\text{fric}} = \begin{cases} k_s(X_w - X_b) + b_d(\dot{X}_w - \dot{X}_b) & \dot{X}_b = 0.0 \\ C_e e^{(|\dot{X}_b|/e1)} + \left[\frac{\mu(k_s(X_w - X_b) + b_d(\dot{X}_w - \dot{X}_b))}{\tan(\theta \mp \Delta\theta)} \right] + \sigma_v \dot{X}_b & \dot{X}_b > 0.0 \\ -C_e e^{(|\dot{X}_b|/e1)} + \left[\frac{\mu(k_s(X_w - X_b) + b_d(\dot{X}_w - \dot{X}_b))}{\tan(\theta \mp \Delta\theta)} \right] + \sigma_v \dot{X}_b & \dot{X}_b < 0.0 \end{cases}$$

This mathematical equation incorporates two primary parts of friction: static and dynamic friction. The latter as two expressions and is influenced by the velocity track. In static friction, the stiction area is exclusively not subject to the velocity because the body velocity should be close to zero velocity or just beyond zero velocity. Frequently, the static models are numbered by the strength adjustment of the test rig when the body sticks while the wheel is moved and depicts the static friction sufficiently precisely. A dynamic model is vital to present an additional state, which can be viewed as the transition, Coulomb, and viscous friction. In addition to these friction models, steady physics state is also briefly discussed in this study.

- **Simple friction model**

If ignoring the Coulomb friction, the previous nonlinear friction model shown in the Equation 4.12, becomes a simple model, as illustrated in Equation 4.23. Despite, losing some features of friction characteristics with this model, in comparison with experimental data, that also obtained close results. From this aspect, another approach should be found to discover which approach obtains more accurate results by comparing with measured results. By using RMS mathematical analysis, the results shown in Table II, prove, as an outcome, that the friction model is more accurate with a consideration of Coulomb.

- **Friction validation**

As mentioned in Section 4.9, in traditional validation for any model or simulation parameters, generally, there is a technique to validate these parameters using a test rig hat has sensors that measure these parameters and specify the type of inputs. However, in our test rig, there are no sensors to measure friction. Therefore, it is useful to use the same single $(X_w - X_b)$ that helps in discovering

the friction effects to assess the friction result accurately. Also, it is possible to use other measured values such as body velocity, to achieve a more precise validation. With these two measured signals and by choosing a suitable input, we could achieve a proper validation of friction.

- **Friction hysteresis**

This section, relative to Section 4.10, describes hysteresis as experienced in the friction force versus velocity behaviour of moving the body relative to the bearing. The hysteretic friction is, moreover, not a unique function of the velocity but instead relies on the displacement and previous history of the movement.

The subsequent hysteresis band is semi-autonomous of the time size of the connected standard position. At the point when an inward circle is closed, the end of the outside loop is taken after, once more demonstrating the nonlocal memory character of the hysteresis, later making the greatest ring curve on the other side.

- **Results**

As illustration in Section 4.10, considering the conduct of friction with regard to the body speed, it is clearly observed that the behaviour qualities at the stick locale, when $X_b = 0.0$, begins from zero friction and reaches a maximum at the breakaway threshold force. In this way, the principal positive position of static friction, because of the heading of uprooting climb, at whatever point the body begins to move, when $X_b > 0.0$, hardly dips in respect of the interpretation region and unmistakably demonstrates the Stribeck effects streaming the framework information sources and speed estimate at \dot{X}_b . The friction drawing initially encases a small positive cycle, from that point onward, the body velocity will return to the second SS, and increment to achieve the extreme incentive before returning to the third SS, drawing a larger encased friction cycle in a positive direction. At the point when $\dot{X}_b < 0.0$, the static values are equal to that for $\dot{X}_b > 0.0$, but in the opposite direction, while the friction drawing the largest enclosed non-zero cycle with values that are twice that in the larger enclosed cycle in the positive direction. This is because the friction value and direction are following the road input forces and the resulting velocity values. These results were obtained from developing a loop within the C++ code in order to simulate the

mathematical passive suspension model with implementation of the nonlinear friction forces.

Note: for more detail about the C++ code see **APPENDIX C**

- **In summary**

An accurate nonlinear dynamic model for friction has been presented. The model is simple yet captures most friction phenomena that are of interest for simulated test results. The low-velocity friction characteristics are particularly important for high-performance pointing and tracking. The model can describe arbitrary steady-state friction characteristics. It supports hysteretic behaviour due to frictional lag, spring-like behaviour in stiction and gives a different breakaway force depending on the rate of change of the applied force. All these phenomena are unified into static, steady state and dynamic friction equations. The model can be readily used in simulations of systems with friction.

It is essential to consider friction in this study, in the hope that the study creates an opening and contributes towards a re-consideration of the role of friction using the current quarter in half and full car suspension models.

Simulation leads to the same conclusion as proven by the experimental results obtained from the test rig test. Comparison between experimental and simulation results show that the proposed general friction model is more accurate than the conventional models (simple model).

Mathematical Modelling for Nonlinear Active Suspension and System Linearity

5.1 Introduction

The primary function of the vehicle suspension system is to enhance ride comfort, stability and driving safety. Hence, the ride quality and the driving stability are two conflicting criteria. Fig. 5.1 illustrates this conflict; this conflict diagram shows the variation of driving safety and comfort with changes in vehicle parameters, such as: body mass, stiffness and damping. The conflict diagram presents the properties of the vehicle driving comfort and safety for a defined manoeuvre as a point in the $\ddot{z}_B - F_{z,dyn}$ diagram. Changing setup prompts to curves clarifies the individual propensities (Fischer and Isermann 2004).

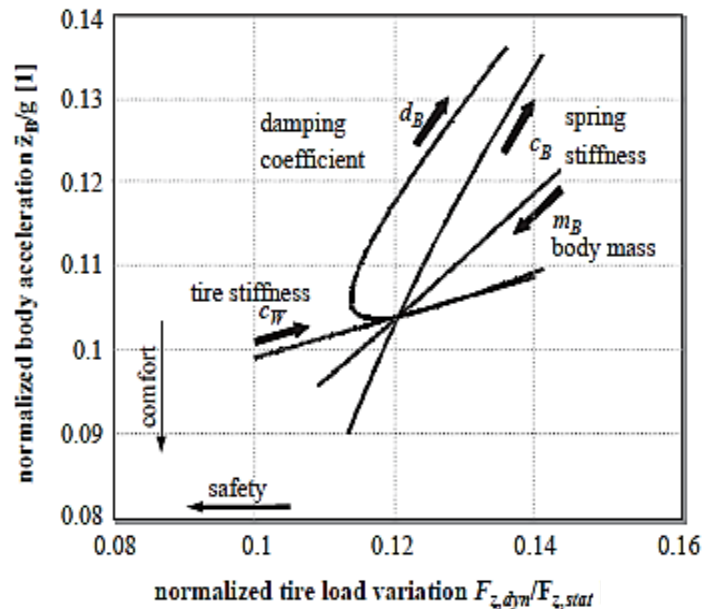


Fig. 5.1. Influence of vehicle parameters, quarter-car simulation (Fischer and Isermann 2004).

As can be seen from Fig 5.1, the stable setup of the passive suspension system is a continuous compromise between comfort and safety for any given input set of road conditions and specific stress. Semi-active or active suspension systems attempt to solve, or at least diminish, this conflict. In such a manner, the mechanism of the semi-active suspension system is the adaptation of the damping and the stiffness of the spring to the original requests. Active suspension systems, in contrast, provide a further force input in adding to possible existing passive systems and, in this way, require considerable covenant energy. This also, clarifies the addiction of a vehicle suspension setup on parameter changes,

accordingly of temperature, deflection, and wear and tear. These progressions must be considered when designing a controller for an active or semi-active suspension to avoid unnecessary performance loss. Therefore, a robust and suitable controller should be implemented. For example, this necessitates a parameter adaptive suspension system, which refers to a control system that is adjusted to conduct the changing settings of the system to be controlled, as mentioned by (Isermann 1992).

Achieving the targets of the suspension system, in both the ride quality (response to road disturbances, which has been investigated in the current study) and handling (response to driver inputs) should be addressed in combination with simple vehicle models. Road disturbances were previously modelled, as mentioned in **Chapter 3**, while driver inputs were considered to be zero load disturbances on the vehicle body. However, in real life, ignoring the driver's input could lead to unsatisfactory performance (Brezas and Smith 2014). The importance of the influence of load disturbance in the suspension model can be estimated by the fact that conventional load forces can be of the same magnitude as the static load of the suspended mass. The issues that handling manoeuvres can cause for active suspension algorithms has been explicitly described in (Venhovens 1995).

However, in the current study, because this study focuses on the investigation and modelling of a real test rig represented by a $\frac{1}{4}$ car, the inertial forces induced by handling manoeuvres, for example: cornering, braking, etc, on the body and changes to static loads, as well as the aerodynamical loads, can therefore be assumed to be zero and are ignored. Rather it was deemed necessary to consider bearing body friction, which was indeed observed with the test rig.

Suspension systems are categorised into the familiar terms of passive, semi-active and active systems. Usual structures are in demand, principally the energy and the particular frequency of the actuator as reported by (Streiter 1996) and depicted in Fig. 5.2. These illustrations highlight the struggle that carmakers encounter in their attempt to upgrade driver safety and comfort, since high performance suspension systems can only be achieved through extensive exploration and with large, expensive and complicated actuator systems.

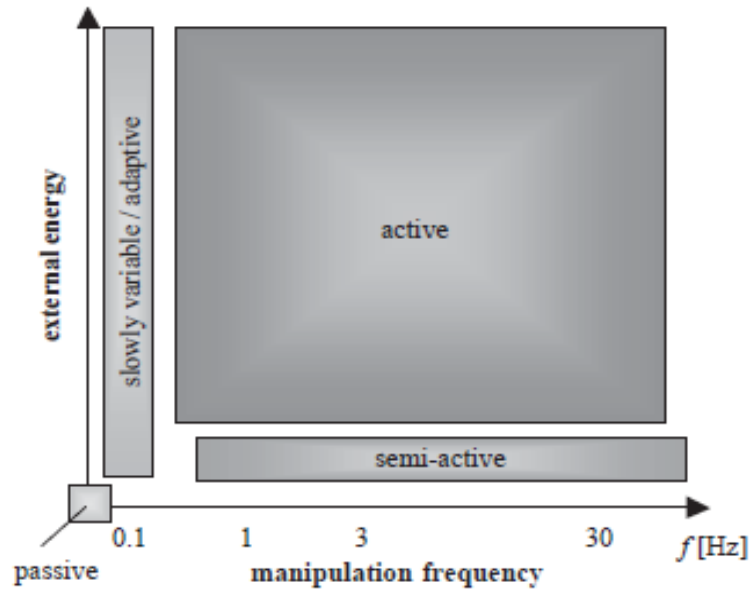


Fig. 5.2. Schematic representation of passive, adaptive, semi-active and active systems (Streiter 1996).

5.2 The Lotus active suspension concept

The Lotus active model was investigated in this section to establish the further advancement. As mentioned in **Chapter 1**, the development of the Lotus model was described by its inventors, P.G. Wright and D.A Williams (Wright and Williams 1984) and numerous reports have appeared in motoring magazines. Nevertheless, a specific account of its operation and performance seems to be lacking. This analysis was corrected and expanded by Thompson and Davis (Thompson and Davis 1991). The mathematical model was examined by means of a simple one-DOF model. A disturbance force, representative of an aerodynamic down-force, was applied directly to a car body in a downward direction, because the model was intended for a racing-car design. However, in the author's opinion, in respect to the dynamic analysis of a general vehicle, it is relatively unimportant if comparing the effect of the aerodynamic down-force to the disturbance force due to road roughness. Therefore, the disturbance force should be applied to a wheel hub instead of the car body and it is categorically to re-derive the Lotus model.

Chapter 1 demonstrates the schematic of the system in Fig. 1.2. An ideal actuator, overlooking the hydraulic system and wheel unit, was used and compared to a one-DOF passive suspension as shown in Fig. 5.3.

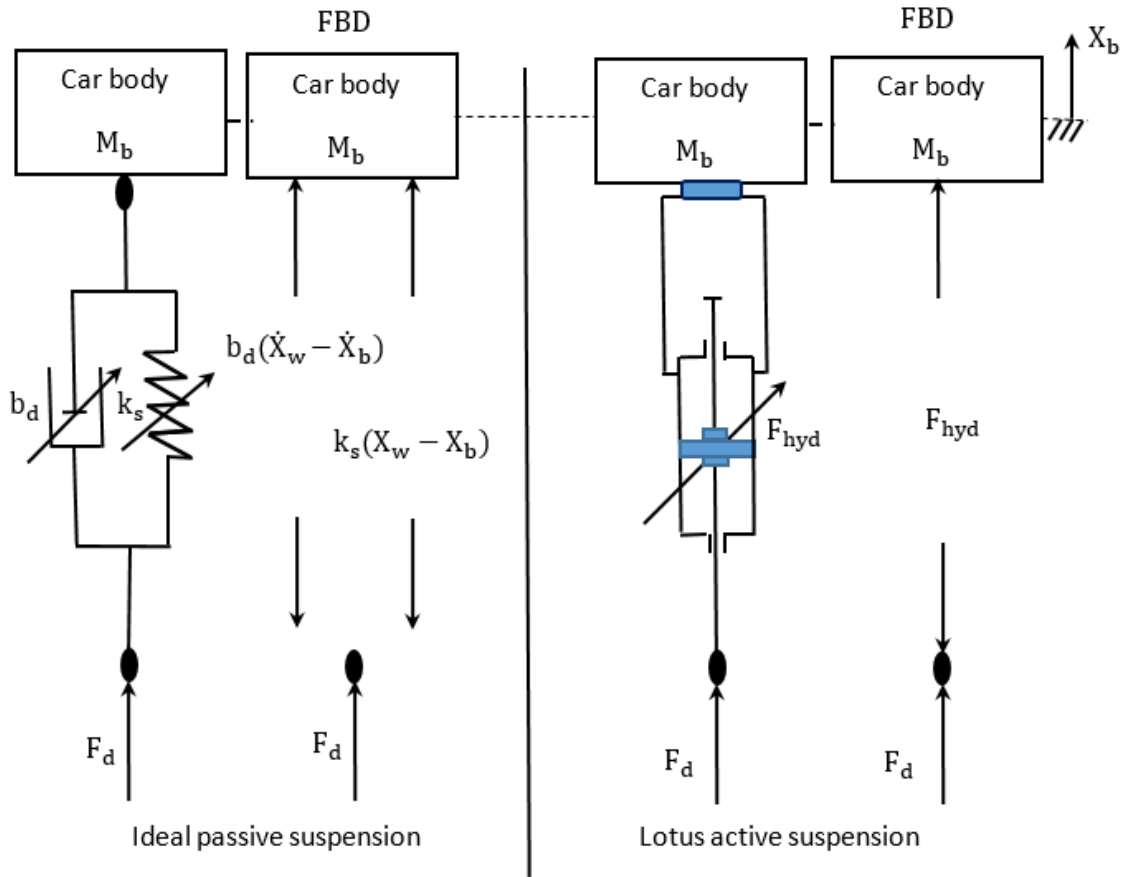


Fig. 5.3. Comparison between ideal passive suspension and Lotus active suspension.

The analysis was conducted so that it endeavours to model the nonlinear active suspension to simulate the behaviour of the adjustable passive suspension, which can adapt its characteristic depending upon the road surface and working conditions. The equations of motion of the passive suspension without considering the body friction force are:

$$F_d = b_d(\dot{X}_w - \dot{X}_b) + k_s(X_w - X_b) \tag{5.1}$$

$$M_b \ddot{X}_b = b_d(\dot{X}_w - \dot{X}_b) + k_s(X_w - X_b) \tag{5.2}$$

where, X_b is car body displacement, X_w is wheel hub displacement and F_d is unmeasured disturbance force.

Also, the equations of motion of the active suspension are:

$$F_d = F_{hyd} \tag{5.3}$$

Therefore, Equation 5.1 becomes:

$$M_b \ddot{X}_b = F_{hyd} \tag{5.4}$$

where, F_{hyd} is the force transferred from the hydraulic actuator to the car body.

The behaviour of the passive suspension is simulated, as F_d is assumed to be the same in both cases, i.e. the passive and active cases. Rearranging the above equations by replacing F_d with F_{hyd} , therefore, means the equations can be written as:

$$F_{hyd} - b_d(\dot{X}_w - \dot{X}_b) - k_s(X_w - X_b) = 0 \quad (5.5)$$

$$(X_w - X_b) = \frac{1}{k_s} F_{hyd} - \frac{b_d}{k_s} (\dot{X}_w - \dot{X}_b) \quad (5.6)$$

Assuming that the car body velocity is comparatively small, then:

$$(\dot{X}_w - \dot{X}_b) \approx \dot{X}_w \quad (5.7)$$

Moreover, Equation 5.6 becomes:

$$(X_w - X_b) = \frac{1}{k_s} F_{hyd} - \frac{b_d}{k_s} \dot{X}_w \quad (5.8)$$

Equation 5.8, is an essential equation for the Lotus model. That is because, if the force, F_{hyd} , and the velocity, \dot{X}_w , can be measured by a load cell and a velocity sensor respectively, they may be used to forecast the relative displacement $(X_w - X_b)$ occurring as a result of the unmeasured disturbance force F_d . Ideally, if the suspension displacement, i.e. the actuator displacement, is ultimately able to offset $(X_w - X_b)$, the disturbance force, F_d should not affect the dynamic of the car body. Consequently, the force transferred to the car body representing the acceleration should be minimised.

Therefore, the required displacement for the actuator is:

$$(X_w - X_b)_d = -\frac{1}{k_s} F_{hyd} + \frac{b_d}{k_s} \dot{X}_w \quad (5.9)$$

In general, this equation may not be exactly correct because the dynamic of the hydraulic actuator does not correctly produce the required motions. Therefore, the displacement demand is compared with the actual displacement measured from an LVDT and the difference $(X_w - X_b)_d - (X_w - X_b)$ amplified to produce an electrical current, or voltage, to control the servovalve. If the amplifier gain connected to the current or voltage is significant, then:

$$(X_w - X_b) \approx (X_w - X_b)_d \quad (5.10)$$

As required. This results in a closed-loop control system, which tries to force $(X_w - X_b)$ equal to $(X_w - X_b)_d$. The schematic diagram in Fig. 5.4 shows how the system works in a servo controller format. Spring and damper rates may be

readily varied adaptively in a computer program by changing the values of k_s and b_d in Equation 5.9.

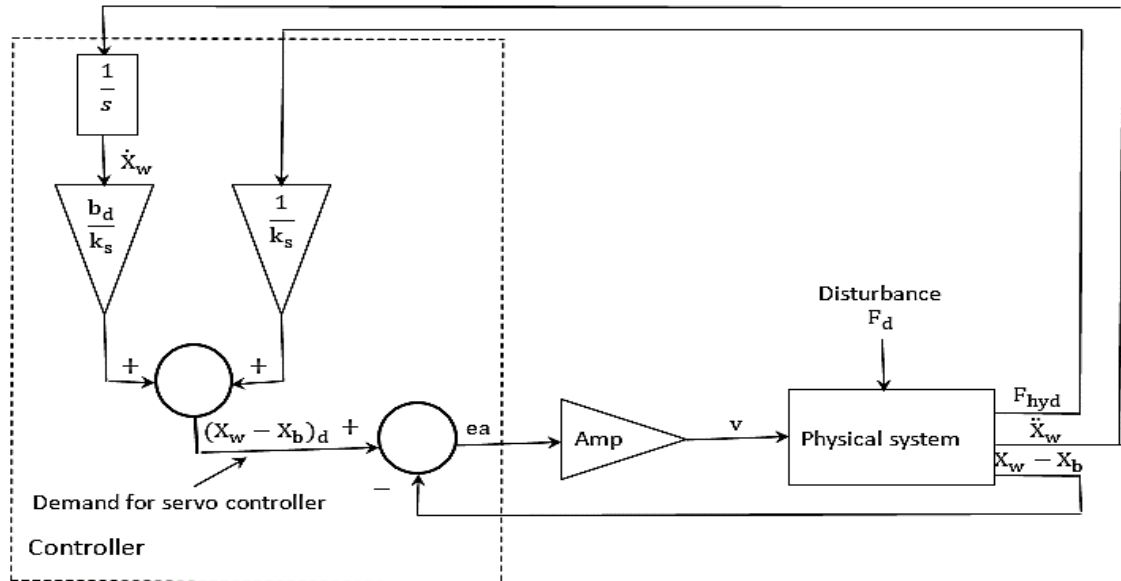


Fig. 5.4. Control block diagram of the Lotus active suspension in servo controller format.

In the case where the disturbance force, F_d , is applied to the system via the wheel unit instead of the car body (as in the original Lotus derivation), it may be assumed that the wheel unit velocity is equivalent to the system disturbance which, can be neglected from the controller design stage. Therefore,

$$(\dot{X}_w - \dot{X}_b) \approx -\dot{X}_b \quad (5.11)$$

By the rearrangement of the block diagram, the original Lotus model proves to be a regulator controller qualified with the unmeasured road input velocity applied at the wheel hub. Fig. 5.5 shows a system block diagram in the organisation of a regulator controller transformed from the original servo controller in Fig. 5.4. This circumstance is interesting because the Lotus model can be classified into either a servo or a regulator controller, depending upon the variable of interest. If the transfer function relating $(X_w - X_b)$ to its demand is considered, the system can be categorised into a servo controller application. On the other hand, if the transfer function relating $(X_w - X_b)$ to the road input disturbance, either displacement or velocity, is considered, the system can be grouped into a regulator controller application instead. However, from a controller design and primary function of active suspension viewpoint, considering the

system as a regulator controller is more appropriate than the servo type; this will be used in subsequent study.

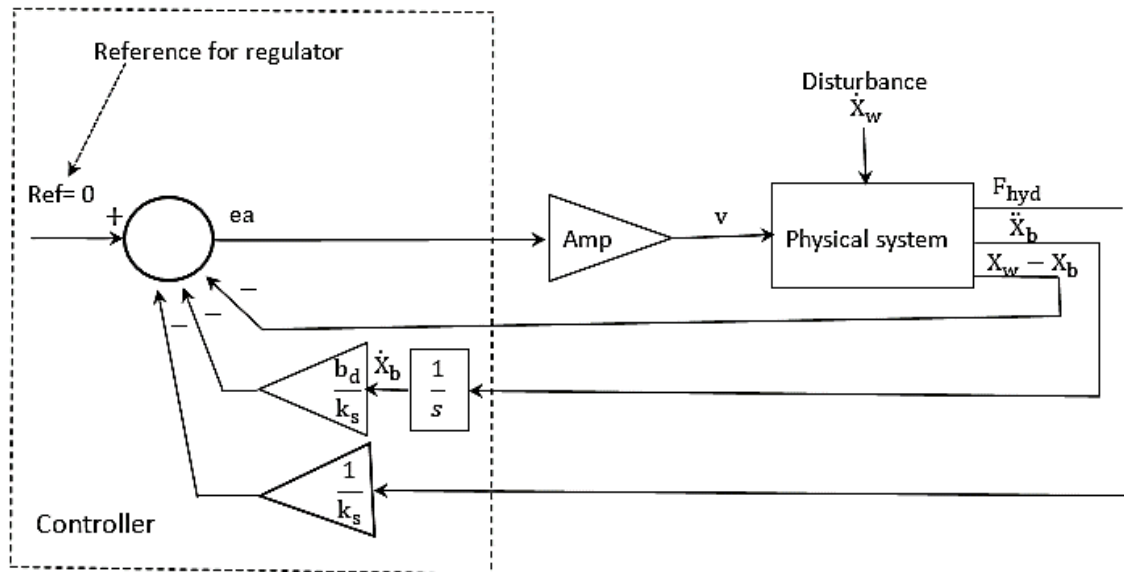


Fig. 5.5. Control block diagram of the Lotus active suspension in regulator controller format.

5.3 Hydraulic nonlinear system modelling

In general, Electro-Hydraulic Servo Systems (EHSS) are widely used in many industrial applications and mobile systems because of their high power-to-weight ratio, high stiffness, fast response, self-cooling, unique positioning capabilities, etc. However, the dynamical models of EHSS have many uncertainties, which are the consequence of physical characteristics, disturbances and load variations (FitzSimons and Palazzolo 1996). The dynamic behaviour of these systems is highly nonlinear due to phenomena such as pressure-flow characteristics, hysteresis in flow gain characteristics, oil leakage, oil temperature variations, characteristics of valves near null and so on. In practice, determining the exact dynamic model that will contain all the physical phenomena of EHSS presents a difficult task. The dynamics of hydraulic systems are highly nonlinear as were mentioned by an old, but still excellent textbook written by (Merritt 1967) and (Arafa and Rizk 1987). In addition, a nonlinear backstepping control technique, in light of a high gain observer design, was displayed for a single-rod electro-hydraulic actuator, with a proportional model changed and utilised for load pressure, to establish the connection between displacement command and virtual command of load weight reported by (Guo et al. 2015). (Fu et al. 2015)

conducted the building-up of the mathematical servovalve model, which established design and control, was added to investigate its characteristics and influential factors in-depth. (Maneetham and Afzulpurkar 2010) presented a proportional derivative controller for high-speed nonlinear hydraulic servo systems. (Alleyne and Hedrick 1995) considered the nonlinear dynamics of an electro-hydraulic actuator in a quarter car active suspension model and used these dynamics to formulate nonlinear control law; their study is interesting and therefore, the current study, tries to modify it.

While it is evident from the previous section that the hydraulic model was overlooked entirely from the Lotus model, it was assumed that the hydraulic system is capable of delivering force infinitely fast. However, in practice, the hydraulic dynamics significantly influence the system response, as will be shown later. Therefore, hydraulic modelling is investigated in this section.

5.3.1 Servovalve nonlinear model

The piston is assumed to support a vertical load acting such that it always attempts to retract the piston, that is, it always moves in the same direction. For open-loop control systems, a critically lapped servovalve spool is assumed, and for closed-loop control systems, an asymmetrically underlapped servovalve spool is always assumed.

The modelling of a single rod actuator under closed loop position control with known actuator seal leakage presents exciting variations from the usual published literature. It will be theoretically shown that this system results in three position offsets due to the seal leakage term, the integrator removal characteristic by the hypothetical open loop transfer function and the dynamic servovalve equation.

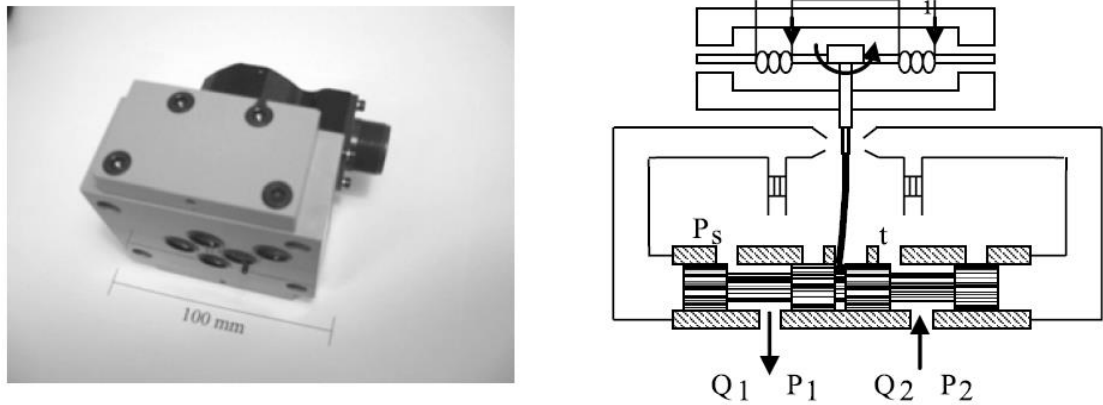


Fig. 5.6. Electrohydraulic servovalve (Watton 2007).

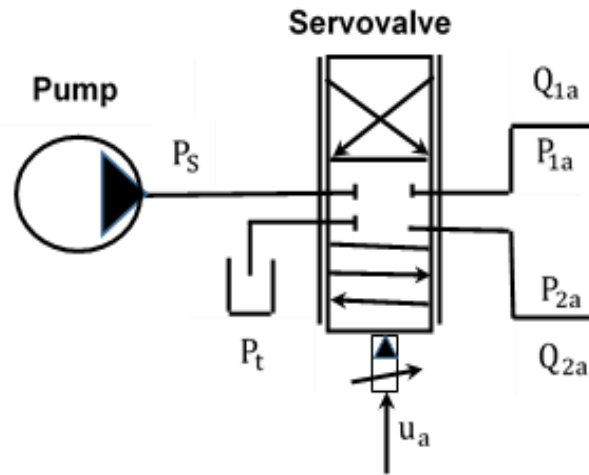


Fig. 5.7. Servovalve schematic diagram.

Considering Figs. 5.6 and 5.7, showing the picture and schematic diagram of the servovalve used with the active system test rig and the schematic diagram of the servovalve connection to the pump and the hydraulic actuator respectively and conventional modelling (Alleyne and Hedrick 1995) and (Watton 2007), the servovalve equations are nonlinear. These equations, whose flow rate passes by the valve, is a function of two inputs: voltage signal and the square root of pressure drop across the valve. Therefore, the flow rate relationships for both sides are given by:

$$Q_{1a} = f(v_{sa}, P_{1a}) \quad (5.12)$$

$$Q_{2a} = f(v_{sa}, P_{2a}) \quad (5.13)$$

Note that: the symbol “a” is refers to active instead of “r” which refers to the road.

Due to the nonlinear dynamics of the actuator, orifice flow of the hydraulic fluid and Coulomb friction forces generated by the actuator seals, linear control techniques often fail to meet performance specifications (Alleyne and Hedrick 1992).

Using a term to cancel-out the effect of the Coulomb friction force inside the actuator, the resulting control law becomes:

$$u_a = v_{sa} + F_f \quad (5.14)$$

where, F_f is the Coulomb friction force inside the actuator. Then,

$$Q_{1a} = f(u_a, P_{1a}) \quad (5.15)$$

$$Q_{2a} = f(u_a, P_{2a}) \quad (5.16)$$

The voltage input, u_a , of the proposed controller given by a first order system is:

$$\dot{x}_{sa} = \frac{1}{\tau_a} (k_a u_a - x_{sa}) \quad (5.17)$$

$$x_{sa} = \int \dot{x}_{sa} dt \quad (5.18)$$

where, τ_a (s) is a time servovalve constant, k_a is the gain of the servovalve, u_a (mv) is the servovalve controller, x_{sa} (m) is the servovalve spool movement and \dot{x}_{sa} (m/s) is spool velocity. The suggested controllers are PA and LQ controllers, as demonstrated in **Chapter 6**.

Therefore, the flowrate equations were developed for two cases dependent on the direction of the active spool movement and assuming negligible tank return pressure.

Case1: if $x_{sa} \geq 0$ when extending, as shown in Fig. 5.8.

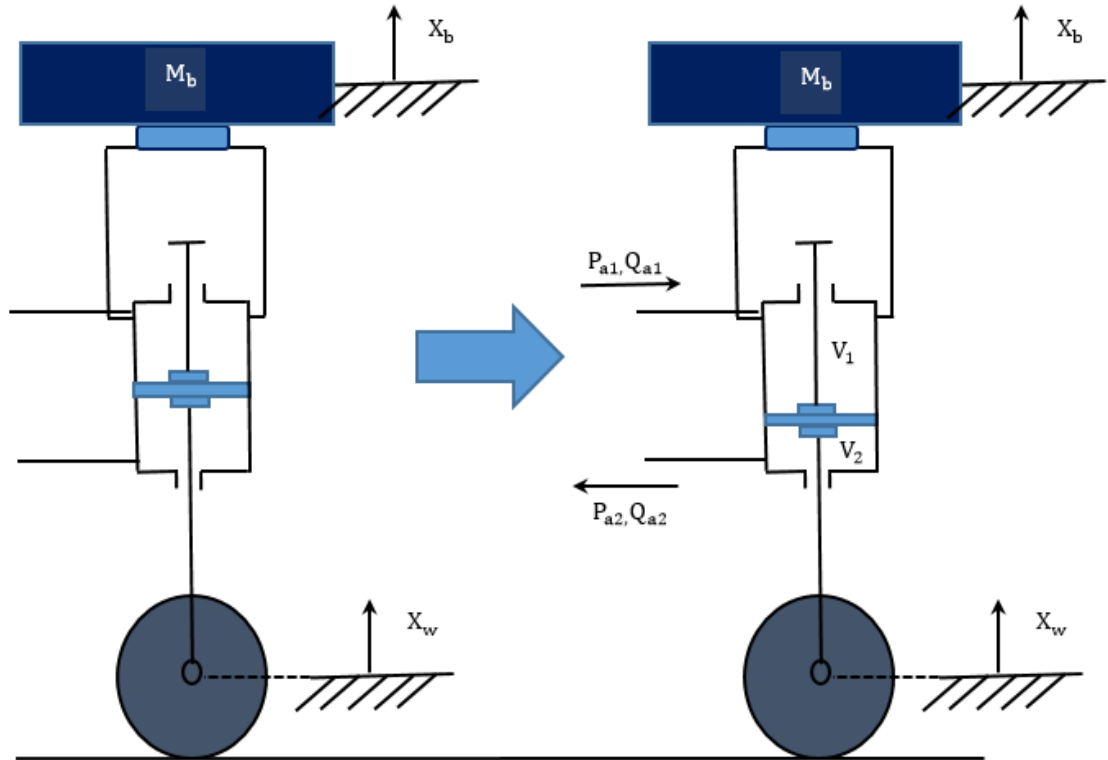


Fig. 5.8. Extending case of the active actuator.

Considering the actuator flow rate equations, the sign of the pressure, or pressure difference, under the square root should be checked. Thus,

$$\text{if } P_{sa} - P_{1a} \geq 0 \quad (5.19)$$

$$Q_{1a} = K_{fa} x_{sa} \sqrt{P_{sa} - P_{1a}} \quad (5.20)$$

$$\text{if } P_{sa} - P_{1a} < 0 \quad (5.21)$$

$$Q_{1a} = -K_{fa} x_{sa} \sqrt{|P_{sa} - P_{1a}|} \quad (5.22)$$

$$\text{if } P_{2a} \geq 0 \quad (5.23)$$

$$Q_{2a} = K_{fa} x_{sa} \sqrt{P_{2a}} \quad (5.24)$$

$$\text{if } P_{2a} < 0 \quad (5.25)$$

$$Q_{2a} = -K_{fa} x_{sa} \sqrt{|P_{2a}|} \quad (5.26)$$

Case 2: If $x_{sa} < 0$ when retracting, as shown in Fig. 5.9.

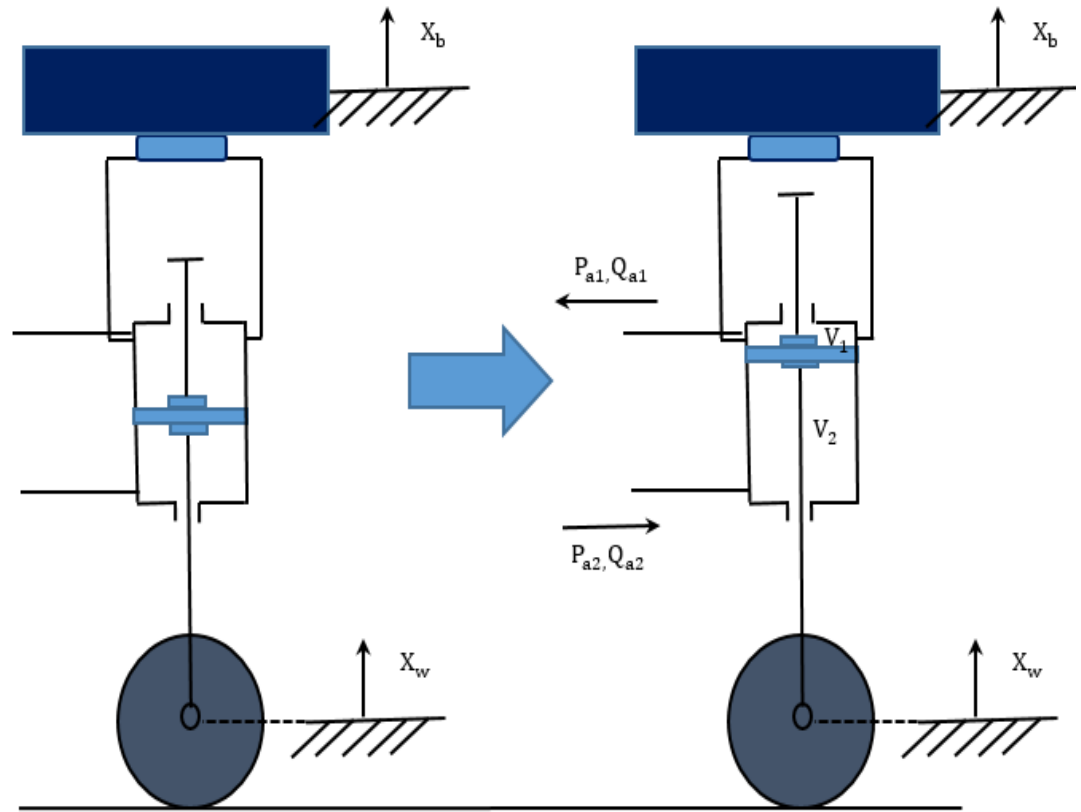


Fig. 5.9. Retracting case of the active actuator.

$$\text{if } P_{sa} - P_{2a} \geq 0 \quad (5.27)$$

$$Q_{2a} = K_{fa} x_{sa} \sqrt{P_{sa} - P_{2a}} \quad (5.28)$$

$$\text{if } P_{sa} - P_{2a} < 0 \quad (5.29)$$

$$Q_{2a} = -K_{fa} x_{sa} \sqrt{|P_{sa} - P_{2a}|} \quad (5.30)$$

$$\text{if } P_{1a} \geq 0 \quad (5.31)$$

$$Q_{1a} = K_{fa} x_{sa} \sqrt{P_{1a}} \quad (5.32)$$

$$\text{if } P_{1a} < 0 \quad (5.33)$$

$$Q_{1a} = -K_{fa} x_{sa} \sqrt{|P_{1a}|} \quad (5.34)$$

In summary, we have two cases depending on the direction of x_{sr} :

For $x_{sr} \geq 0$ when extending, the flowrate equations are:

$$Q_{1a} = K_{fa} x_{sa} \sqrt{|P_{sa} - P_{1a}|} \text{sign}(P_{sa} - P_{1a}) \quad (5.35)$$

$$Q_{2a} = K_{fa} x_{sa} \sqrt{|P_{2a}|} \text{sign}(P_{2a}) \quad (5.36)$$

For $x_{sa} < 0$ when retracting, the flowrate equations are:

$$Q_{2a} = K_{fa} x_{sa} \sqrt{|P_{sa} - P_{2a}|} \text{sign}(P_{sa} - P_{2a}) \quad (5.37)$$

$$Q_{1a} = K_{fa} x_{sa} \sqrt{|P_{1a}|} \text{sign}(P_{1a}) \quad (5.38)$$

If $Q_{1a} \approx Q_{2a}$ then the supply pressure is given by:

$$P_{sa} = P_{1a} + P_{2a} \quad (5.39)$$

Load pressure is defined as:

$$P_L = P_{1a} - P_{2a} \quad (5.40)$$

Assuming $P_L = 0$, then it follows that:

$$P_{1a} = P_{2a} = \frac{P_{sa}}{2} \quad (5.41)$$

From the above equations and the assumption that P_{sa} , P_{1a} and P_{2a} are positive values only, it follows that:

$$Q_{1a} (\text{case } x_{sa} \geq 0) = Q_{1a} (\text{case } x_{sa} < 0) \quad (5.42)$$

$$Q_{2a} (\text{case } x_{sa} \geq 0) = Q_{2a} (\text{case } x_{sa} < 0) \quad (5.43)$$

Simplified servovalve equations for both cases are:

$$Q_{1a} = K_{fa} x_{sa} \sqrt{P_{sa} - P_{1a}} \quad (5.44)$$

$$Q_{2a} = K_{fa} x_{sa} \sqrt{P_{2a}} \quad (5.45)$$

It should be noted that the sign of Q_{1a} and Q_{2a} from the above equations depends on the direction of x_{sa} .

5.3.2 Characteristic servovalve equation within the scope of linearization

Considering a characteristic servovalve, steady-state perfect flow equations will serve to demonstrate the inherent nonlinear characteristic of this crucial hydraulic component used for precision control applications.

To analyse the behaviour of engineering systems, mathematical models are required for the various components. It is standard practice to try to obtain linear models, since a rich mathematical theory exists for linear systems. These models will always be approximate, although possibly entirely accurate for defined ranges of system variables. Inevitably, nonlinear effects will eventually be found for large excursions of system variables. Linear systems have the valuable property of satisfying the superposition principle. This leads to many essential advantages in methods of analysis of them (Atherton 2011).

Traditionally, power systems are designed and operated conservatively in a region where behaviour is mainly linear. In the case of small disturbances, linearised models of the power system around an equilibrium point are adequate for stability analysis and control design.

From the previous section, it is evident that the servovalve equations are nonlinear whose flow rate outputs are functions of two factors: spool movement (applied voltage) and pressure. By considering the relationships given by Equations 5.44 and 5.45 and the servovalve flow characteristics. The small port opening areas on either side vary linearly with spool displacement and the general Bernoulli flow equations, can be used, as used by the servovalve manufacturers (Watton 2007). For the current study, the legacy servovalve test rig leads us to suppose drawbacks occur, such as the erosion of servovalve orifices and so on. Subsequently, the servovalve characteristics should be experimentally validated. As a result, as shown in Figs. 5.10 and 5.11, the servovalve flow rate for both side chambers still has a linear behaviour according to applied voltages within a period of around 0.0 to -1.0 volts, but with a considerable set-off problem that could affect the servo performance.

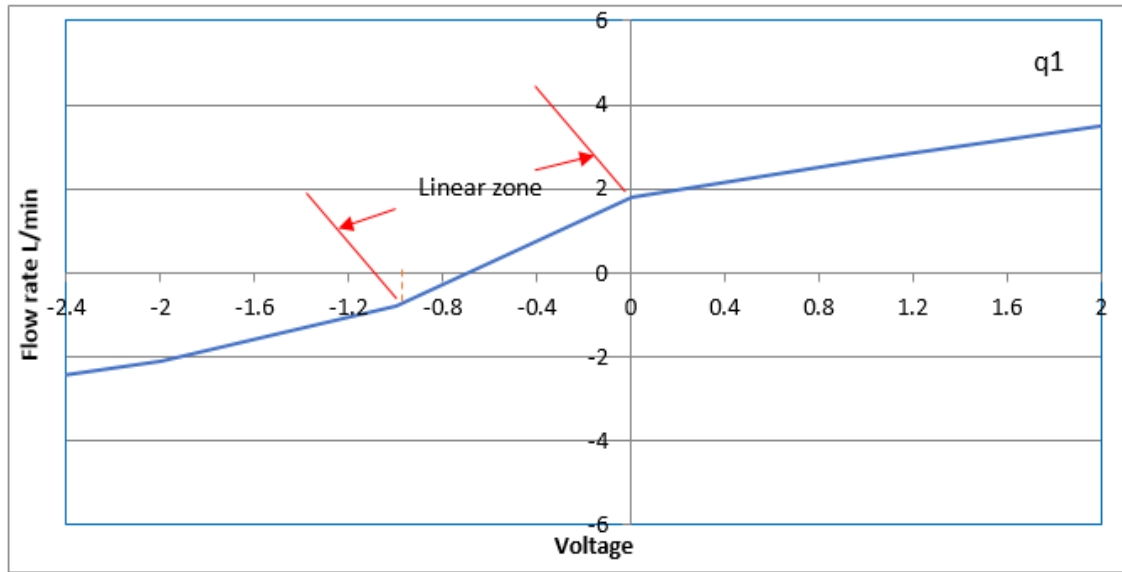


Fig. 5.10. Flow rate/voltage characteristics for servovalve side one.

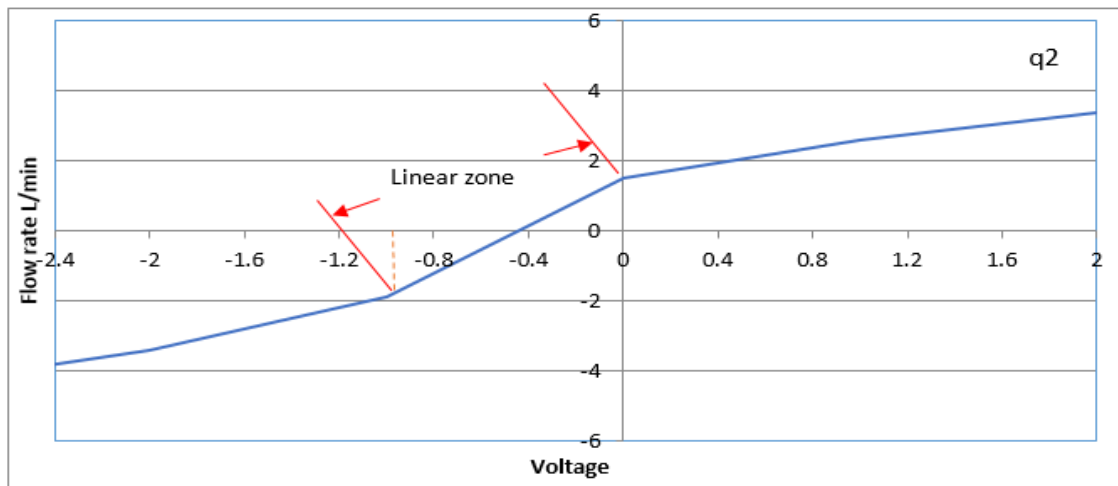


Fig. 5.11. Flow rate/voltage characteristics for servovalves side two.

The linearization technique presented here is valid within the vicinity of the operating conditions. Therefore, to obtain a linear mathematical model, the strategy is connected to servovalve controlled systems, whereby the nonlinear flow features are linearised and then joined with the other system dynamic terms (Watton 2007). Such an approach can give an appreciable vision into the way parameters affect system performance, assuming that the applied voltage, or spool movement, and the pressure drops deviate only slightly from the operating conditions. Consequently, the flow rates in this vicinity have a linear relationship

with the voltages, as mentioned. There follows the question of how to represent this fact. This is achieved using only the first linear term of the Taylor series expansion for a nonlinear function. Accordingly, slight variations in each parameter lead to:

$$\delta Q_{1a} = K_{sa1} \delta x_{sa} - k_{p1} \delta P_{1a} \quad (5.46)$$

$$\delta Q_{2a} = K_{sa2} \delta x_{sa} - k_{p2} \delta P_{2a} \quad (5.47)$$

where,

$$K_{sa1} = \left. \frac{\delta Q_{1a}}{\delta x_{sa}} \right|_{P_{1ass}} = k_{fa} \sqrt{P_{sa} - P_{1ass}} = \frac{Q_{1ass}}{x_{sass}} \quad \text{Flow gain}$$

$$k_{pa1} = - \left. \frac{\delta Q_{1a}}{\delta P_{1a}} \right|_{x_{sass}, P_{1ass}} = \frac{k_{fa} x_{sass}}{2\sqrt{P_{sa} - P_{1ass}}} = \frac{Q_{1ss}}{2(P_{sa} - P_{1ass})} \quad \text{Pressure coefficient}$$

$$K_{sa2} = \left. \frac{\delta Q_{2a}}{\delta x_{sa}} \right|_{P_{2ass}} = k_{fa} \sqrt{P_{2ass}} = \frac{Q_{2ss}}{x_{sass}} \quad \text{Flow gain}$$

$$k_{pa2} = \left. \frac{\delta Q_2}{\delta P_{2a}} \right|_{x_{sass}, P_{2ass}} = \frac{k_{fa} x_{sass}}{2\sqrt{P_{2ass}}} = \frac{Q_{2ss}}{2P_{2ass}} \quad \text{Pressure coefficient}$$

where, x_{sass} is the steady state servovalve spool movement relative to applied voltage and P_{1ass} and P_{2ass} are the steady-state pressures. It can be seen that, at the null condition when, $u_{ass} = 0$ ($x_{sass} = 0$) and $P_{sa}/2 = P_{1ass} = P_{2ass}$, for a critically lapped spool, it therefore follows that:

$$\text{Flow gain} \quad K_{sa1} = K_{sa2} = K_{sa} \quad (5.48)$$

$$\text{Pressure coefficient} \quad k_{pa1} = k_{pa2} = k_{pa} = 0 \quad (5.49)$$

Hence, the characteristic linear servovalve equations are:

$$Q_{1a} = Q_{2a} = k_{sa} x_{sa} \quad (5.50)$$

where,

$$k_{sa} = k_{fa} \sqrt{P_{sa} - P_{1ass}} = k_{fa} \sqrt{P_{2ass}} = k_{fa} \sqrt{P_{sa}/2} \quad (5.51)$$

It is vital to remember that the linearization technique presented here is valid within the vicinity of the operating conditions and can only be considered to help in the design of linear controls. However, because the operating conditions

vary widely, such linearization equations are not adequate. Therefore, the nonlinear equations are considered in the remainder of the current study.

5.3.3 Nonlinear actuator model and hydraulic force

Consider a fluid control volume having input and output flow rates as shown in Fig. 5.12. A flow rate continuity equation is given in the form:

$$Q_i - Q_o = \dot{V} + \frac{V}{\beta_{ea}} \dot{P} \quad (5.52)$$

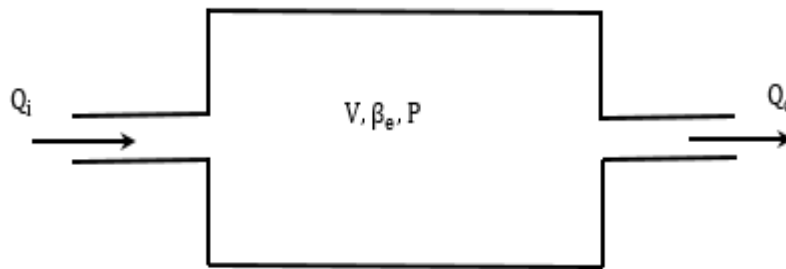


Fig. 5.12. Flows entering and leaving a control volume.

The difference between the input and output flow rates, obtained from dynamic theory, contains two components:

1. Boundary deformation term, \dot{V}
2. Fluid compressibility term, $\frac{V}{\beta_{ea}} \dot{P}$

This flow rate continuity equation is characterised by accepting that deformation is equivalent to the rate of actuator chamber volume. Dynamically, there are two instances of actuator movement, extending and retracting. For mathematical analysis and regular control conditions, at approximately the mid-position of the actuator and the zero-voltage signal of the servovalve, i.e. the operating condition, extending and retracting can be defined by the positive and negative voltage signals, or up and down spool movement, $x_{sa} = f(u_a)$.

For the extending case, when $x_{sa} \geq 0$, as shown in Fig. 5.8, applying the generalised flow continuity equation gives:

$$Q_{1a} - 0 = \dot{V}_1 + \frac{V_1}{\beta_{ea}} \dot{P}_{1a} \quad (5.53)$$

$$0 - Q_{2a} = -\dot{V}_2 + \frac{V_2}{\beta_{ea}} \dot{P}_{2a} \quad (5.54)$$

Since the actuator is a double-rod type and in this study $V_1 = V_2 = V$, then it follows that:

$$Q_{1a} = \dot{V} + \frac{V}{\beta_{ea}} \dot{P}_{1a} \quad (5.55)$$

$$-Q_{2a} = -\dot{V} + \frac{V}{\beta_{ea}} \dot{P}_{2a} \quad (5.56)$$

$$\dot{V} = A_c(\dot{X}_b - \dot{X}_w) \quad (5.57)$$

Substituting Equation 5.57 into Equations 5.55 and 5.56 yields:

$$Q_{1a} = A_c(\dot{X}_b - \dot{X}_w) + \frac{V}{\beta_{ea}} \dot{P}_{1a} \quad (5.58)$$

$$Q_{2a} = A_c(\dot{X}_b - \dot{X}_w) - \frac{V}{\beta_{ea}} \dot{P}_{2a} \quad (5.59)$$

For the retracting case, when $x_{sa} < 0$, as shown in Fig. 5.9, applying the generalised flow continuity gives:

$$0 - Q_{1a} = -\dot{V}_1 + \frac{V_1}{\beta_{ea}} \dot{P}_{1a} \quad (5.60)$$

$$Q_{2a} - 0 = \dot{V}_2 + \frac{V_2}{\beta_{ea}} \dot{P}_{2a} \quad (5.61)$$

Therefore, by using the same assumption as when $x_{sa} \geq 0$, it follows that:

$$-Q_{1a} = A_c(\dot{X}_b - \dot{X}_w) + \frac{V}{\beta_{ea}} \dot{P}_{1a} \quad (5.62)$$

$$-Q_{2a} = A_c(\dot{X}_b - \dot{X}_w) - \frac{V}{\beta_{ea}} \dot{P}_{2a} \quad (5.63)$$

If Q_{1a} and Q_{2a} signs are controlled by the servovalve equations (spool valve direction), simplified actuator equations for both cases are:

$$Q_{1a} = A_c(\dot{X}_b - \dot{X}_w) + \frac{V}{\beta_{ea}} \dot{P}_{1a} \quad (5.64)$$

$$Q_{2a} = A_c(\dot{X}_b - \dot{X}_w) - \frac{V}{\beta_{ea}} \dot{P}_{2a} \quad (5.65)$$

Depending on the characteristic of the servovalve supplied by the manufacturer, no significant spool underlap, or overlap exists. Although often ignored, there are two sources of internal leakage: first, flow through the hydraulic

amplifier, which is relatively constant; second, flow around the spool, which varies with its position (Eryilmaz and Wilson 2000). Maximum internal leakage occurs at null. The problem of position-tracking an electro-hydraulic servo-system with internal leakage within the servovalve was investigated using a fuzzy-logic controller design approach and ignored internal leakages by (Kalyoncu and Haydim 2009). Therefore, it was assumed that the hydraulic leakage characteristic is dominated by the actuator piston radial clearance effect and the leakage effects must be included in the actuator equations. The net effects of cross-port leakage are to increase the damping characteristic of the actuator as the degree of leakage increases (Karpenko and Sepehri 2005).

Therefore, oil leakage is a function of the pressure difference across both sides of the actuator and cross-port leakage resistance. The active system's actuator flow rate equations, including compressibility and cross-line leakage effects for both parties, can be written as:

$$\frac{V}{\beta_{ea}} \dot{P}_{1a} = Q_{1a} - A_c(\dot{X}_b - \dot{X}_w) - \frac{(P_{1a} - P_{2a})}{R_{ia}} \quad (5.66)$$

$$\frac{V}{\beta_{ea}} \dot{P}_{2a} = A_c(\dot{X}_b - \dot{X}_w) + \frac{(P_{1a} - P_{2a})}{R_{ia}} - Q_{2a} \quad (5.67)$$

The actuator hydraulic force is given by:

$$F_{hyd} = A_c(P_{1a} - P_{2a}) \quad (5.68)$$

Depending on the schematic diagram of the active test rig, as shown in Fig. 5.13, and the free body diagrams of the car body and wheel unit, as depicted in Fig. 5.14, the friction forces can be implemented relative to a real dynamic situation that emanates from the effects of sliding the body mass on the lubricant bearings from one side and the real position of the actuator, by defining the dynamic construction angle between the actuator and linkage, from the other side. Therefore, the new equations of motion for active suspension systems considering the new term, body friction, in addition to conventional friction (viscous and Coulomb) that occurs inside the actuator are:

$$M_b \cdot \ddot{X}_b = [F_{hyd} - B_{va}(\dot{X}_b - \dot{X}_w) - F_f] \cos(\alpha \mp \Delta\alpha) - F_{fric} \quad (5.69)$$

$$M_w \cdot \ddot{X}_w = -[F_{hyd} - B_{va}(\dot{X}_b - \dot{X}_w) - F_f] \cos(\alpha \mp \Delta\alpha) + k_t(X_r - X_w) + b_t(\dot{X}_r - \dot{X}_w) \quad (5.70)$$

where, F_{fric} is the total friction force effects at the lubricant supported body bearings. The representation of nonlinear mathematical friction for Active Suspension (AS) is established in the next stage. This is the first-time body friction forces have been implemented with a $\frac{1}{4}$ car AS model.

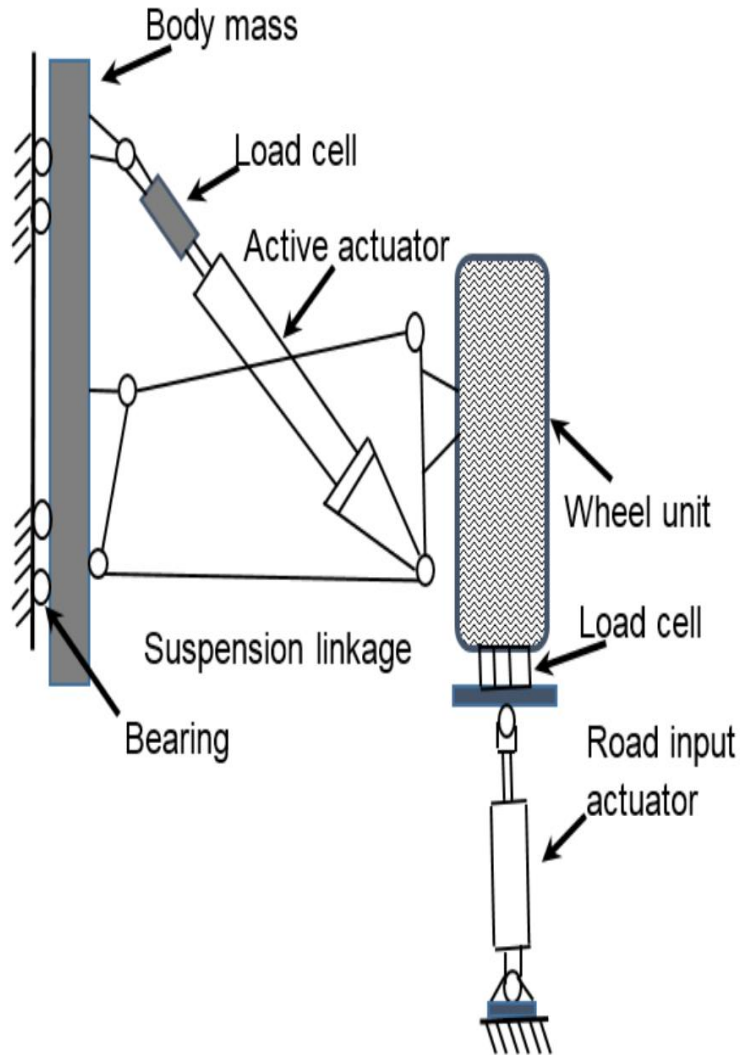


Fig. 5.13. Schematic diagram of the AS test rig.

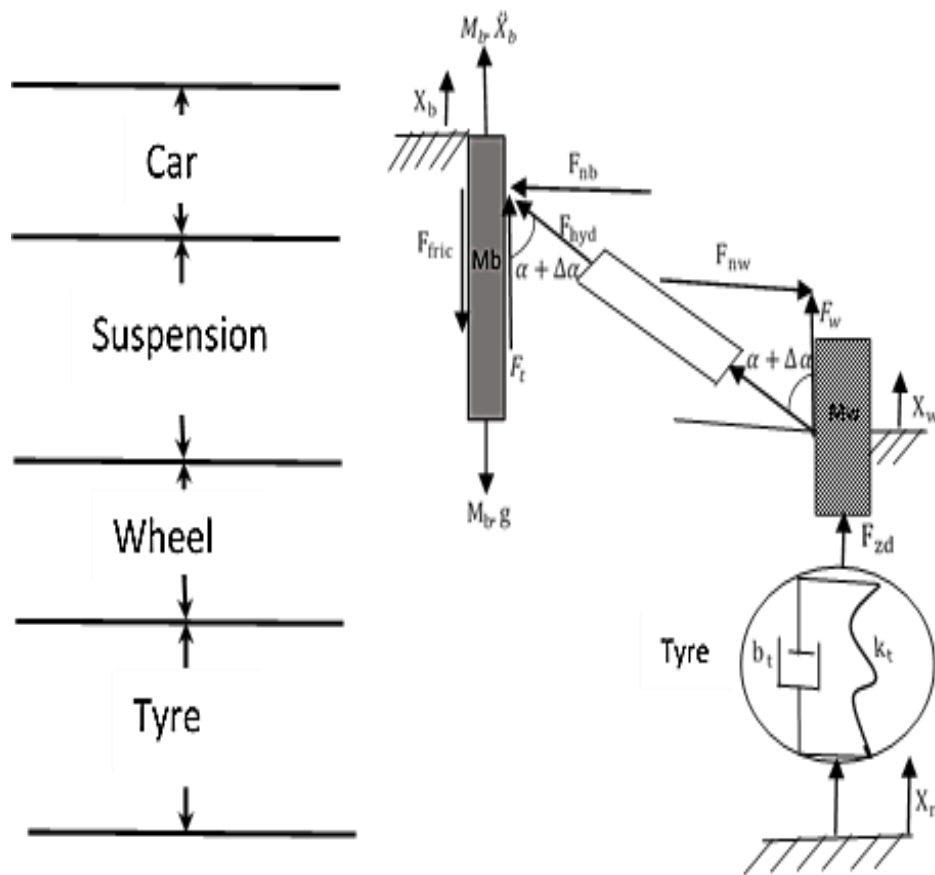


Fig. 5.14. Free body diagram of the 1/4 car and active suspension models.

5.4 Nonlinear friction forces model for AS

Since friction occurs at the linear supported body bearings of the test rig, it can therefore be supposed that the friction has the same behaviours for both experimentally passive and active suspension tests, as mentioned in **Chapter 3** on Passive Suspension (PS) and in **Chapter 4** on the explanation of friction. However, at the current stage, friction presents some different features depending on the type of input force and the quantity of vertical force. These are accounted for in different formulae relating to the constructions of the active test rig. Accordingly, the active hydraulic actuator replaces the spring and viscous damper used with the PS.

The nonlinear friction force for PS was modelled in **Chapter 4**. Friction depended on the history of the relative movements and velocities between the wheel and the body. This model included two main parts: static and dynamic friction. The latter, with two expressions, qualified the velocity value and direction

and vertical force. The friction comprises of: first, the transition behaviour from stiction to slide regimes, including the Stribeck effect; second, Coulomb friction resulting relative to the vertical dynamic force at body bearings, with a suitable friction coefficient, μ ; third, the viscous friction, dependent on the velocity times an appropriate viscous coefficient, σ_v .

Although the friction for the active suspension system includes, the same sectors as the PS system, the relative nonlinear friction model for the AS system contains different formulas as follows:

1. Static friction model

The maximum static friction is determined in a similar way to PS, which was considered depending on the vertical force balance, $\sum F_v = 0$, since the rest of the static friction for the active test rig is as follows:

$$F_{\text{fricS}} = [F_{\text{hyd}} - B_{va}(\dot{X}_b - \dot{X}_w) - F_f] \cos(\alpha \mp \Delta\alpha) \quad (5.71)$$

Alternatively, by applying Equation 5.68 to Equation 5.71, this become:

$$F_{\text{fricS}} = [A_c(P_{1a} - P_{2a}) - B_{va}(\dot{X}_b - \dot{X}_w) - F_f] \cos(\alpha \mp \Delta\alpha) \quad (5.72)$$

where, F_{fricS} is the static friction force.

2. Dynamic friction model

Depending on the direction of the body velocity, the dynamic frictions are:

If $\dot{X}_b > 0.0$

$$F_{\text{fricD}} = C_e e^{(|\dot{X}_b|/e1)} + \left[\frac{\mu M_w \dot{X}_w}{\tan(\alpha \mp \Delta\alpha)} \right] + \sigma_v \dot{X}_b \quad (5.73)$$

If $\dot{X}_b < 0.0$

$$F_{\text{fricD}} = -C_e e^{(|\dot{X}_b|/e1)} + \left[\frac{\mu M_w \dot{X}_w}{\tan(\alpha \mp \Delta\alpha)} \right] + \sigma_v \dot{X}_b \quad (5.74)$$

where, F_{fricD} is the dynamic friction force, C_e is a tracking parameter and $e1$ is the degree of curvature. From the dynamic friction equation, it can be seen that the transition and viscous frictions are in the same form as used in PS. Meanwhile, the Coulomb friction has a new expression relative to modifying the test rig. Therefore, the vertical force depends on the schematic diagram of the active test

apparatus and the type of inputs, as shown in Fig. 5.15 of the free body diagram and can be accounted by:

$$F_{nb} = \mp [M_w \ddot{X}_w] / \tan(\theta \mp \Delta\theta) \quad (5.75)$$

where, F_{nb} is the vertical component of the input forces to the body.

Consequently, the mathematical model for the total nonlinear frictions forces for AS are:

$$F_{fric} = \begin{cases} [F_{hyd} - B_v(\dot{X}_b - \dot{X}_w) - F_f] \cos(\alpha \mp \Delta\alpha) & \dot{X}_b = 0.0 \\ C_e e^{(|\dot{X}_b|/e1)} + \left[\frac{\mu M_w \ddot{X}_w}{\tan(\alpha \mp \Delta\alpha)} \right] + \sigma_v \dot{X}_b & \dot{X}_b > 0.0 \\ -C_e e^{(|\dot{X}_b|/e1)} + \left[\frac{\mu M_w \ddot{X}_w}{\tan(\alpha \mp \Delta\alpha)} \right] + \sigma_v \dot{X}_b & \dot{X}_b < 0.0 \end{cases} \quad (5.76)$$

where, F_{fric} is the total friction force at the lubricant body bearings.

For the active system, the simple form for friction is considered by ignoring Coulomb friction, i.e. only damping friction, qualified by the reasons mentioned in **Chapter 4**. Therefore, the damping frictions are:

$$F_{fricd} = \begin{cases} [F_{hyd} - B_v(\dot{X}_b - \dot{X}_w) - F_f] \cos(\alpha \mp \Delta\alpha) & \dot{X}_b = 0.0 \\ C_e e^{(|\dot{X}_b|/e1)} + \sigma_v \dot{X}_b & \dot{X}_b > 0.0 \\ -C_e e^{(|\dot{X}_b|/e1)} + \sigma_v \dot{X}_b & \dot{X}_b < 0.0 \end{cases} \quad (5.77)$$

where, F_{fricd} is the damping frictions force.

It is important to state here that in contrast to most real-life situations where friction often deteriorates the system, friction here supports the control action, since it will not only diminish body fluctuations, but also reduce body acceleration, which is identical with the primary target of the controller.

5.5 Comparison between one-DOF and Lotus model

As demonstrated in the previous section, if the model comprises the car body and the hydraulic system, supposing that the wheel unit is negligible, the model can be classified as a one-DOF model. It is sensible, to begin with the simplest one-DOF model because it frames the establishment of a two-DOF model and permits comparison between the models, including of the hydraulic system and the

original Lotus model, to be made. The main equations from the previous section that are used in this analysis, are summarised as follows:

$$Q_{1a} = Q_{2a} = k_{sa}x_{sa} \quad (5.78)$$

$$Q_{1a} = A_c(\dot{X}_b - \dot{X}_w) + \frac{V}{\beta_{ea}} \dot{P}_{1a} + \frac{(P_{1a} - P_{2a})}{R_{ia}} \quad (5.79)$$

$$Q_{2a} = A_c(\dot{X}_b - \dot{X}_w) - \frac{V}{\beta_{ea}} \dot{P}_{2a} + \frac{(P_{1a} - P_{2a})}{R_{ia}} \quad (5.80)$$

$$F_{hyd} = A_c(P_{1a} - P_{2a}) \quad (5.81)$$

$$M_b \ddot{X}_b = [F_{hyd} - B_{va}(\dot{X}_b - \dot{X}_w) - F_f] \cos(\alpha \mp \Delta\alpha) - F_{fricd} \quad (5.82)$$

Equations 5.79 and 5.80 represent the general form of the flowrate for both actuator sides. They are also correct in the vicinity of the area of the operating conditions, i.e. it could be possible to match them using Equation 5.78. Therefore, the five equations can be reduced to only two equations, as follows:

$$M_b \ddot{X}_b = [F_{hyd} - B_{va}(\dot{X}_b - \dot{X}_w) - F_f] \cos(\alpha \mp \Delta\alpha) - F_{fricd} \quad (5.83)$$

$$2k_{sa}x_{sa}A_c = 2A_c^2(\dot{X}_b - \dot{X}_w) + \frac{V}{\beta_{ea}} \dot{F}_{hyd} + \frac{2}{R_{ia}} F_{hyd} \quad (5.84)$$

As mentioned, AS can be classified by the experience of the regulator control system with unmeasured disturbances from the road inputs. For the one-DOF model, \dot{X}_w is equivalent to the system disturbance. In the model proposed for the controller design, the disturbances \dot{X}_w , F_f and F_{fricd} are assumed to be zero. The System Equations 5.83 and 5.84 then become:

$$M_b \ddot{X}_b = [F_{hyd} - B_{va}\dot{X}_b] \cos(\alpha \mp \Delta\alpha) \quad (5.85)$$

$$2k_{sa}x_{sa}A_c = 2A_c^2\dot{X}_b + \frac{V}{\beta_{ea}} \dot{F}_{hyd} + \frac{2}{R_{ia}} F_{hyd} \quad (5.86)$$

Taking Laplace transforms and discounting the initial conditions allows the force transfer function to be written as:

$$F_{hyd} = \frac{k_{sa}A_c}{\left(\frac{1}{R_{ia}} + \frac{Vs}{2\beta_{ea}}\right)} x_{sa} - \frac{A_c^2s}{\left(\frac{1}{R_{ia}} + \frac{Vs}{2\beta_{ea}}\right)} X_b \quad (5.87)$$

In addition, the open-loop transfer function relating X_b to x_{sa} can be written as:

$$\frac{X_b}{x_{sa}} = \frac{2k_{sa}A_c \cos(\alpha \mp \Delta\alpha)}{\left(2A_c^2(\alpha \mp \Delta\alpha) + \frac{2Bva}{R_{ia}}\right)s + \left(\frac{2M_b}{R_{ia}} + \frac{BvaV}{\beta ea}\right)s^2 + \frac{M_bV}{\beta ea}s^3} \quad (5.88)$$

Using knowledge of state-space theory, at least three state variables are required to control three closed-loop poles at third-order system. Considering Systems Equations 5.85 and 5.86, the most appropriate state variables are F_{hyd} , \dot{X}_b and X_b . It can be seen that the number of state variables in this analysis is equal to the number of feedback signals used in the Lotus model. Table III shows a comparison between the feedback signals from this analysis, a one-DOF model, and those from the Lotus model.

Table III Comparison of state feedback signals

One-DOF model	Lotus model
1. Hydraulic force (F_{hyd})	1. Hydraulic force (F_{hyd})
2. Velocity of car body (\dot{X}_b)	2. Velocity of wheel hub (\dot{X}_w)
3. Car body travels (X_b)	3. Relative displacement between car body and wheel hub ($X_w - X_b$)

Both hydraulic force signals are duplicated. The wheel velocity in the Lotus model is still related to the car body velocity in the one-DOF model because the Lotus model is adaptable and is approached from $(\dot{X}_w - \dot{X}_b) \approx \dot{X}_w$. Also, for a qualified displacement in the Lotus model, if X_w is considered to be the system disturbance, i.e. X_w is fixed to the ground, this means that $X_w - X_b$ in the Lotus model corresponds to X_b . From this assessment, even though the one-DOF and Lotus model are derived from different methodology, they are similar regarding the use of the same state variables.

5.6 Two-DOF model

To cover a system it is useful to add the wheel unit to the one-DOF model, which yields a more complex and complete model called the two-DOF model. This model is more representative than the one-DOF model and additional physical restriction, i.e. the tyre deflection, can be included in the modelling. Apparently, this more complex model necessitates more state variables to define the system

and more state feedback signals to control the system dynamics. These are investigated in this section. The main equations from the previous section proposed for use in this analysis, in addition to considering an equation of motion for wheel mass, are summarised as follows:

$$M_b \ddot{X}_b = [F_{hyd} - B_{va}(\dot{X}_b - \dot{X}_w) - F_f] \cos(\alpha \mp \Delta\alpha) - F_{fricd} \quad (5.89)$$

$$M_w \ddot{X}_w = [-F_{hyd} + B_{va}(\dot{X}_b - \dot{X}_w) + F_f] \cos(\alpha \mp \Delta\alpha) + k_t(X_r - X_w) + b_t(\dot{X}_r - \dot{X}_w) \dots \quad (5.90)$$

$$2k_{sa}A_c x_{sa} = 2A_c^2(\dot{X}_b - \dot{X}_w) + \frac{V}{\beta_{ea}} \dot{F}_{hyd} + \frac{2}{R_{ia}} F_{hyd} \quad (5.91)$$

By considering Equations 5.17 and 5.18, the control and servovalve spool movement relationship can be written as:

$$\dot{x}_{sa} = \frac{1}{\tau_a} (u_a - x_{sa}) \quad (5.92)$$

$$x_{sa} = f(u_a) \quad (5.93)$$

$$u_a = K_{ba} * ea \quad (5.94)$$

Therefore, Equation 5.91 becomes:

$$2k_{sa}A_c u_a = 2A_c^2(\dot{X}_b - \dot{X}_w) + \frac{V}{\beta_{ea}} \dot{F}_{hyd} + \frac{2}{R_{ia}} F_{hyd} \quad (5.95)$$

Regarding experimental work, the gain is:

$$K_{ba} = GP \quad (5.96)$$

where, $G = D/A$ is the sensor gain convertor, P is the forward gain for the two-DOF model and ea is the active control error signal.

The ¼ car response variables that need to be examined are:

1. Car body acceleration, \ddot{X}_b
2. Suspension displacement, $X_w - X_b$
3. Tyre deflection, $X_r - X_w$
4. The applied voltage to the servovalve, u_a

From a modelling viewpoint, the three variables (\ddot{X}_b , $X_w - X_b$, $X_r - X_w$) may be regarded as system outputs, the control signal, equivalent to u_a , is system input and \dot{X}_r and X_r are unmeasured system disturbances. Fig. 5.15 shows the block diagram representing communication between the system and its environment. Noticeably, the system is a multi-input multi-output model relative to the benefits previously mentioned. The state-space method for system modelling that was used was decided upon because it allowed a multivariable controller design to be directly performed after the modelling process.

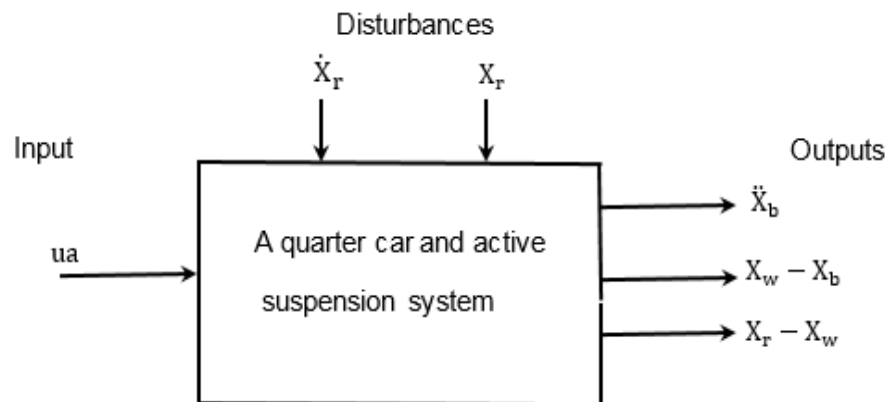


Fig. 5.15. Block diagram representing the interaction between the system and its environment.

5.6.1 Open-loop state-space model

For the state-space model, the first question for this modelling problem is how to select the state variables. The state variables are the factors that determine the feature responses of the system when present states, excitation inputs and the equations defining the dynamics of the system are known. Therefore, the selection principles are that the set of chosen state variables must be sufficient to control the dynamics of the system of interest and the numbers of the state variables should be as few as possible to avoid redundancies and should be measured. According to Equation 5.88, the transfer function relating X_b to x_{sa} could determine that no fewer than three state variables are required to control three closed-loop poles in the third-order system for the instance of the one-DOF model. Theoretically, the wheel unit is represented by a mass, spring and damper. In order to control the motions of the wheel unit, two state variables related to the wheel unit, velocity and displacement, need to be measured. Therefore, when the wheel unit is added to the one-DOF model the total number

of state variables to be measured in order to control the two-DOF model is equal to five.

Some publications employ car, X_b and wheel hub, X_w , displacements to form a set of state variables because it is convenient for the mathematical modelling and controller design (Crolla and Nour 1988) and (Ljung 1999). Although there is no problem for a theoretical study or simulation, in practice, awareness of such sensors is a severe issue. In real life, X_b and X_w cannot be measured because they are referenced mathematically to an ideal ground which does not exist in reality. Displacement sensors, LVDTs, are only able to measure, the relative movement between the car body and the ground, $X_b - X_r$ and the relative movement between the car body and wheel hub, $X_b - X_w$. In this work, therefore, the practical presentation was considered. The mathematical model was repositioned in such a way that the state variables that were practically measurable were chosen.

From Equations 5.89, 5.90 and 5.95, it may be deduced that the most suitable state variables are:

1. Car body velocity, \dot{X}_b
2. Wheel hub velocity, \dot{X}_w
3. Hydraulic force, F_{hyd}
4. Suspension displacement, $X_b - X_w$
5. Tyre deflection, $X_w - X_r$

By using the following state-space notations:

$$x_1 = \dot{X}_b$$

$$x_2 = \dot{X}_w$$

$$x_3 = F_{hyd}$$

$$x_4 = X_b - X_w$$

$$x_5 = X_w - X_r$$

The system equations may be rearranged to first-order differential equations with differential terms isolated on the left-hand side.

$$\ddot{X}_b = -\frac{B_{va} \cos(\alpha \mp \Delta\alpha)}{M_b} \dot{X}_b + \frac{B_{va} \cos(\alpha \mp \Delta\alpha)}{M_b} \dot{X}_w + \frac{\cos(\alpha \mp \Delta\alpha)}{M_b} F_{hyd} - F_f \cos(\alpha \mp \Delta\alpha) - \frac{1}{M_b} F_{fricd} \dots \dots \dots (5.97)$$

$$\ddot{X}_w = \frac{B_{va}(\alpha \mp \Delta\alpha)}{M_w} \dot{X}_b - \frac{(B_{va} + b_t)(\alpha \mp \Delta\alpha)}{M_w} \dot{X}_w - \frac{\cos(\alpha \mp \Delta\alpha)}{M_w} F_{hyd} - F_f \cos(\alpha \mp \Delta\alpha) - \frac{k_t}{M_w} (X_w - X_r) + \frac{b_t}{M_w} \dot{X}_r \dots \dots \dots (5.98)$$

$$\dot{F}_{hyd} = -\frac{2\beta_{ea} A_c^2}{V} \dot{X}_b + \frac{2\beta_{ea} A_c^2}{V} \dot{X}_w - \frac{2\beta_{ea}}{V R_{ia}} F_{hyd} + \frac{2k_{sa} A_c G P \beta_{ea}}{V} e_a \dots \dots \dots (5.99)$$

$$\dot{X}_b - \dot{X}_w = \dot{X}_b - \dot{X}_w \dots \dots \dots (5.100)$$

$$\dot{X}_w - \dot{X}_r = \dot{X}_w - \dot{X}_r \dots \dots \dots (5.101)$$

These equations may be written in the state-space form given by:

$$\dot{x} = Ax + Bea + G_d \dot{X}_r \dots \dots \dots (5.102)$$

where,

$$x = \text{State vector} = \begin{bmatrix} \dot{X}_b \\ \dot{X}_w \\ F_{hyd} \\ X_b - X_w \\ X_w - X_r \end{bmatrix}$$

$$A = \text{System matrix} = \begin{bmatrix} -\frac{B_{va} \cos(\alpha \mp \Delta\alpha)}{M_b} & \frac{B_{va} \cos(\alpha \mp \Delta\alpha)}{M_b} & \frac{\cos(\alpha \mp \Delta\alpha)}{M_b} & 0 & 0 \\ \frac{B_{va} \cos(\alpha \mp \Delta\alpha)}{M_w} & -\frac{(B_{va} + b_t) \cos(\alpha \mp \Delta\alpha)}{M_w} & -\frac{\cos(\alpha \mp \Delta\alpha)}{M_w} & 0 & -\frac{k_t}{M_w} \\ -\frac{2\beta_{ea} A_c^2}{V} & \frac{2\beta_{ea} A_c^2}{V} & -\frac{2\beta_{ea}}{V R_{ia}} & 0 & 0 \\ 1 & -1 & 0 & 0 & 0 \\ 0 & 1 & 0 & 0 & 0 \end{bmatrix}$$

$$B = \text{Input vector} = \begin{bmatrix} 0 \\ 0 \\ \frac{2k_{sa}A_cGP\beta_{ea}}{V} \\ 0 \\ 0 \end{bmatrix}$$

ea = Active control error signal

$$G_d = \text{Disturbance vector} = \begin{bmatrix} 0 \\ \frac{B_t}{M_w} \\ 0 \\ 0 \\ -1 \end{bmatrix}$$

where, \dot{X}_r is the disturbance signal, i.e. the velocity of the road disturbance.

Fig. 5.16 shows a block diagram of the open-loop state-space model. It should be noted that the open-loop state-space model of the active suspension is different from the standard state-space format because of the disturbance term on the right-hand side of the state equation. A further point is that this model includes a tyre damping rate term neglected by the majority of published papers. This is important because, as was shown in **Chapter 3** in Section 3.7, this parameter is one of the vital parameters and cannot be neglected.

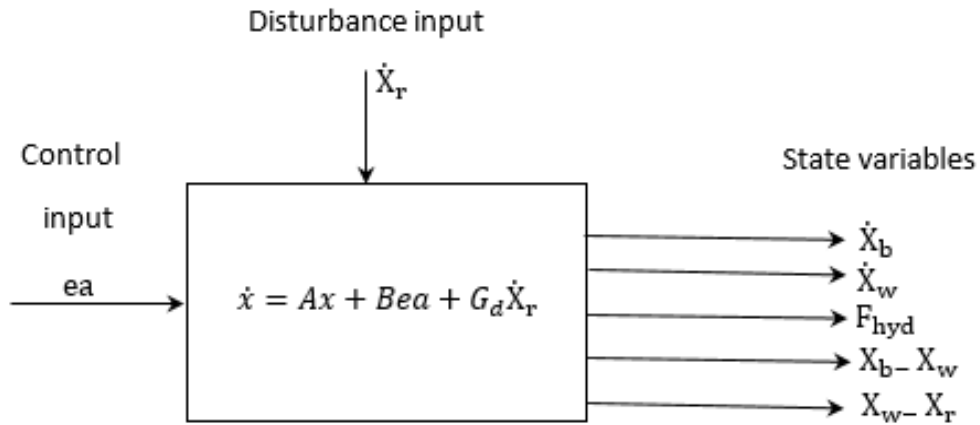


Fig. 5.16. Block diagram of the open-loop state-space model.

5.6.2 Closed-loop system

When a full-state feedback control law is introduced, as shown in Fig. 5.17,

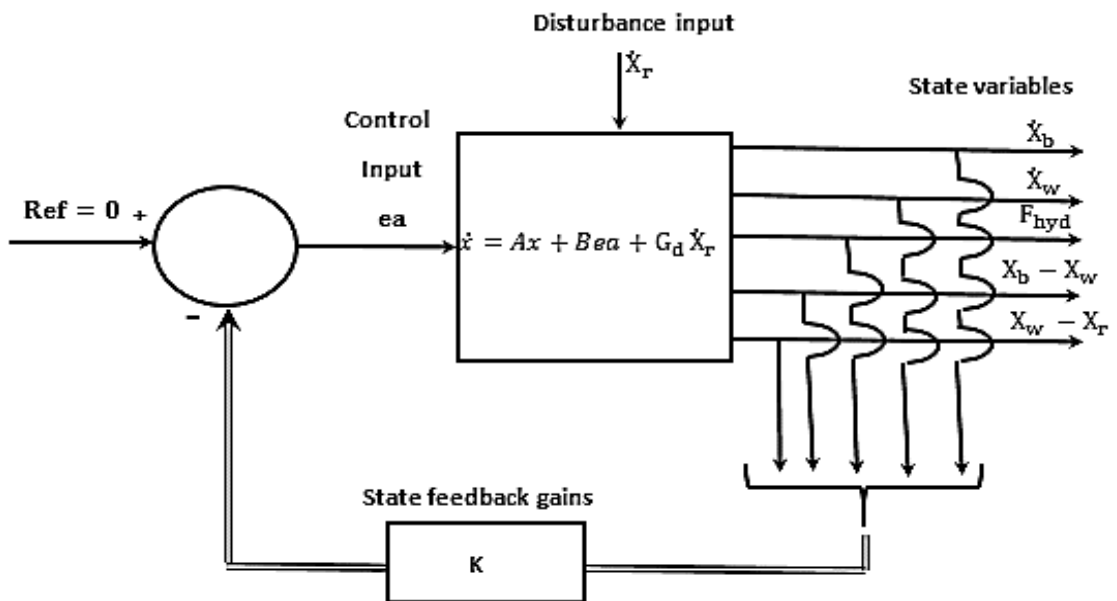


Fig. 5.17. Full-state feedback control applied to the state-space model.

The control signal, ea becomes a function of all five state variables and feedback gains:

$$\begin{aligned}
 ea &= -Kx \\
 &= -NK_1K_2x
 \end{aligned}
 \tag{5.103}$$

$$= -N(I_1I_2\dot{X}_b + J_1J_2\dot{X}_w + H_1H_2F_{hyd} + F_1F_2(X_b - X_w) + L_1L_2(X_w - X_r))$$

where,

$K = 1 \times 5$ State feedback gain vector

$N = A/D$ Gain (data acquisition converted gain)

$K_1 = 1 \times 5$ State feedback gain vector for the controller,

$$K_1 = [I_1 \ J_1 \ H_1 \ F_1 \ L_1]$$

$K_2 = 5 \times 5$ Transducer gain matrix

$$K_2 = \begin{bmatrix} I_2 & 0 & 0 & 0 & 0 \\ 0 & J_2 & 0 & 0 & 0 \\ 0 & 0 & H_2 & 0 & 0 \\ 0 & 0 & 0 & F_2 & 0 \\ 0 & 0 & 0 & 0 & L_2 \end{bmatrix}$$

The problem of the active suspension design is how to achieve the gains of the five state variables that allow the system to minimise \ddot{X}_b within the physical constraints of $X_w - X_b$ and $X_r - X_w$ and the limitation of the control input, u_a . The algorithm controller design is investigated in **Chapter 6**.

5.7 Discussion

This Chapter was set up to question the aspects of the active suspension model that merit inclusion within the $\frac{1}{4}$ car model. After a brief re-stating of the concept of Lotus active suspension, the nonlinear hydraulic system used to generate the control force and how one- and two-DOF models, with frictional considerations, were established. This discussion will review and summarise the findings.

- **The Lotus active suspension concept**

As mentioned in Section 5.2, the unique Lotus model was thought not to be fitting for comprehensive vehicle investigation because the predominant system disturbances ought to be obtained from the road roughness rather than the aerodynamic downforce. Along the same lines, the Lotus model was revisited. Even though this resulted in similar control law, it provides a more practical view for general analysis.

The principal supposition of the Lotus model is that it attempts to design active suspension to reproduce the conduct of passive suspension in an adaptive way, which is able to change conditions. Even though the Lotus model is just a one-DOF model disregarding hydraulic and wheel unit design, it provides an essential understanding of how active suspension works in practice. This became the motivation for further development of this task.

According to the derived control law, the required suspension displacement is generated from the measurement of force and wheel hub velocity. The remarkable reality is that the constant gain for the force signal is equivalent to the inverse of the suspension stiffness and the constant gain for the velocity signal is equal to the ratio of the system damping to the suspension stiffness.

The Lotus model can be defined as either a servo or regulator controller depending upon the parameters concerned. It was shown that the original Lotus model, developed as a servo controller, is equivalent to the regulator type. For further development, it was decided to develop the system using the regulator control scheme because it is more practical regarding controller design.

- **Hydraulic system modelling**

The servovalve equations are, in fact, nonlinear equations whose flow rate outputs are functions of electrical voltage and a square root of pressure drop across the servovalve ports, as illustrated in Section 5.3. The nonlinear servovalve equations were converted to the linear ones using the linearization technique assuming that the voltage and the pressure drop deviate only slightly from the normal operating conditions. It is critical to be aware that the linearization method used in this work is valid in the neighbourhood of the ordinary working conditions and was only used for helping to design a controller. However, in real experimental work, the operating conditions change widely and the linearization equation cannot deal with the problem, so the elaborate, nonlinear equation is used in this study. In addition, the main contribution of the suggested fundamental controller is to be used to drive the nonlinear system by enhancing performance. Regarding the full-state feedback control, all five state variables describing the system dynamics must be fed back to the controller. A transformation from the

pressure difference across the actuator ($P_{1a} - P_{2a}$) into the hydraulic force, F_{hyd} , reduces the number of state variables required for feedback. Consequently, it reduces the number of transducers and signals for processing the workload. This becomes more significant if a full car model were developed instead of the quarter car model because the number of sensors and signal processing units is related to cost.

However, the transformation is valid only for the double-rod actuator:

$$F_{hyd} = A_c(P_{1a} - P_{2a}) \quad (5.104)$$

The pressure difference relates to the force by a constant gain representing a cross-sectional area of the actuator. On the other hand, if a single-rod actuator is used:

$$F_{hyd} = A_1 P_{1a} - A_2 P_{2a} \quad (5.105)$$

The transformation cannot be applied because the pressure difference and the force are not related by a constant gain. Therefore, in this situation, the pressure in both chambers of the actuator must be measured directly instead of using the force to satisfy the requirement of the full-state feedback control scheme.

- **Nonlinear friction forces model for AS**

The friction, for the active test rig, occurs according to same reasons of PS but with some different features, depending on the type of input force and the quantity of the normal force as demonstrated in Section 5.4. Since an active hydraulic actuator replaced the spring and viscous damper used with the PS, the friction force was, thus, accounted for in a different formula relative to this modification of the active construction test rig. In addition, as there is a slight difference between the general and damping friction, damping is consequently used with the AS system.

- **Comparison between one-DOF and Lotus model**

It was found that in order to apply the full-state feedback control to the one-DOF model, including the hydraulic system, the three state variables: (1) force, (2) car body displacement and (3) car body velocity, need to be fed back to the controller. In comparison with the original Lotus model, the three state variables of both

models are similar, even though they are derived from different approaches, as illustrated in Section 5.5.

- **Two-DOF model**

The main difference between the one- and two-DOF models is the wheel unit model, which causes additional design limitations, i.e. tyre deflection. The completed two-DOF model is an accurate multi-input multi-output system. The electrical voltage to the servovalve and the road disturbances may be regarded as the system inputs, while the car body acceleration, suspension displacement, and tyre deflection may be deemed to be the system outputs. State-space modelling was applied to the system because it allows the multivariable controller design to be performed after the modelling process as mentioned in Section 5.6. It was found that at least five state variables are compulsory for the implementation of the full-state feedback control. In comparison to previous publications that disregarded the hydraulic model, at least four state variables must be used to control the quarter car model. The possible measurements were also considered for the determination of five state variables. The car body and wheel hub displacements, which cannot be measured in practice, were rearranged into the relative displacement terms, i.e. the suspension movement and tyre deflection, which can be measured using transducers. Ultimately, it was found that the most suitable five state variables are: (1) car body velocity, (2) wheel velocity, (3) hydraulic force, (4) suspension displacement and (5) tyre deflection.

The hydraulic force equation was shown to be:

$$F_{\text{hyd}} = \frac{k_{\text{sa}} A_c}{\left(\frac{1}{R_{\text{ia}}} + \frac{v_s}{2\beta_{\text{ea}}}\right)} X_{\text{sa}} - \frac{A_c^2 s}{\left(\frac{1}{R_{\text{ia}}} + \frac{v_s}{2\beta_{\text{ea}}}\right)} (X_b - X_w) \quad (5.106)$$

The presence of cross-port leakage changes the actuator dynamic force equation in two ways. Firstly, the relationship with the applied voltage to the servovalve changes from an integral term to a first-order term. Secondly, the concept of static oil stiffness is not valid since the relationship between the generated force and the actuator displacement has a phase advance characteristic that exhibits a derivative behaviour at low frequencies.

According to the three disturbance transfer functions, the hydraulic parameters, i.e. the bulk modulus and oil leakage resistance, are dynamically coupled with all coefficients above the zero-order term in the transfer functions. This provides evidence that the hydraulic parameters influence the dynamic response of the active suspension and generates the motivation for further analysis.

- **In summary**

This chapter displayed the scheme to establish the control of the system by covering Lotus, one- and two-DOF for a $\frac{1}{4}$ car model and a nonlinear hydraulic actuator by implementing the servovalve dynamic equation.

Consideration of the nonlinear friction forces in this study is vital with regard to the role-played in helping to remove body fluctuation and decrease body acceleration. In real life, this has minute affect, relative to the suspension construction; nevertheless, the author hopes this study encourages researchers to rethink the use of the quarter, half and full car models.

For control purposes, therefore, this study focused on the linear behaviour of the servovalve, which is useful in establishing linearization. Consequently, a state space form was chosen to represent the system, which determines the number of state variables to control the system from one side, and to make sure these variables were measured on the other side. All of which helps in designing a fundamental linear control to drive the nonlinear system by enhancing system performance, as shown in **Chapter 6** next.

Design PA and LQ Controllers

6.1 Introduction

Vehicle suspensions have remained a popular research topic due to their essential role in ride comfort, vehicle safety, road damage minimisation and overall vehicle performance. Passive Suspension (PS), which was modelled and discussed in detail in **Chapter 3**, is possibly the most commonly used and is found in most vehicles. However, in the real world, PS has no means of adding external energy to a system because it contains only passive elements, such as a damper and spring. In contrast, Active Suspension (AS) can supply energy from an external source and generate force to achieve the optimal desired performance, as is organised explicitly within the test rig. From this point of view, AS with regard to pole-placement or Pole-Assignment techniques (PA) and Linear Quadratic Regulator (LQR) optimal control are investigated in this study.

A critical question that emerges in the outline of state variable compensators is whether every pole of the closed-loop system can be discretionarily placed in the complex plane. The poles of the closed-loop system are equivalent to the eigenvalues of the system matrix in state variable configuration. If the system is controllable, then it can benefit the planned goal of setting the poles precisely at desired locations to meet performance specifications. Full-state feedback design commonly relies on pole-placement techniques and was reported by (Dorf and Bishop 2011).

A further vital synthesis question examines whether, given a model, one could effectively synthesise a controller such that the closed-loop poles are in predefined areas. The current chapter will demonstrate this is to ascertain that it is conceivable. The term PA is an essential concept in control synthesis (Goodwin et al. 2001). The closed-loop systems, obtained by using either state feedback or output feedback, are described by four system matrices; A, B, C, and D. The purpose of adding feedback is to improve the system attributes to some degree. The impact of feedback on the properties of controllability, observability and stability need to be understood as mentioned by (Brogan 1991).

(Yang et al. 2016) focused on using the state-space representative for a wheel organised drive structure, arranged with vehicle body height changing dimension and wheel driving limit. They designed a PID controller to examine the closed-loop system stability with time-varying sampling.

From another perspective, to improve the stability and ride handling performance of the vehicle, AS systems have attracted a significant amount of research interest in the past few decades and comprehensive surveys on related research are found in publications. These have included classical PID control (Kumar 2008), multi-objective control (Gao et al. 2006), a robust design method of adaptive sliding mode control was derived (Fei and Xin 2012), active force control based architecture in characterising twin rotor multiple-input and a multiple-output (MIMO) system (Ramli et al. 2012).

In addition, distributed control literature provides numerous, beneficial approaches for achieving stability. It was shown by (Fax and Murray 2004) that stability of a formation depends on the agent model and eigenvalues of the Laplacian graph. This fact was later used by (Li et al. 2010) to derive a state-feedback controller, which works for any graph topology. Only the gain of the controller needs to be adjusted. A controller design presented by (Zhang et al. 2011) uses an LQR-like approach to achieve stability. Adaptive approaches can also be used (Li et al. 2013), (Li et al. 2015). (Herman and Sebek 2016) conducted a design state feedback based on a single-agent model. By using a sufficiently large coupling gain and meeting specific criteria, the control law was not only stabilising, but also LQ optimal.

(Surawattanawan 2000) conducted a previous active study for the same test rig and the PA and LQ controllers with a linear hydraulic actuator system without considering the friction forces. This allows for questioning of the validity of Surawattanawan's (2000) experimental results. However, in this study, in contrast to the previous research studies, a new term, friction forces was considered for the first time within the active $\frac{1}{4}$ car model system. However, in order to take into account the actual configuration of the test rig system, a new active suspension system model implementing the nonlinear lubricant friction forces that affect the supporting bearing's body, is considered, as was already established in **Chapter 5**. The general nonlinear friction forces were modelled, as mentioned in **Chapter 4**, and the specific form, damping friction, was used with the active system, as shown in **Chapter 5**. This model captured most of the friction behaviour that was experimentally observed. According to the active test rig, an active actuator is used, instead of the passive stiffness spring and viscous damper to generate the control force as a primary system controller. Therefore,

a nonlinear hydraulic actuator model covered by the dynamic of servovalve, has been modelled as displayed in **Chapter 5**. The controller has been shown in considerable detail using state-space representation.

In the current study, the aim was to design PA and LQ controllers to drive the nonlinear hydraulic active actuator to enhance AS system responses. The same road inputs have been used for the active system that was previously used for PS as modelled in **Chapter 3**. This approach could help in making a satisfactory comparison between the PS and AS systems. Also, bump and random inputs are designed and investigated by simulation to show the comparison between the PS and AS that used the PA and LQ controls, and to clearly demonstrate the robustness of the control.

This study tests control validity in two stages: the primary stage (simulations test) were performed on a C++ compiler and by using MATLAB Control System Toolboxes. A simulated model makes it possible to evaluate the performance with a mathematical approach. The second stage tests were carried out on the experimental test rig to assess the behaviour of the real system. Therefore, a study has been made to develop an active suspension system for the improved performance of a light passenger vehicle, by implementing the PA or LQ controllers with the suspension system and discovering how much improvement occurs in comparison with the inherent trade-off amongst ride comfort, suspension travel and road-holding abilities. Accordingly, the obtained results will be displayed later in this chapter.

6.2 Road simulator input

System input is one of the essential aspects of experimental or simulation work and for the current case; this is the road simulator input. The mixed input, as selected, is a ramp-up phase with various step amplitudes. Further, to avoid abrupt changes, these inputs were subjected to a first order filter, which was designed as a digital filter through the C++ compiler for the PS stage. To ensure the inputs are sufficient for requirements, PI control was selected and successfully achieved its target. The complete details of the road input simulator are documented in Section 3.2, **Chapter 3**.

Therefore, a comparison between the system responses for the AS (the present study) and the PS, which was previously studied in **Chapter 3**, was implemented. It is then of benefit to use the same input. For simulation purposes, the use of bump and random inputs, based upon the existing hydraulic system model, were also investigated.

6.3 Physical Modelling

This investigation considered the $\frac{1}{4}$ car model presented in Fig. 5.14, in **Chapter 5**, for the active test rig after replacing the PS units (spring and viscous damping) with a hydraulic actuator. Where, M_b and M_w are the masses of the chassis (sprung mass) and wheel assembly (unsprung mass), respectively. The mathematical model considering this alteration was previously derived in **Chapter 5**. The wheel unit remains the same as used with PS, with tyre stiffness (k_t) and tyre damping rate (b_t). The displacements of the chassis and wheel are represented by X_b and X_w , respectively and X_r is the road disturbance. F_{hyd} is the hydraulic actuator force applied between the body and wheel, while the suspension travel is given by $(X_w - X_b)$ and the dynamic load experienced by the tyre is denoted by $k_t (X_r - X_w)$ and $b_t (\dot{X}_r - \dot{X}_w)$.

6.4 Control issue and multivariable feedback control

When tackling a control issue, it is crucial to comprehend the essential objective of that control. However, the outlined objective connected in this chapter can be formally restated as the fundamental function of the system:

To minimise \ddot{X}_b within available $X_w - X_b$, $X_r - X_w$ and u_a .

The purpose of the present study is to use fractional representation models in the analysis and synthesis of feedback systems. In comparison with the primary function of the vehicle suspension, it should be noted that the applied voltage to the servovalve u_a is included as one of the physical constraint variables for the design objective. This is due to the voltage amplitude being bounded and limited by the amplifier and the rated voltage of the servovalve, i.e. the restrictions of the spool movement, x_{as} , which depends on the direction and voltage values, undoubtedly limiting regarding servovalve allowance.

A question that inevitably arises is why AS requires multivariable feedback control and whether it is possible to control the system using only single feedback, as typically used in hydraulic position control. Therefore, it is interesting to investigate the dynamic characteristic of the system under single feedback control, in addition to the multivariable case, for MIMO systems. Thus meaning they must be treated with great care. Therefore, one of the goals of the control theory was to capture significant elements of the engineering process of feedback design under the umbrella of a formal mathematical synthesis problem. The motivation for this goal is self-evident. Once formalised under such an umbrella, the elements of engineering art become rigorous tools that can be applied more or less automatically to ever more complex design situations as reported by (Stein and Athans 1987).

This study provides an alternative perspective on the methodology and presents several useful options. These include a formal weight selection procedure, which essentially permits arbitrary specification of system sensitivity functions for minimum phase problems; a classification of all recoverable functions in non-minimum phase problems and certain direct relationships between weights and sensitivities for the latter, which apply to all scalar and certain multivariable cases. The option was to directly synthesise a multivariable controller in terms of minimising some objective function. We utilised the word synthesise rather than design in order to stress a more formalised approach. With respect to the State Equation 5.102 in Section 5.6.1:

$$\dot{x}(t) = Ax(t) + Bea(t) + G_d\dot{X}_r(t) \quad (6.1)$$

A regulator controller type will be considered. Therefore, the disturbance term should be ignored during the controller design stage. Thus, the state equation becomes:

$$\dot{x} = Ax + Bu_a \quad (6.2)$$

$$y = Cx \quad (6.3)$$

where, x is a state vector for the plant (n -vector), u_a is a control signal (scalar), y is the output signal (scalar), $A = n * n$ and is a constant matrix, $B = n * 1$ and is constant matrix and $C = 1 * n$ is a constant matrix.

As stated, it was assumed that both the control signal, u_a , and the output signal, y , are scalars. By the appropriate choice of a set of state variables, it is possible to select an output equal to one or more of the state variables.

From the characteristic equation of the open-loop state-space model given by Equation 6.2, the transfer function relating $X_b - X_w$ to the control signal ea is unstable and if only one feedback signal is used, the feedback of $X_b - X_w$ must be chosen for system stability. Hence, from a practical view, the control signal error, ea , is of the form:

$$ea = -NF_1F_2(X_b - X_w) \quad (6.4)$$

where, N is the A/D converter, F_2 is the LVDT gain for suspension displacement and F_1 is the control gain.

Fig. 6.1 shows the control block diagram of this system, while the pole-zero closed system map for $(X_b - X_w)$ feedback of the state-space model, plotted using the MATLAB Control System Toolboxes (MathWorks 2000), is shown in Fig. 6.2. In particular the commands **sys=ss (A, B, C, D), H= tf (sys)** and **pzmap (H)**, determine the system has five poles and two zeros. Consequently, two loci terminate at two zeros while the other three loci approach infinity.

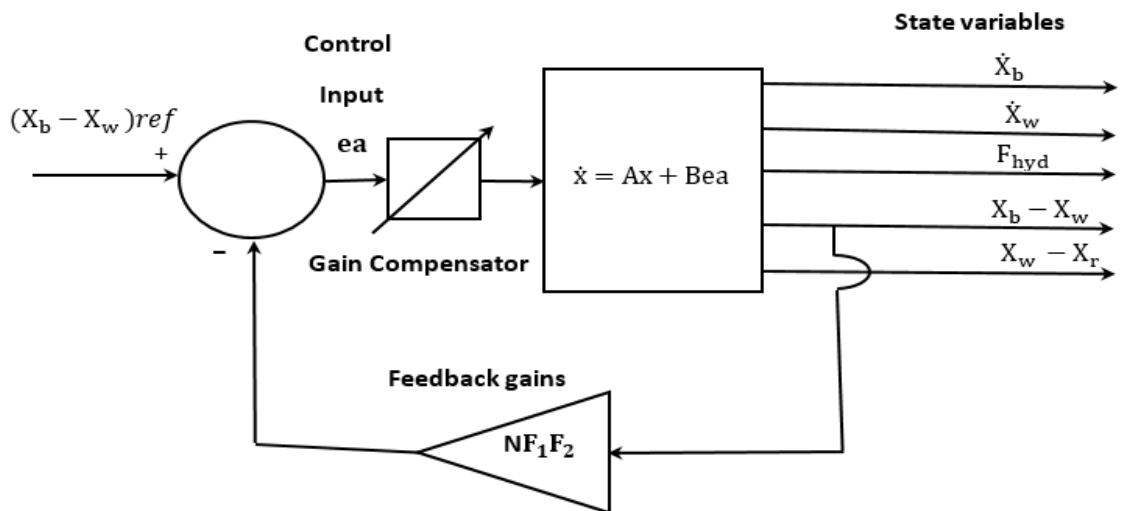


Fig. 6.1. Block diagram of single position feedback control.

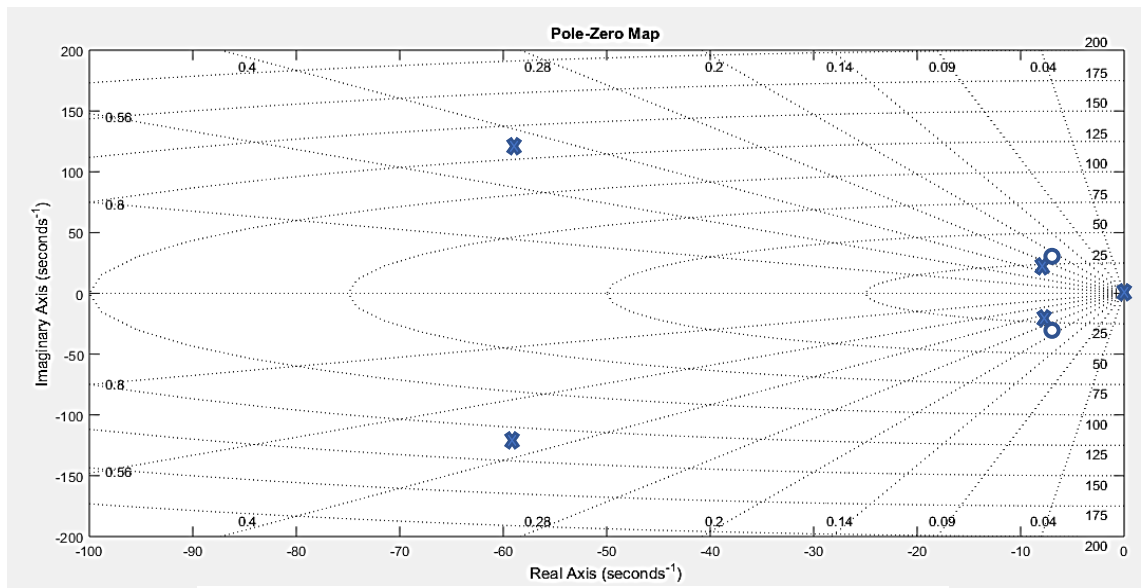


Fig. 6.2. Pole-Zero closed system map for $(X_b - X_w)$ feedback.

However, when considering full-state feedback control, as shown in Fig. 6.3, with three output variables $(X_b - X_w)$, $(X_w - X_r)$ and F_{hyd} , the system configuration is shown in Fig. 6.4.

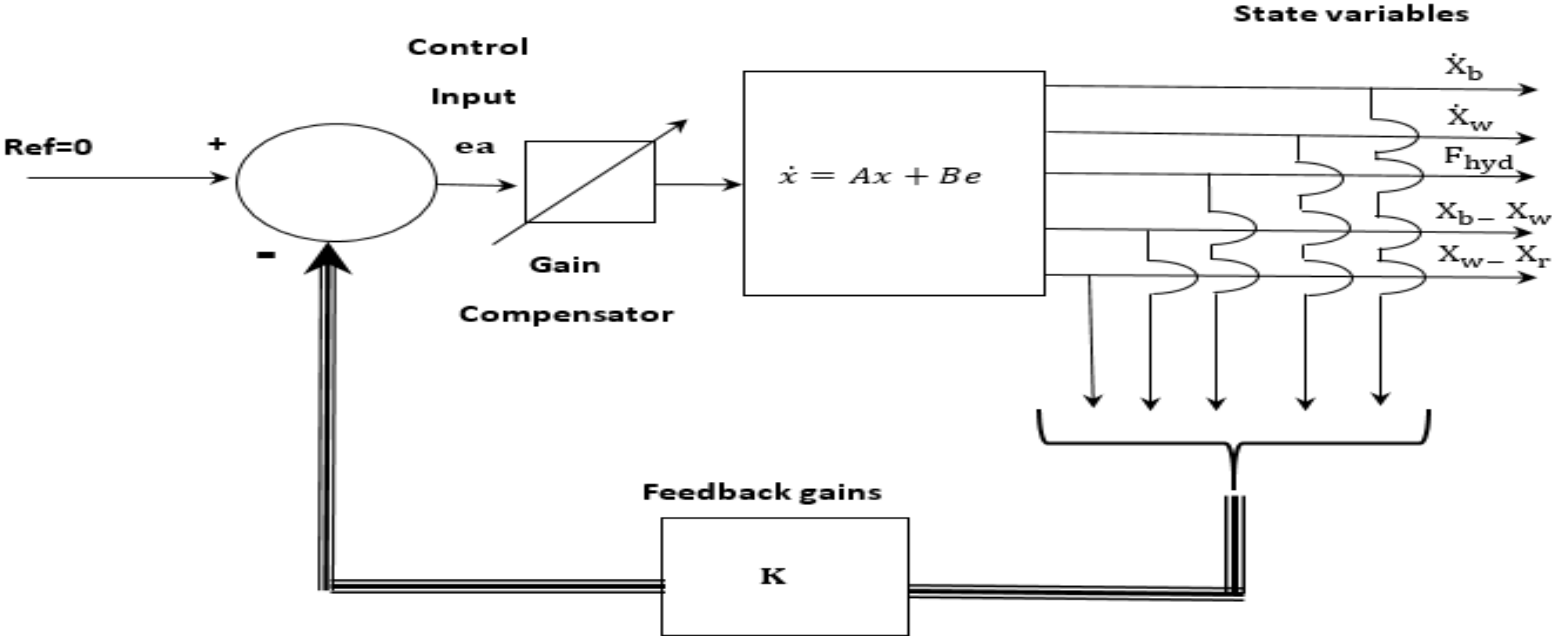


Fig. 6.3. Block diagram of full-state feedback control.

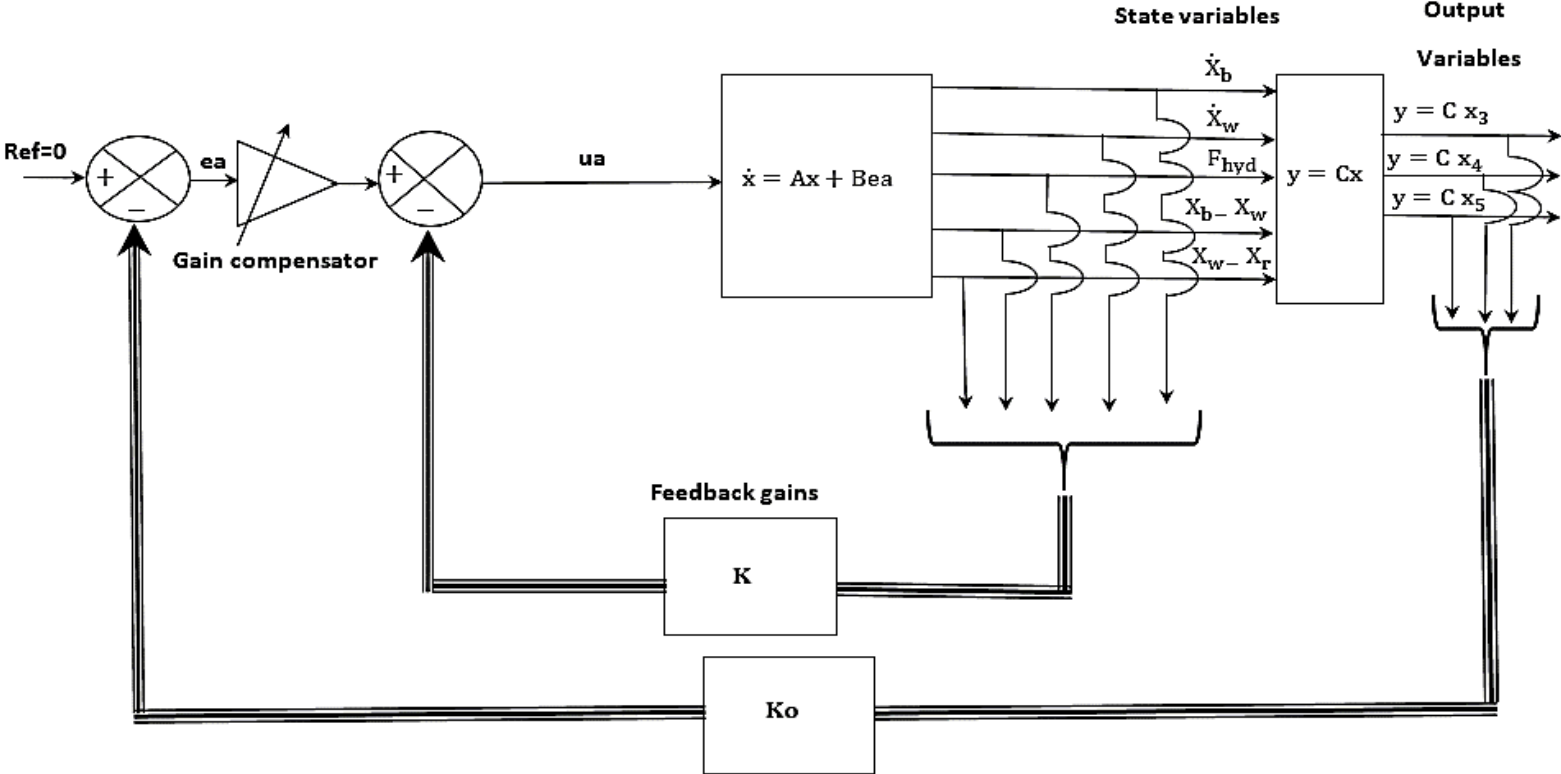


Fig. 6.4. Block diagram of full-state feedback PA controller.

The pole-zero closed system map for these feedbacks was shown in Fig. 6.5, with apparent disappeared zeros. Since the system is stable, according to Routh-Hurwitz, such a condition can be guaranteed if all poles are on the left-hand side i.e. no sign changes in the first column of the Routh table for specific proportional gain values (Nise 2010), as is evidently satisfied in Fig. 6.5. At low natural frequency, the system response is dominated by the three closed-loop poles near the imaginary axis. When the proportional gain increases, the two poles, which are close to an imaginary axis, move towards the imaginary axis for specific gain values. With increases in this gain, they will move following their branches to the right positive area and the system will change to unstable, whilst the other pole at the origin will just move to the left-hand side. Thus, the designer should keep in mind these pole positions before commencing design of a controller, which also helps in selecting a controller type. The primary control target is that the system should be stable with a fast response, i.e. maintain the two dominant poles with their branches on the left-hand side.

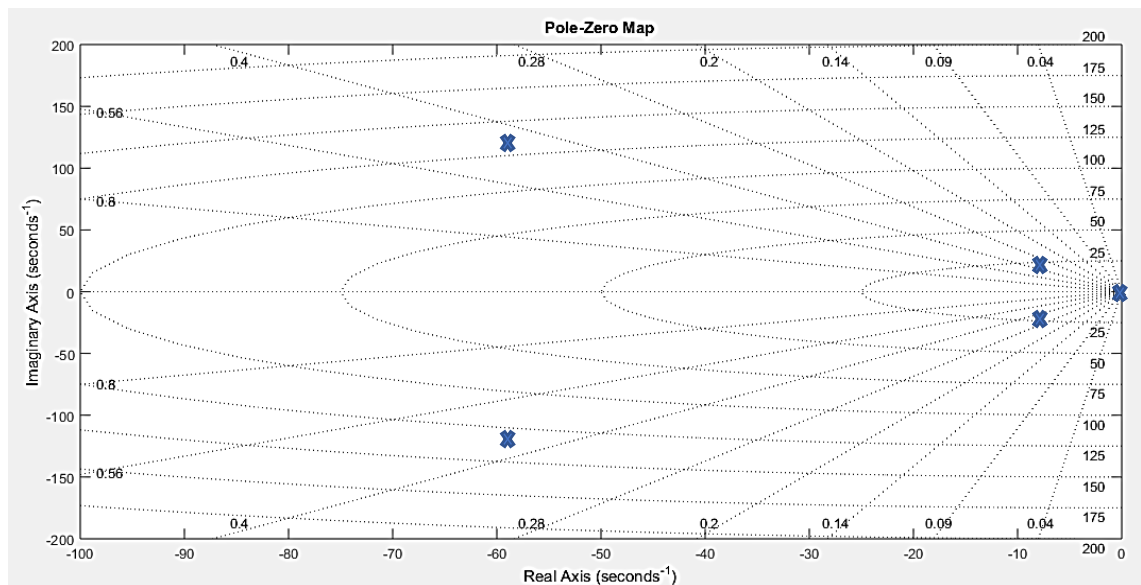


Fig. 6.5. Pole-Zero closed system map for $(X_b - X_w)$, $(X_w - X_r)$ and F_{hyd} feedbacks.

As previously mentioned, the designer should choose the types of feedback and later decide to select controller types. Therefore, depending on the test rig determinants, while using the single feedback control, the adjustment of the gain alone cannot provide a sufficient alteration to the system behaviour to meet the given specifications, i.e. increasing the position feedback gain will result in reduced stability, or even instability. Therefore, this study is considered as a

full-state feedback control scheme, as shown in Fig. 6.4. The control error signal e_a was given by Equation 5.103 in **Chapter 5**. The vital question that arises is how the feedback gains of the five state variables, K , can be chosen to satisfy the design benchmark. In this study, two types of controller design are proposed, i.e. Pole-Assignment (PA) and Linear Quadratic (LQ) optimal control designs.

6.5 Pole-Assignment control (PA)

This section presents the design method commonly called the pole-placement or pole-assignment technique. It is assumed that all variables are measurable and available for feedback. It will be shown that if the system considered is completely state controllable, then poles of the closed-loop system are placed at any desired location by means of state feedback through an appropriate state feedback gain matrix. In general, the present design technique determines the desired closed-loop poles based on the transient-response and frequency-response requirements, such as speed, damping ratio, or bandwidth, as well as steady-state requirements.

In a Single-Input Single-Output (SISO) control system, a controller (compensator) is designed such that dominant closed-loop poles have the desired damping ratio, ξ , and undamped natural frequency, ω_n , i.e. with acceptable values for maximum overshoot, M_{os} , and the settling time, T_{st} . In this approach, the order of the system may be raised by 1 or 2 unless pole-zero cancellation takes place. Note that in the design, effects on the responses of non-dominant closed-loop poles was assumed to be negligible. Unlike specifying only the dominant closed-loop poles, the PA technique, as mentioned by (Katsuhiko 2010) and (Dorf and Bishop 2011), allows the designer to specify all the closed-loop poles. However, there is a cost associated with employing all the closed-loop poles because it requires successful measurements of all state variables and must be completely state-controllable.

As mentioned, the AS is equivalent to the regulator control system experienced with unmeasured road input disturbances. More precisely, it is desirable to keep all the state variables at the zero reference when disturbances occur. When the road input velocity and displacement are applied to the system, the state variables can be carried back to the zero reference by the controller.

According to Section 5.6.1 in **Chapter 5**, the five state variables are:

$$\dot{X}_b, \dot{X}_w, F_{\text{hyd}}, X_b - X_w \text{ and } X_w - X_r$$

While the output variables to be controlled are:

$$\ddot{X}_b, X_w - X_b \text{ and } X_r - X_w$$

It can be seen that $X_w - X_b$ and $X_r - X_w$ are members of a set of state variables and parts of the output variable set, but they are different in sign because of the mathematical representation. The former must be used to follow the state-space modelling and subsequent controller design, while the latter is used for convenience in the derivation of the disturbance transfer functions, as illustrated in Section 5.6. However, there is no problem with cross-referencing between both sets of variables provided the right sign is given to the right variables.

It can be reviewed that:

$$M_b \ddot{X}_b = [F_{\text{hyd}} - B_{\text{va}}(\dot{X}_b - \dot{X}_w) - F_f] \cos(\alpha \mp \Delta\alpha) - F_{\text{fricd}} \quad (6.5)$$

Assuming B_{va} , F_f and F_{fricd} are very small, which is right for the former according to its identified value in Section 3.11, and for the latter regarding its value, as recognised in **Chapter 4**, thus, gives:

$$\ddot{X}_b \propto F_{\text{hyd}} \quad (6.6)$$

Therefore, the three variables that need to be controlled are related to a set of state variables. All the state variables have dynamic closed-loop poles that can be controlled by the PA controller.

With the power of the PA technique, the closed-loop poles can be located at specific locations in the s-plane. In general, the closed-loop poles are specified such that the system dynamic is dominated by an ideal second-order system. This allows the desired damping ratio, ξ , and undamped natural frequency, ω_n , of the dominant poles to be specified.

Substituting Equation 5.102 into Equation 6.2 gives:

$$\dot{x} = (A - BK)x \quad (6.7)$$

Stability and transient-response characteristics are determined by the eigenvalues of the matrix $(A - BK)$, i.e. the regulator poles. If vector K is chosen

properly, the matrix $A - BK$ can be made a stable matrix. When road inputs cause initial state shifting from the zero reference, it is possible to make x approach 0 as t approaches infinity by placing the regulator poles on the left-hand side of the s -plane.

Design steps can be declared as follows:

Step I: Check controllability condition of the system.

The controllability condition states that the system must be completely state controllable so that all of the eigenvalues of the matrix $(A - BK)$ can be controlled by state feedback. An analytical proof can be seen by (Ogata 2010), showing that a necessary and sufficient condition for arbitrary pole placement is that the system is completely state controllable with derivation of the necessary condition. A controllability matrix, M_c , is constructed from the system matrix, A , and the input vector, B , as follows:

$$M_c = [B \ AB \ A^2B \ A^3B \ A^4B] \quad (6.8)$$

The matrix rank information is essential when dealing with the uniqueness of the solutions to sets of simultaneous linear equations and can save a large amount of unnecessary work. The rank of matrix, M_c , can be described as the order of the largest non-zero determinant that can be formed from the elements of the given matrix. The matrix, M_c , having order $n * n$ is said to have rank n if its determinant is non-zero. The condition for the controllability can be written in a mathematical form as:

$$\text{If } |M_c| \neq 0 \quad \text{then rank } [M_c] = n \quad (6.9)$$

If rank $[M_c]$ is equal to n (the necessary condition), i.e. the system order in this work equals five, meaning that there are no linearly independent column vectors in the controllability matrix. Therefore, the matrix $(A - BK)$ can be made an asymptotically stable matrix if matrix K is selected correctly.

Step 2: Determine the coefficients of the characteristic polynomial.

If the system is completely state controllable, Equation 6.9 condition, then all eigenvalues of matrix A can be arbitrarily placed.

From the characteristic polynomial for the matrix A :

$$|sI - A| = a_0 + a_1 s + a_2 s^2 + a_3 s^3 + a_4 s^4 + a_5 s^5 \quad (6.10)$$

Determine the values of a_0, a_1, a_2, a_3, a_4 and a_5 .

Step 3: Determine the transformation matrix T that transforms the system state equation into the control canonical form.

The matrix T is given by:

$$T = M_c W_c \quad (6.11)$$

where, M_c is the controllability matrix, and W_c is given by:

$$W_c = \begin{bmatrix} a_1 & a_2 & a_3 & a_4 & 1 \\ a_2 & a_3 & a_4 & 1 & 0 \\ a_3 & a_4 & 1 & 0 & 0 \\ a_4 & 1 & 0 & 0 & 0 \\ 1 & 0 & 0 & 0 & 0 \end{bmatrix} \quad (6.12)$$

Step 4: Specify a set of the desired eigenvalues.

The closed-loop pole locations must be chosen in such a way that the system outputs behave similarly to a standard second-order system. The closed-loop pole locations can be obtained as follows:

$$\mu = -\sigma \pm \omega_d j \quad (6.13)$$

where,

$$\sigma = \xi \omega_n \quad (6.14)$$

$$\omega_d = \omega_n \sqrt{1 - \xi^2} \quad (6.15)$$

ξ and ω_n were selected depending on which values of settling time and maximum overshoot were accepted. The relation between them is as follows:

$$\text{Mos} = e^{-(\xi\pi/\sqrt{1-\xi^2})} \quad (6.16)$$

$$T_{st} = \frac{4}{\xi \omega_n} \quad (6.17)$$

where, Mos is the maximum overshoot and T_{st} is the settling time.

Therefore, the desired closed-loop poles for the active suspension are

$$\mu_1 = -\sigma + \omega_d j$$

$$\mu_2 = -\sigma - \omega_d j$$

$$\mu_3 = -10\sigma$$

$$\mu_4 = -10\sigma$$

$$\mu_5 = -10\sigma$$

The relationship between ω_n , ξ and the locations of the five closed-loop poles in the s-plane for the ideal second-order response is shown in Fig. 6.6. The terms μ_1 and μ_2 are a pair of dominant closed-loop poles. The remaining three closed-loop poles are located to the far-left of the dominant pair of closed-loop poles to make the system faster, while damping of the system will be mainly caused by the dominance of the closed-loop poles. In this work, the distance, measured along the real axis, between the imaginary axis and the remaining three poles, is assumed to be ten times the distance from the imaginary axis to the dominant poles.

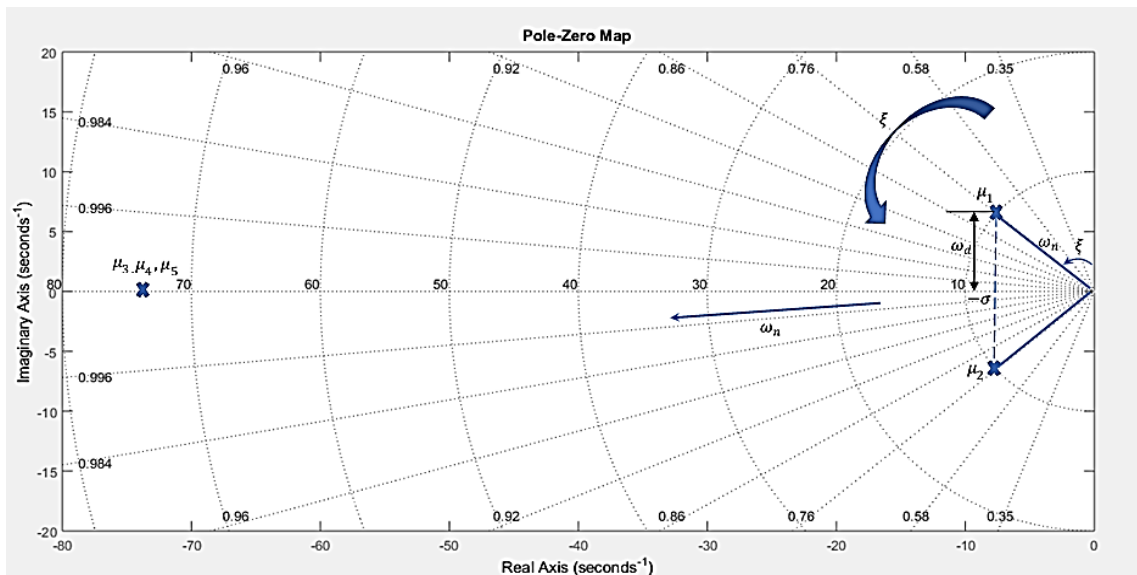


Fig. 6.6. Location of the five suggested closed-loop poles for the PA controller in pole-zero map.

Step 5: Determine the desired characteristic equation.

From the desired characteristic polynomial:

$$(s - \mu_1)(s - \mu_2)(s - \mu_3)(s - \mu_4)(s - \mu_5) = \alpha_0 + \alpha_1 s + \alpha_2 s^2 + \alpha_3 s^3 + \alpha_4 s^4 + \alpha_5 s^5 \quad (6.18)$$

Determine the values of α_0 , α_1 , α_2 , α_3 , α_4 and α_5 .

Step 6: Determine state feedback vector K.

When, $u_a = -Kx$, is used as the control signal and using Equation 6.7, the characteristic equation for this system is therefore:

$$|sI - A + BK| = |T^{-1}(sI - A + BK)T| = |sI - T^{-1}AT + T^{-1}BKT| = 0 \quad (6.19)$$

$$|sI - T^{-1}AT + T^{-1}BKT| = (a_0 + \delta_0) + (a_1 + \delta_1)s + (a_2 + \delta_2)s^2 \\ + (a_3 + \delta_3)s^3 + (a_4 + \delta_4)s^4 + s^5 \quad (6.20)$$

This is the characteristic equation for a system with state feedback. It therefore must be equal to Equation 6.17; the desired characteristic equation. By equating the coefficients of like powers of s , we obtain:

$$\delta_0 = \alpha_0 - a_0$$

$$\delta_1 = \alpha_1 - a_1$$

$$\delta_2 = \alpha_2 - a_2 \quad (6.21)$$

$$\delta_3 = \alpha_3 - a_3$$

$$\delta_4 = \alpha_4 - a_4$$

Let us write:

$$KT = [\delta_0 \ \delta_1 \ \delta_2 \ \delta_3 \ \delta_4] \quad (6.22)$$

The required state feedback gain vector can be determined from the equation:

$$K = [\delta_0 \ \delta_1 \ \delta_2 \ \delta_3 \ \delta_4]T^{-1} \quad (6.23)$$

Thus, if the system is completely state controllable, all eigenvalues can be arbitrarily placed by choosing matrix K according to Equation 6.23, the sufficient condition. It is useful to use the form Equation 5.103 in Section 5.6.2 to make these control gains suitable for the experimental objective. Thus, the state feedback gain vector for the controller is of the form:

$$K_1 = N^{-1}KK_2 \quad (6.24)$$

6.5.1 Design example

Substituting constant parameters of the test rig as follows:

Car body mass, $M_b = 240$ kg

Wheel unit mass, $M_w = 40$ kg

Actuator cross-sectional area, $A_c = 2.46e - 4 \text{ m}^2$

Actuator chamber and hose volume, $V = 7.13e - 5 \text{ m}^3$

Actuator angle, $\alpha = 27^\circ$

Forward gain for two-DOF model, $P = 0.1$

D/A gain, $G = 2.0e-1 \text{ mA/ MC}$

Linearised flow gain of servovalve, $K_{fa} = 2.3e - 11 \text{ m}^3 \text{ S}^{-1}/\text{mA}$

Effective bulk modulus for active suspension system, $\beta_e = 0.24e9 \text{ N/m}^2$

Tyre stiffness, $k_t = 9.2e5 \text{ N/m}$

Actuator viscous damping rate, $B_v = 300 \text{ N/mS}^{-1}$

Cross-port leakage resistance, $R_i = 2.45e11 \text{ N m}^{-2}/\text{m}^3\text{S}^{-1}$

Tyre damping rate, $b_t = 3886 \text{ N/mS}^{-1}$

The system matrix and input vector can be written numerically as

$$A = \begin{bmatrix} -1.25 & 1.25 & 0.003713 & 0 & 0 \\ 7.5 & -104.65 & -0.02228 & 0 & -7000 \\ -407000 & 407000 & -27.478 & 0 & 0 \\ 1 & -1 & 0 & 0 & 0 \\ 0 & 1 & 0 & 0 & 0 \end{bmatrix}$$

$$B = \begin{bmatrix} 0 \\ 0 \\ 7.62e4 \\ 0 \\ 0 \end{bmatrix}$$

Step 1: Check the controllability condition for the system

$$M_c = [B \ AB \ A^2B \ A^3B \ A^4B]$$

$$M_c = \begin{bmatrix} 0 & 2.8e2 & -1.02e4 & -2.48e6 & 4.43e8 \\ 0 & -1.7e3 & 2.26e5 & 4.78e6 & -4.7e9 \\ 7.6e4 & -2.09e6 & -7.48e8 & 1.16e11 & 2.5e11 \\ 0 & 0 & 1.9e3 & -2.36e5 & -7.26e6 \\ 0 & 0 & -1.69e3 & 2.26e5 & 4.78e6 \end{bmatrix}$$

$|M_c| = -8.5978e23$. The rank of M_c is 5; the system is completely state controllable.

Step 2: Determine coefficient terms of the characteristic polynomial from matrix A.

To derive the coefficients of the characteristic polynomial from A, it is sufficient to use the MATLAB control drop-box **Poly (A)** in Matlab, which returns the coefficient as the row vector:

$$\begin{aligned} |sI - A| &= 10817345.3 s + 351225.5 s^2 + 20608.27 s^3 + 133.38 s^4 + s^5 \\ &= a_0 + a_1 s + a_2 s^2 + a_3 s^3 + a_4 s^4 + a_5 s^5 \end{aligned}$$

Step 3: Determine the transformation matrix T that transforms the system state equation into the controllable canonical form.

$$T = M_c W_c$$

where,

$$W_c = \begin{bmatrix} 1.08e7 & 3.5e5 & 2.06e4 & 1.33e2 & 1 \\ 3.5e5 & 2.06e4 & 1.33e2 & 1 & 0 \\ 2.06e4 & 1.33e2 & 1 & 0 & 0 \\ 1.33e2 & 1 & 0 & 0 & 0 \\ 1 & 0 & 0 & 0 & 0 \end{bmatrix}$$

Then matrix T becomes:

$$T = \begin{bmatrix} -4.85e3 & 1.98e6 & 2.75e4 & 2.8e2 & 0 \\ 8.6e3 & 4.5e2 & -3.34 & -1.7e2 & 0 \\ 2.3e8 & 6.65e8 & 5.4e8 & 8.06e6 & 7.6e4 \\ 1.97e6 & 2.7e4 & 1.9e3 & 0 & 0 \\ 4.5e2 & -3.34 & -1.69e3 & 0 & 0 \end{bmatrix}$$

Step 4: Specify desired closed-loop poles

For this design, the undamped natural frequency, $\omega_n = 1.56$ Hz and the damping ratio, $\xi = 0.76$ was used. The desired closed-loop poles that satisfy the requirements are:

$$\mu_1 = -7.45 + 6.37j$$

$$\mu_2 = -7.45 - 6.37j$$

$$\mu_3 = -74.5$$

$$\mu_4 = -74.5$$

$$\mu_5 = -74.5$$

Step 5: Determine coefficient terms of the desired characteristic polynomial.

The desired characteristic polynomial is of the form:

$$(s + 7.45 - 6.37j)(s + 7.45 + 6.37j)(s + 74.5)(s + 74.5)(s + 74.5)$$

$$= 3.97e7 + 7.76e6 s + 6.83e5 s^2 + 2.01e4 s^3 + 2.38e2 s^4 + s^5$$

$$= \alpha_0 + \alpha_1 s + \alpha_2 s^2 + \alpha_3 s^3 + \alpha_4 s^4 + \alpha_5 s^5$$

Step 6: Determine state feedback vector K

The inverse of the transformation matrix, T, can be obtained as:

$$T^{-1} = \begin{bmatrix} 7.01e-9 & -1.16e-9 & 7.43e-25 & 5.05e-7 & 4.75e-7 \\ 5.05e-7 & 8.4e-8 & 1.16e-25 & -9.9e-10 & 8.17e-6 \\ -2.85e-9 & -4.76e-10 & 2.06e-25 & 1.34e-7 & -5.8e-4 \\ 9.87e-8 & -5.8e-4 & -1.87e-24 & 2.57e-6 & 5.75e-6 \\ -4.3e-3 & 6.16e-2 & 1.31e-5 & -2.7e-3 & 4.12 \end{bmatrix}$$

The desired feedback gain vector, K , is of the form:

$$K = [\delta_0 \quad \delta_1 \quad \delta_2 \quad \delta_3 \quad \delta_4]T^{-1}$$

$$K = [-2.27 \quad 6.45 \quad 0.0014 \quad 19.8 \quad 230.7]$$

The control error signal, ea , is obtained by:

$$ea = -Kx$$

$$ea = -[-2.27 \quad 6.45 \quad 0.0014 \quad 19.8 \quad 230.7] \begin{bmatrix} \dot{X}_b \\ \dot{X}_w \\ F_{hyd} \\ X_b - X_w \\ X_w - X_r \end{bmatrix}$$

$$K_1 = N^{-1}KK_2$$

$$N = 3276 \text{ m.c. /v}$$

$$K_2 = \begin{bmatrix} 0.2 & 0.0 & 0.0 & 0.0 & 0.0 \\ 0.0 & 0.2 & 0.0 & 0.0 & 0.0 \\ 0.0 & 0.0 & 0.000002 & 0.0 & 0.0 \\ 0.0 & 0.0 & 0.0 & 0.0000077 & 0.0 \\ 0.0 & 0.0 & 0.0 & 0.0 & 0.000027 \end{bmatrix}$$

The feedback gain vector for the controller K_1 was found to be:

$$K_1 = [-0.0035 \quad 0.0098 \quad 0.21 \quad 785.33 \quad 2608.34]$$

The procedure for the PA design was as written in a C++ compiler, using the MATLAB Control System Toolboxes (MathWorks 2000) to allow systematised designs to be processed. MATLAB includes many engineering toolboxes that

enable engineers to create, analyse and simulate a variety of different projects. In our case, MATLAB included the Control Systems Toolbox, which contains several functions tailored for control system engineering. Also included was the SISO tool, a GUI that allows for interactive system analysis and control design.

The most crucial point after designing the linear PA controller was the implementation of this controller with the original nonlinear system and seeing whether this controller was sufficiently robust and efficient to control the system and how much it was able to enhance system performance. Therefore, a comparison between the dynamic performance of the PS and the AS Pole-Assignment (ASPA) designed controllers for different system responses is displayed and discussed in the next section.

6.6 Simulation results for passive and active suspension designed by pole-assignment

Comparison between the experimental and simulation model results for the PS system was conducted and investigated in **Chapter 3**. To know the extent to which using AS enhances system performance, it is necessary to make a satisfactory comparison between the two systems. Using similar system force inputs is sufficient to discover the extent of these improvements.

The comparison between results of PS and ASPA are placed in two columns: the left representing the PS, while the right shows the ASPA system. Fig. 6.7 shows the desired and real simulation inputs for both the PS and the ASPA systems; an amplitude of 50mm was chosen. Because it is considered a regular controller. Therefore, these road inputs are treated as disturbance inputs.

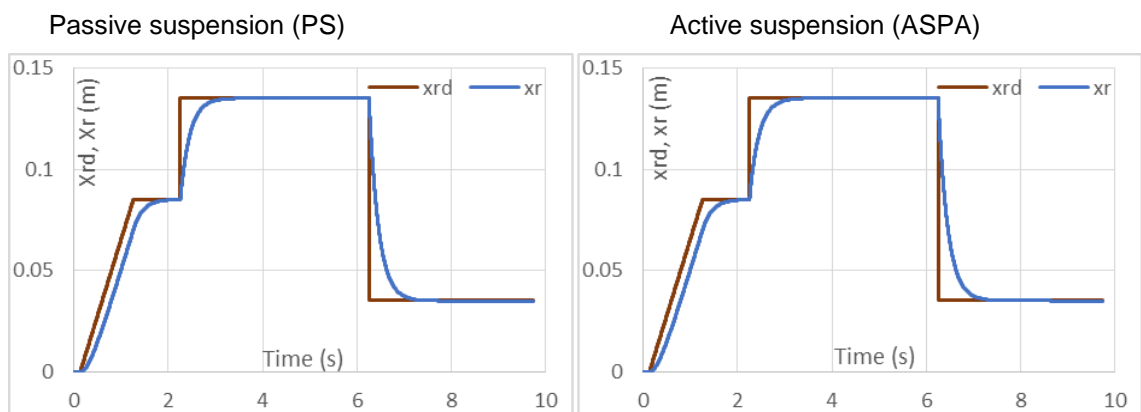


Fig. 6.7. Comparing the road inputs (system inputs) for both systems.

Fig. 6.8 demonstrates the comparison between the wheel and body movements for both PS and ASPA systems. It is evident that the body travel for ASPA has a higher delay than in the PS system, i.e. the body damper increased with regard to control action.

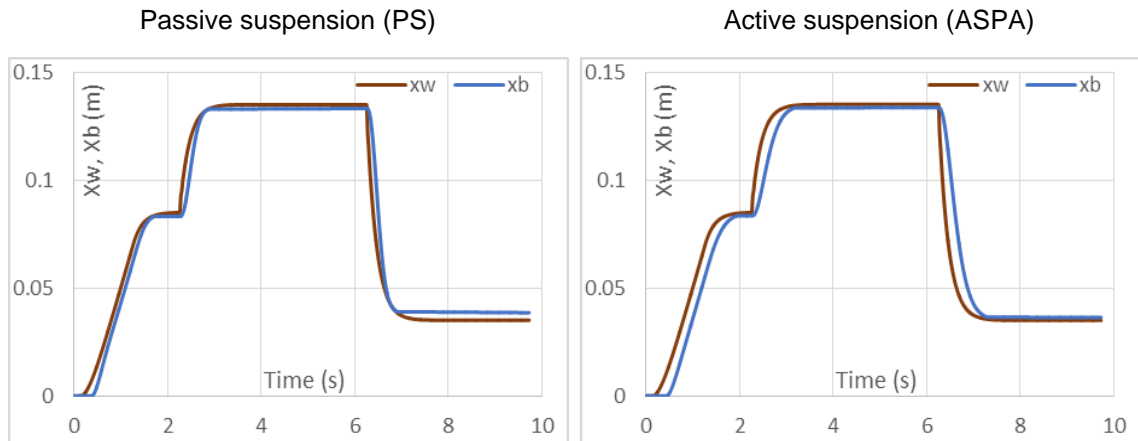


Fig. 6.8. Comparison between the wheel and body travel for both PS and ASPA systems.

The wheel velocity's acceleration and deceleration, as displayed in Fig. 6.9, are relatively similar in both PS and ASPA. This could be because the tyre deflections (wheel inputs) are small and similar for both system in respect of the same inputs.

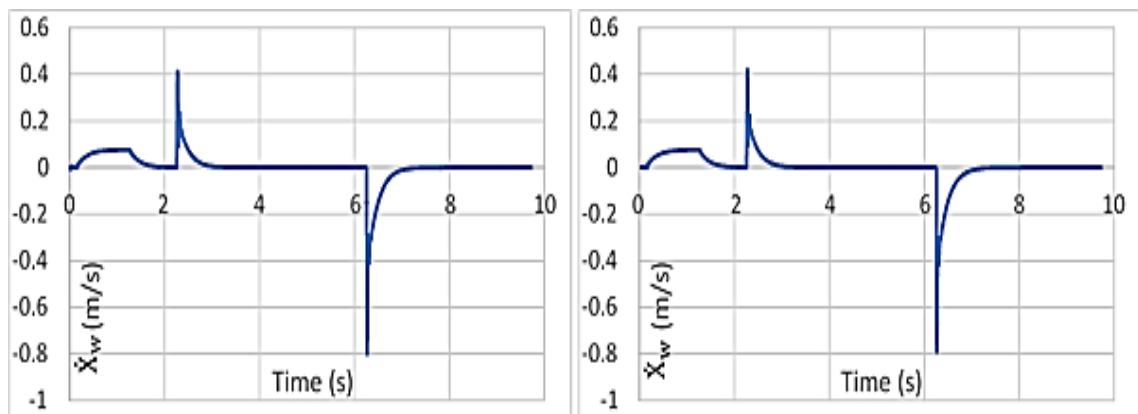


Fig. 6.9. The wheel velocity for PS in comparison with ASPA wheel velocity.

However, the damping of the body velocity for ASPA, close to a 50% reduction in value, is clearly shown in Fig 6.10 in comparison with the velocity behaviour for PS. This matches with the primary target of control; minimising the body acceleration.

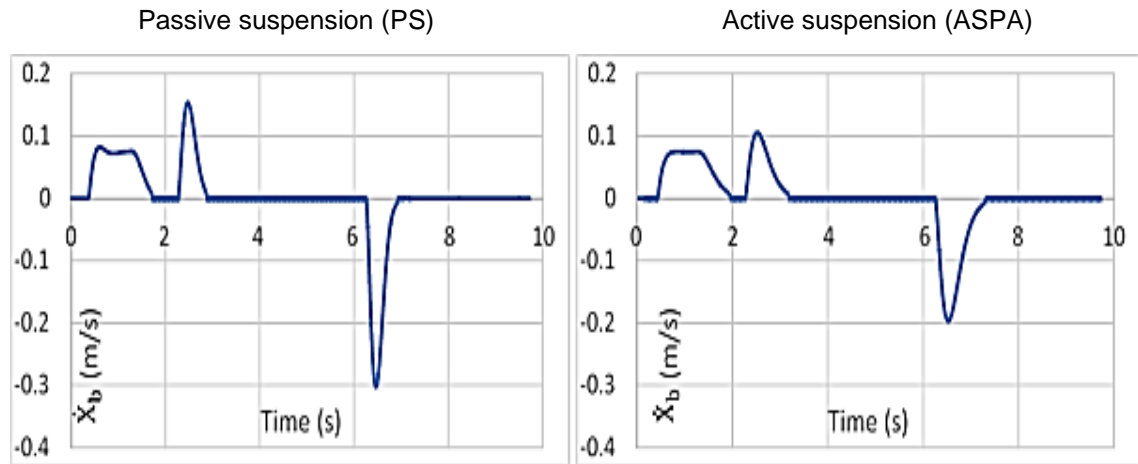


Fig. 6.10. Comparison between the body velocities for both system.

One of the crucial characteristics to be investigated in automobile suspension is suspension displacement; it would be difficult to achieve the goals without monitoring this as it could relate to discovering whether the work allowance in the laboratory environment or in the real world. Therefore, as demonstrated in Fig. 6.11, it is evident that there is a suspension movement cost; it is enlarged as in ASPA in comparing with PS.

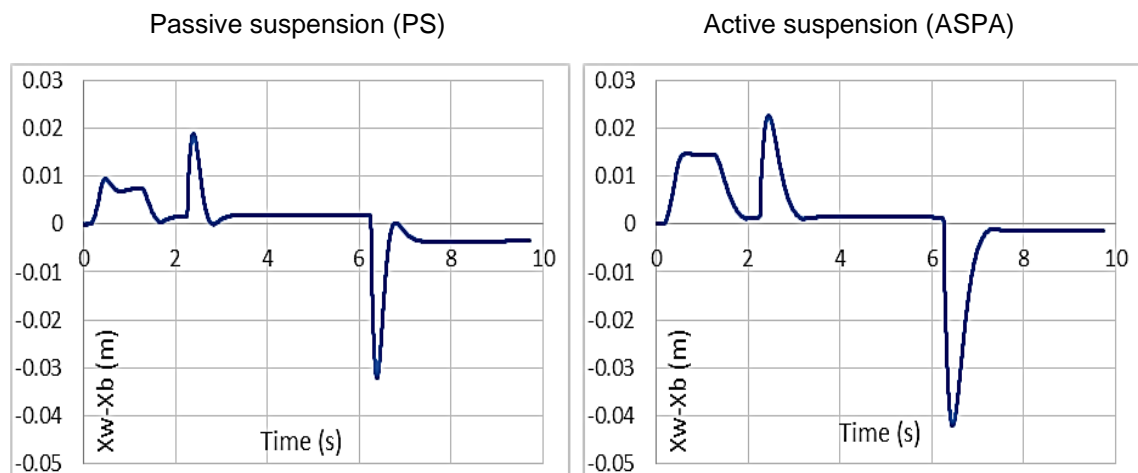


Fig. 6.11. The suspension movement comparison for PS and ASPA.

Fig. 6.12 shows displaced friction force behaviour in both PS and ASPA systems; in ASPA the friction force is lower than that for PS. This has probably occurred proportionally to the body velocity deceleration.

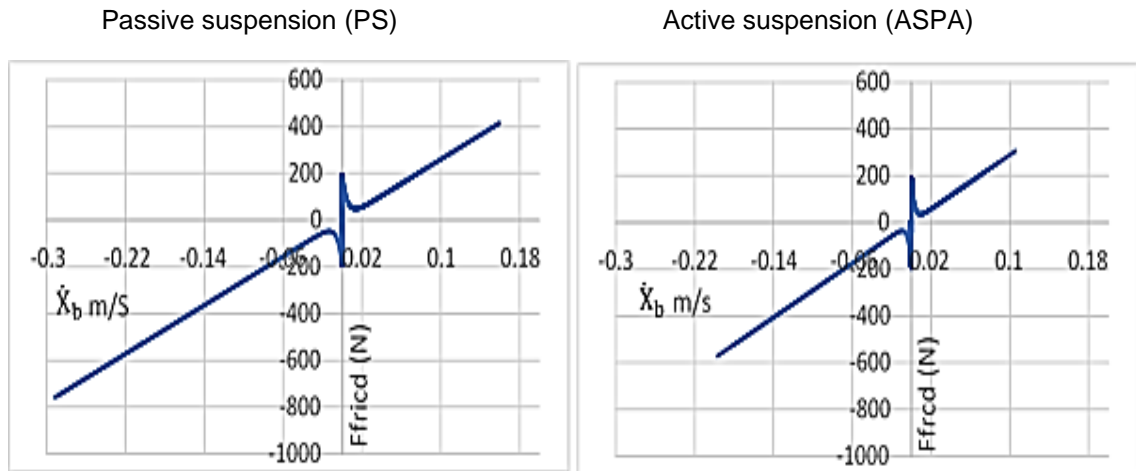


Fig. 6.12. Damping friction force for PA and ASPA as a function of body velocity.

Finally, the contact patch loads are illustrated in Fig. 6.13 for both systems. It is clearly seen that there is a slight difference between them. This could be because of the limitations of the test rig and the lower dynamic weight changing for ASPA in comparison with the PS system.

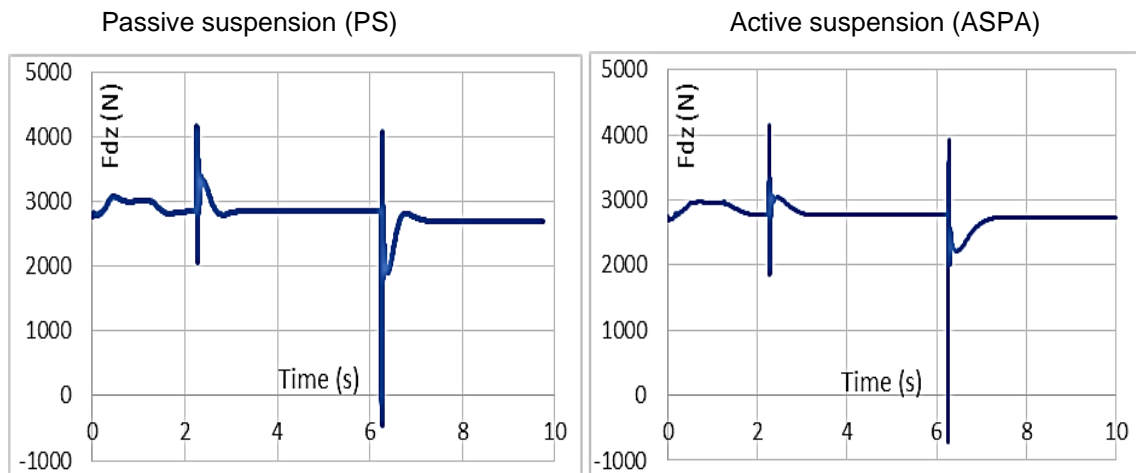


Fig. 6.13. CPL (N) for both systems.

6.7 State observers

In the pole-placement approach to the design of control systems, it was assumed that all state variables are available for feedback. In practice, however, not all state variables are available for feedback. Consequently, there is a need to estimate unavailable state variables.

Estimation of unmeasurable state variables is commonly called observation (Ogata 2010). When the state observer observes all state variables (n) of the system, regardless of whether some state variables are available for

direct measurement, it is referred to as a full-order state observer. However, in this research only observation of the unmeasurable state variables is required. For example, since the measurable output variables are available, and they are linearly related to the state variables, we are only required to observe $(n-m)$ state variables, where, n is the dimension of the state vector and m is the dimension of the output vector.

A state observer estimates the state variables based on the measurements of the output and control variables. Here the concept of observability plays an important role. It will be shown later that state observers can be constructed exactly when the condition of observability is satisfied. In the following discussions of state observers, the notation \tilde{x} is adopted to designate the observed state vector. In many practical cases (Ogata 2010), the observed state vector \tilde{x} is used in the state feedback to generate the desired control vector.

Considering the plant defined by Equations 6.2 and 6.3, the observer is a subsystem to reconstruct the state vector of the plant. The observer's mathematical model is essentially the same as that of the plant, except that it includes an additional term containing the estimation error to compensate for inaccuracies in matrices A and B and the absence of the initial error. The estimated error, or observation error, is the difference between the measured output and the estimated output. The initial error is the difference between the initial state and the initial estimated state. Thus, we define the mathematical model of the observer to be:

$$\begin{aligned}\dot{\tilde{x}} &= A\tilde{x} + Bu_a + k_e(y - C\tilde{x}) \\ &= (A - k_eC)\tilde{x} + Bu_a + k_ey\end{aligned}\tag{6.25}$$

where, \tilde{x} is the estimated state and $C\tilde{x}$ is the estimated output.

The inputs to the observer are the output, y , and the control input, u_a . Matrix, k_e , which is called the observer gain matrix, is a weighting matrix to the correction term involving the difference between the measured output, y , and the estimated output, $C\tilde{x}$. This term continuously corrects the model output and improves the performance of the observer. Fig. 6.14 shows the block diagram of the system and the full-order state observer.

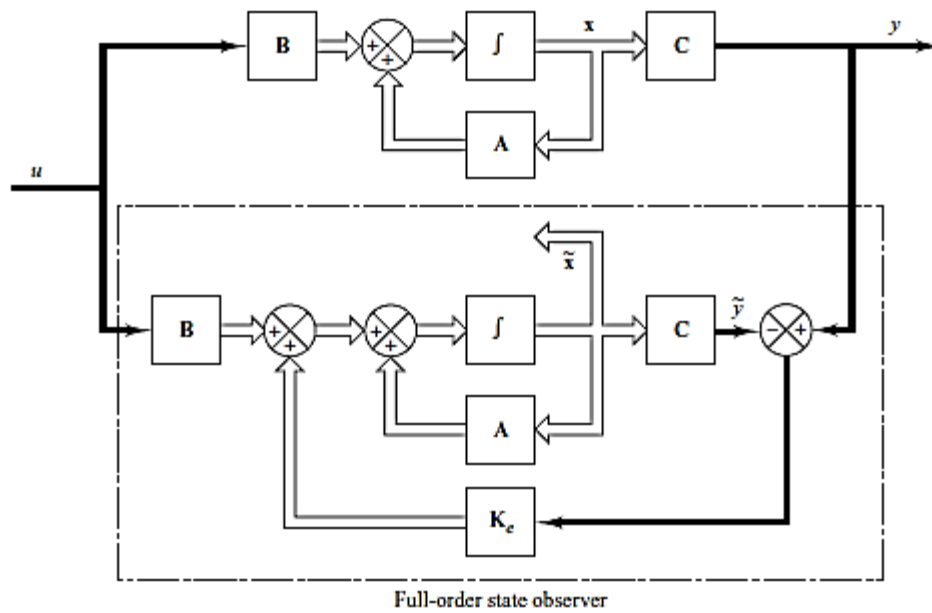


Fig. 6.14. Block diagram of system and full-order state observer (Ogata 2010).

6.8 Linear Quadratic optimal control (LQ)

In control theory, the problem of steering output of interest toward a desired reference trajectory, despite the presence of unknown disturbances and assuming the reference trajectory, as well as the disturbance signals, are produced by an external generator, is usually referred to as output regulation.

The theory of the LQ (Watton 1989), (Ogata 1997), (Ljung 1995) and (Speedy et al. 1970), has been utilised to acquire solutions for an assortment of aerospace engineering issues and also holds considerable promise for other issue areas. The leading theory may be considered a combination of automatic control and maxima-minima theory. The objective of LQ design is to determine control signals that will cause a process to minimise, or maximise, some performance criteria and at the same time satisfy the physical constraints or inevitable practical limitations. In this study, it was decided that a specific class of LQR, a linear regulator type for active suspension control, would be considered.

The LQR is proposed in this work in addition to the PA because of three reasons. Firstly, the control scheme has flexibility for the selection of state variables required for control, i.e. it does not need to cover all state variables. For example, some control methods, such as PA, attempt to minimise all the state variables in similar cases ($\ddot{X}_b, \dot{X}_b, \dot{X}_w, X_b - X_w, X_w - X_r$) rather than the three states ($\ddot{X}_b, X_b - X_w, X_w - X_r$) of concern. Secondly, LQ has the ability to weight

the controlled state variables, in that all five state variables are minimised with the same weights, whereas PA control does not. However, in active suspension control, \ddot{X}_b should have priority over the other states and $X_b - X_w$ and $X_w - X_r$ should be weighted within their physical limitations. Thirdly, with LQ, the physical limitation of the voltage input, u_a in this work, can be considered, which compared with PA, is not possible.

As specified in **Chapter 1**, (Thompson 1976) was the first researcher who applied this theory to the active suspension system. A quarter car system without hydraulic model was utilised. The control issue was at first characterised as a general control following the expansion of a disturbance function input, i.e. road inputs. By making use of a performance index and a mixed ramp and step, bump or random inputs representing the disturbance function inputs, the general tracking control was transformed into an equivalent regulator control. This resulted in a Riccati equation with a specific output matrix appropriate for the inputs. Even though Thompson's (1976) derivation became an essential reference in this area, the method seems to be limited for the type of road inputs. In addition, when the nonlinear hydraulic actuator model is added into the quarter car model, the mathematical model and the performance index will be different from Thompson's (1976) work. Therefore, it was decided to review the derivation of the LQ.

In short, in this work, the mathematical solution differs in two main points differ from Thompson's (1976) work as follows: firstly, a nonlinear hydraulic model is involved in the active suspension system and secondly, by careful selection of the state variables, the mathematics can be applied directly to the LQR type without any complex transformation used in Thompson's (1976) work.

From another perspective, the same modifications from Thompson's (1976) work to Surawattanawan's (2000) work was used, but with two significant modification differences. First, implementation of a new term, the friction force, with the active suspension $\frac{1}{4}$ -car model. Second, using the fundamental linear control to drive the nonlinear hydraulic actuator to generate the hydraulic control force to control the nonlinear AS system.

6.9 Application to the active suspension system

Two major issues were experienced in applying LQR theory to the design of vehicle suspension, as reported by (ElMadany and Abduljabbar 1999). The first problem occurs when a portion of the feedback states are not accessible. However, the guaranteed gain and phase margin results of LQ could be decreased markedly when an estimator has been included (Safonov and Athans 1977). The second problem emerges from the way that the controlled system effectively does not have zero steady-state axle to body deflection in response to external body force because of payload variations, braking, accelerating or cornering forces. In order to overcome these limitations, (Davis and Thompson 1988) suggested that full state feedback, which derived the optimal suspension systems using multivariable integral control. However, the current study extends and revises the work of Davis and Thompson (1988).

As mentioned, active suspension is equivalent to a regular control system experiencing unmeasured road input disturbances. More specifically, it is desirable to keep all the state variables at a zero reference in the presence of disturbances, as mentioned in **Chapter 5**. When the road input velocity and displacement, are applied to the system, the state variables can be brought back to the zero reference by the controller.

According to Section 5.6.1 in **Chapter 5**, and as mentioned in Section 6.5 in the current, the five state variables are:

$$\dot{X}_b, \dot{X}_w, F_{hyd}, X_b - X_w, X_w - X_r$$

While the output variables to be controlled are:

$$\ddot{X}_b, X_w - X_b, X_r - X_w$$

The controllability condition expresses that the system must be completely state controllable so that all the eigenvalues of the system matrix A can be randomly engaged by choosing the correct vector K, as was illustrated for PA control; the system states are entirely controlled.

6.10 LQR algorithm

Previously, in Section 6.5, the design of state feedback controllers using eigenvalue pole placement algorithms were discussed. The closed-loop control system in state-space representation for the LQ controller is shown in Fig. 6.15.

It should be noted that for LQ the state-space model contains an output equation in the model allowing more freedom to select the desired outputs. This is different from the PA. For single input systems, given a set of desired eigenvalues, the feedback gain to achieve this is, provided the system is controllable, unique. For multi-input systems, the feedback gain is not unique, so there is an additional design freedom. How does one utilise this freedom? A more fundamental issue is that the choice of eigenvalues is not obvious. For example, there are trade-offs between robustness, performance and control effort. LQR control can be used to resolve some of these issues by not specifying exactly where the closed loop eigenvalues should be directly, but instead by specifying some sort of objective performance function to be optimised.

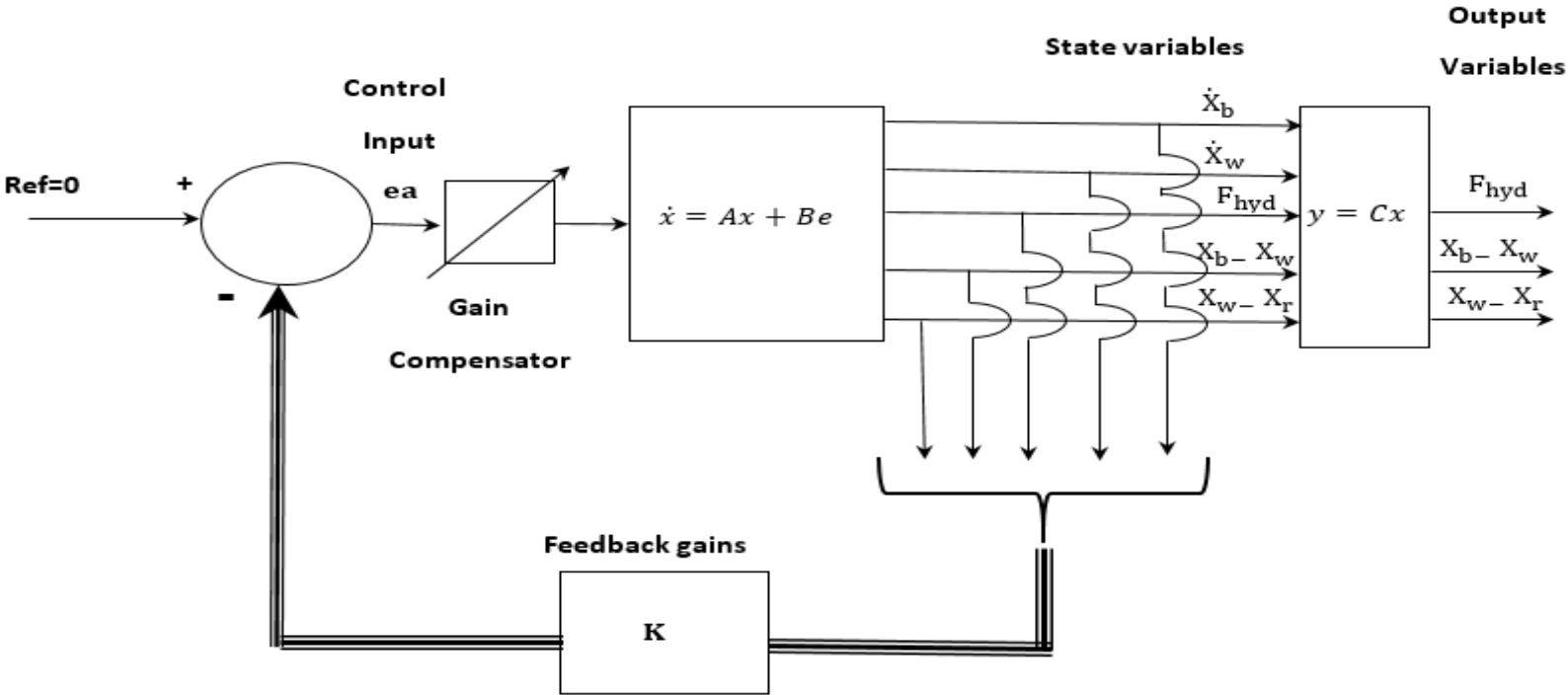


Fig. 6.15. Block diagram of full-state feedback control (linear quadratic optimal control).

The system equation is of the form as previously mentioned:

$$\dot{x}(t) = A(t)x(t) + B(t)ea(t) \quad (6.26)$$

$$y = Cx(t) \quad (6.27)$$

where,

$$C = \begin{bmatrix} 0.0 & 0.0 & 1.0 & 0.0 & 0.0 \\ 0.0 & 0.0 & 0.0 & 1.0 & 0.0 \\ 0.0 & 0.0 & 0.0 & 0.0 & 1.0 \end{bmatrix}$$

The output variables are F_{hyd} (equivalent to \ddot{X}_b), $X_b - X_w$, and $X_w - X_r$. It is vital to note that the output matrix C must comprise of at least the constraint $X_b - X_w$ to preserve system stability.

The control problem is to determine the vector K of the optimal error control signal, ea, in Equation 5.103 so as to minimise a performance index (cost function):

$$J = \int_0^{\infty} (y^T Q_m y + ea^T R ea) dt \quad (6.28)$$

where, Q_m is a positive definite, or positive semi definite, real symmetric matrix and, R is a positive real number.

and,

$$Q_m = \begin{bmatrix} q_1 & 0.0 & 0.0 \\ 0.0 & q_2 & 0.0 \\ 0.0 & 0.0 & q_3 \end{bmatrix}$$

The quadratic form is used in the cost function because it does not differentiate between positive and negative values of the relevant variables. It is seen that the cost function accounts for the output vector, y, and the disbursement of the energy of the control signal, ea, which is equivalent to the applied servovalve voltage, u_a . The matrix Q_m and constant R define the relative significance of the output variables and the expenditure of the input force, or they could be defined as, Q_m is the weighting on the states while the R matrix defines the weighting on the control input in the cost function. The matrix Q_m contains q_1 , q_2 and q_3 which are weighting factors for \ddot{X}_b , $X_b - X_w$ and $X_w - X_r$

respectively. Although the control signal is theoretically assumed to be unbound, its realisation in practice, is impossible. Therefore, designers must bear this in mind and verify the amplitude of the control signal after the design process.

By using the output equation, $y = Cx$, the cost function can be modified to be:

$$J = \int_0^{\infty} (x^T(t)C^T Q_m C x(t) + ea^T(t) R ea(t))dt \quad (6.29)$$

where,

- $x^T(t)C^T Q_m C x(t)$ penalises the transient state deviation.
- $ea^T(t) R ea(t)$ penalises the control effort.

By using Equation 6.7 for,

$$\dot{x}(t) = (A(t) - B(t)K) x(t) \quad (6.30)$$

in the following derivations, the matrix $A - BK$ was found to be stable, i.e. the eigenvalues of the matrix $A - BK$ have negative real parts. Substituting Equation 5.103 into Equation 6.28 yields:

$$\begin{aligned} J &= \int_0^{\infty} (x^T C^T Q_m C x + x^T K^T R K x) dt \\ &= \int_0^{\infty} x^T (C^T Q_m C + K^T R K) x dt \end{aligned} \quad (6.31)$$

By Liapunov's main stability theorem, if the matrix $A - BK$ is stable, the derivative of the quadratic term inside the cost function must satisfy the condition that:

$$\begin{aligned} x^T (C^T Q_m C + K^T R K) x &= -\frac{d}{dt} (x^T P_m x) \\ &= -\dot{x}^T P_m x - x^T P_m \dot{x} \end{aligned} \quad (6.32)$$

where,

P_m is the positive definite real symmetric matrix

Substituting Equation 6.30 into Equation 6.32 yields:

$$x^T (C^T Q_m C + K^T R K) x = -x^T [(A - BK)^T P_m + P_m (A - BK)] x \quad (6.33)$$

Comparing both sides of Equation 6.33 and noting that this equation must hold true for any x , it is required that:

$$(A - BK)^T P_m + P_m (A - BK) = -(C^T Q_m C + K^T R K) \quad (6.34)$$

or,

$$(A^T - K^T B^T) P_m + P_m (A - BK) + C^T Q_m C + K^T R K = 0 \quad (6.35)$$

Supposing that (A, B) is stabilizable; i.e. the matrix $A - BK$ is stable, by the second method of Liapunov's, there exists a positive definite matrix P_m , which satisfies the optimal solution for Equation 6.35. It is important to note that for specific systems, the matrix $A - BK$ cannot be made a stable matrix, whatever feedback gain K is chosen. In such a case, the positive definite matrix P_m does not exist. This means that system stability can be detected at the controller design stage.

The cost function J can be evaluated as:

$$\begin{aligned} J &= \int_0^{\infty} x^T (C^T Q_m C + K^T R K) x \, dt \\ &= -x^T P_m x \Big|_0^{\infty} \\ &= -x^T(\infty) P_m x(\infty) + x^T(0) P_m x(0) \end{aligned} \quad (6.36)$$

Since all eigenvalues of the matrix $A - BK$ are assumed to have negative real parts, $x(\infty)$ approaches zero. Therefore, Equation 6.36 becomes:

$$J = x^T(0) P_m x(0) \quad (6.37)$$

Thus, the cost function can be obtained in terms of the initial condition $x(0)$ and the matrix P_m .

At this stage, there are two methods for obtaining the solution of the LQ, as follows:

1. Analytical method: Using the fact that the cost function is in the form of a polynomial function, the minimisation of J concerning the component k_{ij} of the vector K , can be refined by setting $\frac{\partial J}{\partial k_{ij}}$ equivalent to zero and settling for the optimal values of k_{ij} . However, this technique is not suitable for the active suspension control, which is a high-order system. The organisation of the cost function proves to be an extremely repetitive process and when the design process is rearranged, i.e. changing Q_m and R , the polynomial function must be rearranged every time.

2. Solution via matrix Riccati equation:

- The minimisation of the cost function concerning the element k_{ij} of the vector K is the same as the minimisation of the left-hand side of Equation 6.35 with respect to the vector K (Ogata 1997). Therefore, Equation 6.35 may be rearranged in matrix form appropriate for computer programming. This will aid the repeatability of the design process. However, there is a problem that the equation contains the vector K and K^T so that the minimisation of the equation with respect to the vector K cannot be directly obtained.
- The MATLAB m-file helped to find K_1 gains. Depending on the A , B and C matrices, with a specific Q_m matrix by determining values for q_1, q_2 and q_3 , to find Q using Equation 6.51. In addition, using $R = 1$, allows use of the MATLAB control system drop-box and by printing a “care” order in the m-file determines the P_m matrix as $[P_m] = \text{care}(A, B, Q, R)$. Knowing P_m , B and R and using Equation 6.48, to find the K matrix, knowing the K_2 matrix within, as shown later in Equation 6.52 and by using Equation 6.54, which helps to find the K_1 feedback gains, is quite useful for this particular test rig.

Note: For more detail about m-file, see APPENDIX C.

Therefore, to obtain the solution in a matrix form, by rearranging Equation 6.35, it may be written as:

$$A^T P_m + P_m A + C^T Q_m C + K^T R K - K^T B^T P_m - P_m B K = 0 \quad (6.38)$$

To eliminate the vector K^T , an additional equation is introduced as follows:

$$P_m^T B R^{-1} B^T P_m - P_m^T B R^{-1} B^T P_m = 0 \quad (6.39)$$

Adding Equation 6.39 into Equation 6.38, gives:

$$\begin{aligned} A^T P_m + P_m A + C^T Q_m C + K^T R K - K^T B^T P_m \\ - P_m B K + P_m^T B R^{-1} B^T P_m - P_m^T B R^{-1} B^T P_m = 0 \end{aligned} \quad (6.40)$$

Since the matrix P_m has been assumed to be the symmetric square matrix, i.e. it is symmetrical about the leading diagonal, it follows that:

$$P_m = P_m^T \quad (6.41)$$

R is a positive real number. Therefore, its square root always exists and it may be written as:

$$R = (\sqrt{R})^2 \quad (6.42)$$

Equation 6.40 may be rewritten as:

$$\begin{aligned} A^T P_m + P_m A + C^T Q_m C + K^T (\sqrt{R})^2 K - K^T (\sqrt{R}) (\sqrt{R})^{-1} B^T P_m \\ - P_m^T B (\sqrt{R}) (\sqrt{R})^{-1} K + P_m^T B (\sqrt{R})^{-1} (\sqrt{R})^{-1} B^T P_m - P_m^T B R^{-1} B^T P_m = 0 \end{aligned} \quad (6.43)$$

$$\begin{aligned} A^T P_m + P_m A + C^T Q_m C - P_m^T B R^{-1} B^T P_m \\ + [(\sqrt{R}) K^T - (\sqrt{R})^{-1} B P_m^T][(\sqrt{R}) K - (\sqrt{R})^{-1} B^T P_m] = 0 \end{aligned} \quad (6.44)$$

It can be seen that vector K^T terms do not exist in the first four terms of the equation and the minimum of the left-hand side of this last equation concerning K arises when:

$$\left([(\sqrt{R}) K^T - (\sqrt{R})^{-1} B P_m^T][(\sqrt{R}) K - (\sqrt{R})^{-1} B^T P_m] \right) = \text{minimum} \quad (6.45)$$

or,

$$\left([(\sqrt{R}) K - (\sqrt{R})^{-1} B^T P_m]^T [(\sqrt{R}) K - (\sqrt{R})^{-1} B^T P_m] \right) = \text{minimum} \quad (6.46)$$

Since this last expression is nonnegative, the minimum occurs when it is zero, or when:

$$(\sqrt{R})K = (\sqrt{R})^{-1} B^T P_m \quad (6.47)$$

Thus, the optimal vector K is of the form:

$$K = R^{-1} B^T P_m \quad (6.48)$$

In addition, the optimal control signal is given by:

$$ea = -Kx = -R^{-1} B^T P_m x \quad (6.49)$$

Consequently, from the minimisation of the cost function and Equation 6.45, the matrix P_m in Equation 6.48 must satisfy the following reduced equation:

$$A^T P_m + P_m A + C^T Q_m C - P_m^T B R^{-1} B^T P_m = 0 \quad (6.50)$$

Equation 6.50 is called a reduced Riccati equation. The matrix Riccati equation must be solved numerically to find the matrix P_m and vector K respectively. By using the MATLAB, m-file, as mentioned, and with knowing A , B , C matrices, at the same time the weighting factors, q_1 , q_2 and q_3 , and R -value for matrix Q_m , should be specified, as shown in the next paragraph. Essentially, choosing a large value for R means a designer tries to stabilize the system with less weighted energy; this is usually called expensive control strategy. On the other hand, choosing a small value for R means the designer did not want to penalise the control signal; a cheap control strategy. Similarly, if a large value is chosen for Q_m then the system needs to be stabilised with the least possible changes in the states and a large Q_m implies less concern about changes in the states. Since there is a trade-off between the two, the Q matrix can first be found:

$$Q = C^T Q_m C \quad (6.51)$$

Subsequently, it is possible within the Matlab m-file to use a “**care**” in order to find Q_m . Then, using Equation 6.48 to find K , because this controller totally depends on a practical aspect, the weighting factor for each sensor from the test rig should be known, as shown in the K_2 matrix:

$K_2 = 5 \times 5$ Transducer gain matrix.

$$K_2 = \begin{bmatrix} I_2 & 0 & 0 & 0 & 0 \\ 0 & J_2 & 0 & 0 & 0 \\ 0 & 0 & H_2 & 0 & 0 \\ 0 & 0 & 0 & F_2 & 0 \\ 0 & 0 & 0 & 0 & L_2 \end{bmatrix} \quad (6.52)$$

By using the following equation, it is possible to find the design gains:

$$K = N K_1 K_2 \quad (6.53)$$

Therefore, it is possible to find K_1 from Equations 6.52 and 6.53 as:

$$K_1 = N^{-1} K K_2^{-1} \quad (6.54)$$

where, $N = A/D$ is the converted DAP gain factor.

So far, the controller design meets our transient requirements, but now the

steady-state error must be addressed. In contrast to other design methods, where it was fed back to the output and compared to the reference input to compute an error, with a full-state feedback controller, it was fed back to all of the states. It needed to compute what the steady-state value of the states should be, multiply that by the chosen gain K and use the new value as our reference for computing the input. This can be done by adding a constant gain K_c after the reference; which can be found by employing the user-defined function **rscale.m** in Matlab.

Design steps can be summarised as follows:

1. Specify the cost function.
2. Specify the weighting parameters, i.e. q_1, q_2, q_3 and R .
3. Solve Equation 6.50, the reduced-matrix Riccati equation, for the matrix P_m .
4. Substitute the matrix P_m into Equation 6.48, resulting in the vector K ; the optimal feedback gains and use Equations 6.52, 6.53 and 6.54 to find K_1 .
5. Find the scale factor, K_c , to eliminate the steady state error.

6.10.1 Determination of weighting factors

One of the key questions in LQR design is how to choose the weighting, Q_m . With respect to the cost function in Equation 6.28, there are four weighting factors, R, q_1, q_2 and q_3 , to be identified before the LQR design can be processed. This is a relatively complicated four-dimensional-search problem in order to determine the optimum solution.

There is no loss in the mathematical representation if one of the weighting factors, R , is set to equal unity because LQR is in fact a numerical algorithm used to discover the global minimum point of the cost function. To choose specific values for the cost function weights Q_m , it must use the system information, which be controlled; a particularly simple choice is to use diagonal weighting. (Thompson 1976) proposed an idea to reduce the workload of the numerical search by three facts, as follows:

1. The weighting factors q_2 and q_3 vary with the square of the measured variables $X_b - X_w$ and $X_w - X_r$ in the cost function.

2. $X_b - X_w$ and $X_w - X_r$ terms have the same dimensions because both variables are physically displaced by the same units.
3. In a reflection of the physical limitations, the ratio of the weighting factors for both variables $X_b - X_w$ and $X_w - X_r$ can be practically approximated from the square of the ratio of their physical maximum values.

By applying Thompson's (1976) ideas to this work, an appropriate assessment of the weighting factors q_2 and q_3 can be written as:

$$\frac{q_3}{q_2} = \left(\frac{(X_b - X_w)_{\max}}{(X_w - X_r)_{\max}} \right)^2 = \left(\frac{25}{6.8} \right)^2 = 13.5 \quad (6.55)$$

It should be noted that the maximum physical ranges of $X_b - X_w$ and $X_w - X_r$ are obtained from the test rig as described in Section 3.5.

Therefore, if q_2 is specified, q_3 is mechanically known. With that approximation, the four-dimensional search problem drops to only a two-dimensional search problem. That means, in adding to q_2 , only q_1 needs to be specified. This simplifies the design problem and reduces the calculation time to determine the optimum solution.

6.11 Design example

By considering the state equation of the active suspension system as follows:

$$\dot{x}(t) = A(t)x(t) + B(t)ea(t)$$

$$y = Cx(t)$$

where, A and B matrices are the system and input matrices that were previously used in the design example for the PA controller.

$$C = \begin{bmatrix} 0.0 & 0.0 & 1.0 & 0.0 & 0.0 \\ 0.0 & 0.0 & 0.0 & 1.0 & 0.0 \\ 0.0 & 0.0 & 0.0 & 0.0 & 1.0 \end{bmatrix}$$

The performance index, J as was given by:

$$J = \int_0^{\infty} (x^T(t)C^T Q_m C x(t) + ea^T(t) R ea(t)) dt$$

where, Q_m is the weighting factors matrix, which is:

$$Q_m = \begin{bmatrix} 4.37 & 0.0 & 0.0 \\ 0.0 & 2e6 & 0.0 \\ 0.0 & 0.0 & 2.66e7 \end{bmatrix}$$

Therefore, using Equation 6.51:

$$Q = \begin{bmatrix} 0.0 & 0.0 & 0.0 & 0.0 & 0.0 \\ 0.0 & 0.0 & 0.0 & 0.0 & 0.0 \\ 0.0 & 0.0 & 4.37 & 0.0 & 0.0 \\ 0.0 & 0.0 & 0.0 & 2e6 & 0.0 \\ 0.0 & 0.0 & 0.0 & 0.0 & 2.66e7 \end{bmatrix}$$

and, $R = 1$

Considering we know A , B , Q and R to determine the matrix P_m using the MATLAB m.file, by printing the order $[P_m] = \text{care}(A, B, Q, R)$, P_m was obtained as follows:

$$P_m = \begin{bmatrix} 4.17e5 & 5.01e1 & 9.65e-3 & 7.95e5 & 2.79e5 \\ 5.01e1 & 1.96e1 & 6.84e-5 & -9.60e1 & 1.88e3 \\ 9.65e-3 & 6.84e-5 & 2.74e-5 & 1.85e-2 & 6.24e-3 \\ 7.95e5 & -9.60e1 & 1.85e-2 & 2.04e6 & 1.03e6 \\ 2.79e5 & 1.88e3 & 6.24e-3 & 1.03e6 & 1.02e6 \end{bmatrix}$$

From Equation 6.48 and by printing the order $K = (R^{-1}) * B' * P_m$; in the MATLAB m.file, yield:

$$K = R^{-1} B^T P_m$$

$$K = [7.35e2 \quad 5.21 \quad 2.09 \quad 1.41e3 \quad 4.75e2]$$

From Equation 6.54:

$$K_1 = N^{-1} K K_2^{-1}$$

where, $K_1 = 1 * 5$ is the state feedback gain matrix for the controller.

$$K_1 = [I_1 \quad J_1 \quad H_1 \quad F_1 \quad L_1]$$

$N = A/D$ Gain

$$N = 3276 \text{ m.c/V}$$

$K_2 = 5 * 5$ Transducer gain matrix

$$K_2 = \begin{bmatrix} 0.2 & 0.0 & 0.0 & 0.0 & 0.0 \\ 0.0 & 0.2 & 0.0 & 0.0 & 0.0 \\ 0.0 & 0.0 & 0.000002 & 0.0 & 0.0 \\ 0.0 & 0.0 & 0.0 & 0.0000077 & 0.0 \\ 0.0 & 0.0 & 0.0 & 0.0 & 0.000027 \end{bmatrix}$$

By printing command $K_1 = (N^{-1}) * K * K_2^{-1}$ in the MATLAB m.file, the feedback gain vector for the controller K_1 was found as:

$$K_1 = [1.12 \quad 7.96e - 3 \quad 3.19e2 \quad 5.60e4 \quad 5.37e3]$$

The procedure for the LQ design has been written in the MATLAB m.file and using the same order as mentioned above, allowed the systematic design to be processed. Note: For more detail, see APPENDIX D.

The most significant differences between the two active systems (PA, LQ) were detailed in the previous section. Both are related to the PS system. Therefore, it was decided to only display the comparison between passive and active systems regarding PA control, rather than showing all the responses again.

6.12A new active suspension model

The free body diagrams of both body and wheel masses were demonstrated in **Chapter 5** by Fig. 5.9. The $\frac{1}{4}$ car test rig and model of the actively suspended vehicle were considered by implementing the friction force relative to the real dynamic position and by defining the dynamic construction angle between the actuator and linkage and the reality of the sliding body. The new term, friction force, is considered for the first time with the equation of motion for $\frac{1}{4}$ car model in addition to the systematic friction that already occurs inside the actuator (viscous and Coulomb friction). In fact, for the $\frac{1}{4}$ car research test rig, which is mostly used to investigate and study the dynamic modelling and control of vehicle active suspension system, most of the previous research ignored the friction effects on the body that could result in insufficient information about the system model and control. Therefore, revising the model by considering an accurate form surely contributes to identifying a precise control and pushes the knowledge in

this field. The new equation of body motion, by considering the bearings body friction, damping friction, in addition to the viscous and Coulomb friction, which occurs inside the hydraulic actuator, is:

$$M_b \cdot \ddot{X}_b = [F_{hyd} - b_{va}(\dot{X}_w - \dot{X}_b) - F_f] \cos(\alpha \mp \Delta\alpha) - F_{fricd} \quad (6.56)$$

While the equation of motion for the wheel is:

$$M_w \cdot \ddot{X}_w = -[F_{hyd} - b_{va}(\dot{X}_w - \dot{X}_b) - F_f] \cos(\alpha \mp \Delta\alpha) + k_t(X_r - X_w) + b_t(\dot{X}_r - \dot{X}_w) \dots \dots \dots (6.57)$$

where, M_b and M_w are the masses of the body and wheel, respectively. The displacements of wheel and car body are X_w and X_b , respectively. The damper active actuator coefficient is b_{va} , while the tyre spring stiffness and damping rate are k_t and b_t respectively. The steady-state construction angle is α , while $\Delta\alpha$ is the relative dynamic change in the angle and F_f is the Coulomb friction inside the actuator. It should be noted that X_r , X_w and X_b are mathematically referenced to an ideal ground that does not exist in real world but does exist in the laboratory environment. Although these signals were available to measure with test rig, instead of that, the suspension displacement and tyre deflection signals were used to make the model close to reality. In addition, it is assumed that the tyre behaves as a point-contact follower which is in contact with a road surface at all times.

The active system responds dynamically to road disturbance inputs by inducing relative motion between the body and the wheel through a force generated by the servo-hydraulic actuator. Obtaining the appropriate control voltage for the actuator requires an optimal trade-off between the design objectives in the presence of road disturbance inputs. The optimisation process was conducted but, it was decided to not display it in this study because it is fundamental and usually done for LQ controllers. The success of this process yields a suspension system that is adaptive to road disturbance and other operating conditions.

6.13 Dynamic performance and optimum design of an active suspension system designed by pole-assignment and linear quadratic optimal control

To determine the optimum design of minimising \ddot{X}_b within the available $X_w - X_b$, $X_r - X_w$, and u_a , the dynamic performance of the Active Suspension designed by Pole-Assignment control (ASPA) and by Linear Quadratic optimal control (ASLQ) was investigated by simulation using the mathematical model developed in Section 5.6. The simulation model was built as previously mentioned in **Chapter 5**, by using Equations 5.89, 5.90, 5.91, 5.94 and 5.103 through the C++ compiler environment. This code involved the nonlinear hydraulic actuator equations as a system controller and considered the active $\frac{1}{4}$ car model by implementing the nonlinear friction force model that occurs at the bearings body. The MATLAB m.file was used to find the K gains values, the schematic diagram for this simulation was used with relative to Fig. 6.16. While the experimental setup for the validation of PA and LQ controllers is shown in Fig. 6.17.

Note: the details of C++ program and MATLAB m.file are given in **APPENDIX C**.

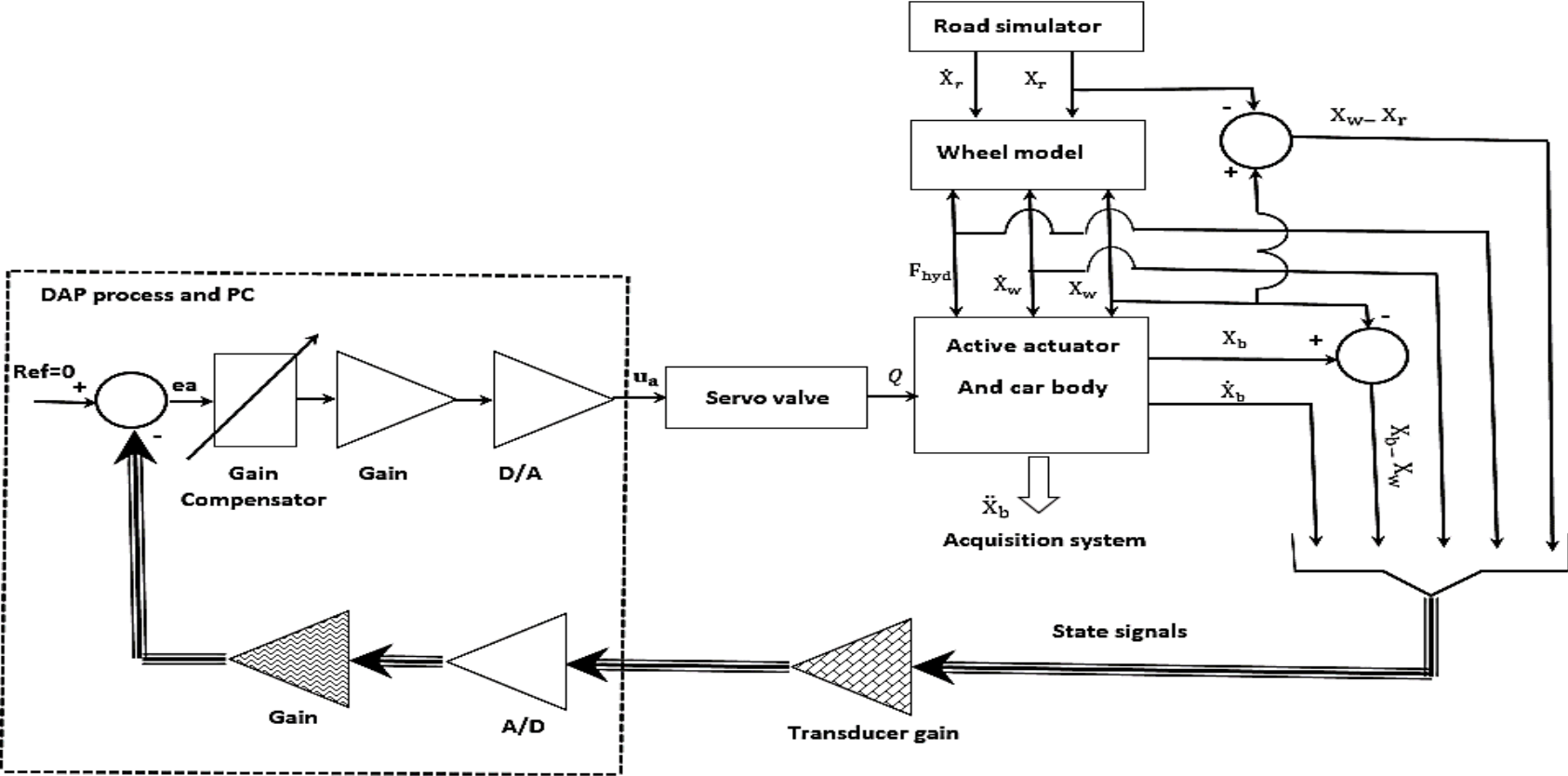


Fig. 6.16. Simulation model for active suspension designed by full-state feedback.

According to the designs of PA and LQ, it can be seen that both are in fact two-dimensional-search problems. Tuning parameters of interest for the PA are ω_n and ξ , whilst for LQ the weighting factors are q_1 and q_2 . The search problems can be globalised by varying these parameters throughout the range of values of practical significance. This resulted in many simulation runs for each case. The ramp and step mixed road input model, developed in Section 3.1 in **Chapter 3**, was used to excite the systems in addition to the ramp and bump or random mixed road input model developed later in this chapter. The three vehicle response variables of interest, \ddot{X}_b , $X_w - X_b$ and $X_r - X_w$, and the control input, u_a , were monitored and printed by running the C++ compiler. The results of the global search are in the form of graphs for each relevant variable with respect to time. This presentation format is similar to the one used in the passive suspension study in Section 3.3. Therefore, a comparison between the global investigation for the passive and active suspensions can be made.

6.14 Comparison between passive suspension and active suspension designed by pole-assignment and by linear quadratic optimal control

To illustrate the influence of active suspension on system performance, the designed model for the PS, developed in Section 3.3, and that of the ASPA and ASLQ controllers are obtained in this chapter. With respect to the test rig construction and the type of the force system inputs, an examination of the values of the relevant variables between the two designs in both positive and negative directions can therefore be conducted, as introduced in Table IV.

Table IV: Performance comparison between PS and ASPA and ASLQ control

Concerned variables	Input force Direction	PS	ASPA	ASLQ	(%) Improvement
Acceleration of car body \ddot{X}_b (m/s^2)	+ ve	1.5	1.43	1.37	9.4
	- ve	2.14	1.35	1.35	58.5
Suspension displacement $X_w - X_b$ (% of max. value) (cm)	+ ve	1.81	2.43	2.21	% Increase 34.2
	- ve	3.29	4.42	4.01	34.3
Tyre deflection $X_r - X_w$ (% of max. value) (cm)	+ ve	0.13	0.133	0.133	% Increase -
	- ve	0.287	0.298	0.298	-
Applied voltage to servovalve u_a (max. value) (v)	+ ve	N/A	- 2.52	- 0.88	% Decrease 286.4
	- ve	N/A	4.65	1.64	283.5

It is evident that the ASPA and ASLQ provide enhanced performance concerning the design objective of this work, i.e. minimising \ddot{X}_b . The ASPA reduce the vibration level to 58.5% of that obtained from the PS in the negative direction relative to the input force (double input) and 4.8% in the positive direction. While ASLQ can be reduced the vibration level, which was closed to a 58.5% reduction in the negative direction and 9.4% in the positive direction, in comparison with that obtained from the PS relative to the input force. ASPA and ASLQ cost more suspension displacement than PS. The wheel movement in all systems (PS, ASPA and ASLQ) is quite close, since the suspension displacement was increased by 34.3% for both controllers in the two directions in comparison to PS, i.e. the body damping increases by 34.3%. There is a slight difference in the tyre deflection response between both passive and active systems. Considering the additional energy consumed for just the AS, ASPA utilises almost the maximum levels of energy, or applied voltage u_a to the AS system; more than 286.4% for the ASLQ control. It is clearly seen that the desired voltage is applied in the direction opposite to the input forces; this is because the main controller contribution is to minimise \ddot{X}_b . The lower consumption of additional energy for the desired in the ASLQ, in comparison with ASPA, is interesting from the viewpoint of controller performance. However, plotting the results of the body acceleration for PS in comparison with AS designed by PA and LQ controllers, clearly illustrates the controller's effectiveness action, as a result they helped to enhance ride comfort, or minimise body acceleration, as shown in Fig. 6.18.

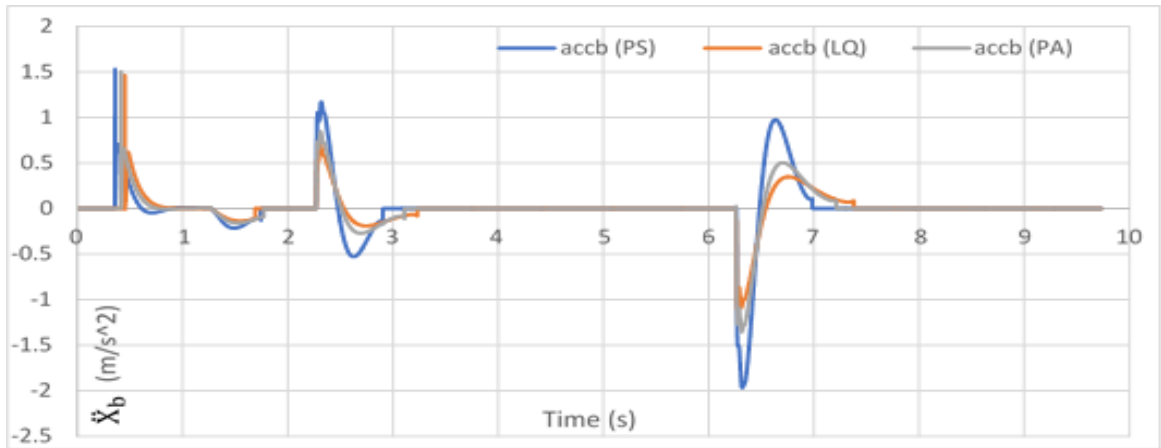


Fig. 6.18. Simulated body acceleration for PS, ASLQ and ASPA under step road excitation.

While, the comparison of body velocity between the PS and AS designed by LQ and PA is shown in Fig. 6.19. The figure clearly shows the deceleration of the velocity according to control achievement.

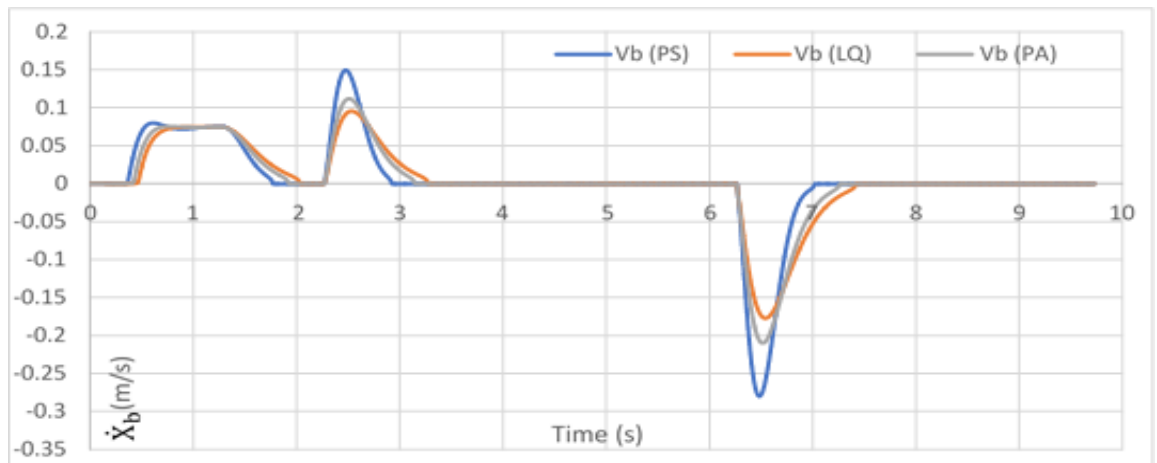


Fig. 6.19. Comparison of body velocity for PS, ASLQ and ASPA under step road excitation ($\dot{X}_b = V_b$).

Fig. 6.20 displays the LQ and PA controller behaviour (applied voltage) relative to the mixed ramp and step roads excitation. It was clearly seen that the energy consumed by the PA controller is significantly higher than that used for the LQ controller.

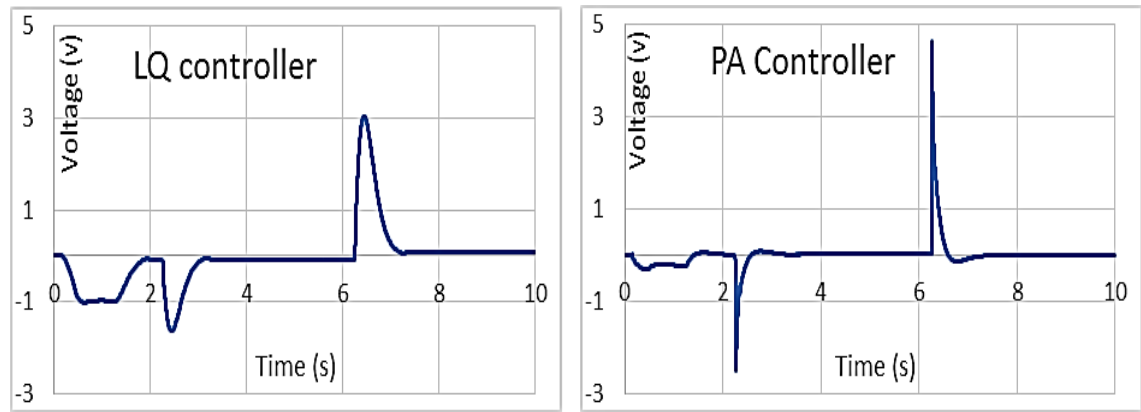


Fig. 6.20. Comparison of PA and LQ controller under step road excitation.

In another perspective, investigating the dynamic characteristics of the suspension designs in more detail; the dominant closed-loop poles of the active suspension designs were plotted in Fig. 6.5. The suggested PA controller poles were elucidated in Fig. 6.6 and added to the dominant natural frequency and damping ratio of each design. The control hydraulic force for both types of control, in addition to the dominant natural frequency and damping ratio of each design, are summarised in Table V.

Table V: Comparisons of natural frequency, damping ratio and hydraulic force for passive and active suspension designs.

Concerned parameters	PS	ASPA	ASLQ
Dominant natural frequency ω_n (Hz)	1.4	1.6	0.1
Damping ration ξ	0.15	0.76	1.0
Hydraulic force F_{hyd} (N)	N/A	+ve 305 -ve 561	368 684

It is apparent that ASPA and ASLQ take place at very high damping regarding the PS system. Even though the PS and the ASPA are entirely different, according to their physical configuration, both systems have one feature in common in that the system dynamics are dominated by a pair of complex conjugate poles or an ideal second-order system. A possible explanation is that both systems use a similar concept in their designs, i.e. constant suspension stiffness and damping rate in the PS is equivalent to the specific desired natural

frequency and damping ratio in the ASPA. With the active principle, the damping ratio of the active system tends to be higher than that of the passive system. More interestingly, optimum ASLQ is dominated by one pole located on the real axis, assuming that the other pole nearby has a small effect, i.e. the system dynamic was dominated by a simple first-order system having extremely low natural frequency and critical damping ratio.

The dominant closed-loop poles were used in the initial investigation in order to investigate the dominant natural frequency and damping ratio. Nonetheless, it was realised that this does not explain all aspects of the system responses because the disturbance transfer functions of both passive and active suspensions contain different zeros.

The real configuration of the PS has a relatively low damping ratio ($\xi = 0.15$). Therefore, the effects of the natural frequency of the car body ($\omega_n = 1.4$ Hz) and the wheel unit ($\omega_n = 13.6$ Hz) are inevitably dominant. It can be clearly seen that the magnitude response is significantly higher at both natural frequencies. When PA is used, it allows the dominant ω_n of the system, along with the dominant system-damping ratio, to be unchanged. In this work, the suggested design solution for ASPA occurs for $\omega_n = 1.6$ Hz and $\xi = 0.76$. The magnitude response is dramatically reduced around the natural frequency of the car body and its peak shifts slightly to a higher frequency. However, the natural frequency of the wheel unit is still dominant at a high-frequency range so that it results in the increment of the magnitude around the natural frequency of the wheel unit.

Interestingly, ASLQ does not affect the natural frequency of the car body and the natural frequency of the wheel unit has a small effect. This may be explained by plotting the dominant closed-loop, as shown in Fig. 6.21. LQ can force the dominant closed-loop pole to lie on the real axis in the s-plane ($\xi = 1.0$) and close to the imaginary axis, i.e. the dominant natural frequency is very small ($\omega_n = 0.1$ Hz). The damping ratio can be increased to critical damping rate with a small inverse effect on transmissibility at a high-frequency range, in comparison to the PS and ASPA, because of the extremely low natural frequency. This results in a significant reduction in the magnitude of the response \ddot{X}_b for the overall frequency range of interest (0-20 Hz). Hence, ASLQ is the most effective solution for vibration isolation.

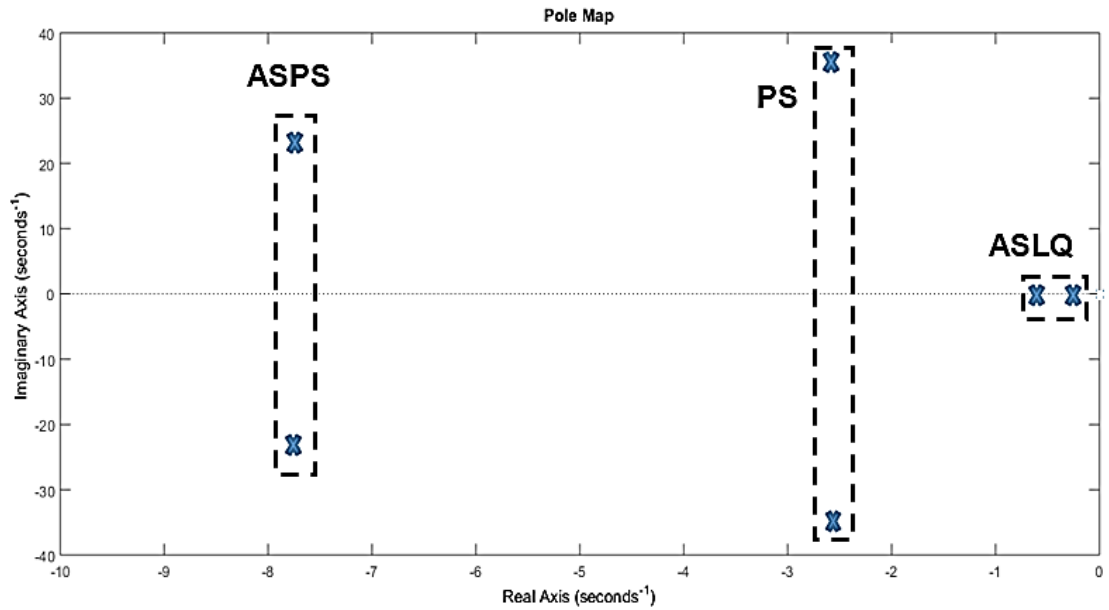


Fig. 6.21. Location of the dominant closed-loop poles of the two suspension designs.

The $X_w - X_b$ response of ASPA and ASLQ are higher than those of the PS at a frequency lower than 1 Hz. This relationship is reversed around the natural frequency of the car body and clearly shows the disadvantages of PS in two aspects, as follows. Firstly, PS can follow the road input displacement sufficiently well in comparison with ASPA and ASLQ at a frequency lower than 1 Hz. Secondly, at the natural frequency of the car body, PS requires a very large movement of $X_w - X_b$ to accommodate the resonance effect of the natural frequency. ASLQ provides the flattest magnitude response among the three suspension designs without any adverse effect from the natural frequency of the car body. This confirms the comparison in Table III that the three optimum designs utilise the same $X_r - X_w$.

It is essential to use the generated hydraulic actuator force to compare between these designs systems. Thus, this force has an active link with the applied voltage relative to the control signal. It can be observed that, although the applied voltage, u_a , for ASLQ is lower than that of ASPA is just 65%, but the generation of the hydraulic actuator force for ASLQ is interestingly higher, by 18%, than ASPA in both directions. This means that ASLQ is undoubtedly better than ASPA control.

So far, our analysis of systems has been in the time domain and based on specific test signals, namely ramp and step. The signal was used to emphasise some aspects of the system's performance, such as: the speed, displacement

and acceleration, of the response. Another particularly important signal is the bump and random input. It is clear that most real signals are not conveniently represented by a step or ramp, as they are normally quite complex waveforms. We can also predict the stability of a closed loop system by looking at its response to bump and random inputs, as we shall see later.

6.15 System bump input exceeds the limit of the test rig

In this study, the experimental system inputs were constrained by the limited movement of the road actuator inputs connected to the test rig. However, in simulation, to broaden the evaluation, a bump input with amplitude of 0.1 m was considered. Thus, providing a chance to check the robustness of the control design. The primary aim of the control was still to reduce the body acceleration i.e. enhance the ride comfort.

The simulated time responses of the passive and active suspensions subject to a bump road profile, as suggested by (Alfadhli et al. 2018), were used:

$$x_r(t) = \begin{cases} \frac{A_m}{2} \left(1 - \cos\left(\frac{2\pi v}{L}t\right)\right) & , 0 \leq t \leq L/v \\ 0 & , t > L/v \end{cases} \quad (6.58)$$

Where, v is the forward speed of the vehicle and A_m and L are the height and length of the bump, respectively. In the current study, it is assumed that the vehicle moves with a constant forward speed. The parameters of the bump road profile were then chosen as $v = 100$ km/h, $A_m = 0.1$ m and $L = 2$ m.

In order to match the previous experimental and simulation studies the previous profile first moved the hydraulic piston from the ground to the midpoint. After the suspension settled the bump input with an amplitude of 0.1m was applied. The bump road excitation is shown for three vehicle speed values, 50, 100 and 150 km/h, in Fig. 6.22. Accordingly, the subsequent responses to the bump action, after approx. 2.3 s, in such figures, are those of interest.

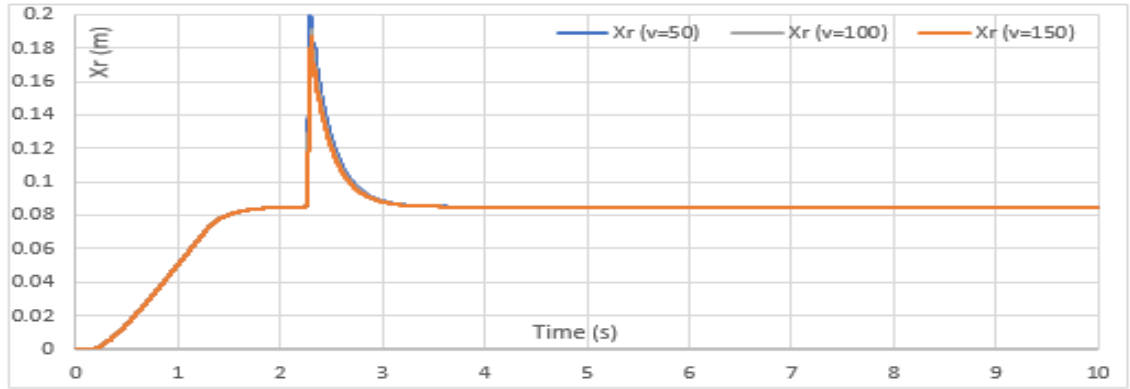


Fig. 6.22. Mixed ramp and bump road inputs for three vehicle speed values, 50, 100 and 150 km/h, with an amplitude of 0.1 m.

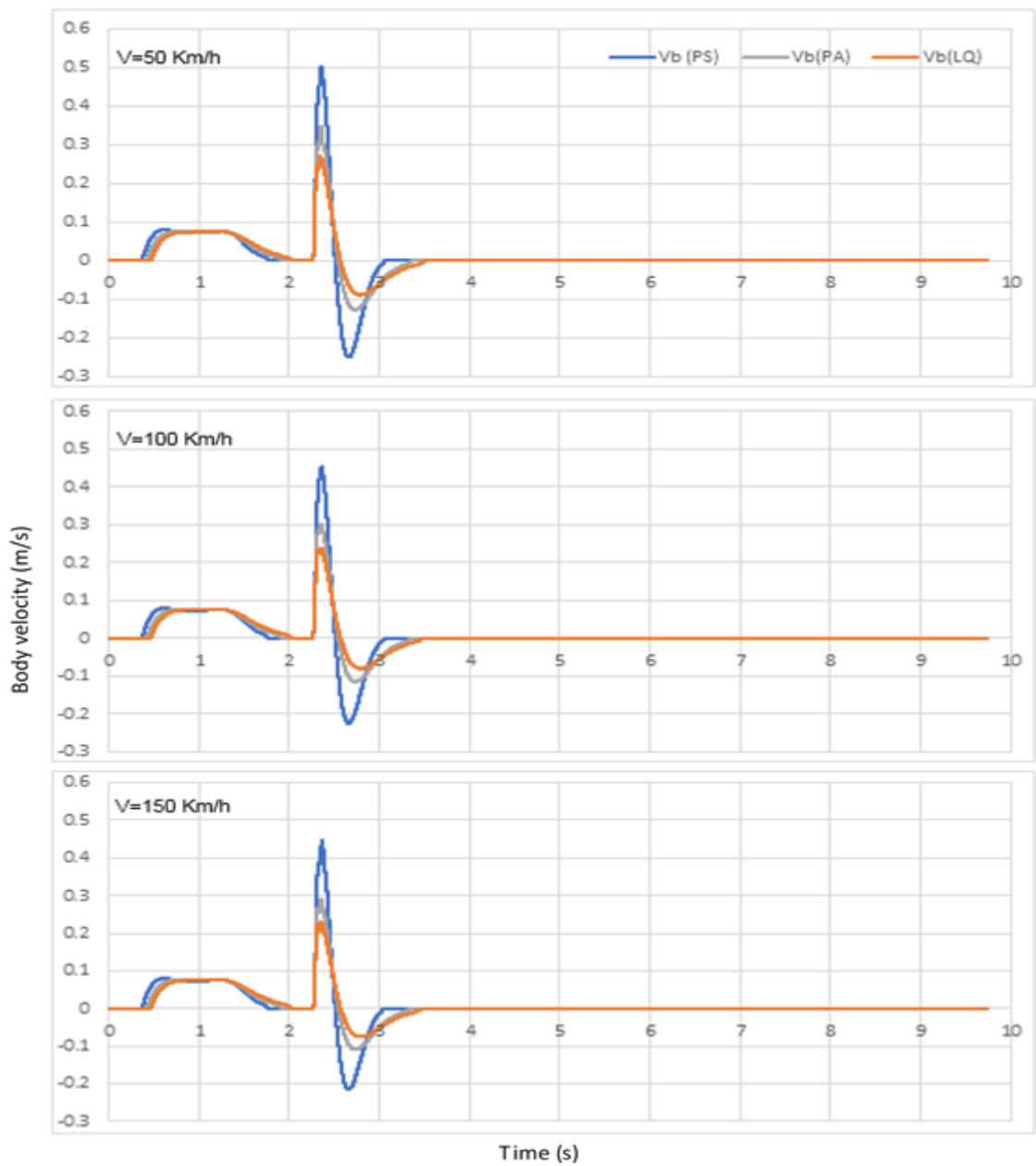


Fig. 6.23. Comparison of the body velocity for PS, ASLQ and ASPA for three vehicle speed values, 50, 100, and 150 km/h under bump road excitation.

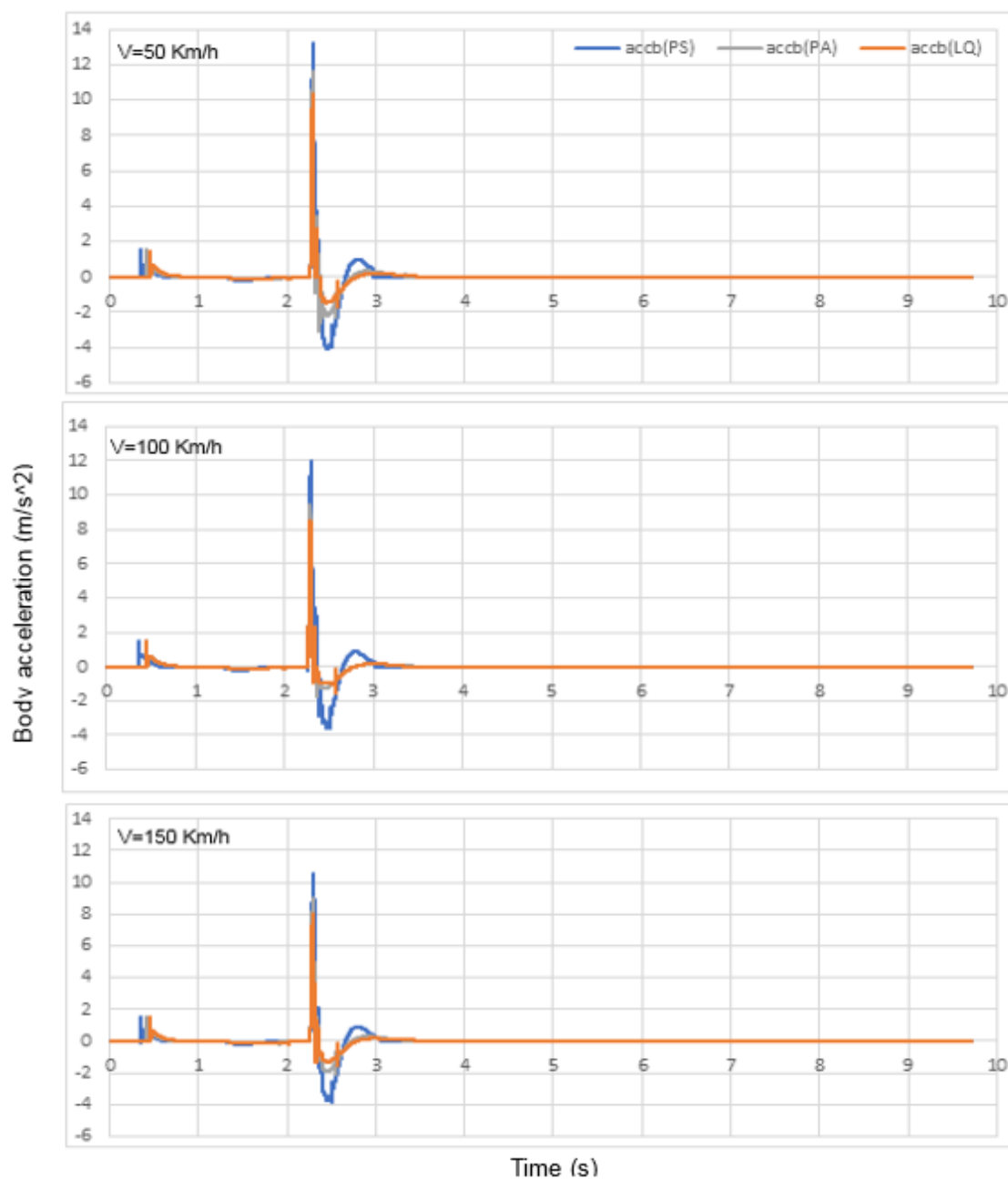


Fig. 6.24. Comparison of the body acceleration for PS, ASLQ, and ASPA for three vehicle speed values, 50, 100, and 150 km/h, under bump road excitation.

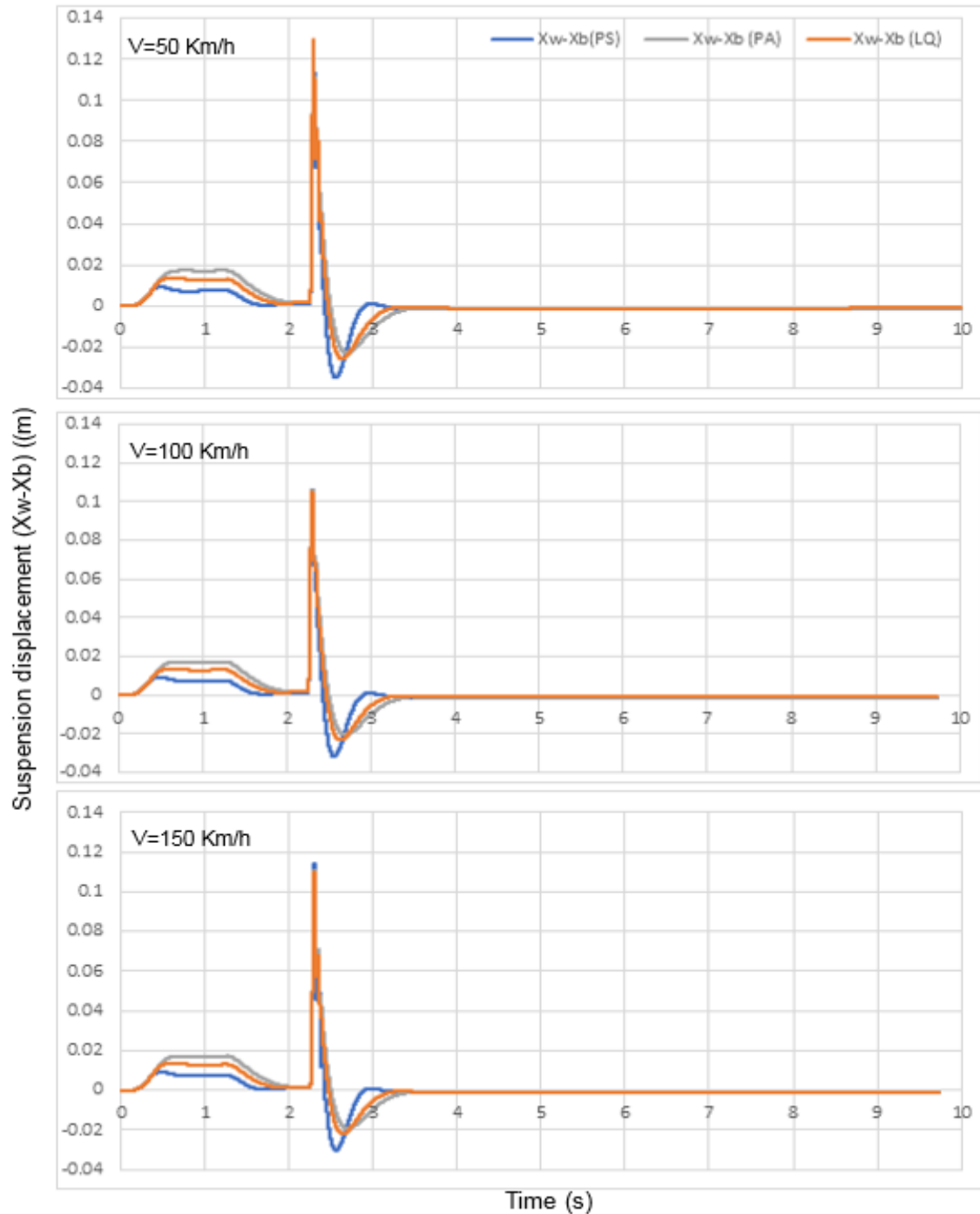


Fig. 6.25. Comparison of suspension travels for PS, ASLQ, and ASPA for three vehicle speed values, 50, 100, and 150 km/h, under bump road excitation.

The simulated time responses of the passive and active suspensions designed by PA and LQ, and the corresponding bump road input, as defined in Equation 6.58 for three different vehicle speeds values, 50, 100, and 150 km/h, are shown in Figs. 6.23, 6.24, and 6.25. It is clear that AS reduces the body velocity and acceleration more efficiently than PS for all vehicle speeds, with a slight difference in the control action between the two controllers, LQ and PA; LQ is better. However, this is at the cost of increasing the suspension displacement,

as shown in Fig. 6.25. The performance of the active suspension at higher vehicle forward speeds is also improved as the suspension travel is reduced compared to that at lower vehicle speeds. These results once again validate that the proposed controllers can advance the ride quality by taking into account the suspension travel limits and saturation of the actuator.

6.16 Random system input for simulation

Vehicle ride and handling are mainly influenced by the road input caused by road roughness. The first step in analysis of vehicle suspension dynamic responses was to determine the mixed ramp and step inputs that were suitable for experimental test rig that was used. The second step in the analysis of simulated time responses of the vehicle system was to use the ramp and bump road excitation. The step road input, such as a bump or a pothole, is used to be representative of a discrete event of relatively short duration and high intensity, as mentioned in **Chapter 3** and Section 6.15. There is another way possible to analytically describe the road input, which can be classified as a random road input, which is characterised by prolonged and consistent excitations.

Random road profiles have been the subject of research for many years. Since the exact nature of the profile was not known, some road profiles were measured and subsequently Fourier analysed to see whether there was a way of characterising their Power Spectral Densities (PSD). It is widely accepted that an adequate approximation for the road profile is integrated white noise, characterised by its PSD as reported by (Sharp and Crolla 1987), (Hrovat 1997b) and (Sharma et al. 1992).

The approximation of road surface roughness has been commonly approximated through the use of ISO 8608 classifications (Agostinacchio et al. 2014) and (Odrigo et al. 2016), which are ranges of proposed PSD for different levels of roughness. They expanded on this by simplifying the approximation for use with MATLAB in order to determine a relation between road surface degradation and dynamic loading of the vehicle. (Tyan et al. 2009) established a one-dimensional sinusoidal approximation method based on these PSD specifications for use with quarter and half-vehicle suspension models. The ISO

8608 standard (Standardization 1995) proposes an approximated formula to obtain the PSD function of road roughness as follows:

$$\Phi(\Omega) = \Phi(\Omega_o) \left(\frac{\Omega}{\Omega_o}\right)^{-\omega} \quad (6.59)$$

where, $\Omega = \frac{2\pi}{l}$ (rad/m) signifies the angular spatial frequency, l is the wavelength and ω is the waviness, which for most road surfaces equal 2, $\Phi(\Omega_o)$, which is equivalent to Φ_o , is the reference PSD value for a given road type at the reference angular spatial frequency $\Omega_o = 1$ (rad/m). The reference values of the PSD at $\Omega_o = 1$ (rad/m) for different road modules are given by ISO 8608 (Standardization 1995), as shown in Table IV. At low spatial frequency, Equation 6.59 tends to infinity, so it was adapted by (Tyan et al. 2009) to designate the pavement roughness PSD as follows:

$$\Phi(\Omega) = \begin{cases} \Phi(\Omega_o) \Omega_1^{-2} & \text{for } 0 \leq \Omega \leq \Omega_1 \\ \Phi(\Omega_o) \left(\frac{\Omega}{\Omega_o}\right)^{-2} & \text{for } \Omega_1 \leq \Omega \leq \Omega_N \\ 0 & \Omega_N \leq \Omega \end{cases} \quad (6.60)$$

Table VI: Road roughness values (Tyan et al. 2009).

Road class	Degree of roughness $\Phi(\Omega_o)$ ($10^{-6}m^3$) for $\Omega_o = 1$ (rad/m)		
	Lower limit	Geometric mean	Upper limit
A (very good)	-	1	2
B (good)	2	4	8
C (average)	8	16	32
D (poor)	32	64	128
E (very poor)	128	256	512

The values of Ω_1 and Ω_N have been suggested by the ISO 8606 standard to be 0.02π and 6π (rad/m), respectively (Tyan et al. 2009), which covers a wavelength band of 0.333-100 m. In the current study, it was decided to use (Alfadhli et al. 2018) analysis to modify the (Tyan et al. 2009). When the vehicle is travelling over a specified road segment of length l and constant velocity v , then the random road profile as a function of a travelled path s can be approximated using a superposition of $N(\rightarrow \infty)$ sine waves as reported by (Alfadhli et al. 2018), as follows :

$$X_r(s) = \sum_{n=1}^N A_n \sin(\Omega_n s - \varphi_n) \quad (6.61)$$

where, the amplitude A_n is given by:

$$A_n = \sqrt{\Phi(\Omega_n) \frac{\Delta\Omega}{\pi}} \quad (6.62)$$

where, $\Delta\Omega = \frac{\Omega_N - \Omega_1}{N-1}$ and φ_n are random phase angles between 0 and 2π . As mentioned by (Alfadhli et al. 2018), the term Ωs in Equation 6.61 is equivalent to:

$$\Omega s = \frac{2\pi}{\lambda} s = \frac{2\pi}{\lambda} vt = \omega t \quad (6.63)$$

In which, λ is the wavelength and ω (rad/s) is the angular frequency in the time domain. From Equations 6.61 and 6.62, the road profile in the time domain is given as follows:

$$X_r(t) = \sum_{n=1}^N A_n \sin(n\omega_0 t - \varphi_n) \quad (6.64)$$

where, $\omega_0 = v\Delta\Omega$ (rad/s) is the fundamental temporal frequency in the time domain. A random road profile is selected in the optimisation process with a very poor road roughness and a vehicle velocity of $v = 100$ km/h because the random road contains most of the human frequency sensitivity range and most of the road profiles are random.

The hydraulic system was used to generate the random inputs, therefore, the inputs consist of ramp and random inputs. Fig. 6.26 shows the road inputs relative to three vehicle speeds, 50, 100, and 150 km/h. The previous procedure of ramping the system up to the mid length was used again. The random inputs were applied after the system had settled, after approx. 2.3 s.

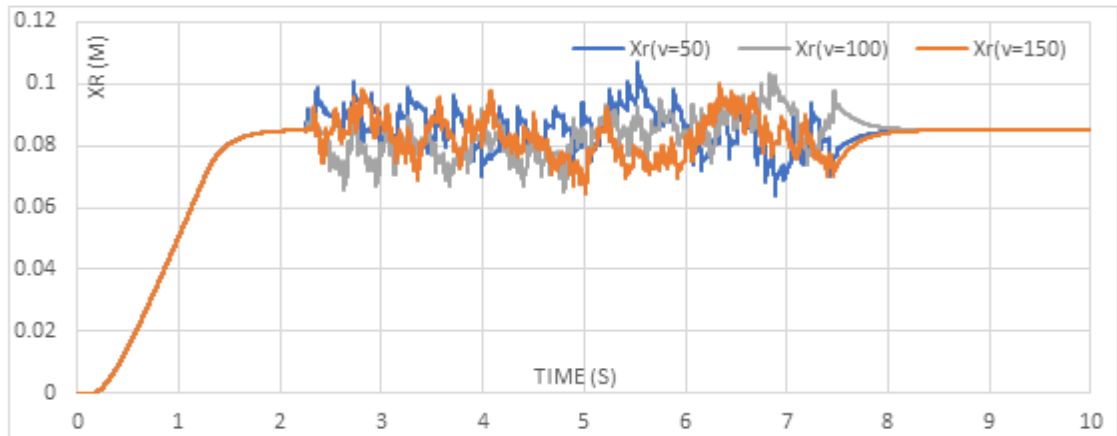


Fig. 6.26. Random road inputs relative to three vehicle speed values, 50, 100, and 150 Km/h.

Comparison of simulation system responses are shown in figs. 6.27 and 6.28. For these figures, the time axis is shifted to show responses from 2.3 s to 4.3 s. Three vehicle speeds were tested, 50, 100 and 150 km/h and, due to the random nature of the road profile, the simulation was carried out several times for each vehicle speed, with a total time duration of 10 s. Excessive accelerations were used at high frequencies; the reference road roughness, $\Phi(\Omega_o)$, used in the simulation was selected as $256 \times 10^{-6} \text{ m}^3$.

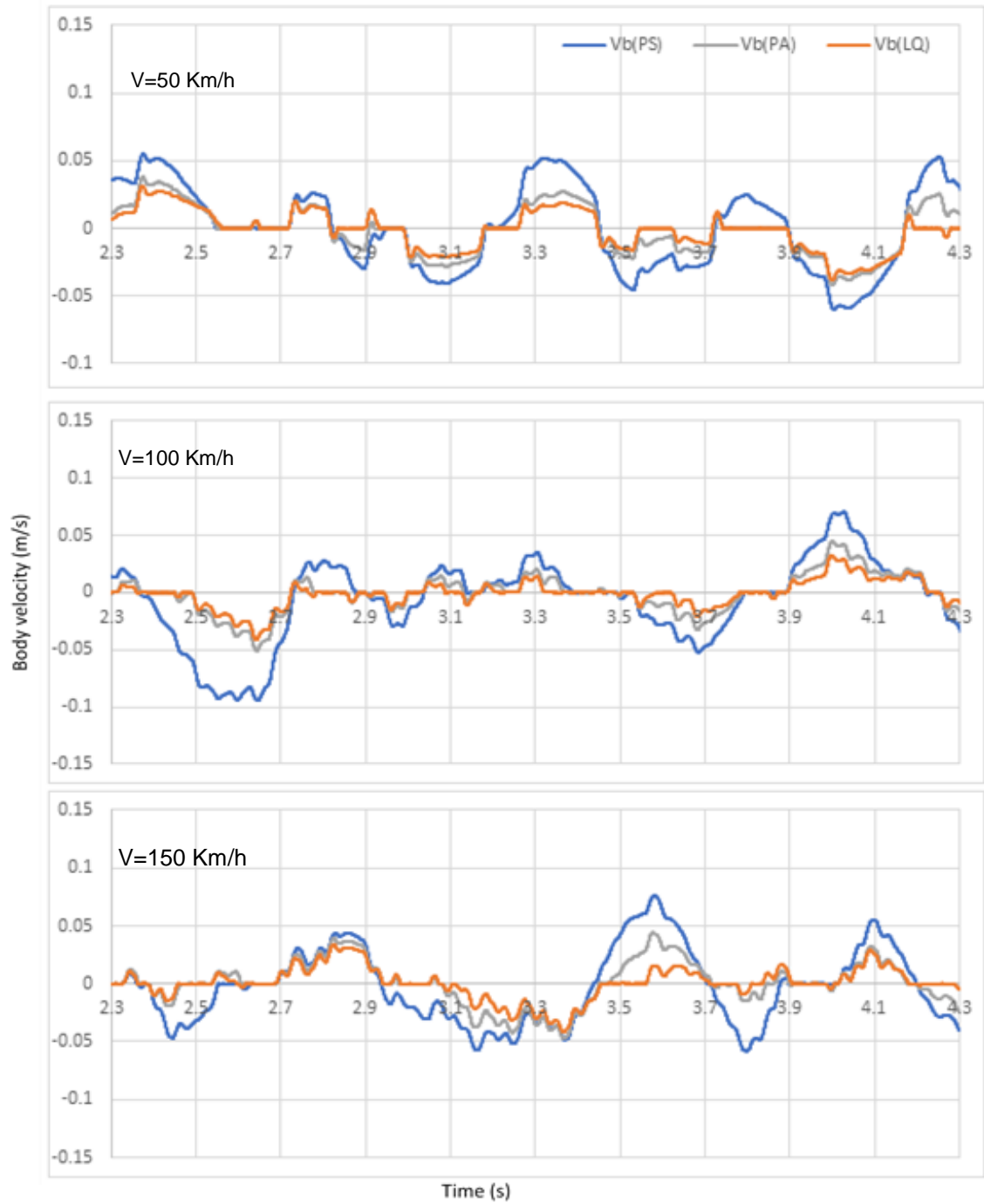


Fig. 6.27. Comparison of the body velocity for PS, ASLQ, and ASPA for three vehicle speed values, 50, 100, and 150 km/h, under random road excitation.

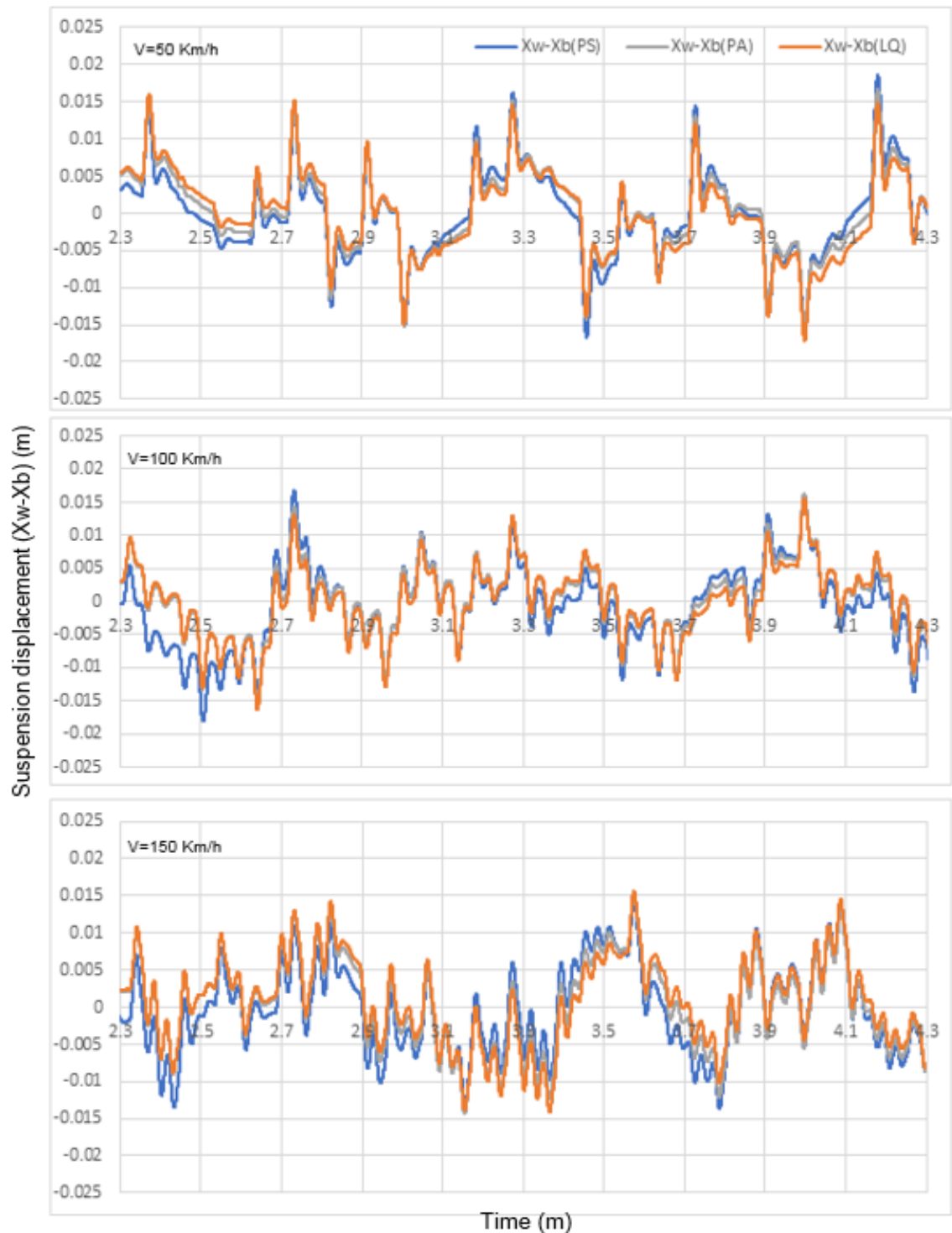


Fig. 6.28. Comparison of suspension travel for PS, ASLQ and ASPA for three vehicle speed values, 50, 100, and 150 km/h, under random road excitation.

It can be clearly seen from Figs. 6.27 and 6.28 that the simulated responses of the active suspension are lower than those of the passive system for all vehicle speeds. Once again, these results confirm the effectiveness of the active suspension and the proposed controllers.

6.17 Discussion

This chapter was set up to test the active suspension system with suitably designed PA and LQ controllers. Ramp, step, bump or random road inputs were variously used, allowing comparisons between the passive and active suspension systems. This, discussion will review and summarise the findings.

- **Pole-assignment control**

Three drawbacks were found in the application of the PA to the active suspension:

- The technique does not enable the designer to accurately determine the three concerned parameters. Instead, it enables the designer to indicate the closed-loop poles of the system matrix. On a basic level, this will influence each of the five state factors simultaneously.
- The strategy is not adaptable on the basis that each one of the five states is controlled with similar weighting.
- The method is not concerned with the constraint of the controller capacity, which is equivalent to an applied voltage to the servovalve. This must be carefully determined because the hypothesis of this method assumes that the controller input is unconstrained. However, this was not correct for the practical design.

- **State observers**

The pole-placement approach for the design of the control system assumed that all state variables were available for feedback. However, in practice, not all state variables are available for feedback, so we have to estimate unavailable status variables.

- **Linear quadratic optimal control**

Even though the theory of LQ, including the knowledge for solving the Riccati equation, is well established, it cannot be utilised directly to by this control problem. The application to active suspension control still requires judgement and adaptation to realise the practical controller design, as was illustrated in Section 6.8.

Some discussion has surrounded the LQ derivation performed by (Thompson 1976) concerning the fact that mathematical modelling affects the derivation, defined cost function, and controlled assessment. When the hydraulic model is added to an ideal active suspension, the model is altered from the original used by Thompson (1976).

The suspension displacement must exist in the output vector to maintain system stability and satisfy the linearised working condition. This is due to the linearised model being performed on the assumption that the actuator is located at the mid-position of the suspension displacement.

By using Liapunov's main stability theorem in combination with minimisation of the defined cost function, the full-state feedback gains can be determined. There are two methods to obtain the solution of the minimisation problem, i.e. an analytical method and by solving equations via the matrix Riccati equation. The former is considered a tedious process when dealing with a high-order system. Therefore, the latter based on matrix calculation and is convenient for computer programming within the MATLAB m.file was used in this work.

One problem was found during the derivation of the optimal solution. There was a vector of state feedback gains and its transpose vector in the derived equation so that the minimisation of the equation concerning the vector of state feedback gains could not be directly obtained. By using a symmetric square matrix and matrix operation theory, the transpose vector could be eliminated and the minimisation process could be performed with the modified equation.

In comparison to the model without the hydraulic system, two main points relating to the cost function can be made. Firstly, when the hydraulic system is added to the model, the number of variables of concern will increase from three to four because of the additional variable, i.e. applied servovalve voltage. Secondly, in the model without the hydraulic system, ideal force is used to represent the car body acceleration and controller input at the same time. However, in the model with the hydraulic system, a hydraulic force is used to represent the car body acceleration, and the applied servovalve voltage is used to represent the controller input.

Four weighting factors must be specified in the cost function. This is a relatively complex problem because mathematically it is a four-dimensional-search problem. The simplification of this problem can be made in two ways. Firstly, set one of the four factors, i.e. the factor of control input in this work, to unity. This can be done without any loss of mathematical representation. Secondly, using the fact that the suspension displacement is similar to the tyre deflection and the maximum available displacements of both variables are physically known, the ratio of both can be specified in the cost function. This simplification will transform the search problem from four to two-dimensions. Nevertheless, it still takes a considerable time to determine the appropriate ranges of the two weighting factors because the initial weighting factors must be randomly chosen and there is no rule to aid this procedure.

- **Dynamic performance and designs of ASPA**

The principal system designs are similar for both the PS and ASPA. For each natural frequency, there exists a damping level at which the car body acceleration level is minimised. This is because the dominant natural frequency and damping ratio in the ASPA are equivalent to the suspension stiffness and damping rate in the PS.

Similar to the concept of PS, the suggested solution of ASPA occurs at the system's lowest natural frequency. In a physical sense, the system's lowest natural frequency is equivalent to incredibly soft passive suspension. The limitation of the system's lowest natural frequency is the control stability. It was found that the ASPA designed using the system's natural frequencies lower than 1.6 Hz was likely to be unstable.

A vast amount of the damping ratio damps down the resonance around the natural frequency of the car body but adversely affects the transmissibility of the frequencies above the car body natural frequency. On the other hand, if the damping ratio is reduced beyond the optimum configuration, the suspension proves to be a deficient damping system. Transmissibility effect is reduced, but the resonance due to the car body natural frequency becomes more pronounced. This results in an increment in the car body acceleration. This phenomenon is similar to that in the PS case. It may be concluded that, even though ASPA provides the better performance in comparison to PS, the conceptual designs of

both are similar. The excellent designs remain a trade-off between the effects of transmissibility and system natural frequency.

Overall trends of the two physical constraints, i.e. suspension displacement and tyre deflection, are similar to those of the PS.

Complex conjugate poles, or an ideal second-order system, dominates PS and ASPA. This fact supports the previous explanation that both systems use the same concepts in their design.

- **Dynamic performances and optimum design of ASLQ**

There is no trade-off between the transmissibility and natural frequency effects for the optimum design of ASLQ. The car body acceleration level is effectively reduced with an increment in its weighting factor. However, the maximum weighting factor is limited by the system stability. This was investigated, and it was found that the system, at the optimum configuration, was dominated by a dominant closed-loop pole close to the imaginary axis. When the weighting factor of the car body acceleration increased, the closed-loop pole was forced towards the imaginary axis. This could be the reason for system instability.

- **Comparison between PS, ASPA and ASLQ systems**

By exciting the models with the defined random road input, simulation results suggest that the optimum active suspension designed by both control methods, ASPA and ASLQ, offer better vibration isolation than the optimum PS because the active system allows the damping rate to be increased with less negative effect on the transmissibility than the passive system.

In comparing the three suspensions, PS, ASPA and ASLQ, for different road input excitation, step, bump and random; the ASLQ provides the most effective solution for vibration isolation, i.e. the lowest level of car body acceleration.

The reason is that the LQ can force the dominant closed-loops to lie on the real axis and move closer to the imaginary axis. Consequently, the system response is dominated by a simple first-order system, assuming that the other poles nearby have a small effect. The damping ratio can be increased to its critical damping rate with the smallest adverse effect on the transmissibility in comparison to PS and ASPA, because the optimum ASLQ has an extremely low

natural frequency. This results in a significant reduction in the magnitude of the response in car body acceleration for the overall frequency range of interest. It was shown that both ASPA and ASLQ could reduce the car body acceleration level to 34.3% of that of PS, with a slim difference between them. Nevertheless, ASLQ is better, regarding the energy consumed 35% lower than for ASPA. There was no difference in the tyre deflections among the three designs.

- **System bump and random input for simulation**

In order to generalise this study, different road input excitation was used, in addition to the step inputs such as: bump and random, to be a system, closed to reality on one hand, and to check the controller robustness and validation on the other hand.

The results for step, bump, and random road input profiles show the active suspension performance was undoubtedly enhanced according to the control effectiveness, since, the body acceleration minimises with the cost of increasing the body suspension travel.

- **Summary**

The results suggest that both controllers use almost identical control inputs but provide different performance for vibration isolation. Both controllers achieved their target to improve the ride comfort by minimising body acceleration and they showed robustness in performance for different kinds of road excitations: step, bump and random. From the viewpoint of controller design, it may be concluded that LQ is theoretically more efficient for the active suspension system than the PA system by lowering added energy.

Conclusion and Future Work

7.1 Introduction

A quarter-car test rig consisting of two sub-systems: (1) an active suspension and (2) a road simulator system, was considered and developed. Efficient use required not only a knowledge of hydraulic and active suspension theory but also instrumentation and signal processing techniques. The instruments were set up and calibrated in such a way that full-state feedback control could be applied to the system. Due to system complexity, it is difficult, in practical terms, to find an accurate $\frac{1}{4}$ -car model. An investigation into establish models for the experimental test rigs of each sub-system. This could extend knowledge to modify the suspension system, not only for a $\frac{1}{4}$ car, but also for a half- and a full-car. The building of these models involved consideration a new term, friction force, in addition to road simulator inputs for passive and active systems. Specifically, the system stability of the fully active suspension mainly relied on the full-state feedback signals.

7.2 Most vital aspects of this study

Firstly, the mathematical modelling of the road input simulator revealed five exciting facts regarding aspects of position control as follows:

- Load pressure due to the system mass always exists for both single-rod and double-rod actuator. This turns out to be a non-linearity offset under position control. However, the application of Laplace transform theory requires zero initial conditions.
- The linearisation technique used for design control in the dynamic analysis outweighs all other considerations, and the offset must, inevitably, be disregarded.
- The presence of cross-port leakage resistance results in an open-loop, third-order system without an integrator for a single-rod actuator. However, for the assumption that leakage resistance is very high, this transforms the transfer into a second-order system with a free integrator.

- The presence of cross-port leakage resistance results in a static position error under closed-loop control in which it cannot be wholly solved by closed-loop gain adjustment alone. Therefore, a power with integral action (PI controller) was considered.
- The hydraulic system was used to generate the different kinds of road profile inputs such as: step, bump and random.

Secondly, the nonlinear mathematical passive suspension system brings a novel contribution to the $\frac{1}{4}$ car model through simulation of the passive experimental tests. Using the conventional $\frac{1}{4}$ car model, a significant difference was discovered between both of the simulation and experimental results. Therefore, it was found that there is a specific term that should be considered within the model, namely, the friction force. Regarding aspects of the PS model, five exciting facts should be highlighted as follows:

- This is the first occasion in which friction force has been implemented with a $\frac{1}{4}$ car model.
- Manipulation of Newton's 2nd law of motion to consider the friction force.
- The design of PS occurs at the lowest suspension stiffness. Inevitably, this is limited by the available suspension working space and the variation in the car body mass.
- For each value of the suspension stiffness, there is a damping level at which car body acceleration is minimised. This mainly results from the effects of transmissibility and natural frequency. Therefore, the design of PS is, in fact, a compromise between both factors.
- Using load cells underneath the tyre to measure the contact patch load.

Thirdly, the nonlinear friction force model relates the test rig construction and the dynamic system analysis. Therefore, the friction model was considered and reflected all the system observations. There are four features regarding the friction model, as indicated, as follows:

- Static friction, or the stiction region: there is a period for the body to depart in the motionless stage.
- Transition friction, or the Strikbeck effect: there is lubricant contact between the body and bearing.
- Coulomb friction: relates the system force inputs and test rig construction.
- Viscous friction: the body has slipped on the lubricated bearing surface.

Fourthly, to provide a baseline for subsequent active suspension development, based on the test rig configuration, the nonlinear hydraulic modelling of AS with the implementation of the friction forces was investigated. The important findings are:

- Transformation of the pressure difference across the actuator into hydraulic force is only valid for a double-rod actuator. If a single-rod type is used, the pressures in both chambers of the actuator must be regarded as state variables rather than a hydraulic force to satisfy the requirements of full-state feedback control theory.
- The presence of cross-port leakage resistance changes the actuator dynamic force equation in two ways. Firstly, the relationship between the applied voltage and the servovalve changes from an integral term to a first-order term. Secondly, the concept of static oil stiffness is not valid since the relationship between the generated force and actuator displacement has a phase advance characteristic that exhibits a derivative behaviour at low frequencies.
- The original Lotus active suspension can be defined as either a servo or a regulator control system, depending upon the variables involved. It was shown that the initial Lotus model and the model including hydraulic components, which is developed in this work, required similar state variables to control the system dynamics.
- A simple, nonlinear friction force model, a damping friction model without considering Coulomb friction, was used. This friction helps to remove body

fluctuations, i.e. it was supporting the controller target to achieve the system response enhancement of minimised body acceleration.

Unknown parameters were experimentally identified, and the mathematical model was validated. The knowledge gained from this work can be summarised as follows:

- The servovalve linearised flow gain may be measured by a steady-state test. However, the assumption used for measurement must be carefully verified, i.e., the supply pressure and load pressure conditions must be well defined and monitored.
- Identifying the effective bulk of the road simulator by considering the line type; for steel pipes a formula was used to calculate the effective bulk modulus as reported by (Watton 2009). Meanwhile, the estimated hose bulk modulus was used for the hose line from a transient test conducted by (Watton and Xue 1994), the values of which are approximately 30% of the bulk modulus of oil.
- Cross-port leakage resistance, actuator viscous damping rate, and tyre viscous damping rate are related to the system damping in which they must be identified based on dynamic measurement only.
- The transfer function relating car body displacement to road input displacement was considered the most appropriate model for the identification of a quarter car model. However, due to the complexity of the transfer function, the model was transformed into two sub-models, i.e., one-DOF and two-DOF models. This approach reduced the model complexity and allowed the parameters to be identified from a series of transfer functions linking vehicle parts to the hydraulic models.
- The dynamic damping due to actuator piston leakage, was found to be substantially more important than that due to viscous actuator damping and Coulomb actuator friction.

- Viscous tyre damping was found to be one of the crucial parameters, which cannot be omitted from the model. This finding went against the assumption used by many publications working on simulation studies in which tyre damping is disregarded.

A hypothetical model, without applying voltage to the servovalve was used for the investigation into the effect of hydraulic parameters on the identified model. The results revealed two dynamic characteristics as follows:

- The presence of actuator piston leakage resulted in significant attenuation of the AS response. A further implication is that fixed gain control schemes may not be appropriate for changes in leakage with wear or replacement/refurbishment of the actuators.
- The low effective bulk modulus of the combination of flexible hose/oil/actuator chamber resulted in an equivalent oil stiffness of a similar order to the tyre stiffness. However, the dynamic contribution appears to only be significant for frequencies beyond 20 Hz, even if a rigid line had been used.

Full-state feedback controls were realised by the LQ optimal method. The main aspects obtained from this investigation can be stated as follows:

- The LQ increases the flexibility of the design process because it allows the designer to individually focus on the system output (car body acceleration), physical constraints (suspension displacement and tyre deflection), and control input (applied voltage to the servovalve) by choosing different weighting parameters.
- Even though the performance of the active suspension designed by the PA is superior to that of the passive suspension, in which the design is a compromise between the natural frequency and transmissibility effects. This was clarified via pole plots on the s-plane of the disturbance transfer functions.

- With a different design concept, the LQ provides a better solution than the PA does, because the method efficiently shifts the dominant natural frequency to a shallow frequency range. This allows the damping rate to be increased to its critical value with the smallest effect on transmissibility. The energy consumed by the LQ controller is significantly lower than for the PA controller.

Fifthly, from the observations of the AS system; although simulation results undoubtedly show the PA and LQ controllers introduced the system response enhancement of minimised body acceleration, the theoretical nonlinear model could predict the dynamic responses of the actual system only within a specific range of weighting factors. However, in the real situation test, the controllers failed. Five aspects should be highlighted for the experimental work as follows:

- Using a physical amplifier to condition the control power to drive the servovalve. Generating the digital control within the PC depending on the measured state variable feedback is quite small.
- Control feedback signals with high noise using 1st or 3rd order filters to cope with this issue.
- Servovalve with offset drawback; this leads to poor experimental results.
- There is no possibility of experimental validation for this work. Therefore, the current simulation parameters are used depending on the parameter's validation of the road simulator passive stage.
- LQ is needed for judgement and experience in the design of a control system. Undoubtedly, LQ provides the analytical capability. However, it does ensure that the result is the best that can be achieved for the given model, cost function and linearised operating condition.

7.3 The main contribution of this study

Finally, the work in this thesis claims to make some original contributions to the areas of passive and electro-hydraulic active suspension systems on the following topics:

- Development of a real quarter car test rig using a full-state feedback control scheme.
- Consideration of a nonlinear hydraulic actuator model for road inputs (system inputs) by covering a dynamic servovalve equation and displaying the inputs (mixed ramp and step inputs after passing through a 1st order filter) with results. Considering the mixed ramp and bump or random inputs for simulation tests. Considering and designing a PI controller for a road simulator.
- Extensive nonlinear mathematical modelling of servovalve and hydraulic actuator applied to active suspension, by considering a real inclined position for both the passive and active suspension sub-system units.
- A new implementation of the frictions force within the equations of motion for passive and active suspension systems for $\frac{1}{4}$ car models by establishing a nonlinear friction model dependant on systematic observations and system dynamic analysis.
- State-space modelling of the active suspension, including hydraulic system and viscous tyre damping.
- Parameter identifications applied to PS.
- Measuring the contact patch load by using load cells beneath the tyre.
- Transformation of the $\frac{1}{4}$ car model to one-DOF and two-DOF models that can significantly simplify modelling problems.
- Influence of the variations of hydraulic parameters to the system responses validation of full state variables.
- Derivation and modification of pole assignment and linear quadratic optimal control applied to drive the nonlinear electrohydraulic active suspension.

- Global studies of PS and AS designed by pole assignment and by linear quadratic optimal control for different kinds of road input excitation.
- Performance comparison for the three suspension systems designs.

7.4 Recommendations for future work

The following can be considered as areas for future work resulting from the above conclusions:-

- The achievement of scheduling control could be further investigated using the knowledge of LQ developed in this work. This would pave the way for actual adaptive active suspension.
- Using the CPL as a feedback control signal regarding the strength link to the stability, leading to driving safely.
- Modifying the test rig by adding a friction transducer sensor to validate the friction model.
- Depending on the knowledge achieved from the new model for the $\frac{1}{4}$ car implementing friction force modifying models for half- and full-car by considering the friction forces.
- Self-adaptive control is another development area. However, this requires a mechanism to classify the road surface condition.
- Various control schemes could be used experimentally with the developed test rig.
- Relating to the system cost, state observation could be used to reduce the number of transducers.
- Using a nonlinear control algorithm to drive the nonlinear modelling could be useful when operating working conditions vary widely. An artificial neural network would be a good condition for the work.

REFERENCES

REFERENCES

Agostinacchio, M. et al. 2014. The vibrations induced by surface irregularities in road pavements—a Matlab® approach. *European Transport Research Review* 6(3), pp. 267-275.

Al-Bender, F. et al. 2004. A novel generic model at asperity level for dry friction force dynamics. *Tribology Letters* 16(1), pp. 81-93.

Al-Zughaibi A. and Davies, H. 2015. Controller Design for Active Suspension System of ¼ Car with Unknown Mass and Time-Delay. *International Journal of Mechanical, Aerospace, Industrial, Mechatronic and Manufacturing Engineering* 9(8).

Al-Zughaibi, A. I. H. 2018. Experimental and analytical investigations of friction at lubricant bearings in passive suspension systems. *Nonlinear Dynamics*.

Alfadhli, A. et al. 2018. The control of an active seat with vehicle suspension preview information. *Journal of Vibration and Control* 24(8), pp. 1412-1426.

Ali Al-Zughaibi et al. 2018. A New Insight into Modelling Passive Suspension Real Test Rig System, Quarter Race Car, with Considering Nonlinear Friction Forces *ImechE, Part D: Journal of Automobile Engineering*.

Alkhatib, R. et al. 2004. Optimal design of passive linear suspension using genetic algorithm. *Journal of Sound and vibration* 275(3), pp. 665-691.

Alleyne, A. and Hedrick, J. K. eds. 1992. *Nonlinear control of a quarter car active suspension*. American Control Conference, 1992. IEEE.

Alleyne, A. and Hedrick, J. K. 1995. Nonlinear adaptive control of active suspensions. *IEEE transactions on control systems technology* 3(1), pp. 94-101.

Altpeter, F. 1999. *Friction modeling, identification and compensation*. École Polytechnique Fédérale de Lausanne.

Arafa, H. and Rizk, M. 1987. Identification and modelling of some electrohydraulic servo-valve non-linearities. *Proceedings of the Institution of Mechanical Engineers, Part C: Journal of Mechanical Engineering Science* 201(2), pp. 137-144.

Armstrong-Helouvry, B. 2012. *Control of machines with friction*. Springer Science & Business Media.

REFERENCES

- Armstrong-Hélouvry, B. et al. 1994. A survey of models, analysis tools and compensation methods for the control of machines with friction. *Automatica* 30(7), pp. 1083-1138.
- Atherton, D. P. 2011. *An introduction to nonlinearity in control systems*. Bookboon.
- Avesh, M. and Srivastava, R. eds. 2012. *Modeling simulation and control of active suspension system in Matlab Simulink environment*. Engineering and Systems (SCES), 2012 Students Conference on. IEEE.
- Baillie, A. S. 1999. *Development of a fuzzy logic controller for an active suspension of an off-road vehicle fitted with terrain preview*. Royal Military College of Canada.
- Ben Mrad, R. et al. 1991. 'A Nonlinear Model of an Automobile Hydraulic Active Suspension System. *ASME Adv. Autom. Technol., DE* 40, pp. 347-359.
- Biglarbegan, M. et al. eds. 2006. *Intelligent control of vehicle semi-active suspension systems for improved ride comfort and road handling*. Fuzzy Information Processing Society, 2006. NAFIPS 2006. Annual meeting of the North American. IEEE.
- Bliman, P.-A. 1992. Mathematical study of the Dahl's friction model. *European journal of mechanics. A. Solids* 11(6), pp. 835-848.
- Bliman, P. and Sorine, M. 1993. Friction modeling by hysteresis operators. Application to Dahl, sticktion and Stribeck effects. *Pitman Research Notes in Mathematics Series*, pp. 10-10.
- Bolton, W. 2003. *Mechatronics: electronic control systems in mechanical and electrical engineering*. Pearson Education.
- Brezas, P. and Smith, M. C. 2014. Linear quadratic optimal and risk-sensitive control for vehicle active suspensions. *IEEE Transactions on Control Systems Technology* 22(2), pp. 543-556.
- Brezas, P. et al. 2015. A clipped-optimal control algorithm for semi-active vehicle suspensions: Theory and experimental evaluation. *Automatica* 53, pp. 188-194.
- Brogan, W. L. 1991. *Modern control theory*. New Jersey: : Prentice Hall.
- Buckner, G. et al. 2015. Intelligent estimation of system parameters for active vehicle suspension control. *CEM Publications*.

REFERENCES

Canal. 2000. Canal used guide, Thoroughbred Digital System Ltd. Cambridge, UK.

Canudas de Wit, C. et al. 1991. Adaptive friction compensation in robot manipulators: Low velocities. *The International journal of robotics research* 10(3), pp. 189-199.

Chikhale, S. and Deshmukh, D. S. 2013. Comparative Analysis Of Vehicle Suspension System in Matlab-SIMULINK and MSc-ADAMS with the help of Quarter Car Model. *International Journal of Innovative Research in Science, Engineering and Technology* 2(8), pp. 4074-4081.

Cho, S.-W. et al. 2005. Smart passive system based on magnetorheological damper. *Smart Materials and Structures* 14(4), p. 707.

Crolla, D. and Nour, A. A. eds. 1988. *Theoretical comparisons of various active suspension systems in terms of performance and power requirements*. Proceedings of IMechE Conference on Advanced Suspensions C.

D2000. 2000. instruction manual. In: Document No. A5/MAN/80950 Issue C, M.I.L. ed. Rankine Road, Daneshill West Industrial Estate, Basingstoke, Hampshire, RG24 8PP, UK.

Dahl, P. R. 1968. *A solid friction model*. DTIC Document.

Darus, R. and Enzai, N. I. eds. 2010. *Modeling and control active suspension system for a quarter car model*. Science and Social Research (CSSR), 2010 International Conference on. IEEE.

Davis, B. and Thompson, A. 1988. Optimal linear active suspensions with integral constraint. *Vehicle System Dynamics* 17(6), pp. 357-366.

De Wit, C. C. et al. 1995. A new model for control of systems with friction. *IEEE Transactions on automatic control* 40(3), pp. 419-425.

Do, A.-L. et al. eds. 2010. *An LPV control approach for semi-active suspension control with actuator constraints*. American Control Conference (ACC), 2010. IEEE.

Dorf, R. C. and Bishop, R. H. 2011. *Modern control systems*. Pearson.

Dowty. sevovalve data sheet. In: Ultra Hydraulic Limited, S.P.D. ed. Arle Court, Cheltenham, Gloucestershire, GL51 OTP, UK.

REFERENCES

- Du, H. et al. 2005. Semi-active H_{∞} control of vehicle suspension with magneto-rheological dampers. *Journal of Sound and Vibration* 283(3-5), pp. 981-996.
- Dupont, P. E. 1994. Avoiding stick-slip through PD control. *IEEE Transactions on Automatic Control* 39(5), pp. 1094-1097.
- ElMadany, M. M. and Abduljabbar, Z. S. 1999. Linear quadratic Gaussian control of a quarter-car suspension. *Vehicle System Dynamics* 32(6), pp. 479-497.
- Engelman, G. and Rizzoni, G. eds. 1993. *Including the force generation process in active suspension control formulation*. American Control Conference, 1993. IEEE.
- Eryilmaz, B. and Wilson, B. H. eds. 2000. *Modeling the internal leakage of hydraulic servovalves*. International Mechanical Engineering Congress and Exposition, ASME.
- Fax, J. A. and Murray, R. M. 2004. Information flow and cooperative control of vehicle formations. *IEEE transactions on automatic control* 49(9), pp. 1465-1476.
- Fei, J. and Xin, M. 2012. Robust adaptive sliding mode controller for semi-active vehicle suspension system. *International Journal of Innovative Computing, Information and Control* 8(1), pp. 691-700.
- Fischer, D. and Isermann, R. 2004. Mechatronic semi-active and active vehicle suspensions. *Control engineering practice* 12(11), pp. 1353-1367.
- FitzSimons, P. M. and Palazzolo, J. J. 1996. Part I: Modeling of a One-Degree-of-Freedom Active Hydraulic Mount. *Journal of Dynamic Systems, Measurement, and Control* 118(3), pp. 439-442.
- Franklin, G. F. and Powell, J. 1981. *Digital Control*. Stanford University.
- Fu, S. et al. 2015. Characteristics and control technology research of three-stage electro-hydraulic servovalve. *J. Appl. Sci. Eng. Innov* 2(2).
- Gao, H. et al. 2006. Multi-objective control of vehicle active suspension systems via load-dependent controllers. *Journal of Sound and Vibration* 290(3), pp. 654-675.
- Ghazaly, N. M. and Moaaz, A. O. 2014. The future development and analysis of vehicle active suspension system. *IOSR Journal of Mechanical and Civil Engineering* 11(5), pp. 19-25.

REFERENCES

Giua, A. et al. eds. 2004. *Design of a control law for a semiactive suspension system using a solenoid valve damper*. Control Applications, 2004. Proceedings of the 2004 IEEE International Conference on. IEEE.

Goodwin, Graham C., Stefan F. Graebe, and Mario E. Salgado. "Control system design." *Upper Saddle River* 13 (2001).

Gordons-tyres. 2018. *Tyre Pressure* [Online]. Scotland: McConechy's Tyre Service Ltd. Available at: <https://www.gordonstyres.co.uk/content/tyre-pressure> [Accessed: 22/0/2018].

Guo, Q. et al. 2015. High-gain observer-based output feedback control of single-rod electro-hydraulic actuator. *IET Control Theory & Applications* 9(16), pp. 2395-2404.

Gysen, B. L. et al. 2009. Design aspects of an active electromagnetic suspension system for automotive applications. *IEEE transactions on industry applications* 45(5), pp. 1589-1597.

Hall, B. and Gill, K. 1987. Performance evaluation of motor vehicle active suspension systems. *Proceedings of the Institution of Mechanical Engineers, Part D: Transport Engineering* 201(2), pp. 135-148.

Hanafi, D. ed. 2010. *PID controller design for semi-active car suspension based on model from intelligent system identification*. 2010 Second International Conference on Computer Engineering and Applications. IEEE.

Hanafi, D. et al. eds. 2009. *Intelligent system identification for an axis of car passive suspension system using real data*. Mechatronics and its Applications, 2009. ISMA'09. 6th International Symposium on. IEEE.

Hardier, G. ed. 1998. *Recurrent RBF networks for suspension system modeling and wear diagnosis of a damper*. Neural Networks Proceedings, 1998. IEEE World Congress on Computational Intelligence. The 1998 IEEE International Joint Conference on. IEEE.

Harnoy, A. et al. 2008. Modeling and measuring friction effects. *IEEE Control Systems* 28(6).

Herman, I. and Sebek, M. eds. 2016. *Optimal distributed control with application to asymmetric vehicle platoons*. Decision and Control (CDC), 2016 IEEE 55th Conference on. IEEE.

REFERENCES

- Hong, K.-S. et al. 1999. *A new model and an optimal pole-placement control of the Macpherson suspension system*. SAE Technical Paper.
- Hrovat, D. 1988. Influence of unsprung weight on vehicle ride quality. *Journal of Sound and Vibration* 124(3), pp. 497-516.
- Hrovat, D. 1990. Optimal active suspension structures for quarter-car vehicle models. *Automatica* 26(5), pp. 845-860.
- Hrovat, D. 1997. Survey of advanced suspension developments and related optimal control applications. *Automatica* 33(10), pp. 1781-1817.
- Isermann, R. 1992. *Identifikation dynamischer systeme Bd. 1 u. 2*. Berlin, Germany: Springer.
- Jamei, M. et al. eds. 2000. *Fuzzy Based Controller of A Nonlinear Quarter Car Suspension System*. Student Seminar in Europe, Manchester, UK.
- Johnson, C. T. and Lorenz, R. D. 1992. Experimental identification of friction and its compensation in precise, position controlled mechanisms. *IEEE Transactions on Industry Applications* 28(6), pp. 1392-1398.
- Kalyoncu, M. and Haydim, M. 2009. Mathematical modelling and fuzzy logic based position control of an electrohydraulic servosystem with internal leakage. *Mechatronics* 19(6), pp. 847-858.
- Karnopp, D. 1983. Active damping in road vehicle suspension systems. *Vehicle System Dynamics* 12(6), pp. 291-311.
- Karnopp, D. et al. 1974. Vibration control using semi-active force generators. *Journal of Engineering for Industry* 96(2), pp. 619-626.
- Karpenko, M. and Sepehri, N. 2005. Fault-tolerant control of a servohydraulic positioning system with crossport leakage. *IEEE Transactions on Control Systems Technology* 13(1), pp. 155-161.
- Katsuhiko, O. 2010. *Modern control engineering*. India: Prentice hal.
- Kermani, M. et al. eds. 2005. *Friction identification in robotic manipulators: case studies*. Control Applications, 2005. CCA 2005. Proceedings of 2005 IEEE Conference on. IEEE.

REFERENCES

Kumar, M. S. 2008. Development of active suspension system for automobiles using PID controller.

KwikFit. 2015. *Tyre Pressure* [Online]. 2015 Kwik-Fit (GB) Limited. Available at: <https://www.kwik-fit.com/tyres/information/tyre-pressure> [Accessed: 15-01-2016].

Leonard, N. E. and Krishnaprasad, P. S. eds. 1992. *Adaptive friction compensation for bi-directional low-velocity position tracking*. Decision and Control, 1992., Proceedings of the 31st IEEE Conference on. IEEE.

Li, Z. et al. 2010. Consensus of multiagent systems and synchronization of complex networks: A unified viewpoint. *IEEE Transactions on Circuits and Systems I: Regular Papers* 57(1), pp. 213-224.

Li, Z. et al. 2013. Distributed consensus of linear multi-agent systems with adaptive dynamic protocols. *Automatica* 49(7), pp. 1986-1995.

Li, Z. et al. 2015. Designing fully distributed consensus protocols for linear multi-agent systems with directed graphs. *IEEE Transactions on Automatic Control* 60(4), pp. 1152-1157.

Lischinsky, P. et al. 1999. Friction compensation for an industrial hydraulic robot. *IEEE Control Systems Magazine* 19(1), pp. 25-32.

Ljung, L. 1995. *System identification toolbox: User's guide*. Citeseer.

Ljung, L. 1999. *System Identification: Theory for the User*, PTR Prentice Hall Information and System Sciences Series. Prentice Hall, New Jersey.

Ljung, L. and Glad, T. 1994. *Modeling of dynamic systems*. PTR Prentice Hall Englewood Cliffs.

Loadcell. 2000. instruction and operation manual. In: Limited, M.I. ed. Rankine Road, Daneshill West Estate, Basingstoke, Hampshire, RG24 8PP, UK.

LVDT. 1994. displacement transducer data sheet. In: Limited, R.E. ed. Grove Street, Heath Town, Wolverhampton, West Midlands, WV10 0PY, UK.

M2000. Moog M2000 PSC user's manual. In: Limited, M.C. ed. Ashchurch, Tewkesbury, GL20 8NA, England, UK.

REFERENCES

- Maneetham, D. and Afzulpurkar, N. 2010. Modeling, simulation and control of high speed nonlinear hydraulic servo system. *Journal of Automation Mobile Robotics and Intelligent Systems* 4, pp. 94-103.
- MathWorks, T. 2000. *Control System Toolbox™ 8 Getting Started Guide*. Natick: The MathWorks, Inc.
- McCloy, D. and Martin, H. R. 1980. Control of fluid power: analysis and design. *Chichester, Sussex, England, Ellis Horwood, Ltd.; New York, Halsted Press, 1980. 505 p.* 1.
- Merritt, H. E. 1967. *Hydraulic control systems*. John Wiley & Sons.
- Microstar, L. 1995. *DAPview for Windows*. Bellevue, WA 98004.
- Microstar, I. 1997. *Developer's Toolkit for DAPL Manual*. Bellevue, WA 98004.
- Microstar, L. 1998. *Application Manual Data Acquisition Processor Analog Accelerator Series*, Bellevue, WA 98004.
- Mokhiamar, O. and Abe, M. 2002. Effects of model response on model following type of combined lateral force and yaw moment control performance for active vehicle handling safety. *JSAE review* 23(4), pp. 473-480.
- Mouleeswaran, S. 2012. *Design and development of PID controller-based active suspension system for automobiles*. INTECH Open Access Publisher.
- Nekoui, M. A. and Hadavi, P. eds. 2010. *Optimal control of an active suspension system*. Power Electronics and Motion Control Conference (EPE/PEMC), 2010 14th International. IEEE.
- Nichols, S. 2007. MANE 6960 Friction & Wear of Materials.
- Nise, N. S. 2010. *CONTROL SYSTEMS ENGINEERING*. John Wiley & Sons.
- Odrigo, A. et al. 2016. Design and development of a road profile generator. *International Journal of Vehicle Systems Modelling and Testing* 11(3), pp. 217-233.
- Ogata, K. 1997. *Modern Control Engineering*. Prentice Hall.

REFERENCES

- Pathare, Y. S. 2014. Design and Development of Quarter Car Suspension Test Rig Model and It's Simulation. *International Journal of Innovative Research and Development*// ISSN 2278–0211 3(2).
- Peng, H. et al. 1997. A Novel Active Suspension Design Technique--Simulation and Experimental. *Ann Arbor* 1001, pp. 48109-42125.
- Preumont, A. 2011. *Vibration control of active structure*. Springer.
- Preumont, A. and Seto, K. 2008. *Active control of structures*. John Wiley & Sons.
- Priyandoko, G. et al. 2009. Vehicle active suspension system using skyhook adaptive neuro active force control. *Mechanical systems and signal processing* 23(3), pp. 855-868.
- Rabinowicz, E. 1965. Friction and wear of materials. *Journal of Applied Mechanics* 33 (1966): 479.
- Rahmat, M. F. a. et al. 2010. Modeling and controller design of an electro-hydraulic actuator system. *American Journal of Applied Sciences* 7(8), pp. 1100-1108.
- Rajamani, R. and Hedrick, J. K. 1995. Adaptive observers for active automotive suspensions: theory and experiment. *IEEE Transactions on control systems technology* 3(1), pp. 86-93.
- Ramli, H. et al. 2012. A Fuzzy-Active Force Control Architecture Based in Characterizing Nonlinear Systems' Behavior. *Procedia Engineering* 41, pp. 1389-1397.
- Rashid, M. M. et al. 2011. Analysis and experimental study of magnetorheological-based damper for semiactive suspension system using fuzzy hybrids. *IEEE Transactions on Industry Applications* 47(2), pp. 1051-1059.
- Ruina, A. and Rice, J. 1983. Stability of steady frictional slipping. *Journal of applied mechanics* 50, pp. 343-349.
- Safonov, M. and Athans, M. 1977. Gain and phase margin for multiloop LQG regulators. *IEEE Transactions on Automatic Control* 22(2), pp. 173-179.
- Sam, Y. M. and Hudha, K. eds. 2006. *Modelling and force tracking control of hydraulic actuator for an active suspension system*. Industrial Electronics and Applications, 2006 1ST IEEE Conference on. IEEE.

REFERENCES

- Segla, S. and Reich, S. eds. 2007. *Optimization and comparison of passive, active, and semi-active vehicle suspension systems*. 12th IFTOMM world congress, France.
- Sharma, K. et al. eds. 1992. *Derivation of a control law for a 3 state switchable damper suspension system for improving road vehicle ride characteristics*. Proceedings of the International Symposium on Theory of Machines and Mechanisms.
- Sharp, R. and Crolla, D. 1987. Road vehicle suspension system design-a review. *Vehicle system dynamics* 16(3), pp. 167-192.
- Sharp, R. and Hassan, S. 1986. The relative performance capabilities of passive, active and semi-active car suspension systems. *Proceedings of the Institution of Mechanical Engineers, Part D: Transport Engineering* 200(3), pp. 219-228.
- Shieh, M.-Y. and Li, T.-H. S. 1998. Design and implementation of integrated fuzzy logic controller for a servomotor system. *Mechatronics* 8(3), pp. 217-240.
- Smyth, A. W. et al. 2002. Development of adaptive modeling techniques for non-linear hysteretic systems. *International journal of non-linear mechanics* 37(8), pp. 1435-1451.
- Sohn, H.-C. et al. 2004. An adaptive LQG control for semi-active suspension systems. *International Journal of Vehicle Design* 34(4), pp. 309-326.
- Speedy, C. B. et al. 1970. *Control theory: identification and optimal control*. Oliver and Boyd.
- Standardization, I. O. f. 1995. *Mechanical Vibration--Road Surface Profiles--Reporting of Measured Data*. ISO 8608:1995, ISO/TC108/SC2, Geneva: International Organization for Standardization.
- Stein, G. and Athans, M. 1987. The LQG/LTR procedure for multivariable feedback control design. *IEEE Transactions on Automatic Control* 32(2), pp. 105-114.
- Streiter, R. H. 1996. *Entwicklung und Realisierung eines analytischen Regelkonzeptes für eine aktive Federung*. na.
- Surawattanawan, P. 2000. *The influence of hydraulic system dynamics on the behaviour of a vehicle active suspension*. Thesis, Cardiff University.

REFERENCES

- Tan, H.-S. and Bradshaw, T. eds. 1997. *Model identification of an automotive hydraulic active suspension system*. American Control Conference, 1997. Proceedings of the 1997. IEEE.
- Technical. 1994. manual of transducer amplifier type E309. In: Limited, R.E. ed. Grove Street, Heath Town, Wolverhampton, West Midlands, WV10 0PY, UK.
- Thompson, A. 1976. An active suspension with optimal linear state feedback. *Vehicle System Dynamics* 5(4), pp. 187-203.
- Thompson, A. and Chaplin, P. 1996. Force Control in Electrohydraulic Active Suspensions. *Vehicle System Dynamics* 25(3), pp. 185-202.
- Thompson, A. and Davis, B. 1991. A technical note on the lotus suspension patents. *Vehicle System Dynamics* 20(6), pp. 381-383.
- Ting, C.-S. et al. 1995. Design of fuzzy controller for active suspension system. *Mechatronics* 5(4), pp. 365-383.
- Tsurata, K. et al. eds. 2000. *Genetic algorithm (GA) based modeling of nonlinear behavior of friction of a rolling ball guide way*. Advanced Motion Control, 2000. Proceedings. 6th International Workshop on. IEEE.
- Türkay, S. and Akçay, H. 2008. Aspects of achievable performance for quarter-car active suspensions. *Journal of Sound and Vibration* 311(1), pp. 440-460.
- Tyan, F. et al. 2009. Generation of random road profiles. *Journal of Advanced Engineering* 4(2), pp. 1373-1378.
- Venhovens, P. J. T. 1995. Optimal control of vehicle suspensions. (1995): 0956-0956.
- Walrath, C. D. 1984. Adaptive bearing friction compensation based on recent knowledge of dynamic friction. *Automatica* 20(6), pp. 717-727.
- Wang, Y. and Winner, H. eds. 2015. *Research of dynamic measurement characteristics of wheel force sensor*. International Tyre Colloquium, 4th, 2015, Guildford, United Kingdom.
- Wang, Z. et al. eds. 2009. *Research on controller design and simulation of electro-hydraulic servo system*. Mechatronics and Automation, 2009. ICMA 2009. International Conference on. IEEE.

REFERENCES

Warminski, J. et al. 2012. *Nonlinear Dynamics Phenomena in Mechanics (Solid Mechanics and Its Applications)*, Vol. 181. Springer-Verlag, Berlin.

Watton, J. 1989. *Fluid power systems: modeling, simulation, analogue and microcomputer control*. Prentice-Hall, Inc.

Watton, J. 2005. *Modelling, monitoring and diagnostic techniques for fluid power systems*. Springer Science & Business Media.

Watton, J. 2007. *Modelling, monitoring and diagnostic techniques for fluid power systems*. Springer Science & Business Media.

Watton, J. 2009. *Fundamentals of fluid power control*. Cambridge University Press.

Westwick, D. T. et al. eds. 1999. *Nonlinear identification of automobile vibration dynamics*. Proc. of the 7th Mediterranean Conference on Control and Automation, Israel.

Williams, D. A. and Wright, P. G. 1984. European Patent Application 84300370.8.

Williams, D. A. and Wright, P. G. 1986. USA Patent 4625993.

Wilson, D. et al. 1986. The application of linear optimal control theory to the design of active automotive suspensions. *Vehicle System Dynamics* 15(2), pp. 105-118.

Wong, J. Y. 2001. *Theory of ground vehicles*. John Wiley & Sons.

Wright, P. 1984. The application of active suspension to high performance road vehicles. *I Mech E Paper C239* 123.

Wright, P. and Williams, D. 1989. *The case for an irreversible active suspension system*. SAE Technical Paper.

Xu, Y. and Ahmadian, M. 2013. Improving the capacity of tire normal force via variable stiffness and damping suspension system. *Journal of Terramechanics* 50(2), pp. 121-132.

Yagiz, N. et al. 2008. Different control applications on a vehicle using fuzzy logic control. *Sadhana* 33(1), pp. 15-25.

REFERENCES

Yang, M. et al. eds. 2016. *PID control for a height adjustable wheel-direct-drive system via time-varying samplings*. Control Conference (CCC), 2016 35th Chinese. IEEE.

Yim, S. et al. 2010. Design of active suspension and electronic stability program for rollover prevention. *International journal of automotive technology* 11(2), pp. 147-153.

Yoshimura, T. et al. 2001. Construction of an active suspension system of a quarter car model using the concept of sliding mode control. *Journal of Sound and Vibration* 239(2), pp. 187-199.

Yukio, H. 2005. Hydrodynamic lubrication. Springer.

Zhang, H. et al. 2011. Optimal design for synchronization of cooperative systems: state feedback, observer and output feedback. *IEEE Transactions on Automatic Control* 56(8), pp. 1948-1952.

Zulfatman, R. and Rahmat, M. eds. 2009. *Modeling and controller design of electro-hydraulic actuator*. Proceeding of the 2nd International Conference on Control, Instrumentation and Mechatronic Engineering.

APPENDIX

APPENDIX A1

- **Design PI controller to drive road actuator**

The reason PI controllers are so popular is that using PI gives the designer a more significant number of options and those options mean that there are more possibilities for changing the dynamics of the system in a way that helps the designer. In particular, starting with a proportional controller, and adding integral terms to the control, the designer can take advantage of the effects; an integral controller gives zero steady-state error for a step input.

The PI controller transfer function adds a pole at the origin and a zero that can be anywhere on the s-plane that the designer wants, depending upon the designer's choice of the two gains. The PI form in s-domain is:

$$PI(s) = [sK_p + K_I]/s \quad (A1.1)$$

Where K_p , K_I are the proportional and integral gains respectively.

- **Characteristic equation of servovalve with scope of linearisation**

Considering a characteristic of servovalve, steady-state perfect flow equations will serve to demonstrate the inherent nonlinear characteristic of this crucial hydraulic component used for precision control applications. Traditionally, power systems are designed and operated conservatively in a region where behaviour is mainly linear. In the case of small disturbances, linearised models of the power system around an equilibrium point are adequate for stability analysis and control design.

The linearisation technique presented here is valid in the vicinity of the operating condition. Therefore, in order to obtain a linear mathematical model, the strategy is connected to servovalve controlled systems whereby the nonlinear flow features are linearised and then joined with the other system dynamic terms (Watton 2007). Such an approach can give appreciable vision into the way parameters affect system performance. Assuming that the applied voltage (spool movement) and the pressure drops deviate only slightly from the operating condition; consequently, the flow rates in this vicinity region have a linear relation to the voltages, as mentioned. Now, how to represent this fact? By using only the

APPENDIX A1

first linear term of Taylor series expansion for a nonlinear function; accordingly, slight variations in each parameter lead to:

$$\delta Q_{1r} = K_{sr1} \delta x_{sr} - k_{p1} \delta P_{1r} \quad (A1.2)$$

$$\delta Q_{2r} = K_{sr2} \delta x_{sr} - k_{p2} \delta P_{2r} \quad (A1.3)$$

Where,

$$K_{sr1} = \left. \frac{\delta Q_{1r}}{\delta x_{sr}} \right|_{P_{1rSS}} = k_{fr} \sqrt{P_{sr} - P_{1rSS}} = \frac{Q_{1rSS}}{x_{srSS}} \quad \text{Flow gain}$$

$$k_{Pr1} = - \left. \frac{\delta Q_{1r}}{\delta P_{1r}} \right|_{x_{srSS}, P_{1rSS}} = \frac{k_{fr} x_{srSS}}{2\sqrt{P_{sr} - P_{1rSS}}} = \frac{Q_{1rSS}}{2(P_{sr} - P_{1rSS})} \quad \text{Pressure coefficient}$$

$$K_{sr2} = \left. \frac{\delta Q_{2r}}{\delta x_{sr}} \right|_{P_{2rSS}} = k_{fr} \sqrt{P_{2rSS}} = \frac{Q_{2rSS}}{x_{srSS}} \quad \text{Flow gain}$$

$$k_{Pr2} = \left. \frac{\delta Q_{2r}}{\delta P_{2r}} \right|_{x_{srSS}, P_{2rSS}} = \frac{k_{fr} x_{srSS}}{2\sqrt{P_{2rSS}}} = \frac{Q_{2rSS}}{2P_{2rSS}} \quad \text{Pressure coefficient}$$

x_{srSS} , is steady state servovalve spool movement relative to applied voltage and P_{1rSS} , P_{2rSS} are the steady-state pressures. It can be seen that at the null condition, $u_{rSS} = 0$ ($x_{srSS} = 0$), and $P_{sr}/2 = P_{1rSS} = P_{2rSS}$, for a critically lapped spool, therefore it follows that:

$$\text{Flow gain} \quad K_{sr1} = K_{sr2} = K_{sr} \quad (A1.4)$$

$$\text{Pressure coefficient} \quad k_{Pr1} = k_{Pr2} = k_{Pr} = 0 \quad (A1.5)$$

Hence, the characteristic linear servovalve equations are:

$$Q_{1r} = Q_{2r} = k_{sr} x_{sr} \quad (A1.6)$$

Where

$$k_{sr} = k_{fr} \sqrt{P_{sr} - P_{1rSS}} = k_{fr} \sqrt{P_{2rSS}} = k_{fr} \sqrt{P_{sr}/2} \quad (A1.7)$$

It is essential to remember that the linearisation technique presented here is valid in the vicinity of the operating condition and will only be considered to help in designing a linear control. Because the operating conditions vary widely, such linearisation equations are not adequate. Therefore, the nonlinear equations should be considered with the rest of the current study.

From **Chapter 3**,

APPENDIX A1

$$\frac{V_{1r}}{\beta_{er}} \dot{P}_{1r} = Q_{1r} - A_{1r} \dot{X}_r - \frac{(P_{1r} - P_{2r})}{R_{ir}} \quad (A1.8)$$

$$\frac{V_{2r}}{\beta_{er}} \dot{P}_{2r} = A_{2r} \dot{X}_r + \frac{(P_{1r} - P_{2r})}{R_{ir}} - Q_{2r} \quad (A1.9)$$

$$F_{hydr} = (P_{1r} A_{1r} - P_{2r} A_{2r}) \quad (A1.10)$$

$$\ddot{X}_r M_r = (P_{1r} A_{1r} - P_{2r} A_{2r}) - B_{vr} \dot{X}_r - k_t (X_r - X_w) - b_t (\dot{X}_r - \dot{X}_w) \quad (A1.11)$$

Since the actuator is a signal-rod type, and in this study for proposed control design, it is assumed that $V_{1r} = V_{2r} = V$ and $A_{1r} = A_{2r} = A_c$ then Equations, (A1.7, A1.8 and A1.9) become as follows:

$$\frac{V}{\beta_{er}} \dot{P}_{1r} = Q_{1r} - A_c \dot{X}_r - \frac{(P_{1r} - P_{2r})}{R_{ir}} \quad (A1.12)$$

$$\frac{V}{\beta_{er}} \dot{P}_{2r} = A_c \dot{X}_r + \frac{(P_{1r} - P_{2r})}{R_{ir}} - Q_{2r} \quad (A1.13)$$

$$F_{hydr} = A_c (P_{1r} - P_{2r}) \quad (A1.14)$$

From Equations (A1.11), (A1.12) and (A1.13) may be written as:

$$2k_{sr} x_{sr} A_c = 2A_c^2 \dot{X}_r + \frac{V}{\beta_{er}} \dot{F}_{hydr} + \frac{2}{R_{ir}} F_{hydr} \quad (A1.15)$$

For the model proposed for controller design, the disturbance \dot{X}_w is assumed to be zero, the system (A1.10) becomes:

$$\ddot{X}_r M_r = F_{hydr} - (B_{vr} + b_t) \dot{X}_r - k_t X_r \quad (A1.16)$$

Taking Laplace transforms and neglecting initial conditions that allow the force transfer function to be written:

$$F_{hydr} = \frac{k_{sr} A_c}{\left(\frac{1}{R_{ir}} + \frac{V_s}{2\beta_{er}}\right)} X_{sr} - \frac{A_c^2 s}{\left(\frac{1}{R_{ir}} + \frac{V_s}{2\beta_{er}}\right)} X_r \quad (A1.17)$$

In addition, the open-loop transfer function relates X_r to x_{sr} , which may be written as:

$$\frac{X_r}{x_{sa}} = \frac{2k_{sr} A_c}{\frac{2k_t}{R_{ir}} + \left(2A_c^2 + \frac{2(B_{vr} + b_t)}{R_{ir}} + \frac{k_t V}{\beta_{er}}\right) s + \left(\frac{2M_r}{R_{ir}} + \frac{(B_{vr} + b_t)V}{\beta_{er}}\right) s^2 + \frac{M_r V}{\beta_{er}} s^3} \quad (A1.18)$$

Using the knowledge of state-space theory, at least three state variables are required to control three closed-loop poles for the third-order system.

APPENDIX A1

Considering systems (A.16) and (A1.17), the most appropriate state variables are F_{hydr} , \dot{X}_r and X_r . These are investigated in this section.

The main equations from the previous section are summarised as follows:

$$\ddot{X}_r M_r = F_{hydr} - B_{vr} \dot{X}_r - k_t (X_r - X_w) - b_t (\dot{X}_r - \dot{X}_w) \quad (A1.19)$$

$$2k_{sr} x_{sr} A_c = 2A_c^2 \dot{X}_r + \frac{V}{\beta_{er}} \dot{F}_{hydr} + \frac{2}{R_{ir}} F_{hydr} \quad (A1.20)$$

The control and the relation with servovalve spool movement, the equation is:

$$\dot{x}_{sr} = \frac{1}{\tau_a} (u_r(t) - x_{sr}(t)) \quad (A1.21)$$

$$x_{sr} = f(u_r) \quad (A1.22)$$

$$u_r(t) = K_{br} * er(t) \quad (A1.23)$$

$$er(t) = ref(t) - X_r(t) \quad (A1.24)$$

Therefore, the control signal is:

$$er(t) = -K_o X_r(t) \quad (A1.25)$$

$$u_a(t) = PI(t) \quad (A1.26)$$

The design of controller in time domain is given by,

$$PI(t) = K_p * ea(t) + K_i \int_0^t ea(t) dt \quad (A1.27)$$

Where, K_o is feedback gain, K_p is proportional gain, K_i is integral gain, er is the error between the reference and the output system,

Therefore, Equation (A1.20) became,

$$2k_{sr} A_c u_r = 2A_c^2 \dot{X}_r + \frac{V}{\beta_{er}} \dot{F}_{hydr} + \frac{2}{R_{ir}} F_{hydr} \quad (A1.28)$$

er = Control signal

From the equations (A1.19) and (A1.28), it may be deduced that the most suitable state variables are:

1. Tyre velocity, \dot{X}_r
2. Hydraulic force, F_{hydr}

APPENDIX A1

3. Tyre deflection, $X_w - X_r$

By using the following state-space notations:

$$x_1 = \dot{X}_r$$

$$x_2 = F_{\text{hydr}}$$

$$x_3 = X_w - X_r$$

The system equations may be rearranged to first-order differential equations with differential terms isolated on the left-hand-side.

$$\ddot{X}_r = -\frac{B_{vr}+b_t}{M_r}\dot{X}_r + \frac{F_{\text{hydr}}}{M_r} - \frac{k_t}{M_r}(X_r - X_w) + \frac{b_t}{M_r}\dot{X}_w \quad (\text{A1.29})$$

$$\dot{F}_{\text{hydr}} = -\frac{2A_c^2\beta_{er}}{V}\dot{X}_r - \frac{2\beta_{er}}{VR_{ir}}F_{\text{hydr}} + \frac{2k_{sr}A_c\beta_{er}}{VR_{ir}}e_r \quad (\text{A1.30})$$

$$\dot{X}_w - \dot{X}_r = \dot{X}_w - \dot{X}_r \quad (\text{A1.31})$$

These equations may be written in the state-space form given by:

$$\dot{x} = Ax + Bea \quad (\text{A1.32})$$

Where,

$$x = \text{State vector} = \begin{bmatrix} \dot{X}_r \\ F_{\text{hydr}} \\ X_w - X_r \end{bmatrix}$$

$$A = \text{System matrix} = \begin{bmatrix} -\frac{(B_{vr} + b_t)}{M_r} & \frac{1}{M_r} & -\frac{k_t}{M_r} \\ -\frac{2\beta_{er}A_c^2}{V} & -\frac{2\beta_{er}}{VR_{ir}} & 0 \\ -1 & 0 & 0 \end{bmatrix}$$

$$B = \text{Input vector} = \begin{bmatrix} 0 \\ \frac{2k_{sr}A_c\beta_{er}}{V} \\ 0 \end{bmatrix}$$

E_r , is the control signal

When a full-state feedback control law is introduced, the control signal e_r becomes a function of all three state variables and feedback gains:

$$\begin{aligned} e_a &= -Kx \\ &= -NK_1K_2x \end{aligned}$$

where,

$K = 1 \times 3$ is the state feedback gain vector.

$N = A/D$ is the converted gain.

$K_1 = 1 \times 3$ is the state feedback gain vector for the controller.

$$K_1 = [I_1 \quad H_1 \quad L_1]$$

$K_2 = 3 \times 3$ is the transducer gain matrix.

$$K_2 = \begin{bmatrix} I_2 & 0 & 0 \\ 0 & H_2 & 0 \\ 0 & 0 & L_2 \end{bmatrix} \tag{A1.33}$$

By using PA method, the PI design step can be declared as follows:

1. Choosing the feedback control signal

As mentioned in our case, the road displacement measurement was chosen as control feedback signal.

2. Find the pole zero system position

APPENDIX A1

Related to A, B, C matrixes and by using the MATLAB DROBOX as shown in the attachment m.file, there is one pole at original and zero on the left side with zero imagery value, as shown in Fig A1.1.

3. Choosing ξ and ω_n

If choosing $\xi = 1.0$ and $\omega_n = 8$, giving a good trade-off between rise time and overshoot, as shown in Fig. A1.3, the location of the zero and pole for PI suggested closed-loop poles in Pole-Zero map is as shown in Fig. A1.2. The PI controller has zero and pole at original, as mentioned.

Therefore, the zeros are:

- $Z_{1,2} = -8 \mp 0.0j$ (A1.34)

- In addition, the pole is:

- $P_1 = 0.0$ (A1.35)

- Therefore, to find the PI gains value is as follows:

- $(s + 8 + 0.0j) = sK_p + K_I$ (A1.36)

- $K_p = 1$ And $K_I = 8$ (A1.37)

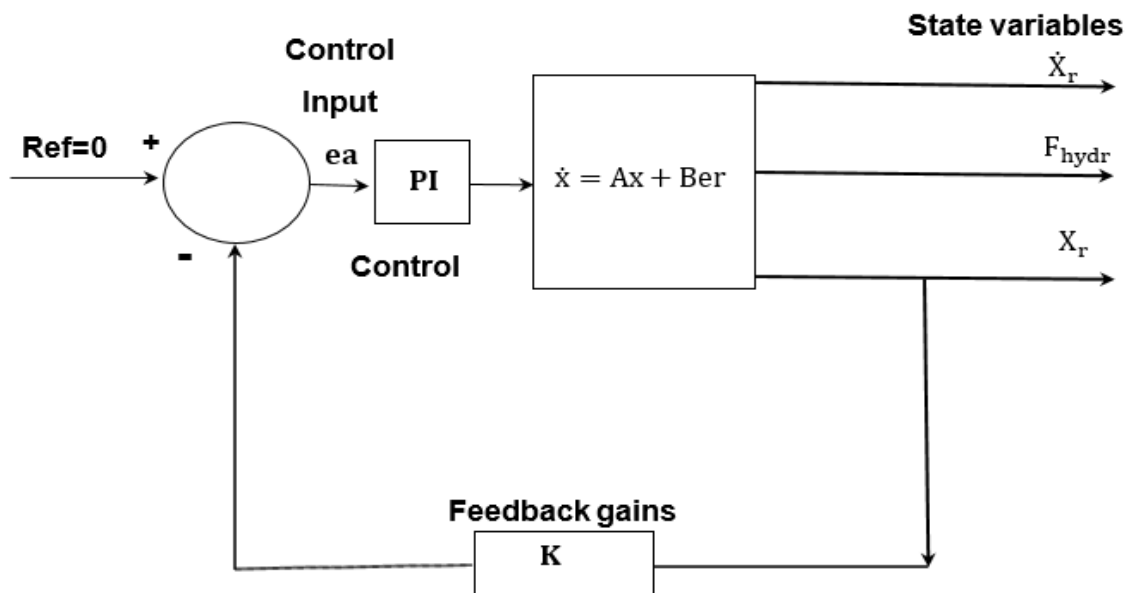


Fig. A1.1. Block diagram of the road measured feedback control.

APPENDIX A1

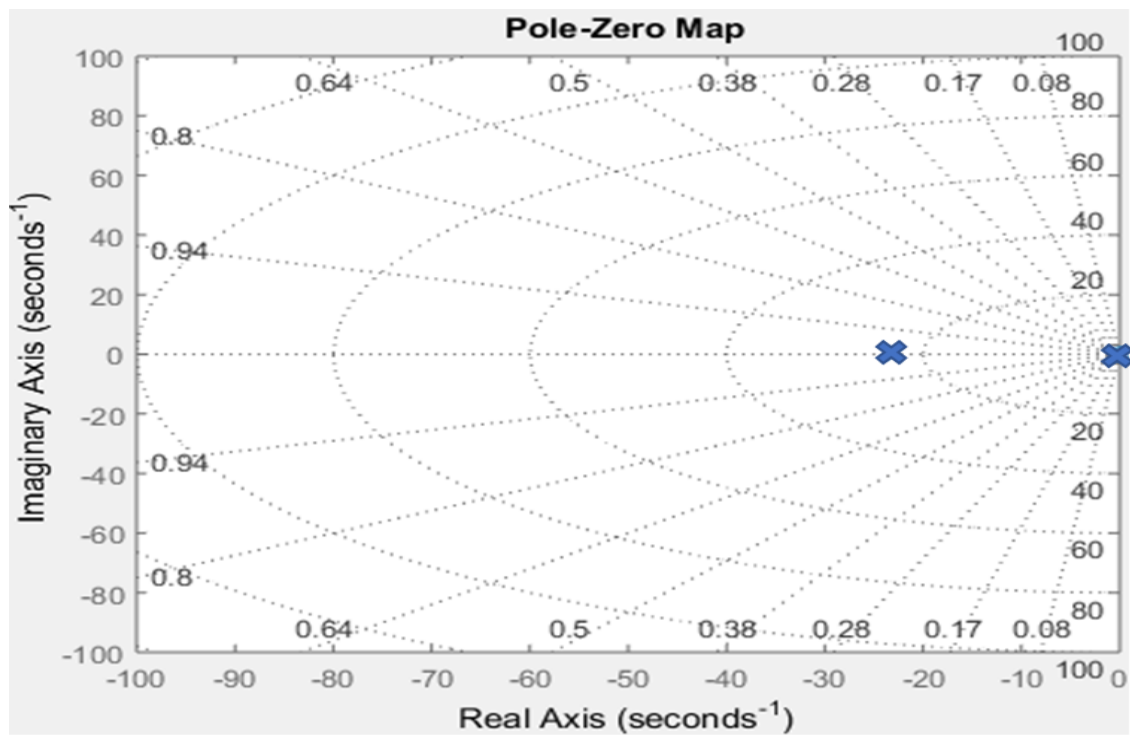


Fig. A1.2. Pole-zero map of the closed system when used X_r as feedback.

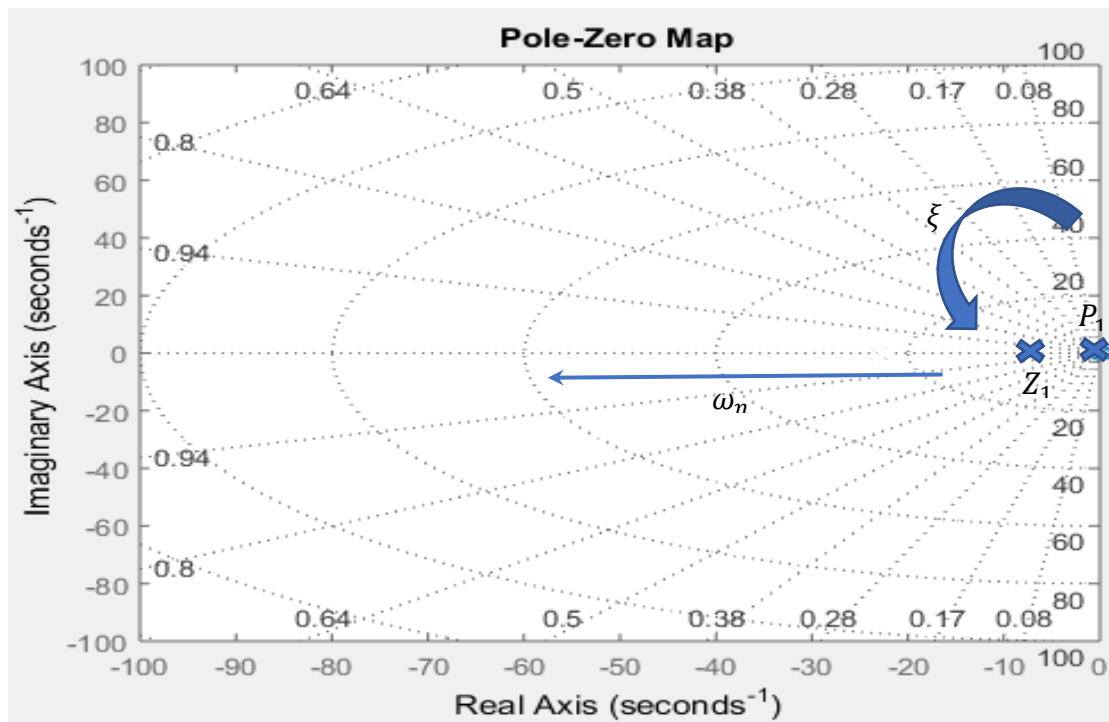


Fig. A1.3 Location of the two suggested closed-loop poles for PI controller in pole-zero map.

APPENDIX A2

- **M.file for plot zero and pole of system and PI controller**

```
%solve PI road input
m1 =5; m2; g=9.81;
kt = 2.8*10^5;
bv = 300;
bt = 3886;
Ac=2.46*10^-4;
V=7.13e-5;
Ri=2.45*10^11;
ki=2.3e-11; %%kfa
Nr=3276;
be=0.22*10^9;
% closed-loop input road
I2=0.2;H2=0.000002;L2=0.000027;
K2=diag([I2,H2,L2]);
% RICCATI Solves an algebraic Riccati equation;
A=[-(bv+bt)/m1 1/m1 -kt/m1; -2*be*Ac^2/V -2*be/Ri*V 0;-1 0 0];
B=[0;(2*ki*Ac*be)/V;0];
C=[1 0 0 ;0 0 0;0 0 0];
D=[0;0;0];
% a0=0.0;a1=10817345.3;a2=351225.5;a3=20608.27;a4=133.38;a5=1.0;
% J=[-1.27+1.27j -1.27-1.27j -12.7 -12.7 -12.7];
Mc=ctrb(A,B);
% elfa0=3.97e7;elfa1=7.76e6;elfa2=6.83e5;elfa3=2.01e4;elfa4=2.38e2;elfa5=1.0;
% Wc=[a1 a2 a3 a4 1;a2 a3 a4 1 0;a3 a4 1 0 0;a4 1 0 0 0;1 0 0 0 0];
% T=Mc*Wc;
Pl=poly(A);
% T1=inv(T);
K=[1 8 0];
%% K1=(N^1)*K*K2^1;
%% find transfer function from stat space
sys=ss(A-B*K,B,C,D);
% H2=tf(sys);
% P=pole(sys);
% pzmap(H2);
% v=[-200 0 -200 200];axis(v)
% grid on
% hold on
%% open loop pole
% sys=ss(A,B,C,D);
H=tf(sys);
P=pole(sys);
Pe=eig(A);
pzmap(H);
v=[-100 0 -100 100];axis(v)
grid on
hold on
```

APPENDIX B1

- **DAP real-time road input controller programs**

```
////////////////////////////////////
// Road-tyre test 13.10.2015
// Active control, Servosuspensor
// Smooth start-bring the actuator to mid_stroke at biginning
////////////////////////////////////

#include "dtd.h"
#include "dtdmod.h"
#include "math32.h"
#define pi      3.141592

//Definition of module name and entry point.
#define COMMAND "CONTROL"
#define ENTRY CONTROL_entry

double  amp1,off1,w1,uc, j1,t, xrd, xr, xr0, error, e1=0.0, Kpa, Kp, t0, t1, Tn, r1, lr1, Tao, Ts, Vb,
Vb1,ua;
int Sn, Sp, sd, ms;

//Implement module identification sequence
int __stdcall          ENTRY (PIB **plib);
extern "C" __declspec(dllexport) int __stdcall
ModuleInstall(void *hModule)
{return (CommandInstall(hModule,COMMAND,ENTRY,NULL));}
int __stdcall          ENTRY (PIB **plib)

{
// Storage for parameters:
void **argv;
int argc;
short int dac0;
short int dac1;
PIPE * in_pipe_amp1;
PIPE * in_pipe_w1;
PIPE * in_pipe_off1;
PIPE * in_pipe_kp;
PIPE * in_pipe_kpa;
PIPE * in_pipe_xr;
PIPE * in_pipe_Tn;
PIPE * in_pipe_Sn;
PIPE * in_pipe_Tao;
PIPE * in_pipe_Ts;
PIPE * in_pipe_sd;
PIPE * in_pipe_Vb;
PIPE * out_pipe_xrd;

//GENERIC_SCALAR pipe_value;

//Access parameters
argv = param_process(plib, &argc,15,15,
```

APPENDIX B1

```
T_PIPE_W, T_PIPE_W,  
T_PIPE_W,T_PIPE_W,T_PIPE_W,T_PIPE_W,T_PIPE_W,T_PIPE_W,T_PIPE_W,T_PIPE_W,T_PIPE  
_W,T_PIPE_W,T_PIPE_W,T_CONST_W,T_CONST_W);  
in_pipe_amp1          = (PIPE *) argv[1];  
in_pipe_w1            = (PIPE *) argv[2];  
in_pipe_off1          = (PIPE *) argv[3];  
in_pipe_kp            = (PIPE *) argv[4];  
in_pipe_kpa           = (PIPE *) argv[5];  
in_pipe_xr            = (PIPE *) argv[6];  
in_pipe_Tn            = (PIPE *) argv[7];  
in_pipe_Sn            = (PIPE *) argv[8];  
in_pipe_Tao           = (PIPE *) argv[9];  
in_pipe_Ts            = (PIPE *) argv[10];  
in_pipe_sd            = (PIPE *) argv[11];  
in_pipe_Vb            = (PIPE *) argv[12];  
out_pipe_xrd          = (PIPE *) argv[13];  
dac0                  = *(short int *) argv[14];  
dac1                  = *(short int *) argv[15];  
  
// Perform initialisations  
pipe_open(in_pipe_amp1,P_READ);  
pipe_open(in_pipe_w1, P_READ);  
pipe_open(in_pipe_off1,P_READ);  
pipe_open(in_pipe_kp, P_READ);  
pipe_open(in_pipe_kpa, P_READ);  
pipe_open(in_pipe_xr, P_READ);  
pipe_open(in_pipe_Tn, P_READ);  
pipe_open(in_pipe_Sn, P_READ);  
pipe_open(in_pipe_Tao, P_READ);  
pipe_open(in_pipe_Ts, P_READ);  
pipe_open(in_pipe_sd, P_READ);  
pipe_open(in_pipe_Vb, P_READ);  
pipe_open(out_pipe_xrd,P_WRITE);  
  
// Begin continuous processing  
amp1 = double(pipe_get(in_pipe_amp1));  
w1  = double(pipe_get(in_pipe_w1));  
off1 = double(pipe_get(in_pipe_off1));  
Kp  = double(pipe_get(in_pipe_kp))/1000;  
Kpa = double(pipe_get(in_pipe_kpa))/1000;  
Tn  = double(pipe_get(in_pipe_Tn))/1000;  
Sn  = pipe_get(in_pipe_Sn)/1000;  
Tao = double(pipe_get(in_pipe_Tao))/1000;  
Ts  = double(pipe_get(in_pipe_Ts))/100000;  
Sd  = pipe_get(in_pipe_sd);  
Vb1 = double(pipe_get(in_pipe_Vb));  
  
t0=sys_get_time();  
xr0 = pipe_get(in_pipe_xr);  
j1  = (off1- xr0)/(Tn*0.5);  
uc=0;  
ms=1;
```

APPENDIX B1

```
//Bring the actuator to offset, 'off1' in time Tn
while(1)
{
    //road control
    t=(sys_get_time()-t0)/1000;
    if(t<Tn) {
        if(t<=Tn*0.5)
            xrd = j1*t+xr0;
        else xrd = off1;
    }
    else {
        j1 = (w1/1000)*pi*2*(t-Tn);
        xrd = amp1*sin(j1); //xrd = amp1*sin(j1)+off1;
        if(Sn==1)
            xrd = xrd + off1;
        else if(xrd>=0)
            xrd=amp1 + off1;
        else
            xrd=off1-amp1;
    }

    if(ms==1) {
        lr1=xrd;
        ms=2;
    }
    //road profile
    r1=((Tao/Ts)*lr1+xrd)/(1+Tao/Ts);
    lr1=r1;

    xr = pipe_get(in_pipe_xr);
    if (sd==1000)
        error = r1-xr;
    else
        error = xrd-xr;
    uc=(Kp)*error;

    Vb = pipe_get(in_pipe_Vb);
    ua = Kpa*(Vb-Vb1);
    Vb1=Vb;

//output limits
    if(uc>32767*0.9) uc=32768*0.9;
    if(ua>32767*0.9) ua=32768*0.9;
    if(uc<-32767*0.9) uc=-32767*0.9;
    if(ua<-32767*0.9) ua=-32767*0.9;

    pipe_put(out_pipe_xrd,int(xrd));
//Send control out
    dac_out (dac0,int(uc));
    dac_out (dac1,int(ua));
}
return 0;
}
```

APPENDIX B1

- **Real time DAPview program to converter D/A or A/D from PC through data acquisition and vice versa for passive suspension system.**

RESET

PIPES amp1,w1,off1, Kp, ti, xrdc, u, ua, kpa, xr, xbw;

PIPES xb, xw, Vb,Vw, Pt, Pb, Qt, Qb, Fa;

PIPES Ts, Sn, Tn, Tao, sd;

Xr Full stroke 170mm;

Xr mid-stroke 6917; fully retracted -7271; Fully extended 21105;

Xr LVDT calibration: 167 m-code/mm;

Xw bottom 16412, top 20164, 22.075 m-code/mm;

Xb bottom 15246, top 19030, 22.254 m-code/mm;

Xbw extended 1.448V, 4824 dap; retracted 0.0V, 0 dap;

Fill Kp 3276 ;1v-3276

fill Kpa 3276 ;1v-3276

fill amp1 3000 ;8350-50mm amplitude. 5010=30mm, 10020-70mm; max 14188 for 8.5cm from mid stroke

fill w1 32 ; 1000 = 1.0 Hz 125 - 1/8 Hz

fill off1 6917 ; 6917 mid stroke; 19442-160mm from bottom

fill Tn 4000 ; 1000 = 1 sec, time expected to reach 'off1'

fill Sn 1000 ; 1000-sine, 2000-step to Sp

fill Tao 200 ;100 - 0.1 seconds, filter for road profile

fill Ts 330 ;100 - 1ms

fill sd 2000 ; 1000-input pass filter, others-no filtering

IFDEF A 11

SET IPIPE0 S0 ; xr

SET IPIPE1 S1 ; xw

SET IPIPE2 S2 ; Vb

SET IPIPE3 S3 ; P_top

SET IPIPE4 S9 ; P_bottom

SET IPIPE5 S7 ; xb

SET IPIPE6 S11 ; ua from DAC1;

SET IPIPE7 S12 ; u_dac0

SET IPIPE8 S8 ; Vw

APPENDIX B1

```
SET IPIPE9 S14 ; load cell
SET IPIPE10 S15 ; xb-xw
;SET IPIPE8 S10 ;Qt ;SET IPIPE9 S15 ;Qb
TIME 300
END
PDEFINE B
xr=IPIPE0
xw=IPIPE1
Vb=IPIPE2
Pt=IPIPE3
Pb=IPIPE4
xb=IPIPE5
ua=IPIPE6
u=IPIPE7
Vw=IPIPE8
Fa=IPIPE9
xbw=IPIPE10
CONTROL(amp1,w1,off1,Kp,Kpa,xr,Tn,Sn,Tao,Ts,sd,Vb,xrdc,0,1)
MERGE (xrdc,u,ua,xr,xb,xw,xbw,Vb,Vw,Pt,Pb,Fa, $BINOUT)
END
ODEFINE C 2
SET OPIPE0 A0
SET OPIPE1 A1
TIME 1650
CYCLE 1
END
START A,B,C
```

APPENDIX B2

- **Simulation program (C++ compiler) used to perform the system identification for passive suspension system with implementation friction force.**

```
// passivewithfrictiondependbodyvelocity.cpp : Defines the entry point for the console application.
// passivewithstaticfriction.cpp : Defines the entry point for the console application.
///  
passive test2.cpp :170517 Defines the entry point for the console application.
//  
//Servo-cylinder positioning
//single-rod, double acting,
//mid-stroke, initial position
//Internal eakage
//non-linear friction
//  
#include "stdafx.h"
#include <stdio.h>
#include <stdlib.h>
#include <math.h>

#define A1r          1.96e-3          //m2, actuator cross-sectional for side 1
#define A2r          0.94e-3          //m2, actuator cross-sectional for side 2
#define w            0.125            //Hz, frequency
#define off1         0.085            //m, mid stroke actuator
#define Am           0.05              //m, amplitude of displacement
#define Ts           0.00036          //second, sampling interval
#define Tn           2.25              //second, time expected to reach 'off1'
#define pi           3.1415           //22/7
#define T            9.73             //sec, simulation time
#define DF           "Opt_CLr.txt"    //output file
#define MT           285               //kg, total mass
#define Mb           240               //kg, body mass
#define Mw           40                //kg, wheel mass
#define Mr           5.0               //kg, tyre mass
#define g            9.81              //m/s2, ground acc.
#define Bvr         500                //N/m/s, actuator viscous damping
#define bd           260               //300 //N/m/s, passive viscous damping
#define bt           3886              //4000 //N/m/s, tyre damping rate
#define kt           9.2e5             //2.8e5 //N/m, tyre stiffness
#define ks           2.89e4            //1.96e4 //N/m/s, spring stiffness
#define Psr         200e5              //N/m2, supply pressure
#define Lr           0.170             //m, full stroke
#define Ld           0.342            //m, total lenth of passive damper
#define Br           1.43e9           //N/m2, road oil bulk modulus
#define Kfr         0.99e-4           // flow constant of servovalve
#define Kp           1.5               //Proportional gain
#define KI          2.5               //Integral gain
#define Sign        1.0                //1 - square wave, others - sine wave
#define tao1        0.2                //second, filter for road profile
#define tao         0.005             //second, time constant, servovalve
#define Rir         2.45e11           // Pa per L, Internal leakage resistance, road cylinder
#define V2r         80e-6             //m^3, Actuator volume for side 2
#define V1r         167e-6           //m^3, Actuator volume for side 1
```

APPENDIX B2

```
double  xr,xb,xw, xrd, dxr, dxr2, dxb, dxb2, dxw, dxw2, p1r, p2r, dp1r, dp2r, q1r, q2r, V01r,V02r, up, ui,
e,md,Sn, ms;
double  jt1, xr0, lr1, r1, sd, xsr, dxsr, Gama, PLr, mu,Deltatheta,A,B,C1,Ce,D,e1,Fn,Fdz,ffmax,ffric;
int      i, N;
float t;

void main()
{
  FILE *fb;
  fb=fopen(DF,"w"); //w-write, r-read

  Sn=2; //Sn=1, sine wave, 2 for square wave
  sd=1; //1 road profile filtered, else for non-filter
  ms=1;
  PLr=MT*g/A1r; p1r=PLr; p2r=0.0;
  up=0.0; ui=0.0;
  N=T/Ts;
  V01r=V1r*100;
  V02r=Lr*A2r+V2r;
  xr0=xr;
  jt1=(off1-xr0)/(Tn*0.50);

  fprintf(fb,"t\txrd\tr1\txr\txw\txb\te\tu\txsr\tVr\tar\tVb\tab\tVw\taw\tp1r\tp2r\tq1r\tq2r\tFdz\tffric\txw-
xb\tFn\n");

  for(i=0; i<N; i++){
    t=i*Ts;
    if(t<0.145){
      //xr=0.0; dxr=0.0; xsr=0.0; dxsr=0.0;
      //xw=0.0; dxw=0.0; xb=0.0; dxb=0.0;
      dp1r=0.0; dp2r=0.0; q1r=0.0; q2r=0.0; xr0=0.0;
      //p2r=0.0; up=0.0; ui=0.0; ffric=0.0;
    }

    //Bring the actuator to offset, 'off1' by time Tn, plus road profile

    else if(t<Tn){
      if(t<=Tn*0.555)
        xrd=(jt1*t-0.010)+xr0;
      else xrd = off1;
    }
    else {
      jt1 = w*pi*2*(t-Tn);
      xrd = Am*sin(jt1);
      if(Sn==1)
        xrd = xrd + off1;
      else if(xrd>=0)
        xrd=Am + off1;
      else
        xrd=off1-Am;
    }

    //road filter
    if(ms==1) {
      lr1=xrd;
      ms=2;
    }
    r1=((tao1/Ts)*lr1+xrd)/(1+tao1/Ts);
  }
}
```

APPENDIX B2

```

        lr1=r1;

        if (sd==1)
            e = r1-xr;
        else
            e = xrd-xr;

    up=Kp*e; //Proportional
    ui+=KI*e*T_s; //Integral
    up+=ui;

    dxsr=(up-xsr)/tao;
    xsr+=dxsr*T_s;

    if(xsr>=0){
        if((Psr-p1r)>=0)
            q1r=Kfr*xsr*sqrt(Psr-p1r);
        else
            q1r=-Kfr*xsr*sqrt(p1r-Psr);

        //q1r in +, out -; q2r out+, in -;
        if(p2r>=0)
            q2r=Kfr*xsr*sqrt(p2r);
        else
            q2r=-Kfr*xsr*sqrt(-p2r);
    }
    else {
        if((Psr-p2r)>=0)

            q2r=Kfr*xsr*sqrt(Psr-p2r);
        else
            q2r=-Kfr*xsr*sqrt(p2r-Psr);

        if(p1r>=0)
            q1r=Kfr*xsr*sqrt(p1r);
        else
            q1r=-Kfr*xsr*sqrt(-p1r);
    }

    dp1r=(Br/(V01r+xr*A1r))*(q1r-dxr*A1r-(p1r-p2r)/Rir);
    dp2r=(Br/(V02r-xr*A2r))*(dxr*A2r+(p1r-p2r)/Rir-q2r);
    dxr2=(p1r*A1r-p2r*A2r-Bvr*dxr-kt*(xr-xw)-bt*(dxr-dxw)-MT*g)/Mr;
    p1r+=dp1r*T_s;
    p2r+=dp2r*T_s;
    xr+=dxr*T_s; //x=x+dx*T_s;
    dxr+=dxr2*T_s;

//passive system
//Nonlinear friction
//ffrics=((ks*(xw+0.081)+bd*dxw)*sin(45*pi/180)-Mb*g);Mb*g=ks*xo;xo=0.081
mu=0.1; D=2600; Ce=193; e1=-0.003;
    B=xw-xb;
    A=0.707*B/(Ld-0.707*B); //((Ld-dltaL)/sin(45)=(xw-xb)/sin(deltatheta),deltaL=(xw-xb)sin(45);
    Deltatheta=asin(A);

//ffric=0.0; // (data acquisition delay or steady state)
ffmax=193.8; //from experment (xw-xb)=0.006974) and (dxw-dxb=-0.02979)[50&35bar]

    if (dxb==0.0) // (static friction)

```


APPENDIX B.3

- **Card program to converter D/A or A/D from PC through data acquisition and vice versa for active suspension system.**

Roadtyre.dap>DAP

RESET

PIPES amp1,w1,off1, Kp, ti, xrdc, r1, u, xr, xwr;

PIPES xb, xw, Vb,Vw, Pt, Pb, Qt, Qb;

PIPES Ts, Sn, Tn, Tao, sd;

Xr; Full stroke 170mm

Xr; mid-stroke 6917; fully retracted -7271; Fully extended 21105

Xr; LVDT calibration: 167 m-code/mm

Xw; bottom 16412, top 20164, 22.075 m-code/mm

Xb; bottom 15246, top 19030, 22.254 m-code/mm

Fill Kp 3276 ; 1v-3276

fill amp1 8350 ;8350-50mm aplitude. 5010=30mm, 10020-70mm; max 14188 for 8.5cm from mid stroke

fill w1 125 ; 1000 = 1.0 Hz 125 - 1/8 Hz

fill off1 6917 ; 6917 mid stroke; 19442-160mm from bottom

fill ti 2000 ; 1000 - 0.1 seconds, time delay for input change

fill Tn 4000 ; 1000 = 1 sec, time expected to reach 'off1'

fill Sn 2000 ; 1000-sine, 2000-step to Sp

fill Tao 200 ;100 - 0.1 seconds, filter for road profile

fill Ts 360 ;100 - 1ms

fill sd 2000 ; 1000-input pass filter, others-no filtering

IDEFINE A 12

SET IPIPE0 S0 ;xr

SET IPIPE1 S1 ;xw

SET IPIPE2 S2 ;Vb

SET IPIPE3 S3 ;P_top

SET IPIPE4 S9 ;P_bottom

SET IPIPE5 S7 ;xb

SET IPIPE6 S11 ;r1 or xrd from DAC1;

SET IPIPE7 S12 ;u_dac0

SET IPIPE8 S10 ;Qt/F suspensor

APPENDIX B.3

```
SET IPIPE9 S15 ;Qb/xb-xw
SET IPIPE10 S8 ;Vw
SET IPIPE11 S14 ;xw-xr
;SET IPIPE11 S14 ;load cell
TIME 300
END
PDEFINE B
xr=IPIPE0
xw=IPIPE1
Vb=IPIPE2
Pt=IPIPE3
Pb=IPIPE4
xb=IPIPE5
r1=IPIPE6
u=IPIPE7
Qt=IPIPE8
Qb=IPIPE9
Vw=IPIPE10
xwr=IPIPE11
CONTROL(amp1,w1,off1,Kp,ti,xr,Tn,Sn,Tao,Ts,sd,xrdc,0,1)
MERGE (r1,xrdc,u,xr,xb,xw,xwr,Vb,Vw,Pt,Pb,Qt, Qb, $BINOUT)
END
ODEFINE C 2
SET OPIPE0 A0
SET OPIPE1 A1
TIME 1800
CYCLE 1
END
START A,B,C
```

APPENDIX B.3

- **Simulation program used to perform the system identification for active suspension system with implementation friction force.**

```
// PID + PA controller.cpp : 020717 Defines the entry point for the console application.
////////////////////////////////////
//Servo-cylinder positioning
//single-rod, double acting, for road simulator
//mid-stroke, initial position, double-rod, double acting, for suspension actuator
//Internal eakage
//Linear friction
////////////////////////////////////
#include "stdafx.h"
#include <stdio.h>
#include <stdlib.h>
#include <math.h>

#define A1r      1.96e-3 //m2, actuator cross-sectional for side 1
#define A2r      0.94e-3 //m2, actuator cross-sectional for side 2
#define off1     0.085      //m, mid stroke actuator
#define Am      0.05        //m, amplitude of displacement
#define w        0.125      //Hz, frequency
#define Ts       0.00036 //second, sampling interval
#define Tn       2.25       //second, time expected to reach 'off1'
#define pi       3.1415     //22/7
#define T        10        //sec, simulation time
#define DF       "Opt_CLa.txt" //output file
#define MT       285       //kg, total mass
#define g        9.81      //m/s2, ground acc.
#define Bvr      500       //N/m/s, actuator viscous damping
#define Psr      200e5     //N/m2, supply pressure
#define Lr       0.170     //m, full stroke
#define Ld       0.700     //m, full free length of active actuator
#define Ber      1.4e9     //N/m2, oil bulk modulus
#define Kfr      0.99e-4 // flow constant of servovalve
#define Kp       1.75      //Proportional gain
#define KI       0.5       //Integral gain
#define Sign     1         //1 - square wave, others - sine wave
#define taof     0.2       //second, filter for road profile
#define taor     0.005     //second, time constant, servovalve road
#define Rir      2.45e11 // Pa per L, Internal leakage resistance, cylinder
#define Vr2      80e-6     //m^3, Actutor volume side 2
#define Vr1      167e-6    //m^3, Actutor volume side 1
#define Mb       240       //kg, body mass
#define Mw       40        //kg, wheel mass
#define Mr       5.0      //kg, Tyre mass
#define ks       2.89e4    //(N/m) ;spring stiffness
#define kt       9.2e5     //(N/m) ;tyre stiffness
#define bv       300      //(N/m*s^-1) ; actuator viscous damping rate
#define bd       260      //(N/m*s^-1) ; passive viscous damping rate
#define bt       3886     //(N/m*s^-1) ; tyre damping rate
#define Be       0.42e9    //N/m2, oil bulk modulus
#define Ac       2.46e-4  //(m^2); actuator cross-sectional area
```

APPENDIX B.3

```
#define Vc 7.13e-5 // (m^3); actuator chamber and hose volume
#define Ri 2.45e13 // (N*m^2/m^3*s^-1); cross-port leakage resistance
#define Kfa 2.3e-11 // (m^3*s^-1/mA); linearized flow gain [need to be identify]
#define elfa 27 // (degree); actuator angle
#define Ps 200e5 // (N/m^2); supply pressure
#define taoa 0.2 // second, time constant, servovalve actuator
#define Kpa 1.0 // proportional gain for active
#define KIa 0.25 // Integral gain for active
#define Kda 0.39 // derivative gain for active
#define V02 5.34e-3 // (m^3); top transmission line volume between Sv and cylinder [need to be identify]
#define V01 1.79e-3 // (m^3); bottom transmission line volume between Sv and cylinder [need to be identify]
#define Lac 0.190 // m, full stroke of actuator

double xr, xrd, dxr, dxr2, xb, dxb, dxb2, xw, dxw, dxw2, p1r, p2r, dp1r, dp2r, q1r, q2r, V01r, V02r, up,
ui, e, Ft, tc, md, Sn, ms, t1, Ce, C, e1, tz, D;
double jt1, xr0, lr1, r1, sd,
xsr, dxsr, Gama, PLr, PL, p1, p2, dp1, dp2, q1, q2, upa, uia, uda, ua, up2, uat, ea, pea, dea, xsa, dxsa, A, B, mu, ffric, ffric,
c, Deltatheta, Fdz, Fhyd, Td;
int i, N;
float t;

void main()
{
FILE *fb;
fb=fopen(DF, "w"); //w-write, r-read

Sn=2; //Sn=1, sine wave, 2 for square wave
sd=1; //1 road profile filtered, else for non-filter
ms=1;
PLr=MT*g/A1r;
p1r=PLr;
N=T/Ts;
V01r=Vr1*100;
V02r=Lr*A2r+Vr2;
xr0=xr;
jt1=(off1-xr0)/(Tn*0.5);
fprintf(fb, "t\txrd\txr\txw\txb\tea\tuasr\txsa\tVr\tp1r\tp2r\tq1r\tq2r\tVb\tab\tVw\taw\tp1\tp2\tq1\tq2\tFdz\tFhyd\tffric\n");

for(i=0; i<N; i++){
t=i*Ts;
if (t<0.145){
//xr=0.0; dxr=0.0; xsr=0.0; xsa=0.0;
xb=0.0; dxb=0.0; xw=0.0; dxw=0.0;
//dp1r=0.0; dp2r=0.0; q1r=0.0; q2r=0.0;
//dp1=0.0; dp2=0.0; q1=0.0; q2=0.0;
//pea=0.0; dea=0.0; Td=0.5;

```

APPENDIX B.3

```
//p1=0.0; p2r=0.0; p2=0.0;
up=0.0; ui=0.0; upa=0.0; uia=0.0; uda=0.0; ua=0.0;
ffric=0.0;
xr0= 0.0;
}
else
//Bring the actuator to offset, 'off1' by time Tn, plus road profile
    if(t<Tn) {
        if(t<=Tn*0.555)
            xrd=(jt1*t-0.01)+xr0;
        else xrd = off1;
    }
    else {
        jt1 = w*pi*2*(t-Tn);
        xrd = Am*sin(jt1);
        if(Sn==1)
            xrd = xrd + off1;
        else if(xrd>=0)
            xrd=Am + off1;
        else
            xrd=off1-Am;
    }
}

//road filter
if(ms==1) {
    lr1=xrd;
    ms=2;
}
r1=((taof/Ts)*lr1+xrd)/(1+taof/Ts);
lr1=r1;

if (sd==1)
    e = r1-xr;
else
    e = xrd-xr;

up=Kp*e; //Proportional
ui+=KI*e*Ts; //Integral
up+=ui;

dxsr=(up-xsr)/taor;
xsr+=dxsr*Ts;

if(xsr>=0){
    if((Psr-p1r)>=0)
        q1r=Kfr*xsr*sqrt(Psr-p1r);
    else
        q1r=-Kfr*xsr*sqrt(p1r-Psr);

    //q1r in +, out -; q2r out+, in -;
    if(p2r>=0)
        q2r=Kfr*xsr*sqrt(p2r);
    else
```

APPENDIX B.3

```
        q2r=-Kfr*xsr*sqrt(-p2r);
    }
    else {
        if((Psr-p2r)>=0)
            q2r=Kfr*xsr*sqrt(Psr-p2r);
        else
            q2r=-Kfr*xsr*sqrt(p2r-Psr);

        if(p1r>=0)
            q1r=Kfr*xsr*sqrt(p1r);
        else
            q1r=-Kfr*xsr*sqrt(-p1r);
    }

    dp1r=(Ber/(V01r+xr*A1r))*(q1r-dxr*A1r-(p1r-p2r)/Rir);
    dp2r=(Ber/(V02r-xr*A2r))*(dxr*A2r+(p1r-p2r)/Rir-q2r);
    dxr2=(p1r*A1r-p2r*A2r-Bvr*dxr-kt*(xr-xw)-bt*(dxr-dxw)-MT*g)/Mr;
    p1r+=dp1r*Ts;
    p2r+=dp2r*Ts;
    xr+=dxr*Ts; //x=x+dx*Ts;
    dxr+=dxr2*Ts;

// active system //LQ control//ea=-(I1*I2*dxb+J1*J2*dxw+H1*H2*(p1-p2)*Ac+F1*F2*(xb-xw)-
L1*L2*(xr-xw)); ea=-(735.4*dxb+5.22*dxw+2.1*Fhyd-1414.2*(xb-xw)-475.5*(xw-xr)); //LQ controll
//ea=-0.2e-1*dxb;
ua=Kpa*ea;
//up2=(735.4*dxb+5.22*dxw+2.1*Fhyd+1414.2*(xb-xw)+475.5*(xw-xr)); //ut=ua-up2;
dxsa=(ua-xsa)/taoa;
xsa+=dxsa*Ts;

if(xsa>=0){
    if((Ps-p1)>=0)
        q1=Kfa*xsa*sqrt(Ps-p1);
    else
        q1=-Kfa*xsa*sqrt(p1-Ps);

    //q1 in +, out -; q2 out+, in -;
    if(p2>=0)
        q2=Kfa*xsa*sqrt(p2);
    else
        q2=-Kfa*xsa*sqrt(-p2);
}
else {
    if((Ps-p2)>=0)
        q2=Kfa*xsa*sqrt(Ps-p2);
    else
        q2=-Kfa*xsa*sqrt(p2-Ps);

    if(p1>=0)
        q1=Kfa*xsa*sqrt(p1);
```


APPENDIX B.3

```
t,xrd,xr,xw,xb,ea,uat,xsr,xsa,dxr,p1r,p2r,q1r,q2r,dxb,dxb2,dxw,dxw2,p1,p2,q1,q2,Fdz,Fhyd,ffric);
```

```
    p1+=dp1*Ts;
    p2+=dp2*Ts;
    xb+=dxb*Ts; //x=x+dx*Ts;
    dxb+=dxb2*Ts;
    xw+=dxw*Ts; //x=x+dx*Ts;
    dxw+=dxw2*Ts;
```

```
    if(abs(xr)>(5*Lr)) i=N;
```

```
    }
    fclose(fb);
```

```
    return ;
}
```

APPENDIX B.4

- **Real time DAP program used to perform the full-state feedback control for active suspension system with considering 3rd order filter.**

```
////////////////////////////////////
// 23.02.2016
// Active control, Servosuspensor
// Third order filter add to Vb
// Zero initial control
//Smooth start
// _ bring the actuator to mid_stroke at biginning
////////////////////////////////////

#include "dtd.h"
#include "dtdmod.h"
#include "math32.h"

#define pi      3.141592

//Definition of module name and entry point.
#define COMMAND "CONTROL"
#define ENTRY CONTROL_entry

double      pt,pb,xwrf[4], xwr[4],xwr0,xbwf[4],xbw0,xbw[4],Vwf[4], Vw[4],Vw0,Vbf[4], Vb[4],
Vb0, dV, amp1,off1,w1,uc, ud, j1,t, xrd, xr,Ac, xr0, error, e1=0.0, Kpa, Kp, t0, t1, tc, Tn, r1, lr1, Tao, Ts,
ua, Tsf, c0,c1,c2,c3,d0,d1,d2,d3;

int Sn, Sp, sd, ms, md, Sa, sg1,i;

double J1,F1,L1,H1,Kia,I1;

//Implement module identification sequence
int __stdcall      ENTRY (PIB **plib);
extern "C" __declspec(dllexport) int __stdcall
ModuleInstall(void *hModule)
{return (CommandInstall(hModule,COMMAND,ENTRY,NULL));}
int __stdcall      ENTRY (PIB **plib)
{
// Storage for parameters:
void **argv;
```

APPENDIX B.4

```
int argc;

    short int dac0;
    short int dac1;

PIPE * in_pipe_amp1;
PIPE * in_pipe_w1;
PIPE * in_pipe_off1;

    PIPE * in_pipe_kp;
    PIPE * in_pipe_I1;
    PIPE * in_pipe_xr;
    PIPE * in_pipe_Tn;
    //PIPE * in_pipe_Sn;
    PIPE * in_pipe_Tao;
    PIPE * in_pipe_Ts;
    //PIPE * in_pipe_sd;
    PIPE * in_pipe_Vb;
    PIPE * in_pipe_Vw;
    PIPE * in_pipe_xbw;
    PIPE * in_pipe_xwr;
    PIPE * in_pipe_pt;
    PIPE * in_pipe_pb;
    PIPE * out_pipe_xrd;
    PIPE * in_pipe_Tsf;
    PIPE * in_pipe_Sa;
    PIPE * in_pipe_Kia;
    PIPE * in_pipe_J1;
    PIPE * in_pipe_F1;
    PIPE * in_pipe_L1;
    PIPE * in_pipe_H1;

//    GENERIC_SCALAR pipe_value;

// Access parameters

    argv = param_process(plib, &argc,25,25,
```

APPENDIX B.4

```
// Perform initialisations

pipe_open(in_pipe_amp1,P_READ);
        pipe_open(in_pipe_w1, P_READ);
pipe_open(in_pipe_off1,P_READ);
        pipe_open(in_pipe_kp, P_READ);
        pipe_open(in_pipe_I1, P_READ);
        pipe_open(in_pipe_xr, P_READ);
        pipe_open(in_pipe_Tn, P_READ);
        //pipe_open(in_pipe_Sn, P_READ);
        pipe_open(in_pipe_Tao, P_READ);
        pipe_open(in_pipe_Ts, P_READ);
        //pipe_open(in_pipe_sd, P_READ);
        pipe_open(in_pipe_Vb, P_READ);
        pipe_open(in_pipe_Vw, P_READ);
        pipe_open(in_pipe_pt, P_READ);
        pipe_open(in_pipe_pb, P_READ);
        pipe_open(in_pipe_xbw, P_READ);
        pipe_open(in_pipe_xwr, P_READ);
        pipe_open(out_pipe_xrd,P_WRITE);
        pipe_open(in_pipe_Tsf, P_READ);
        pipe_open(in_pipe_Sa, P_READ);
        pipe_open(in_pipe_Kia, P_READ);
        pipe_open(in_pipe_J1, P_READ);
        pipe_open(in_pipe_F1, P_READ);
        pipe_open(in_pipe_L1, P_READ);
        pipe_open(in_pipe_H1, P_READ);

// Begin continuous processing

amp1 = double(pipe_get(in_pipe_amp1));
w1  = double(pipe_get(in_pipe_w1));
off1 = double(pipe_get(in_pipe_off1));
Kp  = double(pipe_get(in_pipe_kp))/1000;
I1  = double(pipe_get(in_pipe_I1))/10000;
```

APPENDIX B.4

```
J1 = double(pipe_get(in_pipe_J1))/10000;
F1 = double(pipe_get(in_pipe_F1));
L1 = double(pipe_get(in_pipe_L1))/1000000000;
H1 = double(pipe_get(in_pipe_H1))/10000;
Tn    = double(pipe_get(in_pipe_Tn))/1000;
//Sn  = pipe_get(in_pipe_Sn)/1000;
Tao   = double(pipe_get(in_pipe_Tao))/1000;
Ts    = double(pipe_get(in_pipe_Ts))/100000;
//sd   = pipe_get(in_pipe_sd);
Vb[0] = double(pipe_get(in_pipe_Vb));
Vw[0] = double(pipe_get(in_pipe_Vw));
xbw[0] = double(pipe_get(in_pipe_xbw));
xwr[0] = double(pipe_get(in_pipe_xwr));
pt    = double(pipe_get(in_pipe_pt)); // 1bar=100 m.c, 1bar=10^5N/m^2
pb    = double(pipe_get(in_pipe_pb));
Tsf   = double(pipe_get(in_pipe_Tsf))/1000;
Sa    = pipe_get(in_pipe_Sa);
Kia   = double(pipe_get(in_pipe_Kia))/1000;

t0=sys_get_time();
xr0    = pipe_get(in_pipe_xr);
j1    = (off1 - xr0)/(Tn*0.5);
uc=0;
ud=0.0;
ms=1;
md=1;
sg1=1;
//Tn=4;
Sn=2000; // for sine wave
//Tao=0.2;
//Tsf=3;
sd=1000;
```

APPENDIX B.4

```
//Sa=2000;

//off1 =6917;

//w1=250;

Ac=2.46/10000;

xrd=xr0;

c0=8+8*Ts+4*Ts*Ts+Ts*Ts*Ts;

//c0=23.73964758;

c1=4*Ts*Ts-24-8*Ts+3*Ts*Ts*Ts;

//c1=-23.51365406;

c2=24-8*Ts-4*Ts*Ts+3*Ts*Ts*Ts;

//c2=14.14185796;

c3=8*Ts-8-4*Ts*Ts+Ts*Ts*Ts;

//c3=-2.604840408;

d0=Ts*Ts*Ts;

//d0=1.4703763848;

d1=3*Ts*Ts*Ts;

//d1=4.411129152;

d2=3*Ts*Ts*Ts;

//d2=4.411129152;

d3=Ts*Ts*Ts;

//d3=1.470376384;

//Bring the actuator to offset, 'off1' in time Tn

while(1)

{

    t=(sys_get_time()-t0)/1000;

    if(t<Tsf) {

        uc=0; ua=0;

        dac_out (dac0,int(uc));

        dac_out (dac1,int(ua));

        pipe_put(out_pipe_xrd,int(xrd));
```

APPENDIX B.4

```
xr          = pipe_get(in_pipe_xr);          //This action is needed to prevent data stagnation
Vb[0] = pipe_get(in_pipe_Vb);              //This action is needed to prevent data stagnation
    Vb0=Vb[0];
    }
    else {
        if (md==1) {
            t1=sys_get_time();
            md=0;
        }
        tc=(sys_get_time()-t1)/1000;
        if(tc<Tn) {
            if(tc<=Tn*0.5)
                xrd = j1*tc+xr0;
            else xrd = off1;
        }
        else {
            j1 = (w1/1000)*pi*2*(tc-Tn);
            xrd = amp1*sin(j1);          //xrd = amp1*sin(j1)+off1;
            if(Sn==1)
                xrd = xrd + off1;
            else if(xrd>=0)
                xrd=amp1 + off1;
            else
                xrd=off1-amp1;
        }

        if(ms==1) {
            lr1=xrd;
            ms=2;
        }
    }
}
```

APPENDIX B.4

```
}  
  
//road profile  
r1=((Tao/Ts)*lr1+xrd)/(1+Tao/Ts);  
lr1=r1;  
xr      = pipe_get(in_pipe_xr);  
if (sd==1000)  
    error = r1-xr;  
else  
    error = xrd-xr;  
uc=(Kp)*error;  
  
Vb[0] = pipe_get(in_pipe_Vb);  
Vw[0] = pipe_get(in_pipe_Vw);  
xbw[0] = pipe_get(in_pipe_xbw);  
xwr[0] = pipe_get(in_pipe_xwr);  
pt = pipe_get(in_pipe_pt);  
pb = pipe_get(in_pipe_pb);  
if(sg1==1) {  
    for(i=1;i<=3;i++){  
        Vbf[i]=Vb0;  
        Vb[i]=Vb0;  
        Vwf[i]=Vw0;  
        Vw[i]=Vw0;  
        xbwf[i]=xbw0;  
        xbw[i]=xbw0;  
        xwrf[i]=xwr0;  
        xwr[i]=xwr0;  
        //pt[i]=pt0;  
        //pt[i]=pt0;  
        //pbf[i]=pb0;  
        //pb[i]=pb0;
```

APPENDIX B.4

```
    }
    sg1=0;

}

//Active control
//Vbf=(Vb+8.75*Vbf)/9.75;1storderfilter;
Vbf[0]=(1/c0)*(-c1*Vbf[1]-c2*Vbf[2]-
c3*Vbf[3]+d0*Vb[0]+d1*Vb[1]+d2*Vb[2]+d3*Vb[3]);// 3rdorderfilter
//dV=Vbf[0]-Vbf[1];
Vwf[0]=(1/c0)*(-c1*Vwf[1]-c2*Vwf[2]-
c3*Vwf[3]+d0*Vw[0]+d1*Vw[1]+d2*Vw[2]+d3*Vw[3]);// 3rdorderfilter
xbwf[0]=(1/c0)*(-c1*xbwf[1]-c2*xbwf[2]-
c3*xbwf[3]+d0*xbw[0]+d1*xbw[1]+d2*xbw[2]+d3*xbw[3]);
xwrf[0]=(1/c0)*(-c1*xwrf[1]-c2*xwrf[2]-
c3*xwrf[3]+d0*xwr[0]+d1*xwr[1]+d2*xwr[2]+d3*xwr[3]);
//ptf[0]=(1/c0)*(-c1*ptf[1]-c2*ptf[2]-
c3*ptf[3]+d0*pt[0]+d1*pt[1]+d2*pt[2]+d3*pt[3]);
//pbf[0]=(1/c0)*(-c1*pbf[1]-c2*pbf[2]-
c3*pbf[3]+d0*pb[0]+d1*pb[1]+d2*pb[2]+d3*pb[3]);

//if(dV>=0)
//ua = -Kpa*30*dV;
//else
//ua = -1.5*Kpa*30*dV;

//ua = -Kpa*30*dV; //Proportional
//ud+=-Kia*dV*Ts; //Integral
//ua+=ud;

ua=Kia*(0.2*I1*Vbf[0]+0.2*J1*Vwf[0]+0.053*F1*xbwf[0]+0.0887*L1*xwrf[0]+0.2*10e-6*H1*(pt-
pb)*Ac);// LQ control

//ua=-5*I1*Vbf[0]+0.2*J1*Vwf[0]+0.129*F1*xbwf[0];

for(i=3;i>0;i--) {
    Vbf[i]=Vbf[i-1];
    Vb[i]=Vb[i-1];
```

APPENDIX B.4

```
Vwf[i]=Vwf[i-1];
Vw[i]=Vw[i-1];
xbwf[i]=xbwf[i-1];
xbw[i]=xbw[i-1];
xwrf[i]=xwrf[i-1];
xwr[i]=xwr[i-1];
//ptf[i]=ptf[i-1];
//pt[i]=pt[i-1];
//pbf[i]=pbf[i-1];
//pb[i]=pb[i-1];
}
//output limits
if(uc>32767*0.9) uc=32768*0.9;           if(uc<-
32767*0.9) uc=-32767*0.9;
if(ua>32767*0.9) ua=32768*0.9;           if(ua<-
32767*0.9) ua=-32767*0.9;

pipe_put(out_pipe_xrd,int(xrd));

//test of active suspensor
//uc=0;
//j1 = (w1/1000)*pi*2;
//ua = amp1*sin(j1*tc);
////////
if(Sa==1000) ua=-32768*0.85;
//Send control out

dac_out (dac0,int(uc));
dac_out (dac1,int(ua));
}
}
return 0;}
```

APPENDIX B.4

- **DAP Card program to converter D/A or A/D from PC through data acquisition and vice versa for active suspension system.**

Active-1/acountrol.dap...>DAP

RESET

; First run this programme for less than Tsf time (3 seconds) to zero control outputs

; The run the programme for test

PIPES amp1 , w1, off1, Kp, ti, xrdc, u, ua, kpa, xr, xbw, xrd;

PIPES xb, xw, Vb, Vw, Pt, Pb, xwr, Fa;

PIPES Ts, Sa, Tn, Tao, sd, Sn, Tsf, kia;

Xr; Full stroke 170mm

Xr; mid-stroke 6917; fully retracted -7271; Fully extended 21105

Xr ; LVDT calibration: 167 m-code/mm

Xw; bottom 16412, top 20164, 22.075 m-code/mm

Xb; bottom 15246, top 19030, 22.254 m-code/mm

Xbw; extended 1.448V, 4824 dap; retracted 0.0V, 0 dap

Vb; 5.0 volts/m/s; m-code/3276/5

Fill Kp 3276 ; 1v-3276

fill Kpa 1638 ; 1v-3276, kpa=0.3653, vb gain

fill amp1 3340 ; Maximum 25mm for active suspensor! 3340-20mm, 8350-50mm aplitude. 5010=30mm, 10020-70mm; max 14188 for 8.5cm from mid stroke

fill w1 250 ; 1000 = 1.0 Hz 125 - 1/8 Hz

fill off1 6917 ; 6917 mid stroke; 19442-160mm from bottom

fill Tn 4000 ; 1000 = 1 sec, time expected to reach 'off1'

fill Sn 2000 ; 1000-sine, 2000-step to Sp

fill Tao 200 ; 100 - 0.1 seconds, filter for road profile

fill Ts 720 ; 100 - 1ms

fill sd 1000 ; 1000-input pass filter, others-no filtering

fill Tsf 3000 ; 1000 - 1 second of zero controls, uc, ua

fill Sa 2000 ; 1000 - ua=0, 2000 - ua follows algorithm

fill kia 32760 ; Integral gain,

IFDEF A 12

SET IPIPE0 S0 ;xr

APPENDIX B.4

```
SET IPIPE1 S1 ;xw
SET IPIPE2 S2 ;Vb
SET IPIPE3 S3 ;P_top
SET IPIPE4 S9 ;P_bottom
SET IPIPE5 S7 ;xb
SET IPIPE6 S11 ;ua from DAC1;
SET IPIPE7 S12 ;u_dac0
SET IPIPE8 S8 ;Vw
SET IPIPE9 S10 ;load cell
SET IPIPE10 S15 ;xb-xw
SET IPIPE11 S14 ;xw-xr
;SET IPIPE8 S10 ;Qt ;SET IPIPE9 S15 ;Qb
TIME 600
END
```

.....

; This programme needs to be run first for $t < T_{sf}$ seconds for zero control purpose.

; Run again for the test ;

.....

PDEFINE B

xr=IPIPE0

xw=IPIPE1

Vb=IPIPE2

Pt=IPIPE3

Pb=IPIPE4

xb=IPIPE5

ua=IPIPE6

u=IPIPE7

Vw=IPIPE8

Fa=IPIPE9

xbw=IPIPE10

xwr=IPIPE11

CONTROL(amp1,w1,off1,Kp,Kpa,xr,Tn,Sn,Tao,Ts,sd,Vb,xrdc,Tsf,Sa,kia,0,1)

APPENDIX B.4

```
MERGE (xrdc,u,ua,xr,xb,xw,xbw,xwr,Vb,Vw,Pt,Pb,Fa, $BINOUT)
END
ODEFINE C 2
SET OPIPE0 A0
SET OPIPE1 A1
TIME 1650
CYCLE 1
END
START A,B,C
```

APPENDIX B.5

- **Simulation program used to perform the system identification for active suspension system with implementation friction force.**

// LQwithfriction.cpp : 160717 Defines the entry point for the console application.

// LQcontrol.cpp : 060916 Defines the entry point for the console application.

////////////////////////////////////

//Servo-cylinder positioning

//Singl-rod, double acting, cylinder rod horizontal

//mid-stroke, initial position

//Internal eakage

//Linear friction

////////////////////////////////////

#include "stdafx.h"

#include <stdio.h>

#include <stdlib.h>

#include <math.h>

#define A1r 1.96e-3 //m2, actuator cross-sectional for side 1

#define A2r 0.94e-3 //m2, actuator cross-sectional for side 2

#define off1 0.085 //m, mid stroke actuator

#define Am 0.05 //m, amplitude of displacement

#define w 0.125 //Hz, frequency

#define Ts 0.00036 //second, sampling interval

#define Tn 2.25 //second, time expected to reach 'off1'

#define pi 3.1415 //22/7

#define T 10 //sec, simulation time

#define DF "Opt_CLa.txt" //output file

#define MT 285 //kg, total mass

#define g 9.81 //m/s2, ground acc.

APPENDIX B.5

#define Bvr	500	//N/m/s, actuator viscous damping
#define Psr	200e5	//N/m ² , supply pressure
#define Lr	0.170	//m, full stroke of road actuator
#define Ld	0.700	//m, full free length of active actuator
#define Ber	1.4e9	//N/m ² , oil road bulk modulus
#define Kfr	0.99e-4	// flow constant of servovalve
#define Kp	1.75	//Proportional gain
#define KI	0.5	//Integral gain
#define Sign	1.0	//1 - square wave, others - sine wave
#define taof	0.2	//second, filter for road profile
#define taor	0.005	//second, time constant, road servovalve
#define Rir	2.45e11	// Pa per L, Internal leakage resistance, road cylinder
#define V2r	80e-6	//m ³ , road actuator volum for side 2
#define V1r	167e-6	//m ³ , road actuator volum for side 1
#define Mb	240	//kg, body mass
#define Mw	40	//kg, wheel mass
#define Mr	5.0	//kg, Tyre mass
#define ks	2.89e4	//(N/m) ;spring stiffness
#define kt	9.2e5	//(N/m) ;tyre stiffness
#define bv	300	//(N/m*s ⁻¹) ; actuator viscous damping rate
#define bt	3886	//(N/m*s ⁻¹) ; tyre damping rate
#define Be	0.42e9	//N/m ² , active oil bulk modulus
#define Ac	2.46e-4	//(m ²); active actuator cross-sectional area
#define Vc	7.13e-5	//(m ³); active actuator chamber and hose volume
#define Ri	2.45e13	//(N*m ² /m ³ *s ⁻¹);cross-port leakage resistance active cylinder
#define Kfa	2.3e-11	//(m ³ *s ⁻¹ /mA); linearized active flow gain [need to be identify]
#define taoa	0.2	//second, time constant, active actuator servovalve

APPENDIX B.5

```
#define elfa 27 //((degree); active actuator inclined angle

#define G 1.25e-3 // D/A gain (mA/PSCno.) [Need to be identify]

#define P 0.85e-3 // forward gain

#define Ps 200e5 //(N/m^2); supply pressure

#define Na 3276 //A/D gain (PSCno./V)

#define Kpa 0.1e-2 // proportional gain for active

#define V02 5.34e-3 //(m^3); initial actuator volume for side2 [need to be identify]

#define V01 1.79e-3 //(m^3); initial actuator volume for side1 [need to be identify]

#define Lac 0.19 //m, full stroke of active actuator;

#define I2 0.2 // body velocity weight factor sensor;

#define J2 0.2 // wheel velocity weight factor sensor;

#define H2 0.000002 // pressure weight factor sensor

#define F2 0.0000077 // actuator displacement weight factor sensor

#define L2 0.000027 // wheel road displacement weight factor sensor

#define I1 1.12 // control gain body velocity [Riccatiequ.m 210816 in Matlab]

#define J1 0.008 // control gain wheel velocity

#define H1 319.0 // control gain pressure

#define F1 56063.5 // control gain actuator displacement(xb-xw)

#define L1 5375.67 // control gain wheel road displacement(xb-xw)

double xr, xrd, dxr, dxr2, xb, dxb, dxb2, xw, dxw, dxw2, p1r, p2r, dp1r, dp2r, q1r, q2r, V01r, V02r, up,
ui, e, Ft, tc, md, Sn, ms, t1;

double jt1, xr0, lr1, r1, sd,
xsr, dxsr, Gama, PLr, PL, p1, p2, dp1, dp2, q1, q2, ua, up2, ut, ea, dea, xsa, dxsa, ffric, Ce, D, tz, e1, B, A, Deltatheta, mu,
ffmax, Fhyd, Fdz;

int i, N;

float t;

void main()
```

APPENDIX B.5

```
{  
  
FILE *fb;  
  
fb=fopen(DF,"w");//w-write, r-read  
  
Sn=2;//Sn=1, sine wave, 2 for square wave  
  
sd=1;//1 road profile filtered, else for non-filter  
  
ms=1;  
  
PLr=MT*g/A1r;  
  
p1r=PLr;  
  
N=T/Ts;  
  
V01r=V1r*100;  
  
V02r=Lr*A2r+V2r;  
  
xr0= xr;  
  
jt1=(off1-xr0)/(Tn*0.5);  
  
fprintf(fb,"t\txrd\txr\txw\txb\tea\tua\txsr\txsa\tVr\tar\tp1r\tp2r\tq1r\tq2r\tVb\tab\tVw\taw\tp1\tp2\tq1\tq2\t  
Fdz\tFhyd\tffric\n");  
  
for(i=0; i<N; i++){  
  
    t=i*Ts;  
  
    if (t<0.145){  
  
        //xr=0.0; dxr=0.0; xsr=0.0; xsa=0.0;  
  
        xb=0.0; dxb=0.0; xw=0.0; dxw=0.0;  
  
        //dp1r=0.0; dp2r=0.0; q1r=0.0; q2r=0.0;  
  
        //dp1=0.0; dp2=0.0; q1=0.0; q2=0.0;  
  
        //dea=0.0; p1=0.0; p2r=0.0; p2=0.0;  
  
        up=0.0; ui=0.0; ua=0.0; ffric=0.0;  
  
    }  
  
}
```

APPENDIX B.5

```
xr0= 0.0;

}

//Bring the actuator to offset, 'off1' by time Tn, plus road profile

else if(t<Tn) {

    if(t<=Tn*0.555)

        xrd=(jt1*t-0.01)+xr0;

    else xrd = off1;

}

else {

    jt1 = w*pi*2*(t-Tn);

    xrd = Am*sin(jt1);

    if(Sn==1)

        xrd = xrd + off1;

    else if(xrd>=0)

        xrd=Am + off1;

    else

        xrd=off1-Am;

}

//road filter

if(ms==1) {

    lr1=xrd;

    ms=2;

}

r1=((taof/Ts)*lr1+xrd)/(1+taof/Ts);

lr1=r1;
```

APPENDIX B.5

```
    if (sd==1)
        e = r1-xr;
    else
        e = xrd-xr;

up=Kp*e; //Proportional
ui+=KI*e*Ts; //Integral
up+=ui;

dxsr=(up-xsr)/taor;
xsr+=dxsr*Ts;
if(xsr>=0){
    if((Psr-p1r)>=0)
        q1r=Kfr*xsr*sqrt(Psr-p1r);
    else
        q1r=-Kfr*xsr*sqrt(p1r-Psr);

    //q1r in +, out -; q2r out+, in -;
    if(p2r>=0)
        q2r=Kfr*xsr*sqrt(p2r);
    else
        q2r=-Kfr*xsr*sqrt(-p2r);
}
else {
    if((Psr-p2r)>=0)
        q2r=Kfr*xsr*sqrt(Psr-p2r);
    else
        q2r=-Kfr*xsr*sqrt(p2r-Psr);
```

APPENDIX B.5

```
        if(p1r>=0)
            q1r=Kfr*xsr*sqrt(p1r);
        else
            q1r=-Kfr*xsr*sqrt(-p1r);
    }
    dp1r=(Ber/(V01r+xr*A1r))*(q1r-dxr*A1r-(p1r-p2r)/Rir);
    dp2r=(Ber/(V02r-xr*A2r))*(dxr*A2r+(p1r-p2r)/Rir-q2r);
    dxr2=(p1r*A1r-p2r*A2r-Bvr*dxr-kt*(xr-xw)-bt*(dxr-dxw)-MT*g)/Mr;
    p1r+=dp1r*Ts;
    p2r+=dp2r*Ts;
    xr+=dxr*Ts;
    dxr+=dxr2*Ts;
    // active system
    //ea=-(I1*I2*dxb+J1*J2*dxw+H1*H2*(p1-p2)*Ac+F1*F2*(xb-xw)-L1*L2*(xr-xw)); //LQ control
    ea=-(735.4*dxb+5.22*dxw+2.1*Fhyd-1414.2*(xb-xw)-475.5*(xw-xr)); //LQ controll
    //ea=-0.2e-1*dxb;
    ua=Kpa*ea;
    //up2=(735.4*dxb+5.22*dxw+2.1*Fhyd+1414.2*(xb-xw)+475.5*(xw-xr)); //LQ control
    //ut=ua-up2;
    dxsa=(ua-xsa)/taoa;
    xsa+=dxsa*Ts;
    if(xsa>=0){
        if((Ps-p1)>=0)
            q1=Kfa*xsa*sqrt(Ps-p1);
```

APPENDIX B.5

```
else
    q1=-Kfa*xsa*sqrt(p1-Ps);
    //q1 in +, out -; q2 out+, in -;
    if(p2>=0)
        q2=Kfa*xsa*sqrt(p2);
    else
        q2=-Kfa*xsa*sqrt(-p2);
    }
else {
    if((Ps-p2)>=0)
        q2=Kfa*xsa*sqrt(Ps-p2);
    else
        q2=-Kfa*xsa*sqrt(p2-Ps);

    if(p1>=0)
        q1=Kfa*xsa*sqrt(p1);
    else
        q1=-Kfa*xsa*sqrt(-p1);
    }

//friction
//ffs=((ks*(xw+0.081)+bd*dwx)*sin(45*pi/180)-Mb*g);Mb*g=ks*xo;xo=0.081
mu=0.1; D=2900; Ce=193; e1=-0.003;
B=xw-xb;
A=0.454*B/(Ld-0.891*B); //(Ld-dltaL)/sin(27)=(xw-xb)/sin(deltatheta),deltaL=(xw-xb)sin(63);
```

APPENDIX B.5

```
Deltatheta=asin(A);

//ffric=0.0; // (data acquisition delay or steady state)

ffmax=193.8; //from experment (xw-xb)=0.006974) and (dxw-dxb=-0.02979)[50&35bar]

    if (dxb==0.0) // (static friction)

    {

    if ((Fhyd+bv*(dxw-dxb))<ffmax)

        ffric=Fhyd+bv*(dxw-dxb);

    }

    else if (dxb>0.0) // (transition and dynamic friction)

    {

//ffric=Ce*exp(dxb/e1)+mu*Mw*dxw2/tan((elfa-Deltatheta)*pi/180)+D*dxb;

        ffric=Ce*exp(dxb/e1)+D*dxb; // without Colombo friction

    }

    else if (dxb<0.0) // (transition and dynamic friction)

    {

//ffric=-Ce*exp(dxb/-e1)+(mu*Mw*dxw2/tan((elfa-Deltatheta)*pi/180))+D*dxb;

        ffric=-Ce*exp(dxb/-e1)+D*dxb; // without Colombo friction

    }

dp1=(Be/(V01+(xb-xw)*Ac))*(q1-Ac*(dxb-dxw)-(p1-p2)/Ri);

dp2=(Be/(V02-(xb-xw)*Ac))*(Ac*(dxb-dxw)+(p1-p2)/Ri-q2);

Fhyd=(p1-p2)*Ac*cos((elfa-Deltatheta)*pi/180);

dxb2=(Fhyd+bv*(dxw-dxb)-ffric)/Mb;

dxw2=(-Fhyd-bv*(dxw-dxb)+kt*(xr-xw)+bt*(dxr-dxw))/Mw;
```


APPENDIX C

- **m.file to account the A, B, C, D and to find the K gains value**

```
%solve test1 rig
m1 =240;m2 = 40; g=9.81;
ko = 0.407*10^6;%ko=(2*be*Ac^2/V,be=0.24*10^9,Ac=2.46*10^-5,V=7.13e-5%
kt = 2.8*10^5;
be=0.24*10^9;
bv = 300;
bo=1.482*10^4;%bo=Ri*Ac^2, Ri=2.45*10^11%
bt = 3886;
Ac=2.46*10^-4;
V=7.13e-5;
Ri=2.45*10^11;
ki=2.3e-11; %%kfa
elfa=27;
G=0.2*10^7;
P=1;
Ts=0.00036;
tao=0.2;
%N=1600;
N=3276;
% closed-loop input road
%Pr=4.6 in thesis%
Pr=4.6;% compensator gain
Rr=1;%control gain possible Rr<26
Gr=0.0125;%D/A
F2r=50.6;%LVDT gain
F1r=1;%control gain
% Nr=1600;% A/D
% Kir=5.2*10^-6;%linearised pressure gain of servovalve

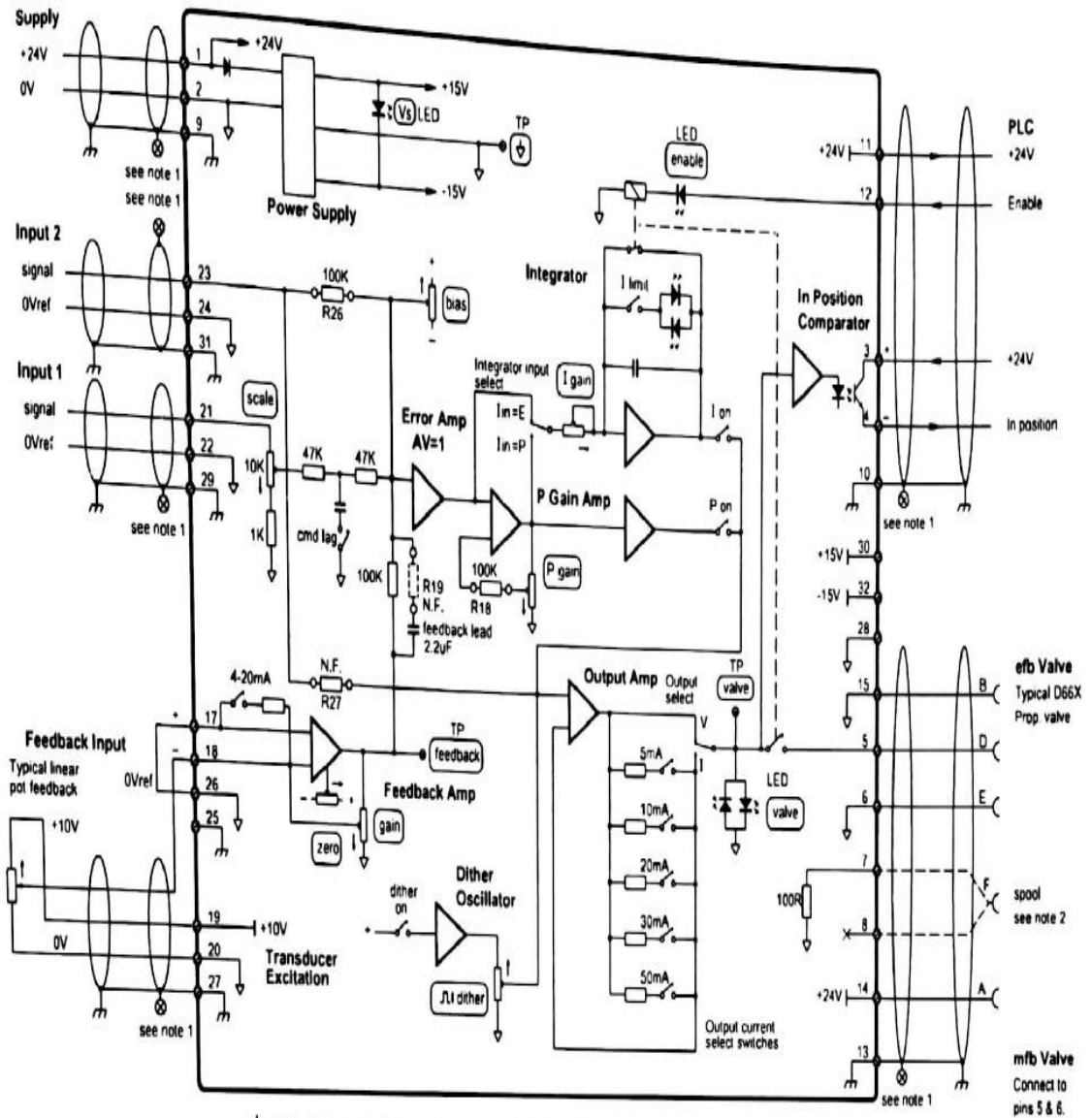
% Rir=2.45*10^11;% leakage resistance
% Bvr=500;
% MT=280;
% A1=1.96*10^-3;
% A2=0.94*10^-3;
% V1=167*10^-6;%actuator volume
% V2=80*10^-6;
% Br=1.4*10^9;%bulk modulus
% Ps=200; %supply pressure
% Kfr=1.78*10^-9; %flow constant of servovalve
%end
%feedback gain
%I2=5;J2=5 ;;H2=66.7*10^-6;F2=57.2;L2=18.2;thesis gains weight
I2=0.2;J2=0.2 ;H2=0.000002;F2=0.0000077;L2=0.000027;
K2=diag([I2,J2,H2,F2,L2]);
%I1=-5.26*10^-2;J1=2.11*10^-1;H1=5.85*10;F1=1.54*10^-2;L1=-2.78*10^-1;
%I1=-5.26*10^-2;J1=2.11*10^-1;H1=5.85*10^-3;F1=1.75*10^-1;L1=-2.5*10^-2;
% RICCATI Solves an algebraic Riccati equation;
A=[-bv/m1 bv/m1 0.891/m1 0 0;bv/m2 -(bv+bt)/m2 -0.891/m2 0 -kt/m2;
 -ko ko -(2*be)/(V*Ri) 0 0;1 -1 0 0 0;0 1 0 0 0];
B=[0;0;(2*ki*Ac*G*P*be)/V;0;0];
```

APPENDIX C

```
C=[0 0 1 0 0;0 0 0 1 0;0 0 0 0 1];
%q1=0.1; q2=3*10^9;q3=13.5*q2; optimal one
q1=4.37;q2=2*10^6; q3=2.66*10^7;
Qm=diag([q1,q2,q3]);
R=1;
Q=C'*Qm*C;
% A'*Pm+Pm*A-Pm'*B*R^-1*B'*Pm =-(C'*Qm*C);
% Q=Pm'*B*(R^-1)*B'*Pm-A'*Pm-Pm*A;
[Pm]=care(A,B,Q,R);
% [K,S,E] = lqr(A,B,Qm,R);
% Controllability Matrix (Mc)
% Mc=[B A*B A^2*B A^3*B A^4*B];
Mc=ctrb(A,B);
% det(Mc)=-6.5879e-11;det(Mc)/=0.0; rank(Mc)=5;
% To create the observability matrix Mb
% Mb=obsv(A,C)
a0=0.0;
a1=10817345.3;
a2=351225.5;
a3=20608.27;
a4=133.38;
a5=1.0;
%% mu1=-7.45+6.37j;mu2=-7.45-6.37j;mu3=-74.5;mu4=-74.5;mu5=-74.5;
elfa0=3.97e7;elfa1=7.76e6;elfa2=6.83e5;elfa3=2.01e4;elfa4=2.38e2;elfa5=1.0;
Wc=[a1 a2 a3 a4 1;a2 a3 a4 1 0;a3 a4 1 0 0;a4 1 0 0 0;1 0 0 0 0];
K=(R^-1)*B'*Pm;
% K1=(N^-1)*K*K2^-1;
% I1=K1(1);J1=K1(2);H1=K1(3);F1=K1(4);L1=K1(5);
% K1(thesis)=[-5.26*10^-2 2.11*10^-1 5.85*10^-3 1.75*10^-1 -2.5*10^-2];
% K/N=[-0.0392 0.3506 0.0005 0.4317 -5.0235]
T=Mc*Wc;
I=eye(5);
Pl=poly(A);%%
Kp=[3.97e7 -3.05e6 3.3e5 -508.2 104.6];
T1=inv(T);
% K=Kp*T1;
K1=(N^-1)*K*K2^-1;
D=0;
sys=ss(A,B,C,D);
H=tf(sys);
```

APPENDIX D

- Block-wiring diagram of road actuator servovalve amplifier

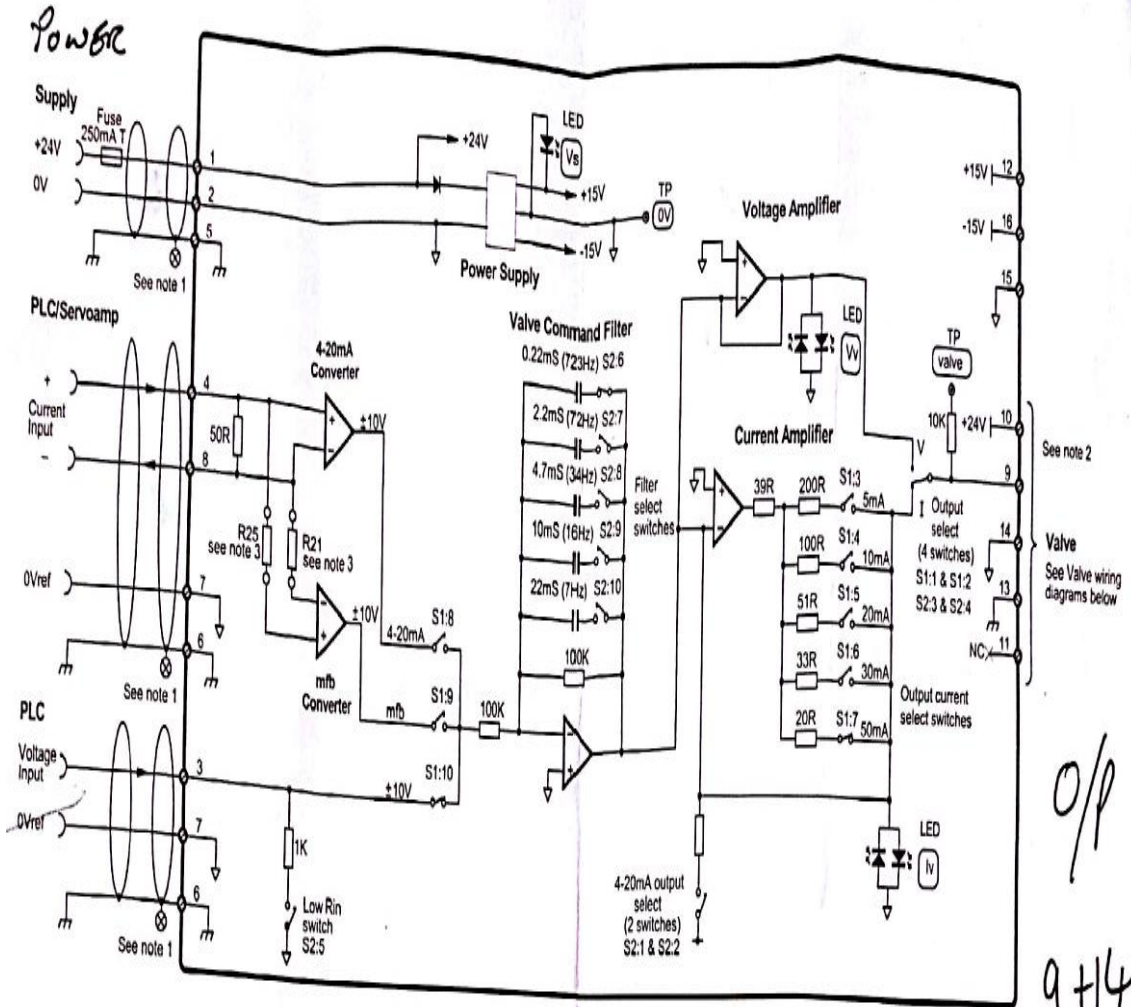


Note 1. Connect cable screen to enclosure cable gland or chassis ground terminal on G122-824.

Note 2. Connect spool (pin F) to terminal 7 if current, to terminal 8 if voltage.

APPENDIX D

- Block-wiring diagram of active actuator servovalve amplifier



Notes:

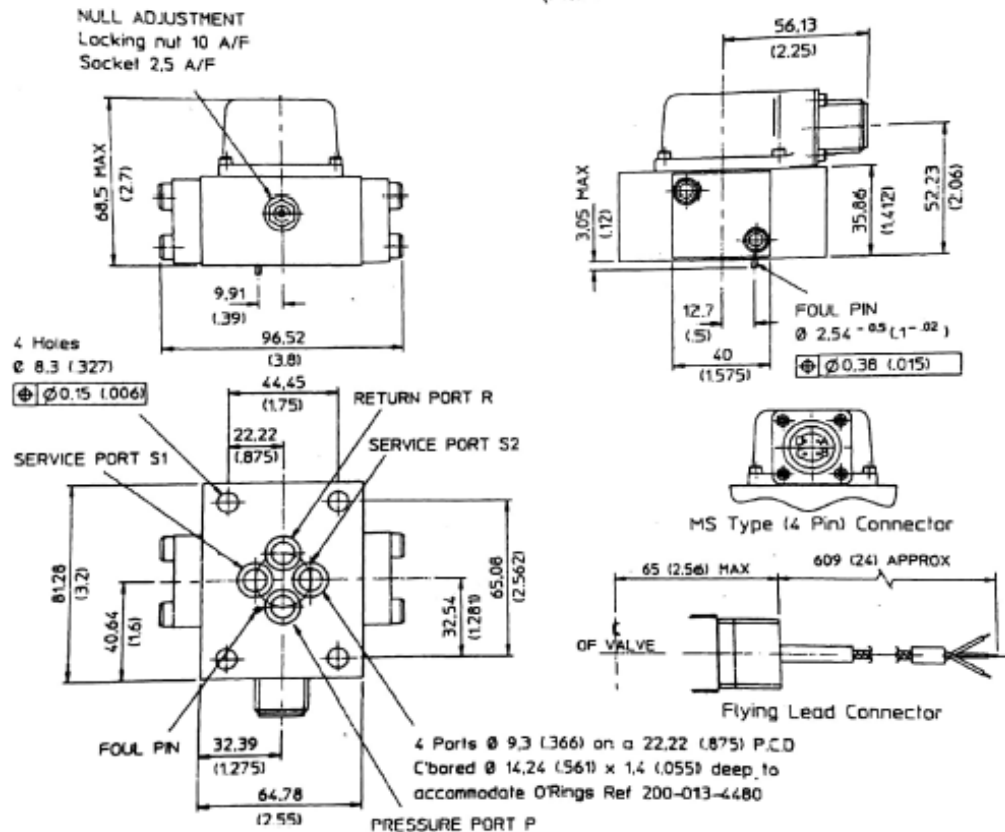
1. Connect cable screen to enclosure cable gland.
2. Terminal 10 max output current is 500mA. It cannot power a DDV.
3. R21 and R25 are 1/4W plug-in resistors on P.C.B. to select mfb input current. Default 390K. See 5.3.
4. Switches shown in default positions.

APPENDIX D1

- Servovalve 4551 installation data

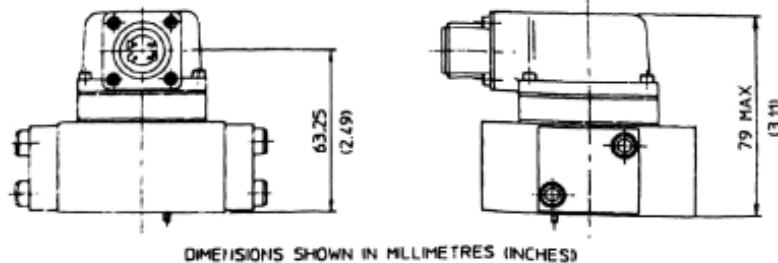
INSTALLATION DATA - 4551 SERIES VALVE

- 1 Before installation refer to Application Data.
- 2 Suggested mounting screws: M8 x 50 long (5/16 UNC or UNF x 2 long) high tensile steel socket head cap screws.
- 3 **Null adjustment:** Flow out of service port 1 will increase with clockwise rotation of bushing pin.
- 4 Surface to which valve is mounted requires 0,8 microns (32 micro inches) finish flat within 0,025 (.001).
- 5 Electrical connector: MS 3102E-14S-2P.
- 6 Replacement base mounting O'Rings: 200-013-4480 are 10,82 (.426) I/D x 1,78 (.07) sect'.
- 7 Motor cap normally positioned with electrical connector over pressure port, may be rotated 90° or 180° to suit particular installations.
- 8 Optional electrical mating connector: MS 3106E/MC-14S-2S (maximum cable size 7,75mm (.305) diameter).



INSTALLATION DATA - INTRINSICALLY SAFE 4851 SERIES VALVE

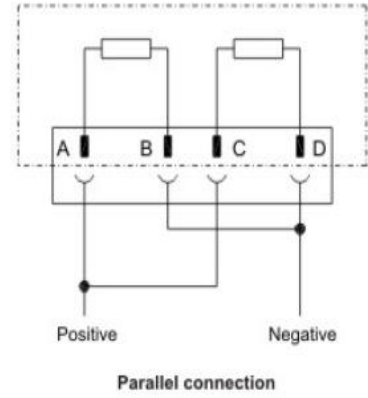
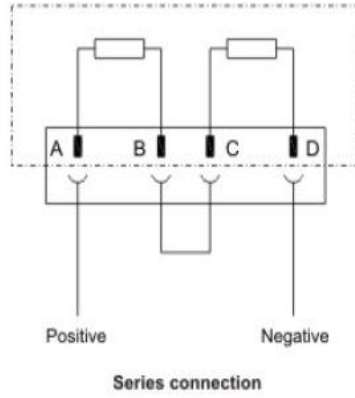
NOTE: TO COMPLY WITH I.S. APPROVALS THIS VALVE MUST NOT BE DISMANTLED.



APPENDIX D1

- **Servo valve connection**

Electrical Details



APPENDIX E

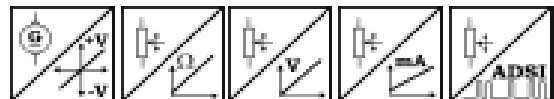
- (W)GS2 Velocity Sensor with Analog or A/D converted synchronous serial output.

(W)GS2 Velocity Sensor with Analog or A/D converted synchronous serial output



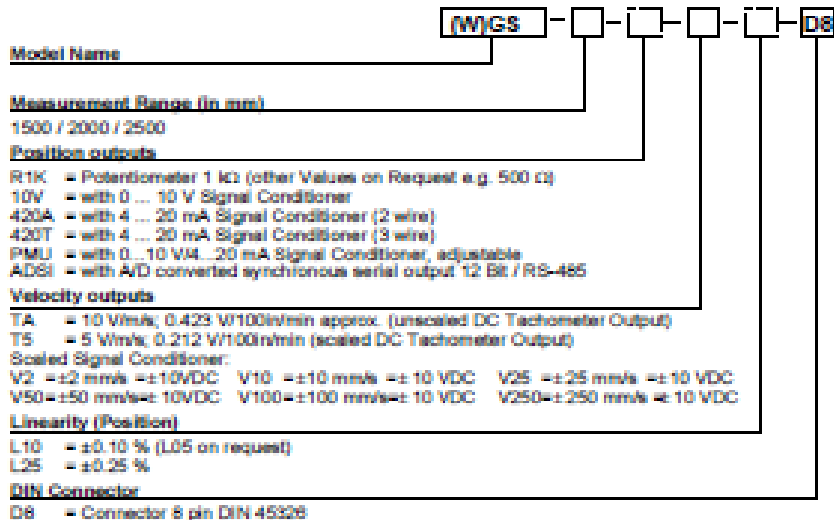
Velocity Sensor with Position Option

- Protection Class IP50
- Measurement Range:
0 ... 1500 mm to 0 ... 2500 mm
0 ... 59.06 In to 0 ... 98.43 In
- With Analog Output or A/D converted synchronous serial output



Specifications	Output	Scaled / unscaled DC Tachometer Potentiometer: 1 kΩ Voltage: 0...10 V Current: 4 ... 20 mA, 2 or 3 wire Voltage and Current Output, adjustable A/D converted synchronous serial 12 Bit RS-485
	Resolution	Essentially infinite / AD81: 12 Bit Full Scale
	Material	Aluminium and Stainless steel. Cable: Stainless Steel. Housing: Anticorrosive Sheet Steel
	Sensing Device	Precision Potentiometer
	Connector	Male Socket 8 pin DIN 45326
	Position Linearity	Up to ±0.05 % Full Scale
	Velocity Linearity	Up to ±0.25 % Full Scale
	Protection Class (IEC 529)	IP50

Order Code (W)GS2



Order Code Mating Connector (see accessories page 105)

WS-CONN-D8

Order Example: WGS2 - 2500 - 10V - V10 - L10 - D8

APPENDIX E

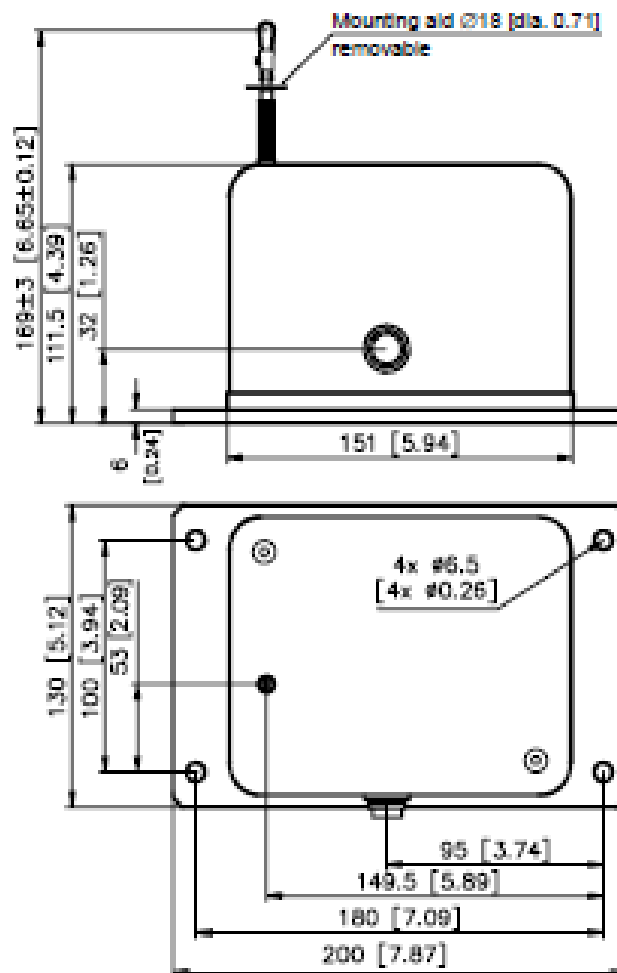
(W)GS2 Velocity Sensor with Analog or A/D converted synchronous serial output



Specifications (Continuation)	Weight	2.1 kg approx.
	Environmental	
	Immunity to Interference (EMC)	Refer to Output Specification
	Temperature	Refer to Output Specification

Cable Forces typical at 20 °C	Range		Maximum Pull-out Force	Minimum Pull-In Force
	[mm]	[in]	[N]	[N]
	1500	59.09	10.2	8.7
	2000	78.74	8.4	5.4
	2500	98.43	7.2	4.8

Outline drawing



Dimensions in brackets are inches.
For guaranteed dimensions consult factory